Silicon, iron and titanium doped calcium phosphate-based glass reinforced biodegradable polyester composites as bone analogous materials

Maziar Shah Mohammadi

Department of Mining and Materials Engineering

McGill University, Montréal, QC, Canada

April 2012

A thesis submitted to the Faculty of Graduate and Postdoctoral Studies of McGill University in partial fulfillment of the degree of doctor of philosophy

ABSTRACT

Bone defects resulting from disease or traumatic injury is a major health care problem worldwide. Conventional surgical techniques are associated with several limitations such as donor site morbidity, infection, pain and additional cost of operation in autogenic transplantation, or availability and immunological rejection in allogenic transplantation. Tissue engineering offers an alternative approach to repair and regenerate bone through the use of a cell-scaffold construct. The engineered scaffold should provide an appropriate environment for the osteoblasts to proliferate, differentiate, and ultimately induce bone formation. The scaffold should be biodegradable, biocompatible, porous with an open pore structure, and should be able to withstand the applied forces. Degradable synthetic polymers have been considered as scaffolding materials; however, they lack bioactivity and do not have the capacity to withstand certain load bearing conditions. Phosphate-based glasses (PGs) may be used as reinforcing agents in degradable composites since their degradation can be predicted and controlled through their chemistry.

This doctoral dissertation describes the development and evaluation of PGs reinforced biodegradable polyesters for intended applications in bone augmentation and regeneration. This research was divided into three main objectives:

1) Investigating the composition dependent properties of novel PG formulations by doping a sodium-free calcium phosphate-based glass ($50P_2O_5$-40CaO, in mol.%) with SiO_2, Fe_2O_3, and TiO_2. Accordingly, ($50P_2O_5$-40CaO-xSiO_2-(10-x)Fe_2O_3, where x = 10, 5 and 0 mol.%) and ($50P_2O_5$-40CaO-xSiO_2-(10-x)TiO_2 where x = 10, 7, 5, 3 and 0 mol.%) formulations were developed and characterised in terms of physico-chemical and surface properties, as well as cytocompatibility using MC3T3-E1 pre-osteoblasts. SiO_2 incorporation led to increased solubility, ion release, pH reduction, as well as hydrophilicity, surface energy, and surface polarity. In contrast, doping with Fe_2O_3 or TiO_2 resulted in more durable glasses, and improved cell attachment and viability. The cytocompatibility of Ti-doped PGs was further investigated in terms of cell proliferation and alkaline phosphatase (ALP) activity. It was found that 3 mol.% TiO_2 was adequate for stabilising the PG network resulting in controlled degradation, and improved cell

viability and proliferation; however, higher ALP activity was achieved at 5 to 7 mol.% SiO_2 incorporation. It was hypothesised that the presence of SiO_2 in the TiO_2-doped formulations could up-regulate the ionic release from the PG leading to higher ALP activity of MC3T3-E1 cells.

2) Incorporating Si, Fe, and Ti doped PGs as fillers, either as particulates or fibres, into biodegradable polyesters (polycaprolactone (PCL) and semi-crystalline and amorphous poly(lactic acid) (PLA and PDLLA)) with the aim of developing degradable bone analogous composites. Degradation and ionic release in deionised water (DW), changes in structural and mechanical properties of the composites as-processed and when conditioned in phosphate buffered saline (PBS) were investigated. It was shown that composite properties can be modulated by incorporating PG particulate (PGPs) blends of different formulations or through the incorporation of PG fibres (PGFs) as randomly oriented fibres. It was found that PG composition and geometry dictated the weight loss and ionic release of the composites. PGF reinforcement resulted in greater enhancement of mechanical properties compared to PGP. This was also reflected upon ageing in PBS, where composites reinforced with PGFs maintained their mechanical properties for longer times compared to those reinforced with PGPs. In addition, it was found that degradation time of PGF could be altered through its composition to coincide either with matrix degradation making it suitable for longer-term applications such as bone fixation devices, or with bone regeneration period suggesting its suitability for applications in bone tissue engineering (BTE) when converted to porous scaffolds. It was also hypothesised that a potential reaction between Si and the ester bond led to the formation of carboxylate by-products resulting in a lower molecular weight polymer, thus affecting the mechanical properties of the composites. This reaction was found to depend on both PG composition and surface area, as well as composite processing temperature. In addition, an apatite precursor was formed upon conditioning in simulated body fluid only on the surface of certain composites with enhanced ion release rates. Cytocompatibility assessment with MC3T3-E1 pre-osteoblasts showed that these composites were cytocompatible, and cell alignment along the PGFs was observed possibly due to their favourable ionic release properties.

3) Investigating the solid-state foaming (SSF) using carbon dioxide (CO_2) of PDLLA-PGP composites with up to 30 vol.% filler content. While PDLLA foams resulted in 92% porosity, the porosity of the composites ranged between 79 and 91% which decreased with PGP content. In addition, a reduction in pore size was observed with increasing PGP content; however, the pore size maintained its range of 200-500 μm in all composite foams, suitable for BTE applications. The percentage of open pores increased significantly with PGP content (up to 78% at 30 vol.% PGP). Compressive strength and modulus of PDLLA-PGP foams showed up to approximately 3-fold increase at 30 vol.% PGP content compared to neat PDLLA foams.

In conclusion, calcium phosphate glass properties could be tailored by doping with SiO_2, Fe_2O_3, and TiO_2, and its versatility could be translated into a degradable composite to be suitable for applications as bone analogous materials. SSF using CO_2 is an effective method of producing PDLLA-PG scaffolds with appropriate pore morphology for BTE applications.

RÉSUMÉ

Les défauts osseux découlant de maladies ou de traumatismes constituent un problème de santé majeur à l'échelle mondiale. Les techniques chirurgicales traditionnelles sont associées à plusieurs facteurs limitatifs tels que la morbidité du site donneur, l'infection, la douleur et le coût additionnel dans les cas de greffes autogènes ou la disponibilité et le rejet immunologique dans les cas de greffes allogènes. Le génie tissulaire représente une autre option pour réparer et régénérer des os en faisant appel à l'échafaudage cellulaire. L'échafaudage ainsi produit devrait fournir un milieu adéquat pour la prolifération et la différentiation des ostéoblastes et entraîner, à terme, la formation d'os. L'échafaudage doit être biodégradable, biocompatible, poreux à structure ouverte, et doit pouvoir résister aux forces appliquées. Si la possibilité d'utiliser des polymères synthétiques dégradables comme matériaux d'échafaudage a été examinée, ces substances ne sont pas bioactives et ne peuvent résister à certaines conditions de charge appliquées. Des verres à base de phosphate (PG) peuvent être utilisés comme agents de renforcement dans des composites biodégradables puisque leur dégradation peut être prédite et maîtrisée par l'intermédiaire de leurs propriétés chimiques.

La présente thèse de doctorat décrit la mise au point et l'évaluation de polymères biodégradables renforcés avec des PG pour des applications d'augmentation et de régénération osseuses. La recherche présentée visait les trois principaux objectifs suivants :

1) l'étude des propriétés dépendantes de la composition de nouvelles formulations de PG par le dopage de verres de calcium à base de phosphate exempts de sodium ($50P_2O_5$-40CaO, en % molaire) avec du SiO_2, du Fe_2O_3 et du TiO_2. Ainsi, des formulations de ($50P_2O_5$-40CaO-xSiO_2-(10-x)Fe_2O_3, où x = 10, 5 et 0 % mol) et ($50P_2O_5$-40CaO-xSiO_2-(10-x)TiO_2 où x = 10, 7, 5, 3 et 0 % mol) ont été mises au point et caractérisées en ce qui concerne leurs propriétés physicochimiques et de surface, ainsi que leur cytocompatibilité en utilisant des pré-ostéoblastes MC3T3-E1. L'incorporation de SiO_2 s'est traduite par une augmentation de la solubilité, de la libération d'ions, de la réduction du pH, ainsi que de l'hydrophilicité, de l'énergie de surface et de la polarité. En revanche, le dopage au Fe_2O_3 ou au TiO_2 a donné des verres plus durables, en plus d'améliorer la fixation et la

viabilité cellulaires. La cytocompatibilité des PG dopés au Ti a fait l'objet d'études plus approfondies sur la prolifération cellulaire et l'activité de la phosphatase alcaline (ALP). Il a ainsi été établi que 3 % mol de TiO_2 convient pour stabiliser le réseau de PG, ce qui se traduit par une dégradation contrôlée et l'amélioration de la viabilité et de la prolifération cellulaires. Une activité de l'ALP accrue a toutefois été obtenue avec l'incorporation de 5 à 7 % mol de SiO_2. Il a été postulé que la présence de SiO_2 dans les formulations dopées au TiO_2 pourrait accroître la libération d'ions des PG, entraînant ainsi une activité de l'ALP accrue des cellules MC3T3-E1;

2) l'incorporation de PG dopés aux Si, Fe et Ti comme charges, sous forme de particules ou de fibres, dans des polyesters biodégradables (polycaprolactone (PCL) et acides polylactiques amorphes (PLA et PDLLA)) dans le but de mettre au point des composites dégradables analogues aux os. La dégradation et la libération d'ions dans l'eau désionisée et les modifications aux propriétés structurales et mécaniques des composites tels quels ou conditionnés dans une solution saline dans un tampon phosphate (PBS) ont été étudiées. Il a ainsi été démontré que les propriétés de composites peuvent être modulées en y incorporant des mélanges de particules de PG (PGP) de différentes formulations et de fibres de PG (PGF) aléatoirement orientées. Il a été établi que la composition et la géométrie des PG déterminent la perte de poids et la libération d'ions des composites. Comparativement aux PGP, le renforcement par PGF a produit une amélioration plus marquée des propriétés mécaniques. De même, après vieillissement dans une PBS, les composites renforcés aux PGF ont conservé leurs propriétés mécaniques plus longtemps que ceux renforcés aux PGP. En outre, il a été établi que la durée de dégradation des PGF pouvait être changée en modifiant leur composition afin que cette durée corresponde avec celle de la dégradation de la matrice, les rendant ainsi convenables pour des applications à plus long terme telles que des dispositifs de fixation osseuse, ou encore avec la durée de régénération osseuse, de sorte qu'ils conviendraient à des applications en génie tissulaire osseux (BTE) une fois convertis en des échafaudages poreux. Il a également été postulé qu'une réaction potentielle entre le Si et le lien ester entraînait la formation de sous-produits de carboxylate, ce qui se traduirait par un polymère de poids moléculaire réduit et aurait ainsi une incidence sur les propriétés mécaniques des composites. Il a été établi que cette réaction dépend de la composition et de la surface active du PG, ainsi que de la

température de traitement du composite. De plus, lors du conditionnement dans un fluide organique simulé, la formation d'un précurseur de l'apatite n'a été observée qu'à la surface de certains composites présentant des taux de libération d'ions accrus. L'évaluation de la cytocompatibilité avec les pré-ostéoblastes MC3T3-E1 a démontré que ces composites étaient cytocompatibles, et un alignement de cellules le long des PGF a été observé, qui pourrait être dû à leurs propriétés de libération d'ions favorables;

3) l'investigation du moussage en milieu solide (SSF) avec du dioxyde de carbone (CO_2) de composites de PDLLA-PGP contenant jusqu'à 30 % vol de charge. Alors que les mousses de PDLLA présentaient 92 % de porosité, la porosité des composites allait de 79 % à 91 %, diminuant avec la teneur en PGP. En outre, une réduction de la taille des pores a été observée avec l'augmentation de la teneur en PGP; la fourchette de dimensions des pores est toutefois demeurée la même (de 200 µm à 500 µm) pour toutes les mousses de composites, qui conviennent à des applications en BTE. Le pourcentage de pores ouverts a augmenté significativement avec la teneur en PGP (jusqu'à 78 % à 30 % vol de PGP). La résistance à la compression et le module d'élasticité en compression des mousses PDLLA-PGP avaient à peu près triplé à 30 % vol de PGP par rapport à celles des mousses seulement constituées de PDLLA.

En conclusion, les propriétés des verres de calcium à base de phosphate peuvent être adaptées par dopage au SiO_2, au Fe_2O_3 et au TiO_2, et leur versatilité peut se traduire par la mise au point de composites dégradables convenant à des applications comme matériaux analogues aux os. Le moussage en milieu solide avec du CO_2 constitue une méthode efficace pour produire des échafaudages de PDLLA-PG dont la morphologie des pores convient à des applications en BTE.

ACKNOWLEDGEMENTS

I would like to start by expressing my sincere thanks and gratitude to my inspiring thesis supervisors, Dr. Showan N. Nazhat and Dr. Martin N. Bureau, for their trust, and continuous guidance throughout my PhD. I would like to deeply acknowledge their generosity in providing all of the materials, equipments, facilities, and trainings necessary for my research from which I have gained invaluable experience in numerous experimental skills and analytical methods. I have to acknowledge appreciable amount of time they spent discussing my data and opening new windows towards completing my PhD. In addition, obtaining a PhD is a long journey, and one might face several difficulties during that period. Therefore, I would like to also thank my PhD supervisors who kindly listened to my words whenever I encountered a problem, and have always been supportive.

I would like to take this opportunity to express my admiration and gratefulness to all the co-authors of the manuscripts that I have generated during my PhD, particularly Dr. Ifty Ahmed who kindly answered my questions. I would like to thank all the members of Professor Nazhat's group (Dr. Naser Muja, Dr. Vahid Serpooshan, Dr. Benedetto Marelli, Chiara E Ghezzi, Florencia Chicatun, and Christoph Stähli) for their help and support. All the research associates and technicians at McGill university and National Research Council-Industrial Materials Institute (NRC-IMI) who helped me with organizing or conducting my experiments are gratefully acknowledged, specially, Monique Riendeau and Pierre Vermette at McGill University, and Richard Gendron, Chantal Coulombe, Dominique Desgagnés, Karine Théberge, and Manon Plourde at NRC-IMI. The completion of this thesis would not have been possible without their help and support.

I would like to acknowledge the funding sources that made this research to be done without financial restraints. McGill Engineering Doctoral Award (MEDA), McGill International Doctoral Award (MIDA), Provost's fellowship, and Dr. Y. Lin-Alexander's fellowship are thankfully acknowledged. Moreover, Department of Mining and Materials Engineering at McGill University is gratefully acknowledged for conferring on me the Research Excellence Recognition Award, and Graduate Research Enhancement and

Travel (GREAT) Award. Following funding sources are also deeply acknowledged: Canadian Natural Sciences and Engineering Research Council, le Fonds Québécois de la Recherche sur la Nature et les Technologies, Hatch Faculty Fellowship and Canadian Foundation for Innovation: Leaders Opportunity Fund.

I would like to express my deepest gratitude to my family for their continuous love, support, and encouragement. Last, but not least, I would like to thank my lovely wife for her patience, understanding and love which made this dissertation possible.

TABLE OF CONTENTS

LIST OF FIGURES

CHAPTER 2

CHAPTER 4

CHAPTER 5

CHAPTER 6

CHAPTER 7

CHAPTER 8

CHAPTER 9

LIST OF TABLES

CHAPTER 6

CHAPTER 7

CHAPTER 8

GLOSSARY OF ABBREVIATIONS AND SYMBOLS

2D	Two dimensional
3D	Three dimensional
α-MEM	Alpha-minimum essential medium
AA	Atomic absorption
AB	AlamarBlue™
ALP	Alkaline phosphatase
ATR-FTIR	Attenuated total reflectance Fourier transform infra red
β-TCP	Beta-tricalcium phosphate
BMU	basic multicellular units
BO	Bridging oxygen
BTE	Bone tissue engineering
CA	Contact angle
CaP	Calcium phosphate
CHA	Carbonated hydroxyapatite
CLSM	Confocal laser scanning microscopy
DII	Diiodomethane
DMA	Dynamic mechanical analysis
DTA	Differential thermal analysis
DW	Deionised water
ECM	Extracellular matrix
FBS	Foetal bovine serum
FDA	Food and drug administration
GPC	Gel permeation chromatograph
HA	Hydroxyapatite
IC	Ion chromatography
ICP-OES	Inductively coupled plasma/optical emission spectrophotometer
M_n	Number average molecular weight
M_w	Weight average molecular weight

micro-CT	Micro computed tomography
mol.%	Mole percent
NBO	Non-bridging oxygen
NMR	Nuclear magnetic resonance
PBS	Phosphate buffered saline
PCL	polycaprolactone
PDLLA	Poly(D,L-lactic) acid
PGs	Phosphate-based glasses
PGA	Poly(glycolic acid)
PGF	Phosphate-based glass fibre
PGP	Phosphate-based glass particulate
PLA	Poly(lactic acid)
PLGA	Poly(lactic-co-glycolic acid)
SA	Surface area
SBF	Simulated body fluid
$scCO_2$	Supercritical carbon dioxide
SE	Surface energy
SE^d	Dispersive surface energy
SE^p	Polar surface energy
SE^t	Total surface energy
SEM	Scanning electron microscopy
SGs	Silicate-based glasses
T_c	Crystallisation temperature
T_g	Glass transition temperature
T_m	Melting temperature
TE	Tissue engineering
THF	Tetrahydrofuran
TIPS	Thermally induced phase separation
vol.%	Volume percent
wt.%	Weight percent
X^p	Surface polarity

CONTRIBUTIONS OF AUTHORS

This dissertation presents a collection of five published and to be submitted manuscripts written by the candidate under the supervision of Prof. Showan N Nazhat and Dr. Martin N Bureau. As the first author of all the manuscripts, I proposed, designed and conducted the bulk of the experiments. In addition, material preparation and testing, data collection and analysis, and writing the manuscripts have been my commitment. As the candidate's supervisors, Prof. Nazhat and Dr. Bureau guided me throughout the whole process and extensively reviewed all the manuscripts.

Since this was a multidisciplinary field of research from materials processing, physical, chemical and mechanical characterisations to cell-material assessments, collaborations were necessary in order to cover all the required experiments that were needed to fulfill the objectives of this research project. The role of each of the contributors and co-authors of the manuscripts is explained below:

Dr. Christopher D Rudd is a professor at the University of Nottingham and collaborated on the development of the initial Si and Fe-doped glass formulations and composites. Therefore, he was considered as a co-author on manuscript 1 (Chapter 4), manuscript 2 (Chapter 5), and manuscript 3 (Chapter 6).

Dr. Ifty Ahmed is a research associate at the University of Nottingham and collaborated on the production of the initial Si and Fe-doped glass formulations and composites. Therefore, he was considered as a co-author on manuscript 1 (Chapter 4), manuscript 2 (Chapter 5), and manuscript 3 (Chapter 6).

Dr. Naser Muja is a research associate and collaborated on the cell-material assessments in Prof. Nazhat's group who trained me to conduct the Live/Dead® assay, and helped with interpretation of the results. Therefore, he helped with the generation of Figures 5.8, 6.5, 6.6 and 7.5.

Dr. Benedetto Marelli was a PhD student in Prof. Nazhat's group working on "*In vitro* mineralization of an osteoid-like dense collagen construct for bone tissue engineering", and provided the expertise on the FTIR investigations for manuscript 1 (Chapter 4). He conducted the experiment and generated Figure 4.5 and supplementary Figure 4.1. (Other

FTIR investigations present in manuscript 2 and 3 were carried out by the candidate). He also provided the expertise for micro-CT analysis for manuscript 5 (Chapter 8) and generated Figure 8.5.

Florencia Chicatun is a PhD student in Prof. Nazhat's group working on "Development and characterization of dense collagen/chitosan hybrid gel scaffolds for tissue engineering", and provided the expertise for the cell metabolic and alkaline phosphatase activities. Therefore, she helped with the conduction and data interpretation of these assays. She contributed to the generation of Figures 7.6 and 7.7.

Christoph Stähli is a PhD student in Prof. Nazhat's group working on "Copper-releasing phosphate-based glass for the stimulation of angiogenesis", and helped with conducting the ICP-OES measurements. Therefore, he contributed to the generation of Figure 7.4 (a, b, c and d).

Sergio Almeida was a visiting student in Prof. Nazhat's group. I, the candidate, trained him for using the DMA instrument, and he helped with conducting the DMA test for manuscript 2 (Chapter 5). Data collection, analysis and interpretation were my commitment.

Jason Bertram was an undergraduate student at McGill University who was performing his co-op program at NRC-IMI. I, the candidate, trained and supervised him during his Co-op at NRC-IMI, and he helped with the fabrication of PDLLA-PGP composites. He also helped with experimental aspects of the PDLLA-PGP composite characterisation. Data collection, analysis and preparation were my commitment.

Richard Gendron is a researcher at NRC-IMI, and collaborated on the foaming process. He helped me with using the autoclave and conducting the foaming process. His expertise and advice was very helpful in the development of the foams. Therefore, he was considered as a co-author on manuscript 5 (Chapter 8).

It should be noted that all the mentioned results due to these contributions were obtained under the lead and supervision of the candidate, and generated for the manuscripts included in this dissertation, and will not be used elsewhere.

CHAPTER 1

INTRODUCTION

1.1. Introduction

Skeletal system defects, for example after trauma or tumour resection, impede the normal human organism function. Although bone has a high regenerative capacity, particularly in young people, which allows the majority of fractures to be healed without the need for major intervention, large bony defects need surgical intervention since they lack the template for an orchestrated regeneration [1]. Current methods of restoring tissues include surgical transfer of relevant tissue from healthy parts of the same patient (autogenic transplantation) or from a donor (allogenic transplantation). However, there are several limitations associated with these surgical techniques, including donor site morbidity, infection, pain and the additional cost of operation in autogenic transplantation, as well as availability and immunological rejection in allogenic transplantation [2]. Therefore, the search for new bone regeneration strategies is essential due to increasing medical and socioeconomic challenges of our ageing population. Biomaterials-based treatment in orthopaedics is rapidly growing due to this tremendous clinical need. In order to replace the autologous or allogenic bone usage, many bone substitute materials have been evaluated in the last two decades which generally include bioactive ceramics and glasses, natural or synthetic polymers, as well as their composites [1, 3-5].

Composites are an attractive approach as biomaterials since the required mechanical and physiological demands of the host tissue can be fulfilled by combining the advantageous properties of different materials [6, 7]. Composites based on biodegradable polymers (e.g. poly(lactic acid) (PLA), poly(glycolic acid) (PGA), their copolymers (poly(lactic-co-glycolic acid) (PLGA)), as well as polycaprolactone (PCL)) and bioactive ceramics (e.g. hydroxyapatite (HA), β-tricalcium phosphate (β-TCP), and Bioglass®) have been extensively studied as bone analogous materials [8]. They provide the potential for reduced stress shielding, and would negate additional surgical intervention, as alternatives to metals [9]. It is also well recognised that the addition of bioactive glasses and ceramics into a polymeric matrix should improve the mechanical and biological properties of the composites. However, not all calcium phosphate materials (e.g. silicate-based glasses (SGs) or HA) provide controlled solubility properties [10] to coincide with either the bone regeneration rate or degradation of the matrix.

Phosphate-based glasses (PGs) have emerged as a potential alternative inorganic phase for producing composites of controllable degradation [11, 12]. PGs are a unique class of materials that are degradable and biocompatible containing elements that are natural constituents of the human body. They provide a diverse range of solubility, which can be predicted and controlled through their chemistry [12-14]. The advantage of using PGs as fillers in composites compared to conventional stoichiometric additives, e.g. HA [15-18], is the greater flexibility in the composition of the glass filler phase, thus allowing for the tailoring of the end properties of the composites [11]. Moreover, they can be used as reinforcing agents as both particulates and fibres since their structural polymeric nature allows them to be easily drawn into fibres [19]. The use of fibres as filler could result in a higher mechanical reinforcing effect, compared to particulates, when incorporated into a polymer matrix.

Tissue engineering (TE) is a promising approach to treat severely damaged tissues and overcome the problems associated with current surgical techniques. This approach develops a scaffold to provide an appropriate environment for the cells to proliferate and differentiate in order to induce tissue regeneration. TE scaffolds are highly porous structures which serve as three-dimensional (3D) templates for the seeded cells to lay

down the extracellular matrix (ECM), and therefore facilitate the formation of functional tissues and organs. Therefore, along with biodegradability and biocompatibility, the materials being used for scaffold production should have the ability to be processed into a porous structure with well-defined architecture and mechanical properties suitable for the end application.

1.2. Aim, research hypothesis and objectives

It is hypothesised that the versatility of PG properties may be translated into a composite system by incorporation into a degradable polymer. However, this largely depends on the glass composition. Therefore, the global aim of this doctoral research was to develop novel PG formulations, and produce biodegradable composite systems by incorporating the PGs into biodegradable polymers for intended applications in bone repair and regeneration. The objectives were to:

A. Develop PG formulations by incorporating SiO_2, Fe_2O_3 or TiO_2 into a calcium phosphate-based glass composition ($50P_2O_5$-$40CaO$-$xSiO_2$-$(10-x)Fe_2O_3$, where x = 10, 5 and 0; $50P_2O_5$-$40CaO$-$xSiO_2$-$(10-x)TiO_2$, where x = 10, 7, 5, 3 and 0). Investigate the bulk and surface properties of the PGs as well as solubility and ionic release rates. Assess pre-osteoblastic cell line (MC3T3-E1) attachment and cytocompatibility on the PGs.

B. Incorporate PGs into biodegradable polyesters such as PCL and PLA (semi-crystalline and amorphous (PDLLA)) and investigate the effect of PG formulation and/or geometry (particulate or fibre) on the composite properties as-produced, and upon conditioning in aqueous environments. Assess MC3T3-E1 pre-osteoblastic cell attachment and cytocompatibility on the composites. These composites may have potential applications as bone fracture fixation devices and scaffolds for bone tissue engineering.

C. Investigate the foamability of PDLLA-PG composite systems by solid-state gas foaming technique with high pressure carbon dioxide (CO_2). Study the effect of PG

filler content on morphology and mechanical properties of porous PDLLA-PG composites.

In order to meet the first objective, and assess the effect of Si, Fe and Ti doping on PG properties, sodium-free PG formulations with fixed P_2O_5 and CaO content were developed. Na_2O is deemed an important component of bioactive SGs in order to reduce the high network connectivity and increase the surface reactivity [20, 21]. However, PGs are readily soluble in aqueous environments as a consequence of their low network connectivity and may not require Na_2O as a modifying oxide. In addition, the positive effect of Na^+ ions on cells has been questioned [22, 23]. Therefore, while the majority of PG formulations that have been investigated to date included Na_2O, this research aimed to produce sodium-free PGs doped with SiO_2, Fe_2O_3 or TiO_2.

PCL and PLA were selected as the composites matrices for the second objective. Both of these aliphatic polyesters are US Food and Drug Administration approved for use as sutures, controlled drug delivery devices and temporary orthopaedic plates for bone fracture repair. They have also received attention for use as scaffolds for TE as they can be degraded via hydrolysis under physiological conditions, where the degradation rate of PCL is much slower than that of PLA [24]. At room and physiological temperatures, PCL is in the crystal reinforced rubber state due to its low glass transition temperature (T_g) of approximately -60 ^oC, while PLA (semi-crystalline or amorphous) is below its T_g of approximately 55 ^oC, and is a relatively high strength and modulus polymer [25]. In addition, the melting temperature (T_m) of PCL (60 ^oC) allows it to be processed at relatively low processing temperatures (100 ^oC) compared to PLA (above 200 ^oC) since its T_m is approximately180 ^oC. Since the composite processing temperature impacts the filler/matrix interaction, investigating the effect of PG formulation surface properties on the polymer matrix during processing required different matrices with distinct processing temperatures.

To achieve the third objective, $50P_2O_5$-40CaO-$10TiO_2$ (Ti10) PG and PDLLA were selected as the filler and matrix, respectively. PDLLA is a mixture of two stereoisomeric forms of PLA (D- and L-lactic acid). Due to the amorphous nature of D,L-PLA, it is usually considered for applications such as drug delivery systems allowing a

homogenous dispersion of the active species within a monophasic matrix [25, 26]. This amorphous structure can also be beneficial when producing TE scaffolds through gas foaming due to an increased gas dissolution in less organised morphologies; hence, amorphous polymers foam more easily than the crystalline polymers [27]. This allowed for investigating the effect of PG fillers on the foamability of the composite system without being hindered by the crystallinity of the polymer matrix.

1.3. Thesis outline

The research work outlined herein is directed towards the development of calcium phosphate-based glass-reinforced biodegradable polymer composites as materials for bone repair and regeneration. The thesis includes: general introduction, literature review, statement of the problem, PGs, modulation of composite properties through incorporation of PGs, foamability of polymer-PG system, general discussion, conclusions and future perspectives.

In the present chapter (Chapter 1), an introduction, research hypothesis, objectives and outline are presented followed by a summary of original contributions. Chapter 2 provides a review of published literature on bone repair and regeneration, bone tissue engineering (BTE), biomaterials in bone repair and regeneration including bioactive ceramics and glasses with a focus on PGs, polymeric biomaterials with a focus on synthetic biodegradable polymers and polymer-ceramic composites, porous structures for BTE scaffolds, scaffold requirements and fabrication techniques. Chapter 3 refers to the statement of the problem outlining the motivations behind this research.

Chapter 4 reports on the results generated when PG particles ($50P_2O_5$-40CaO-10x, in mol.%) where x is either Fe_2O_3 or SiO_2 were incorporated into PCL to serve as a degradable composite biomaterial for potential applications in bone repair and regeneration. It was hypothesised that PCL incorporated with PG particulate blends of different formulations will tailor the composite properties. Changes in the structural and mechanical properties of as-processed composites, when aged in deionised water and phosphate buffered saline, and the potential for calcium phosphate deposition by conditioning in simulated body fluid were investigated. This manuscript has been published in peer-reviewed *Acta Biomaterialia*.

Chapter 5 reports on the results of the effect of doping PGs with Si and Fe on the properties of the glass alone and when incorporated into the PCL matrix as randomly orientated fibres (PGFs), with the aim of developing a degradable bone analogous composite. A series of parameters were used to characterise the properties of the various composites, as produced and as a function of degradation time. The capacity for calcium phosphate formation and pre-osteoblastic cytocompatibility were also investigated. This manuscript has been published in peer-reviewed *Acta Biomaterialia.*

Chapter 6 reports on the results of investigating the effect of PGF surface properties on polyester matrix composites. PG composition influences its surface properties in terms of hydrophilicity and surface energy which considerably affect its degradation, as well as filler/matrix interaction when incorporated into hydrolysable polyesters. The effect of Si and Fe doped PG composition on the surface energy which was correlated with their solubility and reactivity with the PLA matrix was investigated. The effect of these PGFs on a series of composite properties was also investigated. In addition, the cytocompatibility of the composites was assessed using MC3T3-E1 pre-osteoblasts to investigate their potential application in bone repair and regeneration. This manuscript has been published in peer-reviewed *Journal of Materials Science: Materials in Medicine.*

In Chapter 7, the incorporation of TiO_2 into PGs was attempted to control their degradation rate and improve their biological properties. Therefore, PG formulations were developed and characterised by replacing Fe_2O_3 with TiO_2, which has been shown to enhance cell growth and osteoblastic differentiation [28, 29]. Therefore, Fe_2O_3 was replaced by TiO_2 in the glass composition to investigate the effect of Si and Ti doping on PG properties for potential applications in BTE. This manuscript is under preparation to be submitted for peer-review.

In Chapter 8, the foamability of PDLLA-PG composite system was studied. For this purpose, a TiO_2 doped PG (Ti10), which was investigated in Chapter 7, was selected and incorporated into PDLLA as PG particulate (PGP) to produce PDLLA composites of 5, 10, 20 and 30 vol.% PGP content. Having characterized the composites in terms of density, PG content, morphology and mechanical properties, CO_2 solid-state gas foaming technique was applied to fabricate composite foams with controlled morphology for

potential applications as BTE scaffolds. The effect of PG incorporation and filler content on the foamability and foam morphology as well as mechanical properties was investigated. This manuscript is under preparation to be submitted for peer-review.

This dissertation ends by providing a general discussion (Chapter 9) and overall conclusions and future perspectives (Chapter 10).

1.4. Summary of original contributions

The original contributions of this research can be summarised by the following publications:

1.4.1. Journal publications

- ✓ **Shah Mohammadi M**, Ahmed I, Marelli B, Rudd C, Bureau MN, Nazhat SN. Modulation of polycaprolactone composite properties through incorporation of mixed phosphate glass formulations, *Acta Biomaterialia* 2010; 6:3157-3168.

This article (Chapter 4) presents the modulation of PCL composite properties through incorporation of mixed PG formulations. This confirmed the hypothesis that blends of Si and Fe doped PG particulate will tailor the composite properties.

- ✓ **Shah Mohammadi M**, Ahmed I, Muja N, Almeida S, Rudd C, Bureau MN, Nazhat SN. Effect of Si and Fe doping on calcium phosphate-based glass fibre reinforced polycaprolactone bone analogous composites. *Acta Biomaterialia* 2012, doi:10.1016/j.actbio.2011.12.030.

In this work (Chapter 5), Si and Fe doped PGs were investigated alone and when incorporated into PCL as randomly dispersed fibres. PG properties could successfully be translated into a composite system. Composites were developed for longer term applications (e.g. fracture fixation devices) or potential applications as BTE scaffolding materials, based on the compositional dependence of PGFs degradation rate, which could be coincided with either the degradation time of the polymer matrix or regeneration period of bone.

- ✓ **Shah Mohammadi M**, Ahmed I, Muja N, Rudd C, Bureau MN, Nazhat SN. Effect of calcium phosphate-based glass fibre surface properties on poly(lactic acid) matrix composites. *Journal of Materials Science: Materials in Medicine* 2011; 22:2659-2672.

The third article (Chapter 6) presents the effect of PG surface properties on the PLA matrix composite properties. Having characterized the surface properties of the Si and Fe doped PG in terms of contact angle and surface energy, the surface polarity dependence of PGs on the glass composition was correlated with the solubility in aqueous environments, ionic release, filler/matrix interaction, and consequently matrix molecular weight and composite mechanical properties.

- ✓ **Shah Mohammadi M**, Chicatun F, Stähli C, Muja N, Bureau MN, Nazhat SN. Effect of silica and titania doping on sodium-free calcium phosphate-based glass properties for bone tissue engineering. To be submitted.

In the fourth manuscript (Chapter 7), Fe_2O_3 was replaced with TiO_2 in the glass composition to further control the degradation of the glass, and potentially improve cell attachment and cytocompatibility. This study showed controlled degradation as well as improved cell attachment, proliferation and alkaline phosphatase (ALP) activity in sodium-free PGs doped with SiO_2 and TiO_2.

- ✓ **Shah Mohammadi M**, Bertram J, Marelli B, Gendron R, Nazhat SN, Bureau MN. Calcium phosphate glass particulates-reinforced poly(D,L-Lactic acid) composite foams through solid-state foaming using carbon dioxide. To be submitted.

The fifth manuscript (Chapter 8), presents the foamability of polymer-PG composite system by applying CO_2 gas foaming to investigate the potential of creating controlled porous structures to serve as BTE scaffolds. The effect of PG filler on foamability and foam cellular morphology is addressed in this manuscript.

CHAPTER 2

BACKGROUND AND LITERATURE REVIEW

2.1. Bone

2.1.1. Structure

Two types of bone tissue can be distinguished in the adult skeleton (Figure 2.1a):

(i) Cortical or compact bone: This type of bone is dense with a porosity of approximately 10% and is usually found in the external part of long bones (femur, tibia, etc.) and flat bones (mandible, skull and scapula).

(ii) Cancellous or trabecular bone: Cancellous bone is 50-90% porous. Consequently, its mechanical properties, including compressive strength, are approximately 10 times lower compared to cortical bone. The sponge-like structure of trabecular bone is made of bars and rods of various sizes called trabeculae and mainly present in the metaphysis of long bones.

The overall ratio between cortical and cancellous bone is 80:20, and is dependent on the location in the skeleton. However, bones with predominantly trabecular structure are also present [30-32].

Bone has a multi-scale architecture, and several hierarchical levels have been considered to explain its structure [33-35]. A recognised model based on seven

hierarchical levels is available in the literature [36] (Figure 2.1b). According to this model, molecular components of bone (e.g. water, collagens, carbonated hydroxyapatite (CHA) and non-collagenous proteins) are the main constituents of the first level [37]. The second hierarchical level includes mineralized collagen fibrils (organized CHA crystals) formed by the molecular components of bone. The third level of hierarchy is made up of bundles or other arrangements of mineralized collagen fibrils organized in arrays and aligned along their lengths. Fibril arrays are organised in a variety of patterns (parallel or radial fibril arrays, woven fibre structure and plywood-like structures) to make the fourth level [36]. These patterns can be considered as the extension of the third level structure into a higher scale size range (micron and even millimetre).

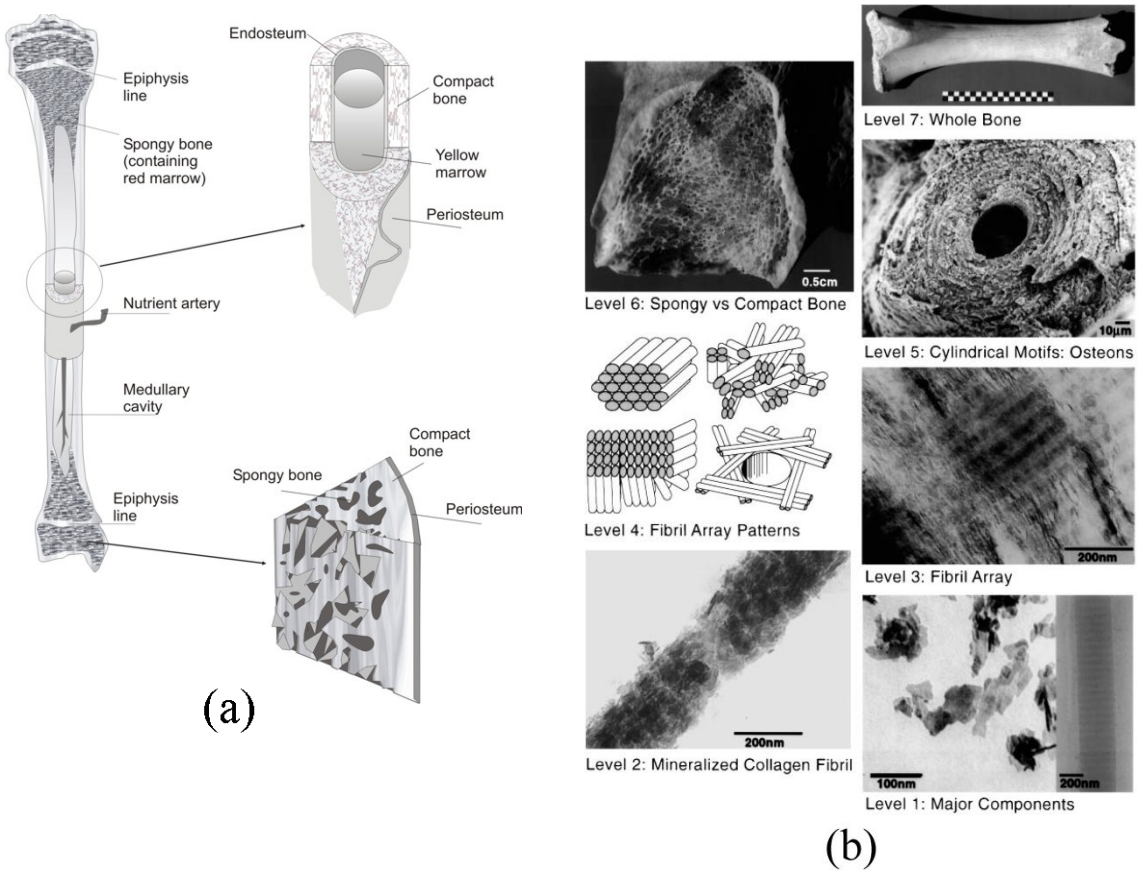

Figure 2.1 (a) The structure of the skeletal long bone comprising outer cortical (compact) bone, and inner trabecular (spongy) bone [38]. (b) The seven levels of hierarchical structure of bone [36].

The fifth level is composed of channels (e.g. Haversian canal) which are conduits for nerves and blood capillaries [34]. These cylindrical structures are called osteons. Cortical and cancellous structures are considered as the sixth level of hierarchy [36], and the seventh level of the osseous tissue organization is the whole bone.

2.1.2. Composition

Bone is an organic-inorganic biocomposite with a unique architecture [39]. Bone composition depends on the anatomical location, age and general health condition. Adult bone represents 50-70 wt.% mineral, 20-40 wt.% organic matrix, about 5-10 wt.% water, and about 1-5 wt.% lipids [40].

Bone mineral represents about 70% (by weight) of the bone tissue which is mainly composed of small CHA crystals [$Ca_{10}(PO_4)_6(OH)_2$]. It also contains many impurities such as carbonate and magnesium [30, 40].

Bone organic matrix is mostly composed of type I collagen fibres which is 90% of total protein content. Collagen is synthesised and secreted by the bone forming cells (osteoblasts), and then deposited in the form of preferentially oriented layers, or lamellae. The ground substance of bone matrix includes proteoglycans and glycoproteins which are involved in the calcification of the mineral [30, 32, 40]. Non-collagenous proteins are also present in the bone matrix with endo- and exo-genous origins. The endogenous proteins that are synthesised by osteoblasts are primarily growth factors and osteocalcin, and have been assumed to be important for bone growth, metabolism and turnover [30]. The exogenous proteins such as plasma-derived albumin and alpha2-HS-glycoprotein are involved in the mineralization of the matrix [31].

2.1.3. Mechanical properties

The mechanical properties of bone vary based on the type of the bone, age, gender, and anatomical site of the body. For example, it has been reported that the ultimate compressive strength for trabecular bone from human mandibles ranges from 0.2 to 10.4 MPa [41]. The strength values for vertebra, tibia and femur range from 0.8 to 5.8 MPa, with modulus values in the range of 1 to 3.2 GPa [42]. The mean values of jaw

bone modulus of elasticity in bending vary from 3.9 to 5.5 GPa, and failure strain from 3.0 to 4.1% [43].

The need to understand the role of trabecular bone in age-related bone fracture and the design of bone-implant systems have been the motivation for research on the trabecular bone biomechanics for over 30 years [44]. Trabecular bone heterogeneity is a critical issue which distinguishes it from many other biological tissues. For instance, the compressive modulus can vary 100-fold from one location to another within a single proximal tibia [45], and the strength can vary 5-fold within the proximal femur [46]. Modulus and strength can vary by more than an order of magnitude across different sites and species. A substantial loss of mechanical properties should also be considered with ageing in humans. For example, there are almost 7 and 11% reductions per decade in ultimate strength for the human proximal femur and spine, respectively, from the ages of 20 to 100 [47]. Until after about the age of 30, and perhaps even later depending on site, strength does not decrease in any significant manner [48]. Therefore, due to the substantial heterogeneity of trabecular bone, factors such as age and site need to be designated when discussing the specifics of the mechanical properties which is a key concept and has a direct relevance to fields as tissue engineering (TE), where the aim is to replace damaged trabecular bone with a substitute having appropriate mechanical properties for that site [44].

Morgan *et al.* [49] investigated the dependence of the mechanical properties of human trabecular bone on anatomic site and apparent density. It was hypothesized that yield strain depended on anatomic site in both compression and tension. Compressive yield strains ranged from 0.70% strain for the trochanter to 0.85% for the femoral neck. Tensile yield strains ranged from 0.61% for both the femoral neck and trochanter to 0.70% for the vertebra. The yield strain was higher in compression than tension for each site. The modulus ranged from 0.344 and 0.349 GPa (for vertebra) to 3.230 and 2.700 GPa (for femoral neck) in compression and tension, respectively. The yield stress ranged from 2.02 and 1.72 MPa (for vertebra) to 17.45 and 10.93 MPa (for femoral neck) in compression and tension, respectively. Apparent density or porosity is also an important determinant of the mechanical properties of bone [50]. The apparent density of cortical bone is 5-fold greater than that of cancellous bone [49, 50]. The mechanical properties of

cortical bone are significantly higher than those for cancellous bone; as summarised in Table 2.1.

Table 2.1 Mechanical properties of cortical (compact) and cancellous (spongy) bone [21, 51].

Property	Cortical bone	Cancellous bone
Compressive strength (MPa)	100-230	2-12
Flexural, tensile strength (MPa)	50-150	10-20
Strain to Failure (%)	1-3	5-7
Fracture toughness ($MPam^{1/2}$)	2-12	-
Young's modulus (GPa)	7-30	0.05-0.5

2.2. Clinical needs for bone repair and regeneration

Bone loss due to injury or disease severely affects the quality of life at significant socio-economic cost. Furthermore, bone related illnesses have become more prevalent due to the ageing population worldwide. For example, in the USA alone, 10 million people have osteoporosis according to the National Osteoporosis Foundation. In addition, another 34 million are at increased risk of osteoporosis due to low bone mass [52], and 1.5 million fractures occur each year as a result of osteoporosis along with other bone diseases. Annual direct care expenditures of $12.2-$17.9 billion (in 2002) have been reported for osteoporosis-related fractures [53].

The gold standard of bone replacement is based on autologous grafting. Autologous bone graft is taken from another part of the patient's body which provides osteogenic cells and osteoinductive factors needed for bone healing and regeneration [54, 55]. However, the cases in which it can be used are restricted mainly due to limited amount of autograft that can be obtained as well as donor site morbidity [56-58]. Allografts could be alternatives, which are taken from another person's body. However, allografts have the potential of immune rejection and of pathogen transmission. In addition, infection may possibly occur in the recipient's body after transplantation [59, 60]. The most widely used alternative for transplantation involves replacing tissues and organs with biomaterials which can be mechanical devices or artificial prosthesis. However, they will not restore the biological function of the living structure. Furthermore, these devices may undergo failure due to wear which could also induce an

inflammatory response in the host tissue. Therefore, development of bone augmentation strategies has been an increasing demand.

TE emerged in the mid 1980s as a promising approach in order to overcome the problems associated with current surgical techniques used to treat severely damaged tissues [61], and bone repair is considered as one of its major applications [62]. The general concept of bone tissue engineering (BTE) includes the formation of a cell-scaffold construct with an appropriate environment for the cells to proliferate and differentiate in order to induce tissue regeneration [63-65]. Cell extraction is an important consideration; for example, cells extracted from an individual patient may have the advantage of no immune response after transplantation, but it also includes numerous disadvantages such as limited cell numbers can be harvested from the patient tissue, it is time consuming, and cells taken from elderly patients biopsies may not be suitable for transplantation [63]. Non-human cells can be used as an alternative to the above method. In this approach, xenotransplantation is used to obtain a high number of cells from genetically engineered animals. However, there is a possibility of infectious agents' transmission. In addition, there are ethical, moral and social concerns discouraging its use [55]. To overcome the above mentioned limitations, stem cells and/or progenitor cells can be used instead. Figure 2.2 summarises the TE cycle, which includes: 1) harvesting cells from specific body tissues; 2) *in vitro* cell expansion; 3) cell seeding within a three-dimensional (3D) scaffold prior to implantation of the construct for tissue repair. This scaffold functions as a biomechanical support during the regeneration period while degrades gradually [64, 65]. From a materials engineering point of view, the starting point is scaffold material selection and design.

2.3. Biomaterials in bone repair and regeneration

Bone repair strategies using metal and non-degradable implant materials (e.g. titanium) have existed for decades. Although these implants are able to replace the structural functions, they do not reflect the other important functions of the skeleton such as maintaining ion homeostasis, storing biological factors and cues within the matrix or remodelling to the external load bearing. Moreover, the lifespan of the repair is short and ultimately leads to failure due to implant loosening and a lack of integration with the

living tissue [32]. Therefore, TE seeks a repair strategy to meet all the biological functions by replacing metal implants with donor cells and degradable scaffolds which drastically reduce the need for revision operations. Table 2.2 represents some of the biomaterials that have been extensively used for this purpose with their degradation time.

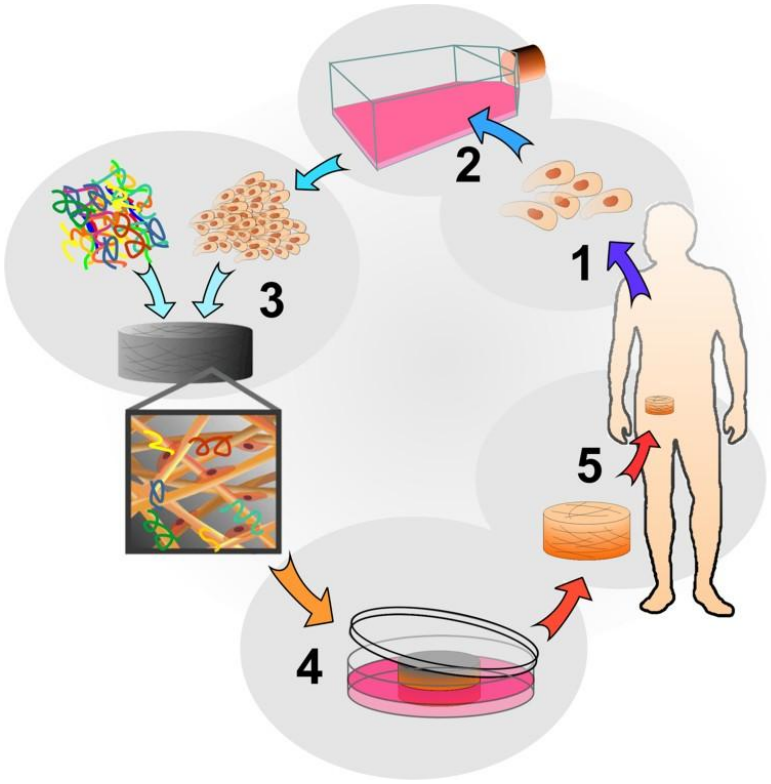

Figure 2.2 Tissue engineering cycle; 1: Cell extraction from a tissue biopsy. 2: Cell proliferation. 3: Cell seeding within a 3D porous scaffold. 4: *in vitro* Culture of cellular scaffold to generate a graft. 5: Implantation of the construct (cellular scaffold) into the damaged site to integrate with the native tissue [66, 67].

Table 2.2 Biomaterials used for bone repair and regeneration [32, 68, 69].

Name	Degradation time	3D structure
Naturally derived materials		
Collagen	< A few months	Fibrous, sponge hydrogel
Starch	A few months	Porous
Chitosan	< A few months	Sponge, fibres
Alginates	Weeks to a few months	Hydrogel, sponge
Hyaluronic acid (HA)	< A few months	Hydrogel
Polyhydroxyalkanoates (PHA)	Months	Porous, hydrogel
Synthetic materials		
Polyurethane (PU)	> 1 year	Porous
Poly(α-hydroxy acids) (e.g. Poly(lactic acid)(PLA))	1 months to a few years	Porous
Poly(ε-caprolactone) (PCL)	> 1 year	Sponge, fibres
Poly(propylene fumarates) (PPF)	Weeks to a few months	Hydrogel
Titanium	Non-degradable	Mesh
Calcium phosphate	Varied	Porous

2.3.1. Bioactive and biodegradable ceramics and glasses

Ceramics have been widely used in orthopaedic and dental applications [70]. Some ceramics such as sintered HA, silicate-based glasses (e.g. Bioglass®), and apatite-wollastonite glass-ceramic have the ability to form a bone-like apatite layer on their surface in the living body and bond to bone. These materials are generally termed bioactive and are clinically important for use as bone-repairing materials [20]. The word "bioactive" was coined by Larry Hench in 1971 and has several uses. The most general use is that the material stimulates an advantageous biological response from the body upon implantation. Calcium phosphate ceramics, bioactive glasses and glass-ceramics are considered as bioactive ceramics [71]. Bioactive glasses are the focus of this section since this research addresses these materials.

Glass is an inorganic fusion product as a result of cooling a melt through its glass transition to a rigid condition without crystallization. Generally, oxides that are used in glasses may be divided into three groups: network forming oxides such as SiO_2, B_2O_3 and P_2O_5; network modifying oxides such as Na_2O, K_2O, CaO and MgO; and intermediate oxides such as Al_2O_3, TiO_2, V_2O_3 and Bi_2O_3 [11]. Figure 2.3 shows schematic structures

of a glass forming units using SiO_2 as the network forming oxide. Two types of bonds exist in the glass or crystal network; bridging oxygen (BO) bonds between neighbouring Si atoms which hold the network together, and non-bridging oxygen (NBO) bonds between Si and modifier atoms which disrupt the network. Based on the glass network former, glasses for biomedical applications may be divided into silicate- and phosphate-based glasses

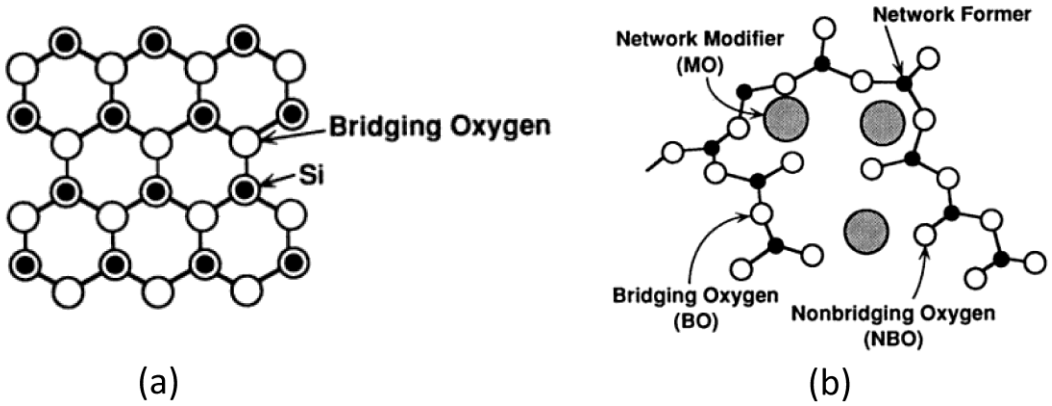

Figure 2.3 Schematic structure of (a) a silica network, all $Si(O_4)$ tetrahedral are bonded by –Si-O-Si (siloxane bonds). (b) A random glass network composed of network modifiers (MO), and network formers (SiO_2) [21].

2.3.1.1. Silicate-based glasses

Bioactive silicate-based glasses (SGs) were developed by Hench *et al.* (1971) for biomedical applications [72-75]. Bioglass® is a commercially available bioactive glass which is based on 45S5 composition that corresponds to $46.1SiO_2$-$26.9CaO$-$24.4Na_2O$-$2.5P_2O_5$ (mol.%). 45S5 refers to the SiO_2 content (45 wt.%) and the Ca/P molar ratio (5). Over the last three decades, SGs have generated significant interest for bone tissue regeneration applications [76].

When exposed to physiological fluids *in vivo*, these glasses form a surface CHA layer which has the ability to create a direct bond with bone through interactions with collagen synthesized by osteoblasts [76]. The biological behaviour of glasses depends on the relative proportion of BO to NBO bonds in the phases of the materials [21]. The bone bonding mechanism has been extensively researched by Hench and co-workers [21]. The following reaction mechanism has been proposed, which is divided into a number of stages:

Stage 1: Rapid exchange of Na^+ with H^+ or H_3O^+ from solution

$$Si\text{-}O\text{-}Na^+ + H^+ + OH^- \longrightarrow Si\text{-}OH^+ + Na^+ (solution) + OH^-$$

Stage 2: Loss of soluble silica in the form of $Si(OH)_4$ to the solution resulting from the breakage of Si-O-Si bonds and formation of Si-OH at the glass-solution interface

$$Si\text{-}O\text{-}Si + H_2O \longrightarrow Si\text{-}OH + OH\text{-}Si$$

Stage 3: Condensation and repolymerisation of a SiO_2 rich layer on the surface depleted in alkali and alkaline earth cations

Stage 4: Migration of Ca^{2+} and PO_4^{3-} groups to the surface through the SiO_2 rich layer forming $CaO\text{-}P_2O_5$ rich film on top of the SiO_2 rich layer followed by growth of the amorphous $CaO\text{-}P_2O_5$ rich film by incorporation of soluble calcium and phosphate from solution

Stage 5: Crystallization of the amorphous $CaO\text{-}P_2O_5$ film by incorporating OH^- and CO_3^{2-} or F^- ions from solution to form a mixed CHA layer

In summary, three general processes occur when a bioactive glass is immersed in an aqueous solution; leaching, dissolution, and precipitation. Leaching occurs due to the release of alkali or alkaline earth elements usually by cation exchange with H^+ or H_3O^+. Since these cations; e.g. Na^+, are not part of the glass network, and only modify the network by forming NBO bonds, ion exchange occurs easily. Network dissolution occurs by breaking of –Si-O-Si-O-Si- bonds through the action of hydroxyl (OH) ions. This occurs locally and releases silica into the solution. The hydrated silica (SiOH) formed on the glass results in silica-rich gel layer formation. In the precipitation reaction, phosphate and calcium ions released from the glass along with those from the solution form a calcia-phosphate-rich layer on the surface. The nucleation and formation of apatite layer, which is considered as the main responsible factor for the bioactivity of Bioglass® is due to the solubility of phosphate species [77].

Kokubo *et al.* [78] also showed that the formation of a bone like apatite on the surface of bioactive materials is induced by functional groups, such as Si-OH, Ti-OH, Zr-

OH, Ta-OH, Nb-OH, and -COOH. As an example, a schematic of the apatite formation process on the surface of amorphous sodium titanate is shown in Figure 2.4. It was found that the surface was highly negatively charged immediately after it was soaked in simulated body fluid (SBF). The ionic concentration of SBF solution (in mM) is Na^+: 142, K^+: 5, Mg^{2+}: 1.5, Ca^{2+}: 2.5, Cl^-: 147.8, HCO_3^-: 4.2, HPO_4^{2-}: 1, SO_4^{2-}: 0.5, pH: 7.4; nearly equal to that of human blood plasma. The Ti-OH groups formed on the surface of sodium titanate after soaking in SBF are negatively charged and can selectively combine with the positively charged Ca^{2+} in the fluid to form calcium titanate, and the surface gradually gains an overall positive charge. Consequently, the positively charged surface combines with negatively charged phosphate ions to form calcium phosphate.

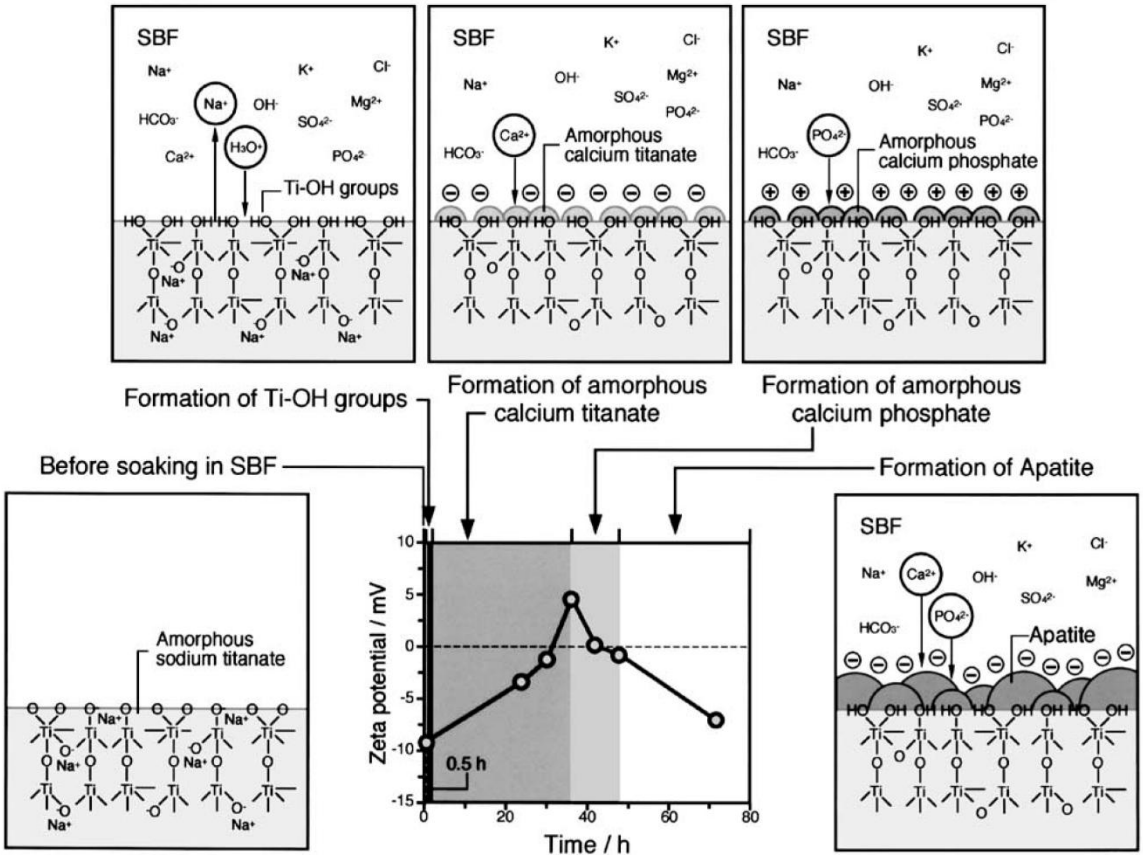

Figure 2.4 Schematic illustration of the relationship between the changes in the surface structure and the potential of amorphous sodium titanate in the apatite formation process on its surface in SBF [78].

SGs have been successful in orthopaedic, dental, and many other clinical applications. For example, the traditional 45S5 Bioglass® is US Food and Drug Administration (FDA) approved as bone filler in the treatment of periodontal diseases, and in middle ear surgery [79]. A wide range of other compositions have been developed by incorporating additional elements such as magnesium, boron, silver, potassium, zinc, iron, strontium or fluorine [80-84]. Other clinical applications have been proposed for bioactive glasses; e.g. in endodontology [85], periodontology [86] and as coating on metallic orthopaedic implants [87]. They have also been used in the development of TE scaffolds and regenerative medicine [3, 88-90]. In addition, extensive work has been carried out on the potential of bioactive glasses in antibacterial properties [91] and stimulation of angiogenesis [92] making them a potential candidate for wound healing applications [93].

In BTE, the regenerating periods which can be extended over weeks, should ideally coincide with a material with controlled degradation rates [94]. However, bioactive SGs do not reflect the required dissolution properties as they are not fully degradable [10]. In addition, while incorporation of certain metal oxides (e.g. Ga_2O_3, Ag_2O and CuO) is beneficial in antibacterial and angiogenesis properties through the release of metal ions [95-97], the range of glass formulations is limited in SGs because of the nature of the silicate network. More rapid solubility is also required in wound healing applications [93].

2.3.1.2. Phosphate-based glasses

The limitations associated with SGs have led to continued research for new materials for bone defect repair. Soluble phosphate-based glasses (PGs) are an example of one of these materials, which provide a diverse range of solubility that can be predicted and controlled by altering the glass composition [13, 14, 98]. In recent decades numerous PG formulations of binary, ternary and quaternary compositions have been developed for biomaterials and TE applications [13, 14, 19, 29, 98-101].

A. Structure and chemistry of phosphate-based glasses

The 3D network structure of SGs is a SiO_4 tetrahedron due to the strong affinity of silicon towards oxygen [12]. Since phosphorous has an affinity towards oxygen, phosphates also have a tetrahedral unit; though, the PO_4 unit is quite different from that of SiO_4 (Figure 2.5). Phosphorous has a charge of 5^+ while silicon has a charge of 4^+ and, in the case of P_2O_5, a terminal double bond oxygen forms since the oxygen atoms that are not shared between phosphate tetrahedral share their two unpaired electrons with the P^{5+}. The terminal oxygen limits the connectivity of PGs and decreases their interatomic forces and rigidity. In addition, PGs contain fewer cross-links while having a higher number of terminal oxygen atoms when they are mixed with metal oxides resulting in more flexibility of PO_4^{3-} tetrahedral [102]. Therefore, the range of glass formations are wider in binary PG compared to the silicate glass system [12].

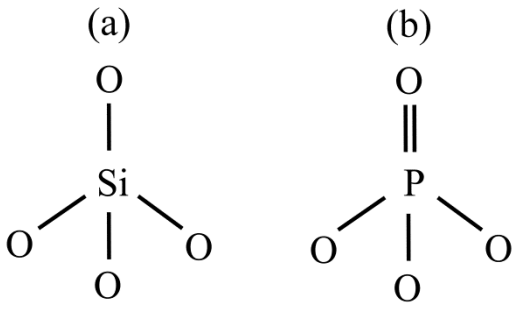

Figure 2.5 Tetrahedral unit of (a) silicate and (b) phosphate (Adapted from [12]).

Phosphate tetrahedra can be classified by the number of oxygen atoms that are shared with other phosphate tetrahedra, which are referred to as BO atoms. This classification leads to phosphate tetrahedra labelled with Q^i where i is the number of BOs and ranges between 0 and 3. Figure 2.6 shows the various Q species. While the 3D vitreous P_2O_5 has Q^3 tetrahedra, the addition of modifying oxides results in depolymerisation of the network through the cleavage of P-O-P bonds. The negatively charged NBO will coordinate with the modifying cations to optimize the coordination number of metal ions [102-105].

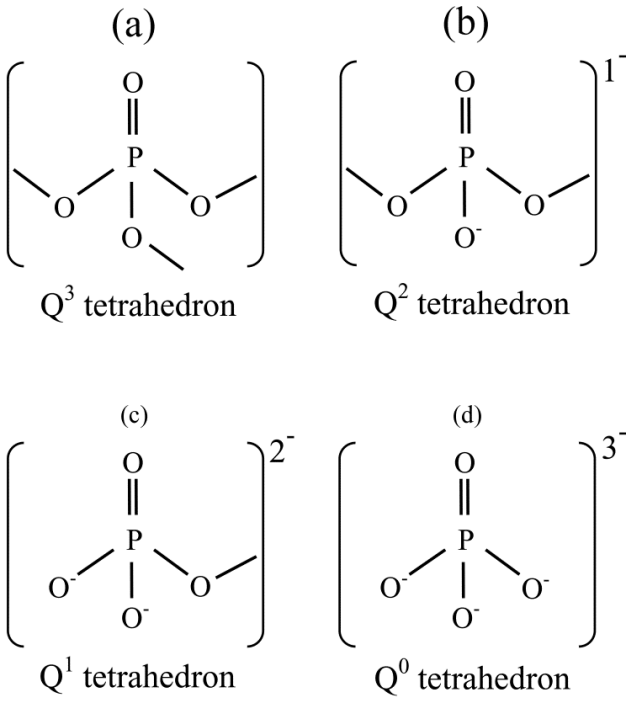

Figure 2.6 Representation of PO_4 tetrahedra (Adapted from [106]).

Kirkpatrik and Brow proposed the depolymerisation model predicting that the dominant Q^i varies based on $Q^3 \rightarrow Q^2 \rightarrow Q^1 \rightarrow Q^0$ as the amount of modifying oxides (M_2O) increases as follows [106]:

$$2Q^3 + M_2O \rightarrow 2Q^2$$
$$2Q^2 + M_2O \rightarrow 2Q^1$$
$$2Q^1 + M_2O \rightarrow 2Q^0$$

Therefore, the amount of metal oxides (x) in the glass and consequently the oxygen/phosphorus ratio sets the number of linkage of each tetrahedron via BO to other tetrahedra. Q^2 and Q^3 units are dominant in the glass network which is called ultra phosphate, where $0 \leq x \leq 0.5$. The glass network will be dominated by Q^2 units forming indefinitely long chains and/or rings in metaphosphate region, where x = 0.5 or O/P = 3 [12, 107]. It has been shown that the properties of metaphosphate glasses are more dependent on the P-O-M bonding between chains than the nature of the P-O-P bonding. There is an increase in the rigidity of the metaphosphate network and an associated

increase in glass transition temperature (T_g) as the field strength of the modifying cation increases [105]. The glass network will be based on Q^2 units terminated by Q^1 units in the polyphosphate region (x>0.5, O/P>3). At x = 0.67, the structure is based on phosphate dimer, i.e. two Q^1 tetrahedra units linked by one BO, termed a pyrophosphate unit. At x = 0.75, the network consists of isolated orthophosphate Q^0 units [107]. Therefore, in a binary system, the ratio of P_2O_5 to M_2O can be classified into four different groups [11]:

$$P_2O_5 + 3\ M_2O \rightarrow \text{Orthophosphates}$$
$$P_2O_5 + 1 - 2\ M_2O \rightarrow \text{Pyrophosphates}$$
$$P_2O_5 + 1\ M_2O \rightarrow \text{Metaphosphates}$$
$$P_2O_5 + <1\ M_2O \rightarrow \text{Ultraphosphates}$$

B. Melt-derived bulk phosphate-based glasses

Most PGs are fabricated using melt-quenching methods. In this procedure, oxide precursors are mixed and melted in a furnace at temperatures above 1000 ^oC depending on the final glass composition. The glass can be formed by casting different shapes; i.e. rods and plates. The melt is normally cooled quickly through the T_g, and often followed by cooling very slowly to room temperature in an annealing step to remove residual stress [12].

PGs have been used in a wide range of technological applications; e.g. solid-state batteries, sensors, laser devices, and air tight seals for metals with high coefficient of thermal expansion [108]. However, all the PG formulations that will be discussed in this dissertation were specifically designed for potential biomedical applications. Table 2.3 summarizes main PG compositions present in the literature developed for biomedical applications.

C. Ternary phosphate-based glasses

In the binary sodium phosphate glasses (Na_2PO_4H-$NaPO_4H_2$), which was developed by Gough *et al*. [101, 109], the liable surface prevented cell attachment to these highly soluble glasses due to lack of physical anchorage. A significant portion of studies on PGs focused on ternary P_2O_5-CaO-Na_2O system [98, 110].

Table 2.3 PG compositions (in mol.%) present in the literature developed for biomedical applications.

P_2O_5	CaO	Na_2O	K_2O	MgO	ZnO	Fe_2O_3	SiO_2	TiO_2	SrO	Ga_2O_3	Ag_2O	CuO	ZrO_2	Intended Application	Ref.
50	50													Bone	[111]
45	x=8-40	55-x												Bone	[110]
45	30,35,40	25, 20,15												Hard/soft tissue	[112]
45	12-36	19-43												Bone	[98]
45,50,55	30,35,40	5-25												Bone	[100] [19]
50	50-x	x=2-10												Bone	[23]
50	30-48	2-20												Hard/soft tissue	[113]
45	20,24, 28,32	35-x	x=0-25											Bone	[114]
45	32-x	23		x=0-22										Hard/soft tissue	[115]
50	40-x	10			x=0-20									Bone	[116] [117]
50	30	20-x				x=0-5								Skeletal muscle	[118]
50	30,35,40	20-x				x=1-5								Muscle	[119]
50	30	15-x				5	x=0-5							Hard/soft tissue	[13]
50	30	20-x						x=0-15						Bone	[28] [29] [120]
50	40	10-x						x=0-5						Bone	[121]
50	30	20-x							x=0-5					Bone	[122]
50	30-x	15						5	x=0-5					Sr ion delivery	[123]
45	16,15,14	39-x								x=0-5				Antimicrobial	[124] [125]
50	30	20-x									x=0-20			Antimicrobial	[126] [127] [128]
45	18,20,22	22-35										0-15		Antimicrobial	[129]
50	30	20-x										x=0-10		Antimicrobial	[130]
40	50	1.5		1.5				6					1	Bone	[131]
50	30	9	5-x		3		3	x=0-5						Hard/soft tissue	[132, 133]

A ternary glass system based on $45P_2O_5$-xCaO-(55-x)Na_2O where x was between 8 and 40 mol.% was developed by Franks *et al.* [98]. An inverse relationship between CaO content and the degradation rate was observed which was found to be linear over time for glasses containing up to 20 mol.% CaO. It was suggested that Ca^{2+} and its interaction with the glass network was a dominant factor in the solubility rate of these formulations. In high CaO containing glasses, an ion exchange process accompanied by a gradual breakdown of the glass network were two suggested responsible processes for degradation. The potential application of this glass system for bone regeneration was studied by Salih *et al.* [110]. Low soluble glasses were found to enhance bone cell growth and antigen expression. In contrast, highly soluble glasses considerably reduced cell proliferation, and down-regulated antigen expression. The authors suggested that greater amounts of Ca^{2+} are released with low dissolution rate glass which has an essential role in cells activation mechanisms, thus affecting their growth. However, a sharp change in pH associated with high release rates of Na^+ and PO_4^{3-} may have an adverse effect on cells in highly soluble glasses. Therefore, another ternary system by complete replacement of Na_2O with K_2O ($45P_2O_5$-xCaO-(55-x)K_2O, where x was between 16 and 32 mol.%) was also developed due to the higher degradation and unfavourable cellular response associate with high sodium content [98]. In fact, this system showed a higher dissolution rate compared to analogous P_2O_5-CaO-Na_2O system; therefore, no biocompatibility study was performed on this system. Ahmed *et al*. [100] developed and investigated ternary glass systems based on (45, 50 and 55)P_2O_5-(30, 35 and 40)CaO-Na_2O. There was a linear increase in T_g and crystallisation temperature (T_c) with increasing CaO content. Nuclear magnetic resonance (^{31}P NMR) revealed that Q^1 and Q^2 species are present at 45 mol.% P_2O_5; whilst only Q^2 was detected for 50 and 55 mol.% P_2O_5. Bitar *et al*. [113] investigated the $45P_2O_5$-xCaO-(55-x)Na_2O (x = 30-48) glass system. There was little or no cell adhesion and survival with less than 40 mol.% CaO in the glass composition which was attributed to the high solubility of the surface layer of these glasses. However, it was concluded that ternary glasses with high CaO content (46 and 48 mol.%) support cell attachment and viability, and maintain cellular function as indicated by phenotype gene expression up to 7 days. The effect of ternary PGs ($50P_2O_5$-(50-x)CaO-xNa_2O, where x was either 2, 4, 6, 8 or 10) on the behaviour of osteoblast and osteoblast-like

cells was investigated by Skelton *et al.* [23]. It was found that exposure to PGs resulted in inhibition of cell adhesion and proliferation and increased cell death. However, a greater number of cells were found on the composition that contained the highest Ca^{2+} and the lowest Na^{+}, and this composition was capable of supporting osteogenic proliferation and early differentiation. Other studies has also demonstrated that the least or no detrimental effect on cell numbers or morphology were found with the high Ca^{2+} and low Na^{+} glasses (the least soluble) [110, 113].

Based on these studies, glass degradation, loss of PG surface integrity due to dissolution, associated ion release and pH change of the environment are factors that affect the biocompatibility. Therefore, a more biologically compatible substrate with the potential to support osteogenic grafting could be produced by chemical modifying the glass [23]. For this purpose, the addition of metal oxides that increase the chemical durability of the PG would have a positive influence on biocompatibility. Therefore, quaternary systems were developed as a result of such additions [12].

D. Quaternary phosphate-based glasses

In developing quaternary systems, Franks *et al.* [115] synthesized $45P_2O_5$-(32-x)CaO-$23Na_2O$-xMgO, where x was between 0 and 22 mol.%, by the partial substitution of Ca^{2+} with Mg^{2+}, which has the same valance but a smaller ionic radius. The degradation rate changed from exponential to linear with decreasing CaO content. In addition, the degradation rate decreased by substituting CaO with MgO. The glass compositions with little or no MgO showed a slight decrease in the proliferation of human osteoblast-like cell line (MG63) after two days. However, all glass formulations showed equal or greater cell proliferation than the control after five days.

Knowles *et al.* [114] investigated the $45P_2O_5$-(20, 24, 28 and 32)CaO-(35-x)Na_2O-xK_2O, x = 0-25 mol.%, in order to study the effect of replacing Na^{+} with larger K^{+} ions. The degradation of this system was influenced by both CaO and K_2O content. At 20 mol.% CaO, the addition of K_2O initially reduced the degradation which then increased with further addition of K_2O. At high CaO content (32 mol.%), an anomaly was observed in degradation, and a weight gain was observed before weight loss. It was found that K^{+} ions have a positive effect on cell proliferation only at high content (20 mol.%),

regardless of the associated increase in degradation.

Zinc was added to PGs by Salih *et al.* [116] with the aim of promoting osteoblastic cell adhesion. The cells were found to attach to the glass surface, but maintained rounded morphology with lack of spreading on the glass surface. In addition, although cell proliferation increased with increasing ZnO content, it was consistently lower than the positive control.

In order to provide more flexibility in the degradation rate, Ahmed *et al.* [100] incorporated iron oxide into PG by the partial substitution of Na_2O leading to evolution of $50P_2O_5$-(30, 40 and 45)CaO-Na_2O-xFe_2O_3 (x was between 1 and 5 mol.%). Fe_2O_3 addition up to 5 mol.% resulted in a decrease in degradation rate by one order of magnitude and an increase in T_g. Abou Neel *et al.* [118] also investigated the incorporation of Fe_2O_3 into PGs, and showed that the overall surface energy of the glass decreased with increasing Fe_2O_3 leading to a significant decrease in the degradation rate which can be due to the formation of more hydration resistant P-O-Fe bonds.

Based on the soluble nature of these glasses in aqueous environments, they may be particularly interesting for controlled release of certain antimicrobial ions. Therefore, a range of PGs (P_2O_5-CaO-Na_2O) doped with Ga_2O_3, AgO and CuO have also been developed for potential antimicrobial properties. For example, Vallapil *et al.* [124, 125] has shown that Ga_2O_3-doped PGs hold promise as antimicrobial agents and could provide some advantages over conventional therapeutic agents. PGs doped with 0-15 mol.% silver have been investigated by Ahmed *et al.* [126]. It was found that incorporating 3 mol.% Ag was adequate to demonstrate a potent antimicrobial effect while still being cytocompatible in terms of silver release. P_2O_5-CaO-Na_2O-CuO system has also been developed and investigated by Mulligan *et al.* [129] and Abou Neel *et al.* [130] for potential antimicrobial properties.

Glasses and glass-ceramics containing titanium dioxide (TiO_2) are preferred for specific applications which require special properties such as bioactivity [134]. Abou Neel *et al.* [28, 29, 120, 121] incorporated TiO_2 into PGs to investigate the hypothesis that the combination of Ti^{4+} and Ca^{2+} ions would improve their biological behaviour. It has been suggested that TiO_2 could decrease the degradation rate probably due to the formation of TiO_5 or TiO_4 structural unit and the strong Ti-O-P bonds. Reduced

degradation rate of PGs by incorporating TiO_2 into the glass composition has also been confirmed by Navarro *et al.* [135] in the P_2O_5-CaO-Na_2O-TiO_2 system. $50P_2O_5$-(20-15)Na_2O-30CaO-(0-5 mol.%)TiO_2 formulations have been studied in terms of bioactivity in SBF and gene expression with an osteoblast cell line (MG63) [28]. It was found that the proliferation and gene expression was enhanced on the TiO_2 containing PG surfaces particularly for those with 3 and 5 mol.% TiO_2. This enhancement was suggested to be associated with the low degradation rate of these two compositions which maintained appropriate pH levels that are favoured by osteoblasts or may be attributable to the release of Ti ions. In addition, PG particles doped with 5 mol.% TiO_2 were implanted in rat calvarium, and bone formation was observed after 5 weeks of implantation. However, there was no evidence of apatite layer formation after 14 days incubation in SBF despite the favourable cell response and gene up-regulation. Elsewhere, increasing TiO_2 content was shown to have a profound effect on the maturation of primary osteoblasts [136]. It has been reported that the maximum amount of TiO_2 that can be incorporated into the ternary formulations while maintaining their amorphous nature was 15 mol.%, which was associated with increased density and Tg and reduced hydrophilicity and surface energy [120]. The incorporation of TiO_2 from 5 to 15 mol.% into PGs was effective in enhancing cell viability. Considerable control on the glass degradation rate by TiO_2 incorporation, the associated release of beneficial ions such as different phosphate species, Ca^{2+} and Ti^{4+}, and higher hydrophilicity and surface reactivity compared to the positive control (Thermanox®) were considered as the factors which mediated this enhancement.

E. Dissolution mechanisms of phosphate-based glasses in aqueous environments

The aqueous dissolution mechanisms and the stability of resultant anionic species of phosphate- and silicate-based glasses are different. While silicate species can be repolymerised, phosphates remain in solution, they dissolve and form new structures without any resemblance to the original glass structure [137]. In order to determine the dissolution mechanisms of these glasses, the types of reactions that can occur between the glasses and water should be considered which involve [138]:

(1) Acid/base reactions: Three types of acid/base sites on polymeric phosphates have

been indicated based on studies on short chain polymers (Figure 2.7). Sites 1 and 2 in Figure 2.7 can be protonated in solution at appropriate pH values. The chain terminating groups (Sites 2 and 3) are weak diprotic acids. These acid/base reactions can aid glass dissolution by disrupting the ionic interactions between chains.

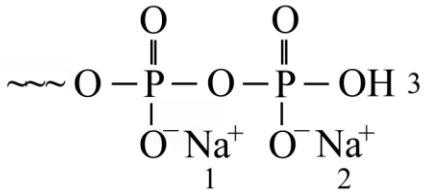

Figure 2.7 Acid/base sites on polymeric phosphates (Adapted from [138]).

(2) Hydration of the entire phosphate chains, and

(3) Hydrolysis reactions (Figure 2.8) which results in the cleavage of P-O-P bonds and could lead to the ultimate destruction of the phosphate network to produce orthophosphate

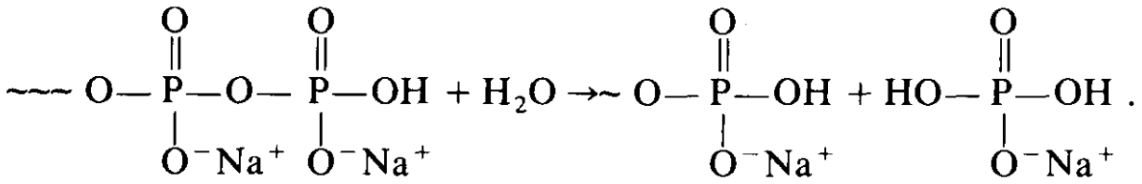

Figure 2.8 Hydrolysis reaction of the polymeric phosphates [138].

Given that pure P_2O_5 is chemically unstable due to the hydrolysis of the P-O-P bond, the addition of glass modifying metal oxides improves its stability by forming P-O-M bonds that are generally more stable [139]. P_2O_5 has a connective polymer structure (Figure 2.9a) with an infinite cross-link density. The addition of modifiers disrupts the bonds in the network resulting in lower cross-link density and an increase in the number of anionic NBOs which are present in the glass (Figure 2.9b). Therefore, it is evident that divalent cations can serve as ionic cross-links between the NBOs of two different chains increasing the chemical durability of the glass (Figure 2.9c).

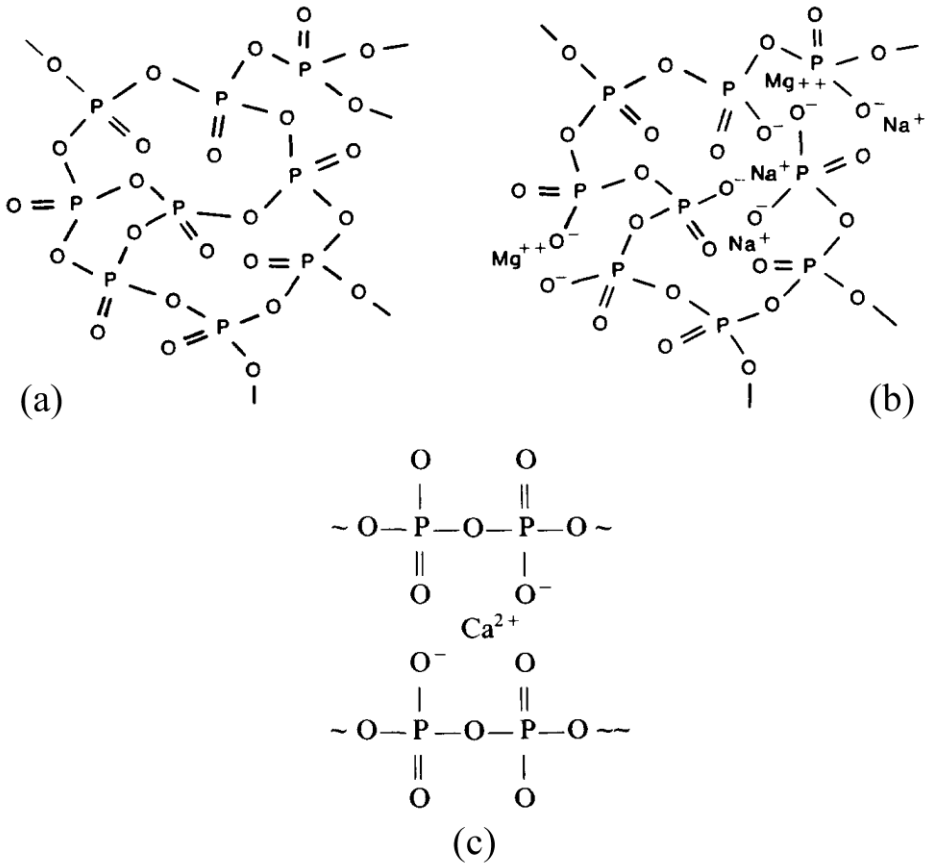

Figure 2.9 PG structure. (a) Connective polymer structure of P_2O_5. (b) Modifiers disrupt the bonds in the network which lowers cross-link density and increases the number of anionic non-bridging oxygen atoms. (c) Divalent cations, i.e. calcium, can serve as ionic cross-links between the non-bridging oxygens of two different chains which enhances the chemical durability of the glass [138].

F. Surface properties of phosphate-based glasses

Glasses are generally considered as high energy surfaces; hence, should easily be wetted by water. Although high energy materials tend to adsorb low-energy compounds, e.g. water vapour or organic contaminants, from the environment, this will in turn cause a rapid reduction in the surface energy which results in having low-energy surfaces [118, 140, 141]. Contact angle measurement is a technique to characterise the outmost layer (~ 0.5 nm) of the material. The term "surface energy", for solids, reflects the affinity of the surface to other materials. More energy is gained upon bringing a surface with higher surface energy into contact with other materials. In other words, the surface energy

describes the adhesive properties of the material. Surface free energy (SFE) can be calculated based on contact angle measurements quantifying wettability of the solid material. This procedure involves testing the material with well-characterized wetting liquids in terms of the polar and dispersive components of their surface tensions. According to Owens and Wendt, the relevant surface free energy equation is [142-145]:

$$\gamma_l(1 + \cos\theta)/\gamma_{ld}{}^{\frac{1}{2}} = (\gamma_{sp})^{\frac{1}{2}}\left[\frac{(\gamma_{lp})^{\frac{1}{2}}}{(\gamma_{ld})^{\frac{1}{2}}}\right] + (\gamma_{sd})^{1/2}$$

where θ is the contact angle, γ_l is the liquid surface tension, and γ_s is the solid surface tension, or free energy. The d and p subscripts are the dispersive and polar components, and the sum of these two component forces is merely the total free surface energy. If $\frac{(\gamma_{lp})^{\frac{1}{2}}}{(\gamma_{ld})^{\frac{1}{2}}}$ is plotted versus $\gamma_l(1 + \cos\theta)/\gamma_{ld}{}^{\frac{1}{2}}$, the equation is the y = mx + b. Therefore, the y intercept will be $(\gamma_{sd})^{1/2}$.

The surface properties of PGs have been investigated using four different test liquids: water and ethylene glycol having polar characteristics, as well as diiodomethane and α-bromonaphthalene with non-polar (or dispersive) property [118]. It is generally expected that low surface tension liquids will give rise to a smaller contact angle, on a given solid, when compared to higher surface tension liquids. Lowest contact angles were obtained by water on the surface of the PGs ($50P_2O_5$-30CaO-(20-x)Na_2O-xFe_2O_3, where x=0-5 mol.%) [118]; though, water has the highest surface tension of all tested liquids. This phenomenon indicates the polar characteristic of the PGs which can be attributed to the P-O-P bonds. The interactions between polar liquids and the glass surface decreased with increasing iron oxide content and greater contact angle values were obtained highlighting the network modifier character of iron oxide. Contact angles of the dispersive test liquids remained constant within the experimental errors. Iron-free glass showed the highest surface energy. By incorporating Fe_2O_3 into the glass composition, the polar component of the surface energy decreased. Consequently, the surface polarity (γ^p/γ^t) decreased.

Another study investigated the surface properties of P_2O_5-CaO-Na_2O-TiO_2 by static contact angle measurement. The angles were directly measured after a droplet was placed on the glass surface using water and diiodomethane as the test liquids [120]. The

contact angles of ultrapure water showed statistically significant higher values compared to TiO_2-free glass suggesting that the addition of TiO_2 to the ternary composition resulted in less hydrophilic glasses. However, since the contact angle of the studied compositions was less than 90^o [146], they are still considered as having hydrophilic surfaces. It is worth considering that these glasses were relatively hydrophilic and had a higher surface energy compared to Thermanox® [120] and Bioglass® [147]. It is well-known that increased surface hydrophilicity or wettability has been associated with enhanced protein adsorption which can mediate anchorage-dependent cells, e.g. osteoblasts, fibroblasts and endothelial, adhesion on the surface of biomaterials [148]. The incorporation of TiO_2 as a modifying oxide considerably reduced the surface free energy compared to 0 mol.% TiO_2 glass.

Surface free energy measurements of Strontium-doped PGs have been showed that strontium (Sr^{2+}) had no effect on surface free energy [122].

G. Phosphate-based glass fibres

PGs of certain compositions (i.e. more than 45 mol.% P_2O_5) can be easily drawn into fibres because of their polymeric nature. The spinnability or fibre drawing ability is associated with the entanglement capacity of longer chains with other chains allowing for continuous filaments to be formed instead of droplets or clusters [149]. Phosphate-based glass fibres (PGFs) can be fabricated by drawing from a melt at high temperature onto a rotating drum [150, 151]. An appropriate viscosity is required for fibre drawing which is adjusted by the temperature [119]. Moreover, this temperature should be above the glass crystallisation temperature to prevent difficulty in fibre drawing [152], or reduction of the glass bioactivity [153]. The diameter of the fibres can be controlled by adjusting the drum speed. For example, smaller fibre diameter is achieved by higher drum speed [12]. It has been shown that the fibre diameter can influence cell orientation [154]. The cells will orient along the long axis of the fibre if the fibre diameter is comparable to the size of the cells. They incline to wrap around the smaller diameter fibres. However, cells can also grow perpendicular or parallel to the long axis of the fibres. In this case, the fibres can be used as a contact guide.

Iron containing PGFs ($50P_2O_5$-30CaO-(20-x)Na_2O-xFe_2O_3, x=1-5), fabricated and characterised by Ahmed *et al.* [119], showed a dramatic improvement in immortal muscle precursor cell line attachment for fibres with 4 and 5 mol.% Fe_2O_3 (Figure 2.10).

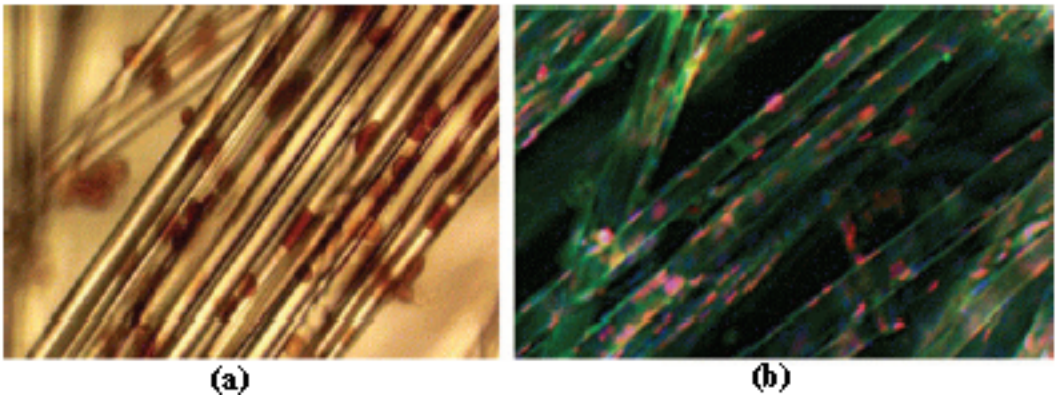

Figure 2.10 Muscle cells (a) attached to iron containing phosphate-based glass fibres, and (b) fused and form multinucleate myotubes (a cytoplasmic marker of skeletal muscle cells, Desmin, stained green. A nuclear marker of differentiation, Myogenin, stained pink, and the nuclei stained blue [119].

It has also been found that fibres containing 3 mol.% Fe_2O_3 are compatible with both primary human osteoblasts and fibroblasts which support a clear proliferation pattern with an even growth morphology [113]. Moreover, Fe_2O_3 containing PGFs have been shown to form capillary-like channels upon degradation in aqueous environments (Figure 2.11). The degradation process of these fibres includes a combination of surface hydration and internal hydrolysis. The hydration of the outer surface creates a protective barrier against degradation. However, over long periods, bulk degradation occurs by hydrolysis of the long Q^2 chains into shorter phosphate chains resulting in Q^1 and Q^0 to be the dominating units of the resultant channel structure [155]. PGFs with the composition of $50P_2O_5$-30CaO-(15-x)Na_2O-5Fe_2O_3-xSiO_2 have been studied by Patel *et al*. [13]. While the substitution of 1 and 3 mol.% Na_2O for SiO_2 resulted in a significant decrease in degradation rate up to 7 days and a mass loss of 20%, the substitution of 5 mol.% NaO_2 for SiO_2 led to rapid non-linear degradation of the glass fibres and resulted in 60% mass loss at 4 days.

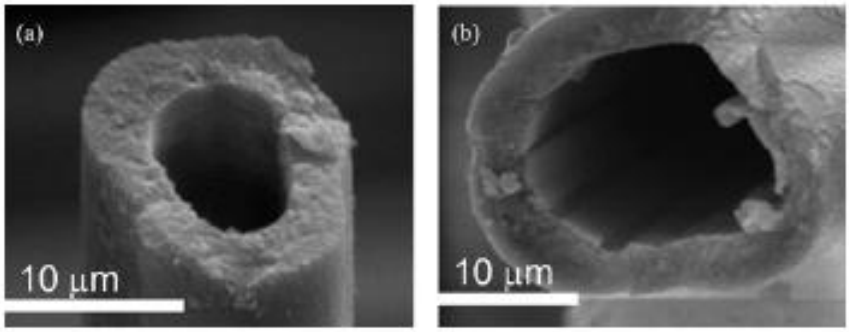

Figure 2.11 SEM micrographs illustrating the tubular structures formed from degradation of phosphate-based glass fibres after 18 months for (a) 3 and (b) 5 mol.% Fe_2O_3 in the glass composition [155].

2.3.2. Polymeric Biomaterials

While biocompatible polymers (e.g. polyethylene), metals (e.g. titanium), and ceramics (e.g. alumina) have been used in biomedical applications, biodegradable polymers have emerged as the principal scaffolding materials used for TE applications since metals and ceramics (except for magnesium alloys or some calcium phosphate based bioceramics) are not biodegradable [156-159]. These polymers can be divided into two main categories:

2.3.2.1. Naturally derived polymers

These polymers are proteins that mimic various extracellular matrices (ECMs) in living species such as collagens, fibrin and silk fibroin, as well as polysaccharides such as chitosan, hyaluranon, alginic acid, and glycosaminoglycans [159]. There are several advantages associated with naturally occurring biopolymers for potential applications in TE, as well as drug delivery and gene therapeutics [160, 161]. For example, natural polymers best simulate the native ECM due to their biocompatibility, abundance, and swelling capability in water. They mimic the hydrated state of tissues since they are principally composed of a polymeric network that can contain up to 99 % water content (also known as hydrogels) [162, 163]. However, limited mechanical properties, lack of control on degradation rate, lack of reproducibility, and the risk of immunogenicity or the potential harbouring microbes or viruses are certain limitations regarding the use of natural polymers [164-166].

2.3.2.2. Synthetic polymers

Synthetic polymers have been used in a broad diversity of biomedical applications. The most widely investigated biodegradable synthetic polymers include: poly(ortho esters) such as poly(glycolic acid) (PGA), PLA, and their copolymers (poly(lactic-co-glycolic acid) (PLGA)), PCL, polyanhydrides, polycarbonate, and polyfumarate [156, 159]. Biodegradable synthetic polymers provide many advantages over other materials as scaffolds for TE applications. For example, the ability to tailor the mechanical properties and degradation kinetics to suit a variety of applications are key advantages. In addition, they can be fabricated into different shapes with required pore morphologic features contributing to tissue in-growth. Moreover, polymers can be designed with chemical functional groups that induce tissue in-growth [167-169]. Since PCL and PLA have been used as the polymer matrix of the composites in this study, these polymers will be discussed in detail.

A. PCL: Polycaprolactone is an aliphatic polyester ($[\text{-O-}(CH_2)_5\text{-CO-}]_n$) which has been extensively studied as a potential biomaterial [170]. It is a semi-crystalline polymer with a low T_g of approximately -60 ^oC being always in a crystal reinforced rubber state at room temperature. This is a unique property among the more common aliphatic polyesters which contributes to the high permeability of PCL for many therapeutic drugs [171]. While PCL can be degraded by microorganisms [172], it has been shown that, under physiological conditions, PCL can also be degraded by hydrolysis [173]. In addition, it has been reported that low molecular weight fragments of PCL are taken up by macrophages and degraded intracellularly [174]. The degradation of PCL is considerably slower than PLA and PGA. Therefore, it is more suitable for longer-term implantable drug delivery systems such as Capronor^{TM} which serves as a one year implantable contraceptive device [170]. The tendency to form compatible blends with a wide variety of other polymers is another interesting property of PCL [175]. Furthermore, ε-caprolactone can be copolymerised with numerous monomers such as ethylene oxide, chloroprene and methyl methacrylate. In particular, copolymers of ε-caprolactone and lactic acid have been extensively investigated [24]. PCL is regarded as a non-toxic and

tissue compatible material and its products are US FDA approved for suture use, drug delivery devices and temporary orthopaedic plates for bone fracture repair [170].

B. PLA: Poly(lactic acid) ([-O-CH(CH_3)-CO-]$_n$) also belongs to the family of aliphatic polyesters commonly made from α-hydroxy acids and is biodegradable and compostable [176, 177]. PLA exists in two stereoisomeric forms since lactic acid is a chiral molecule. Two stereo regular polymers include D-PLA and L-PLA. A mixture of D- and L-lactic acid also exists as D,L-PLA (PDLLA) [25]. The polymers which are derived from optically active D and L monomers are semi-crystalline while the optically inactive D,L-PLA is amorphous. Due to the amorphous nature of D,L-PLA, it is usually considered for applications such as drug delivery systems as it is important to have a homogenous dispersion of the active species within a monophasic matrix. In contrast, L-PLA is preferred in applications where high mechanical strength and toughness are required, e.g. sutures and orthopaedic devices [25, 26]. The degradation of PLA occurs by simple hydrolysis of the ester bond and does not need the enzymes to catalyze this hydrolysis. The degradation rate depends on the shape and size of the article, the isomer ratio, time and temperature of the hydrolysis, low-molecular-weight impurities, and catalyst concentration [176]. PLA is of a relatively high strength and modulus polymer with a T_g and melt temperature (T_m) of approximately 55 and 175 ^oC, respectively [178]. At temperatures above 200 ^oC, PLA undergoes thermal degradation due to hydrolysis, oxidative main chain scission, lactide formation, and inter-/intra-molecular transesterification reactions [179].

2.3.3. Polymer-ceramic composites

Although bioactive ceramics provide the potential for TE applications, their brittleness and relatively low fracture strength impede their load-bearing applications. Therefore, incorporating these materials into biodegradable polymers has been of interest particularly for BTE [16-19]. Figure 2.12 shows the schematic diagram of the composite material approach using different combinations of biodegradable polymers and bioactive inorganic particles.

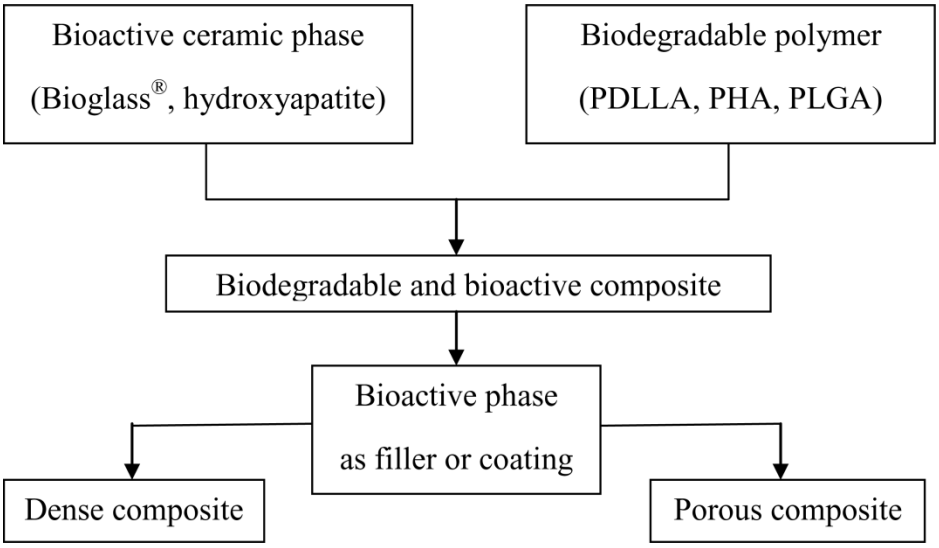

Figure 2.12 A schematic diagram showing the composite approach using biodegradable polymers and bioactive inorganic particles. PDLLA: poly(D,L-lactic acid), PHA: polyhydroxyalkanoate, PLGA: poly(lactic-co-glycolic acid) [180].

Biodegradable composites for TE must have controlled strength and modulus retention *in vivo* to provide the necessary support for cell attachment and proliferation as well as augment the tissue capacity to regenerate. Polymers alone generally lack strength and stiffness, as well as a bioactive function. On the other hand, polymers can be easily formed to fabricate complex shapes and structures. Therefore, there are several reasons for the combination of biodegradable polymers and bioactive ceramics and glasses for BTE applications [88, 181-183], which are highlighted below:

i) The combination of polymers and inorganic materials leads to composite materials with improved mechanical properties owing to the intrinsic stiffness and strength of the inorganic phase.

ii) Incorporation of a bioactive phase into a polymer matrix would induce the potential of bioactivity (calcium phosphate deposition on the surface), and improve the bone bonding ability.

iii) Incorporation of bioactive phases into the bioresorbable polymers can alter the degradation behaviour of the polymer. Increased water absorption due to the internal interfaces between the polymer and more hydrophilic bioactive phase

would provide a means of controlling the degradation kinetics of the scaffold [184, 185].

Fibres and particulates are two types of reinforcements that are normally used in biomedical composites [7]. The mechanical properties are influenced by the shape, size and distribution of the reinforcement in the matrix as well as the reinforcement-matrix interfacial bonding. While particulate composites are easy to manufacture, fibre reinforced composites have been shown to result in greater increase in mechanical properties [111, 186, 187]. Increased volume fraction and higher surface area to volume ratio of inclusions have also been shown to favour bioactivity [88]. Therefore, the incorporation of fibres is preferred for certain applications [184].

Calcium phosphate ceramics and glasses incorporated into biodegradable polymers have been extensively studied for BTE applications [186-188]. Since the composition, content and solubility of the filler component are parameters that can influence composite properties, their tailoring is essential for bone repair and regeneration. However, not all calcium phosphate materials provide controlled solubility properties with either bone regeneration rate or degradation of the matrix such as in the case of SGs or HA. Therefore, PGs may be a potential alternative inorganic phase for the purpose of producing composites of controllable degradation [11, 12]. In addition, their polymeric nature allows them to be easily drawn into fibres [19], which could result in a mechanical reinforcing effect when incorporated into a polymer matrix. Dense and porous PGs-reinforced polyester composites available in the literature for bone repair and regeneration applications are presented in Table 2.4. Their mechanical properties and the cell type used to investigate their cytocompatibility have also been reported.

Ahmed *et al*. [111] used a binary PGF formulation ($50P_2O_5$-50CaO) to reinforce PCL. Flexural strength and modulus of up to 30 MPa and 2.5 GPa respectively were reported which are comparable with human trabecular bone. Mass loss of 8% for low PGF content (18 wt.%) composites was observed which increased to 20% for a higher content (39 wt.%). It was suggested that, *in vivo*, cells from the surrounding tissue may migrate into the porous matrix resulting from the leaching of the fibres.

Table 2.4 Biodegradable PG-reinforced polyester composites available in the literature developed for bone repair and regeneration, and their properties.

Polymer matrix	PG formulation (mol.%)	Type of PG	Percentage of PG (wt.%)	Porosity (%)	Mechanical properties	Cell Type used to investigate the cytocompatibility	Ref.
PDLLA	$44.5P_2O_5$-44.5CaO-$6Na_2O$-$5TiO_2$	Particle	40	97	Compressive strength: 20 KPa Compressive modulus: 120 KPa	SAOS-2 osteoblast-like	[189]
PLA	$50P_2O_5$-46CaO-$4Na_2O$	Particle	5 / 10 / 20	> 75	Compressive modulus: 90 MPa	human primary osteoblasts	[190]
PLA	$50P_2O_5$-40CaO-$5Na_2O$-$5Fe_2O_3$	Fibre	26	Dense composite	Flexural strength: 90 MPa Flexural modulus: 5 GPa	human osteosarcoma cell line (MG63)	[191]
PLA	$50P_2O_5$-40CaO-$5Na_2O$-$5Fe_2O_3$	Fibre	37 / 56 / 83	Dense composite	Flexural strength: 50-130 MPa Flexural modulus: 7-11.5 GPa	-	[192]
PCL	$50P_2O_5$ -50CaO	Fibre	18 / 39	Dense composite	Flexural strength: 25-30 MPa Flexural modulus: 1 / 2.4 GPa	-	[111]
PCL	$45P_2O_5$-xCaO-(55-x)Na_2O, x=20-50	Particle	10	Dense composite	-	Osteoblast-like MG63	[184]
PCL	$40P_2O_5$-16CaO-$20Na_2O$–24MgO	Fibre	18 / 45	Dense composite	Flexural strength: 55 / 105 MPa Flexural modulus: 2 / 6 GPa	-	[193]
PLGA	$50P_2O_5$-30CaO-(19-x)Na_2O-xAg_2O, x=1-5	Particle	3 / 5 / 20	Porous macro-spheres (up to 2 mm in diameter, pore size: 30-70 μm)	-	-	[194]

PGFs with 5-22.5 wt.% Fe_2O_3 have also been used as reinforcing agents to develop biodegradable composites for orthopaedic applications [195]. Biocompatibility assessments of these glasses showed no inflammatory response up to five weeks. Degradable PGFs reinforced several different degradable polymers including poly(ε-caprolactone/L-lactide) and poly(ortho ester) have been shown to be non-toxic composites with no inflammatory response [196]. Figure 2.13 shows human osteosarcoma cell line (MG63) grown on PLA-PGF of composition $50P_2O_5$-40CaO-$5Na_2O$-$5Fe_2O_3$ (mol.%). *In vivo* studies of PGFs embedded in PCL also demonstrated that these materials are well tolerated with minimal inflammation [197].

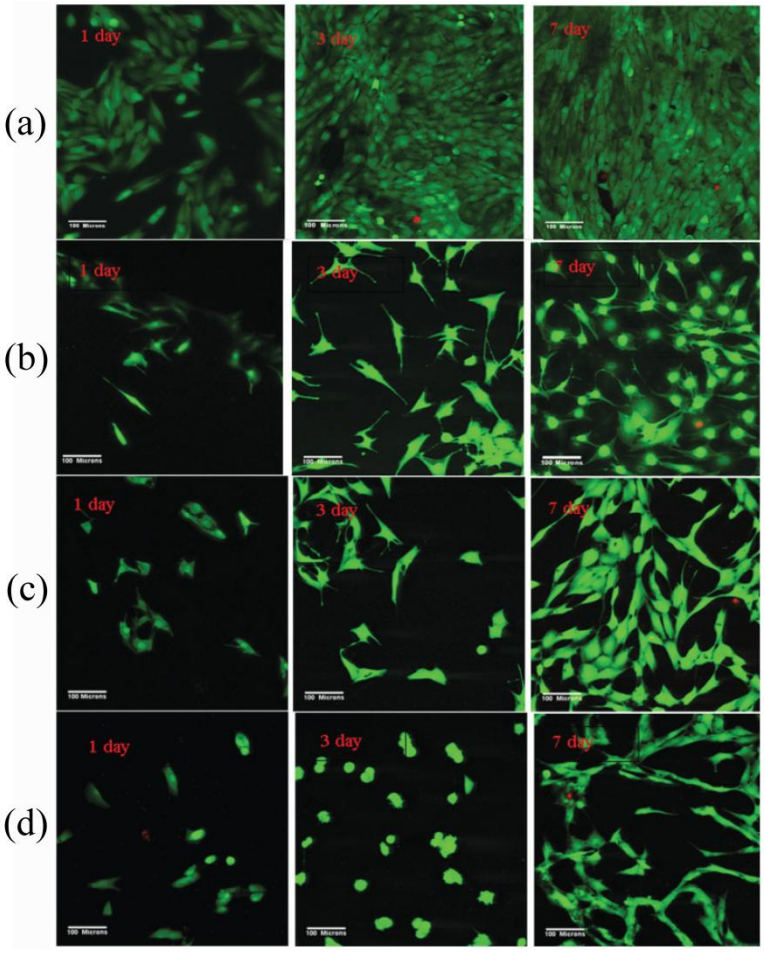

Figure 2.13 Cytocompatibility assessment of (a) Thermanox® (control), (b) PLA, (c) PLA-PGF (heat treated) composites, and (d) PLA-PGF (non-treated) over 1, 3, and 7 days using human osteosarcoma cell line (MG63) [191].

In situ formation of unidirectional aligned channels in 3D dense collagen has been attempted by incorporation of PGFs containing 3 mol.% Fe_2O_3 [198]. The channels were continuous in nature and were of similar diameter dimensions as the fibres (30-40 µm). Human oral fibroblasts maintained excellent viability after 24 hours when cultured in this construct. The cells showed packed spindle shaped appearance spreading over the glass fibres and the collagen matrix with no preference.

2.4. Porous structures for bone tissue engineering scaffolds

Scaffolds are highly porous structures (artificially or biologically derived) which serve as a 3D environment for the seeded cells to attach, proliferate, lay down the reconstituted ECM, and therefore facilitate the formation of functional tissues and organs [199, 200]. Hence, producing tailored *in vitro* cell culture scaffolds mimicking the complex and organized structure of native ECM is of importance [201]. Scaffolds can also be carriers of cells, growth factors, drugs, and other macromolecules [202, 203]. An example of a porous scaffold to promote cartilage and bone tissue formation is shown in Figure 2.14.

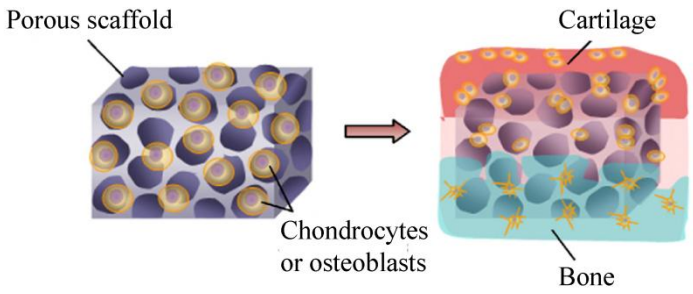

Figure 2.14 Schematic example of scaffold application to induce regeneration of bone and cartilage, by seeding cells within the scaffold [204].

2.4.1. Scaffold required properties

Since the primary function of the scaffold is tissue conduction, it should possess the following basic requirements for TE applications [55, 156, 157, 200]:

- Bioresorbability/Biodegradability: post implantation, scaffold materials must have the capacity to be degraded or metabolised in a controlled manner in order to match tissue growth,

- Biocompatibility: the scaffold material and its degradation by-products must not induce cellular toxicity or inflammation *in vivo*,
- High surface area to volume ratio with suitable topography and surface chemistry to promote cell adhesion, growth, and differentiation,
- Open/interconnected porosity to facilitate mass transfer and homogenous tissue regeneration. The minimum required pore size of approximately 100-150 μm has been reported for bone ingrowth,
- Appropriate mechanical properties to be able to stand the applied forces, and
- Be able to be processed in a reproducible manner.

2.4.2. Scaffold engineering

A critical challenge in TE is the biomaterial from which the scaffold is fabricated as these provide physical, mechanical, and chemical cues to direct various cell growth programs [158, 159, 205]. In addition, modulation of cell function and neotissue formation significantly depends on engineering design of a 3D scaffold [156, 206]. For example, the size, orientation, and surface chemistry of the pores in the engineered tissue considerably manipulate tissue ingrowth, and biomechanical signals transmission within the scaffold [65, 207]. Moreover, the regeneration process can be deteriorated due to lack of oxygen and nutrients as new blood vessel formation takes several days post implantation [208]. In BTE, besides designing issues, there is also a challenge regarding the fabrication of reproducible biodegradable 3D scaffolds that are also able to work for a certain period of time under load-bearing conditions [68].

2.4.3. Scaffold fabrication techniques

Numerous techniques have been used to produce BTE scaffolds [209], which include textile technologies, solvent casting, phase separation, gas foaming, freeze drying, electrospinning, UV and laser radiation, salt leaching, 3D pore architecture designs (CAD/CAM and rapid prototyping). The selection of the scaffolding technique can have a critical effect on the properties of the scaffold and its *in vivo* performance. Despite the progress made in the fabrication of 3D scaffolds, there are still some

problems that need to be overcome which include accurate and consistent technique, and minimal variations in the properties in different scaffold batches [55].

Solvent casting and particulate leaching is the most widely used and one of the simplest methods to prepare the scaffold which was first described by Mikos *et al.* in 1994 [210]. This technique involves the dissolution of the polymer in an organic solvent followed by mixing with ceramic granules and dispersing calibrated minerals, such as sodium chloride, sodium tartrate and sodium citrate, or organic (e.g. saccharose) particle in the polymer solution. The salt particles are leached out by selective dissolution to create a porous polymer matrix [55, 180]. Ease of manufacturing and the ability to incorporate drugs and chemicals into the scaffold are the main advantages of this technique. However, there are several limitations, i.e. only simple shapes can be formed [211]. Furthermore, the very low pore interconnectivity usually makes it unsuitable for TE applications. In addition, highly toxic solvents are used [68] and residual solvent may remain trapped which would reduce the activity of bioinductive molecules, i.e. if proteins had been incorporated [180]. Moreover, the mechanical properties of these scaffolds are lower than the ideal required mechanical properties even compared to trabecular bone [212].

Thermally induced phase separation (TIPS) approach is to rapidly lower the temperature of a homogenous solution of polymer and inorganic material to solidify the solvent and induce solid-liquid phase separation. Solidified solvent forces the polymer and ceramic mixture into the interstitial spaces. Using a freeze-dryer, the frozen mixture is lyophilised to remove the solvent and create the foam structure [6, 213]. Highly porous scaffolds with anisotropic tubular morphology and extensive pore interconnectivity can be produced with this fabrication technique [6, 183, 214]. Sensitivity of the technique regarding its processing parameters, use of toxic solvents, low mechanical stability and pore size in the range of 10 to 100 μm are main disadvantages [157, 211]. Nevertheless, polymer-bioactive glass composite microspheres have been fabricated using TIPS, and were investigated for potential tissue regeneration and drug delivery applications [194, 215]. In order to produce fully degradable microspheres, Blaker *et al.* [194] incorporated PGPs (3, 5, and 20 wt.%) into PLGA. TIPS technique was used to enable the rapid formation of monodisperse porous macro-

spheres. Macro-spheres (up to 2 mm in diameter) with isotropic pore morphology (interconnected spherical pores of 30-70 μm) were produced to be potentially suitable for localized drug delivery, tissue regeneration/augmentation, and TE applications.

Solid free form (SFF) fabrication refers to techniques including selective laser sintering, 3D printing, and fused deposition modeling (FDM) which are based on computer-aided manufacturer (CAD/CAM) methodologies [180, 213]. These methods have been developed to manufacture scaffolds for BTE with specific designed properties [51, 216-218] and has been used for polymer composites containing calcium phosphate as the bioactive phase. For example, PLLA-TCP composites has been fabricated by Xiong *et al.* [219] with up to 90% porosity by a layer-by-layer manufacturing method. PLA scaffolds with computationally designed pores (wide channels) in the range of 500-800 μm and solvent derived local pores of 50-100 μm were also produced by Taboas *et al.* [15]. Complex equipment requirement and increased fabrication time compared to other direct techniques are the shortcoming of this method [180]. There are also specific disadvantages associated with each SFF technique; e.g. use of organic solvents as binders, and lack of mechanical properties due to the combination of several stack up powdered layers in 3D printing [220]. FDM does not use organic solvents; however, the non-incorporation of growth factors and range of polymers that can be used due to the processing requirements and temperatures are the main disadvantages of this method [220].

2.4.4. Gas foaming using carbon dioxide

This technique was developed for producing highly porous foams without the use of organic solvents. Carbon dioxide (CO_2) can be used as a porogen to create 3D polymeric structures to be used as scaffolds. There are different approaches in using CO_2 such as supercritical fluids or high pressure to process polymers into 3D TE scaffolds [221].

2.4.4.1. Supercritical CO_2

CO_2 exists at supercritical condition above a critical temperature (T_c=304.1 K) and pressure (P_c=73.8 bar) (Figure 2.15). It has the properties of both a gas and a liquid in

this state. By changing the temperature and pressure in Figure 2.15a, the phase changes from solid to liquid and to gas. However, at the intersection of T_c and P_c, the liquid and gas phases cannot be distinguished, and the single fluid phase CO_2 is said to be supercritical carbon dioxide ($scCO_2$) [221] (Figure 2.15b(iii)). $ScCO_2$ is inexpensive, non-flammable, non-toxic, and its properties can be tuned through its density [222].

Supercritical CO_2 has been found to be soluble in some polymers [223]. Plasticization occurs when $scCO_2$ diffuses into the polymer matrix and separates the polymer chains resulting in lower resistance to chain rotation resulting in a reduction of the polymer T_g. By reducing the CO_2 pressure, the solubility of the gas in the polymer decreases [224] generating nuclei (or bubbles) which then grow to form the pores in the foam. The T_g begins to increase once the CO_2 vacates the polymer making it glassy and the pores cannot grow further. The porous structure becomes fixed by this event [223-225]. Controlling the nucleation and the diffusion of the gas are very important in creating suitable scaffolds for TE. The nucleation is rapid leading to a large number of nucleation sites if the venting rate is high and the structure will have a uniform and homogenous pore size distribution.

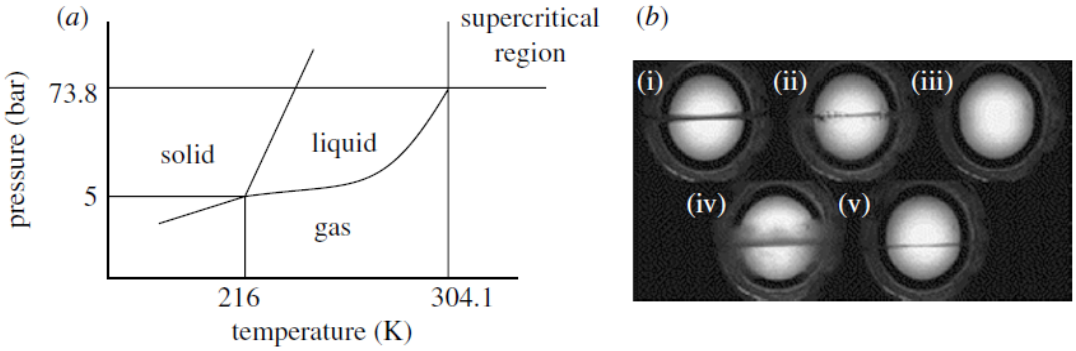

Figure 2.15 (a) Phase diagram of carbon dioxide indicating critical points and supercritical region [221, 226]. (b) The creation of the single supercritical fluid phase (iii) by increasing the temperature and pressure of liquid CO_2 above its critical points (i and ii). The process is reversed by subsequent reducing the temperature and pressure (iv and v) [227].

In contrast, the pores which nucleate initially will be significantly larger than others because of greater diffusion of gas from the surrounding matrix. Therefore, a wide dispersion in pore size would be present in the resultant structure [228]. The effect of

changing the molecular weight of the polymer, pressure and venting rate on pore structure has been demonstrated using different gases (CO_2, N_2 and He) [224, 225, 229-232]. Sheridan *et al*. [231] compared CO_2, N_2 and He gas foaming by fabricating 3D porous matrices from bioabsorbable materials (e.g. PLGA). It was demonstrated that the choice of gas and polymer has a large influence on the final scaffold structure. Highly porous matrices were produced by using CO_2. However, N_2 and He led to no measurable pore formation. While the mechanism is not known, greater degree of foaming with CO_2 compared to N_2 and He may be due to a specific interaction between CO_2 and carbonyl groups of PLGA. It has been demonstrated that specific interactions with CO_2 occur in polymers with electron donating functional groups; as in the case of the carbonyl groups, most probably because of Lewis acid-base nature. In this case, the electron lone pairs of the carbonyl oxygen interact with the carbon atom of the CO_2 molecule [233]. The effect of gas type on porosity and a micrograph of typical scaffold by foaming PLGA are presented in Figure 2.16.

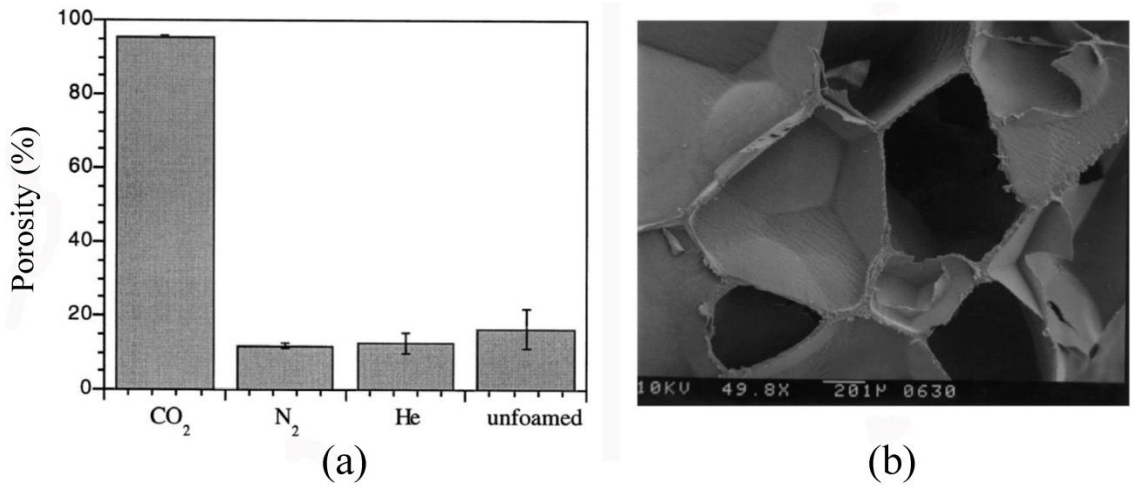

Figure 2.16 (a) The influence of gas type on porosity. (b) Photomicrograph of typical PLGA scaffold foamed for 24 h in 850 psi CO_2. PLGA (85:15) discs were equilibrated for 1 h in 850 psi gas prior to pressure release (340 psi/min) [231].

Amorphous polymers have the ability to foam more easily than the crystalline polymers due to increased gas dissolution in less organised morphologies [27]. In addition, scaffolds made of a high molecular weight polymer have less porosity compared to the same polymer with lower molecular weight. Longer polymer chains in

high molecular weight polymers are likely to be entangled to a greater extent which provides a stronger resistance to expansion during phase separation step compared to shorter polymer chains. Tai *et al.* [234] demonstrated that the pore size and structure of PDLLA and PLGA scaffolds produced by $scCO_2$ can be modified by altering the processing conditions. A longer soaking time and higher pressure resulted in a higher nucleation density due to more CO_2 molecules diffusion into the polymer matrix leading to a structure with smaller pores. Foams with larger pores were produced when higher temperatures were applied because increased diffusion rates facilitated pore growth. Moreover, a reduction in the depressurisation rate led to larger pores since it allowed for longer period of pore growth. Increasing amount of glycolic acid content in the PLGA copolymer decreased the pore size of the scaffold. Mathieu *et al.* [235, 236] investigated supercritical fluid foaming of PLA and PLA-ceramic (HA and β-TCP). Neat PLA foams with 78 to 92% porosities and interconnected pores (200-400 μm) were prepared. The addition of fillers reduced the foam porosity. In addition, a higher density of smaller and more closed pores were achieved as a consequence of increased matrix viscosity due to the presence of fillers. The compressive strength and modulus were increased up to 6 MPa and 250 MPa, respectively, with fillers for a given porosity.

PLA-PG composite foams have also been produced and studied for BTE by Georgiou *et al*. [190] using $scCO_2$. The glass content was shown to affect the foam morphology. Smaller pores were created with increasing amounts of glass content. However, foaming of PLA-20 (wt.%) PG was not efficient. The addition of fillers increased the foam densities; nevertheless, the required level of porosity for BTE remained above 75%. Direct contact of PLA-PG foams with human foetal bone cells and their proliferation showed similar results compared to foams of PLA with HA or β-TCP.

2.4.4.2. High pressure carbon dioxide

Gas foaming can also be performed with high pressure CO_2 at low temperatures. In this CO_2-based foaming process, the polymer is initially saturated with CO_2, and then followed by an expansion step [237]. The process with some important foaming parameters is schematically illustrated in Figure 2.17.

The polymer is plasticised during the saturation step since the T_g of the polymer decreases to a value below the saturation temperature. In addition, the polymer matrix swells, and reduced viscosity allows the polymer-CO_2 mixture to be processed at lower temperatures. Once the polymer matrix is saturated with CO_2, a rapid decrease in pressure provokes a shift in the thermodynamic equilibrium. Consequently, an oversaturation of CO_2 occurs in the polymer. However, foaming (nucleation and cell growth) will not occur below the T_g because the polymer matrix can still be in the glassy state; e.g., if the saturation temperature is relatively low, and T_g has not been adequately depressed by CO_2 sorption. Therefore, phase separation and nucleation will only occur when the saturated specimen is heated to a temperature above the T_g. It should be noted that the foaming will take place instantaneously if the saturation temperature is high enough, and the polymer is in the rubbery state due to sufficient decrease of Tg. When the polymer returns to the glassy state; either by a decrease in temperature or a decrease in the CO_2 concentration, cell growth will stop [237].

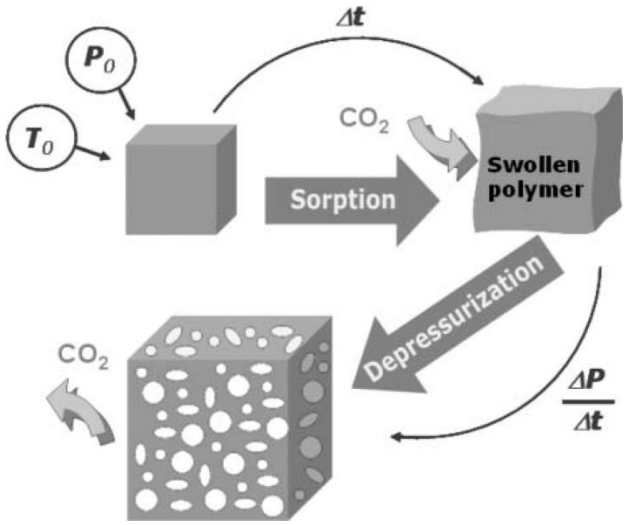

Figure 2.17 Schematic demonstration of CO_2-foaming process [237]. P_0, T_0 and Δt are the saturation pressure, temperature and time, respectively.

Mooney *et al*. [238] developed this technique by foaming poly($_{D,L}$-lactic-co-glycolic acid) which was exposed to high pressure CO_2 (5.5 MPa) for 72 hours at room temperature. By reducing the CO_2 pressure to atmospheric levels, the solubility of the gas in the polymer matrix decreased rapidly resulting in thermodynamic instability of the

dissolved CO_2 leading to the nucleation and growth of gas cells within the polymer matrix. Large pores (~100 μm) and up to 93% porosity could be produced using this technique. The porosity and pore structure depends on the amount of gas dissolved in the polymer and the rate and type of nucleation as well as the diffusion rate of gas molecules through the polymer to the pore nuclei [27, 230]. By changing the gas pressure and temperature, the mount of dissolved gas can be controlled. Homo-/heterogeneous nucleation and the diffusion rate of dissolved gas can be regulated by the processing temperature and the rate at which the gas pressure is changed. By increasing the amount of dissolved gas in the polymer matrix or increasing the gas diffusion rate after thermodynamic instability, a more interconnected pore structure could be created [238]. Singh *et al.* [239] has also investigated the fabrication of PLGA foams for biomedical applications. Porosity of 89% with a pore size ranging from 30 to 100 μm was achieved at CO_2 pressures of 100-200 bar and temperatures up to 40 ^oC. Hu *et al*. [240] suggested that the foamability of the PLA depends on solubility, diffusion coefficient of CO_2 into the material, and the polymer degree of crystallinity. It was found that the presence of CO_2 induced crystallinity in PLA, and the degree of crystallinity increased with increasing saturation pressure. Foaming was performed by saturating the polymer for two days with CO_2 at different pressures and at room temperature. The pressure was rapidly released and samples were subsequently allowed to foam at a range of temperatures from 25 to 160 ^oC for 5, 10, 30 and 90 seconds. A more uniform cellular structure obtained when PLA samples were saturated at 2.8 MPa and room temperature followed by foaming at 100 ^oC. Figure 2.19 (a) represents SEM micrograph of PLA foam saturated at 2.8 MPa at 25 ^oC and foamed at 100 ^oC. The effect of CO_2 pressure on crystallinity, solubility and diffusion coefficient have been shown in Figure 2.18 (b, c and d), respectively.

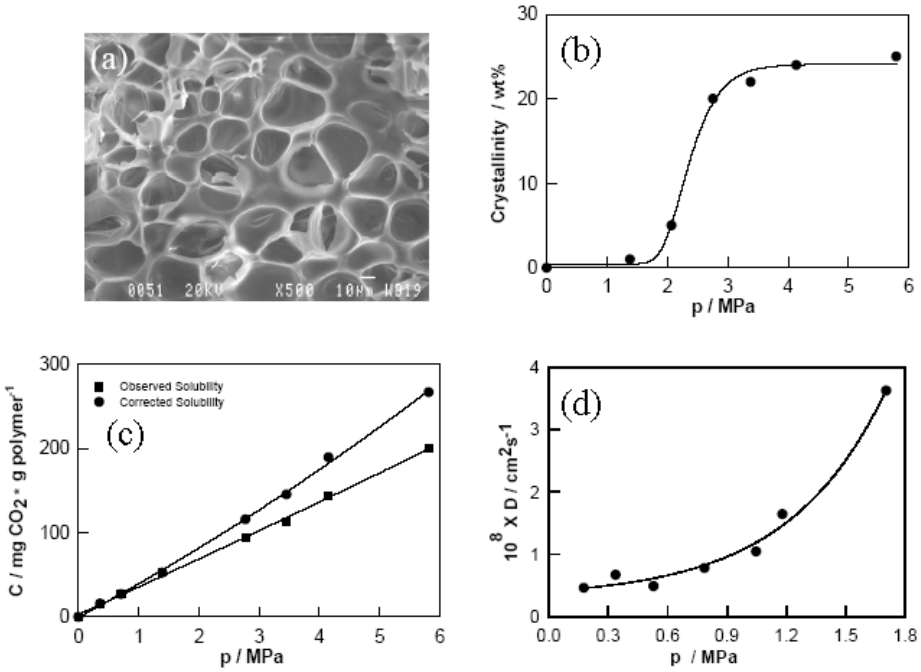

Figure 2.18 (a) SEM micrograph of PLA foam saturated at 2.8 MPa at 25 ^{o}C and foamed at 100 ^{o}C. (b) CO_2-induced crystallization as a function of pressure. (c) Solubility of CO_2 dependence on pressure at 25 ^{o}C. (d) Effect of pressure on the diffusion coefficient of CO_2 in amorphous PLA at 25 ^{o}C [240].

CHAPTER 3

STATEMENT OF THE PROBLEM

Research into developing new materials for bone defect repair has led to the generation of phosphate-based glasses (PGs) and their composites as an interesting class of materials with unique properties. Numerous PG formulations of binary, ternary and quaternary compositions have been developed and investigated either alone or incorporated into polymers for biomaterials and tissue engineering applications. However, there are three issues associated with the development of PG formulations, polyester-PG composites and foams, and these will be addressed each in the following manner:

1) PG formulation: The majority of PG formulations that have been developed for biomedical applications to date are based on the P_2O_5-CaO-Na_2O system. This was probably based on the original bioactive silicate-based glasses (SGs) developed in the SiO_2-CaO-Na_2O system, and SiO_2 was replaced by P_2O_5 as the network forming oxide while still maintaining CaO and Na_2O as modifying oxides. Na_2O is used as a major component of SGs in order to reduce the network connectivity and increase the resorption and surface reactivity through the ionic exchange of Na^+ with H^+/H_3O^+ from physiological solutions as the initiating step of calcium phosphate (CaP) deposition [20,

21]. However, PGs have low network connectivity due to the presence of terminal double bond oxygen in their structure [102] and are unstable and readily soluble in aqueous environments due to the hydrolysis of the P-O-P bonds. Therefore, while the incorporation of metals with charges equal or greater than two (e.g. Ca^{2+}) is required to cross-link the phosphate chains and increase their stability [138], the incorporation of Na_2O would only increase the instability of the phosphate network, which will lead to greater degradation and ion release rates. Increased PO_4^{3-} release is unfavourable to cells due to considerable reduction in pH [23]. In addition, sodium ions have been reported to be detrimental to cells [22]. Therefore, the addition of Na_2O to PGs may not be required. On the other hand, the positive effect of Si on bone metabolism has been reported [241-243], and Si-substituted CaPs have shown enhanced biological behaviour [241]. Therefore, the approach of this study was to develop sodium-free PGs doped with SiO_2 and Fe_2O_3 or TiO_2. The replacement of Na_2O with SiO_2 would change the degradation and ionic release properties of PGs. In addition, PGs doped with Fe_2O_3 have been shown to be cytocompatible attributable to reduced degradation rate due to the formation of P-O-Fe bones [119]. The incorporation of TiO_2 into PGs has also been associated with reduced degradation rate due to the formation of P-O-Ti bonds [120], and with improved biological response potentially due to the release of Ti^{4+} ions [28, 136].

2) Composite systems: Composites of biodegradable polymers and ceramics or glasses are of interest due to enhanced mechanical properties. Several composite systems have been developed; however, these have been generally based on one type of filler. Since the properties of PGs significantly depend on their composition, it was hypothesised that the use of filler blends of mixed PG formulations can modulate composite properties. For example, while highly degradable PGs would facilitate ion release, CaP deposition and creation of pores within the structure, slower degrading PGs would remain for longer time periods thus maintaining composite mechanical properties. In addition, the filler/matrix interaction has a significant influence on the composite properties. It has been demonstrated that there is a potential reaction between bioactive SGs and the ester bond in polyesters at elevated processing temperatures [188]. However, there have been no reports on whether Si-doped PGs would induce similar interaction. Therefore, in this

study, the potential interaction between Si-doped PGs and hydrolysable polyesters was investigated by varying the PG geometry (particulate or fibre), composition (ternary or quaternary), and composite processing conditions. For this purpose, polycaprolactone as well as semi-crystalline and amorphous poly(lactic acid) were selected which require different processing temperatures, and exhibit different physico-mechanical properties.

3) Foaming the polyester-PG composites: In order to develop a scaffold for bone tissue engineering (BTE), the composites need to be converted into porous structures. Gas foaming using carbon dioxide (CO_2) is a scaffold producing technique without the use of organic solvents. However, there are few studies on the foamability of polymer-PG systems. Among which, supercritical CO_2 ($scCO_2$) has demonstrated limited foamability extent in the presence of the fillers [190]. Herein, solid-state CO_2 foaming was demonstrated as a potential alternative to $scCO_2$ foaming.

Through these investigations, this dissertation provides new insights into developing novel PG formulations, composites with modulated properties for different potential applications as either fracture fixation devices or scaffolds for BTE, and an effective foaming technique to produce scaffolds with relatively high filler content. It questions the need for incorporating Na_2O in the PG formulations, and validates that doping PGs with both SiO_2 and TiO_2 increased osteoblastic attachment, proliferation and alkaline phosphatase activity. In addition, PG formulation, its surface properties, type of the polymer matrix and processing conditions should be taken into account when producing polyester-PG composites. Overall, this work will impact the development of biodegradable constructs for bone repair and regeneration applications.

CHAPTER 4

INCORPORATION OF MIXED PHOSPHATE-BASED GLASS PARTICULATES MODULATES POLYMER MATRIX COMPOSITE PROPERTIES

Owing to their controllable degradation, phosphate-based glasses (PGs) have emerged as novel biocompatible materials for bone repair and regeneration. However, like most ceramic materials, the major disadvantage of PGs could be low fracture toughness; e.g. brittleness. On the other hand, synthetic polymers such as the Food and Drug Administration (FDA) approved α-hydroxy-polyesters; e.g. poly(lactic acid), poly(glycolic acid), and polycaprolactone (PCL), are degradable; however, their main limitations include lack of bioactivity function as well as the incapacity to withstand certain load bearing conditions. The versatility of PG properties may be translated into a composite system by incorporation into a degradable polymer, thus potentially improving their mechanical and bioactivity properties.

The main objective of this work was to incorporate PG particulates (PGPs), ($50P_2O_5$-40CaO-10x), where x is either Fe_2O_3 or SiO_2, into PCL to serve as a degradable composite biomaterial for potential applications in bone repair and regeneration. It was

hypothesised that incorporating blends of different PG formulations into PCL will tailor the composite properties. Along with being an FDA approved biodegradable polyester for use as sutures, controlled drug delivery devices and temporary orthopaedic plates for bone fracture repair, PCL has also received attention for use as an implantable biomaterial as a scaffold for tissue engineering. Moreover, it is a semi-crystalline polymer, which at room and physiological temperature, exists within the crystal reinforced amorphous rubber region; i.e. above its glass transition temperature. In this study, changes in structural and mechanical properties in deionised water and phosphate buffered saline, as well as the potential for a calcium phosphate deposition by conditioning in simulated body fluid were investigated.

The findings of this work were reported in a manuscript published in the peer-reviewed journal, *Acta Biomaterialia*.

Modulation of polycaprolactone composite properties through incorporation of mixed phosphate glass formulations

Maziar Shah Mohammadi[a], Ifty Ahmed[b], Benedetto Marelli[a], Christopher Rudd[b], Martin N Bureau[c,a], Showan N Nazhat[a]

[a] *Department of Mining and Materials Engineering, McGill University, Montreal, QC, Canada*

[b] *Faculty of Engineering, Division of Materials, Mechanics and Structures, University of Nottingham, UK*

[c] *Industrial Materials Institute, National Research Council Canada, QC, Canada*

Keywords: Phosphate-based glass particles, Polycaprolactone, Biodegradable composites, Dissolution, Bioactivity

4.1. Abstract

Phosphate-based glasses (PGs) and their composites are of interest as bone repair and tissue engineering scaffolds due to the totally degradable nature of the materials. This study has investigated the effect of Si and Fe on the properties of PG particulate-filled polycaprolactone (PCL) matrix composites. Two glass compositions were investigated (mol.%): 50 P_2O_5, 40CaO and 10 SiO_2 or Fe_2O_3 (Si10 and Fe10 respectively). All composites contained 40 vol.% particulate filler, either Si10, Fe10, or a blend (40Si10/0Fe10, 30Si10/10Fe10, 20Si10/20Fe10, 10Si10/30Fe10, 0Si10/40Fe10). Ion release, weight loss and composite mechanical properties were characterized as a function of time in deionised water (DW) and phosphate-buffered saline (PBS), respectively. The potential for calcium phosphate deposition was assessed in simulated body fluid (SBF). Calcium and phosphate ion released in DW increased in tandem with the rate of composite weight loss, which increased with Si10 content. A Si10 content dependent rate of pH reduction was observed in DW. After 56 days, the PG in the 40Si10/0Fe10 composite was completely dissolved, whereas 67% of that in 0Si10/40Fe10 composite remained. The initial flexural strength of 40Si10/0Fe10 composites was significantly lower when compared with the other materials. An increase in Si10 content led to an increase in Young's modulus and a concomitant decrease in flexural strain. It was found that the PCL molecular weight (M_w) decreased dramatically with increasing Si10 content. FTIR analysis showed that Si incorporation into PG led to reaction with the PCL ester bonds, resulting in a reduction in PCL M_w when processed at elevated temperatures. Changes in mechanical properties with time in PBS were glass blend dependent and a more rapid rate of reduction was observed in higher Si10 content composites. After 28 days in SBF, surface deposited brushite was formed in 20Si10/20Fe10 PG containing composites. Thus, the properties of PCL-PG composites could be tailored by controlling the phosphate glass blend composition.

4.2. Introduction

Composites are an attractive approach as biomaterials since the advantageous properties of different materials can be combined to satisfy the required mechanical and physiological demands of the host tissue [6, 7]. Composites based on biodegradable polymers and bioactive ceramics have been considered for bone tissue engineering, reconstruction and repair [8, 17, 244]. Incorporation of ceramics and glasses into the polymer matrix should improve not only the mechanical properties of the material, but also its bioactivity and biological behaviour [190]. Therefore, bioactive calcium phosphate fillers have been incorporated in degradable polymers [196, 245-249]. Since the composition of the filler, its content and solubility are parameters that can influence the composite properties; the tailoring of such properties is paramount. However, not all calcium phosphate materials are necessarily ideal. For example, hydroxyapatite (HA) or bioactive silicate-based glasses (SGs) do not have the required dissolution properties as they are not fully degradable [10]. While many factors affect bone healing (e.g. anatomical site, age and sex of the patient), the regenerating period can be extended over weeks, and ideally this should coincide with a controlled degradation rate of the material. Therefore, producing a fully biodegradable composite material with controllable mechanical property retention characteristics is essential in bone repair and regeneration. For this purpose, phosphate-based glasses (PGs) may be a potential alternative as the inorganic phase of biodegradable composites [11, 12].

PGs have a wide range of solubility, which can be predicted and controlled by altering their composition [13, 14, 98, 138]. Numerous binary, ternary and quaternary PGs have been developed [13, 14, 19, 29, 98-101, 109, 138]. A ternary glass system based on $45P_2O_5$-xCaO-(55-x)NaO_2, where x was between 8 and 40 mol.%, was developed by Franks *et al.* [98]. An inverse relationship between CaO content and the solubility was observed, which was linear over time for glasses containing up to 20 mol.% CaO. It was suggested that Ca^{2+} and its interaction with the glass network were the dominant factors of dissolution. In high CaO content PGs, an ion exchange process and a gradual breakdown of the glass network were two suggested processes responsible for dissolution. Salih *et al.* [110] investigated the potential of this glass system for bone regeneration and suggested that at higher CaO content greater amounts of Ca^{2+} are

released with lower dissolution rates, which has an essential role in cell activation mechanisms affecting cell growth. However, a sharp change in pH associated with high release rates of Na^+ and PO_4^{3-} has an adverse effect on cells in highly soluble glasses and unfavourable cellular responses associated with glasses of high Na^+ content. Ahmed *et al.* [119] partially substituted Na_2O by Fe_2O_3 in PG to provide more control over solubility. Fe_2O_3 addition up to 5 mol.% resulted in a decrease in solubility by one order of magnitude and an increase in the glass transition temperature due to the formation of more hydration resistant P-O-Fe bonds [118]. This formulation also allowed the adhesion and proliferation of myoblasts *in vitro*. Incorporation of SiO_2 into PG, on the other hand, has been shown to increase their solubility. PG with the composition of $50P_2O_5$-30CaO-(15-x)Na_2O-5Fe_2O_3-xSiO_2 was investigated by Patel and Knowles [13]. The substitution of SiO_2 at up to 3 mol.% resulted in glasses with a linear solubility behaviour reaching 20% weight loss at day 7, whereas the addition of 5 mol.% led to glasses with a non-linear solubility behaviour reaching 60% weight loss by day 4.

The versatile properties of PG may be translated to a composite system by incorporation into a degradable polymer. However, this has largely depended on the glass composition, which has tended to be based on one type of filler [190, 196, 245, 246]. Therefore, in this study, PG particles ($50P_2O_5$-40CaO-10x) where x is either Fe_2O_3 or SiO_2) were incorporated into polycaprolactone (PCL) to serve as a degradable composite biomaterial for potential applications in bone repair and regeneration. PCL is a biodegradable polyester that is US Food and Drug Administration approved for use as sutures, controlled drug delivery devices and temporary orthopaedic plates for bone fracture repair. Recently it has also received attention for use in scaffolds for tissue engineering, as it can be degraded via a hydrolytic mechanism under physiological conditions [250]. Therefore, it was hypothesised that PCL incorporating PG particulate blends of different formulations will tailor the composite properties. Changes in structural and mechanical properties in deionised water (DW) and phosphate-buffered saline (PBS) and the potential for a calcium phosphate deposition by conditioning in simulated body fluid (SBF) were investigated.

4.3. Experimental

4.3.1. Materials

4.3.1.1. Phosphate glass particulate (PGP) production

Two melt-derived glass compositions were prepared using P_2O_5, $CaHPO_4$, Fe_2O_3, and SiO_2 (Sigma Aldrich, UK) as starting materials. The precursors were mixed and placed into a Pt/5%Au crucible (Birmingham Metal Company, UK), and heated to 400 °C for 30 min to remove moisture. They were then melted at 1150 °C for 90 min, poured onto a steel plate and quench cooled to room temperature. Table 4.1 lists the glass compositions and codes. Bulk glass was ground using agate media in a vibratory cup mill (KHD Humboldt Wedag AG MN 954/2, Christison Scientific Equipment Ltd, Gateshead, UK) for 6 min and sieved for 20 min using three sieve stacks of 105, 75, and 53 μm. Approximately 67% passed through the 53 μm sieve in the allocated grind time.

Table 4.1 Glass compositions and codes

Glass code	Components (mol.%)			
	P_2O_5	CaO	SiO_2	Fe_2O_3
Si10	50	40	10	-
Fe10	50	40	-	10

4.3.1.2 PCL-PG composite production

PCL-PGP composites were prepared by first dissolving PCL (average molecular weight ~65,000, Sigma Aldrich, U.K.) in chloroform (Laboratory grade, Fisher Scientific) at 7% (w/v) followed by addition of appropriate amounts of PGP and the solution was allowed to mix for 20 min. The solution was then ultrasonicated (Precision Ultrasonic Cleaner from Ultrawave Limited, Cardiff, UK) for 1 min, and poured into a 13.5 cm diameter petri dish. Films were then prepared by solvent casting at room temperature for 2 days. Composites of approximately 1.6 mm thickness were produced from five films placed in a metal shim, and heat pressed (Down-stroke Press, Daniels, UK) at 100 °C. The films were heated for 30 min and pressed for 30 min at 38 bar, after which they were immediately cooled in a second press (Up-stroke Press, Daniels, UK) at room temperature for 30 min at the same pressure. Table 4.2 lists composite

compositions and codes. Composites containing 40 vol.% PG particles, either of Si10, Fe10, or a blend (40Si10/0Fe10, 30Si10/10Fe10, 20Si10/20Fe10, 10Si10/30Fe10, 0Si10/40Fe10), were prepared.

Neat PCL plaques (also 1.6 mm thick) were also produced by melt pressing PCL for 30 min at 38 bar and cooling in the cold press at room temperature for a further 30 min at 38 bar.

Table 4.2 Composites compositions and codes

Composite code	Components (vol.%)		
	PCL	Si10	Fe10
PCL	100	0	0
PCL-PGP 1	60	40	00
PCL-PGP 2	60	30	10
PCL-PGP 3	60	20	20
PCL-PGP 4	60	10	30
PCL-PGP 5	60	0	40

4.3.2. Characterisation of the PCL-PGP composites

4.3.2.1. Ageing in deionised water (DW)

PCL-PGP composites were aged in DW for up to 56 days by placing 10×10×1.6 mm^3 specimens (n=3) into vials containing 25 ml of ultra-pure deionised water (18.2 MΩ cm resistivity) and incubating at 37 °C. Ion release, composite weight, and pH of the ageing environment were measured at 14 different time points: 0, 2, 4, 8, 24, 48, 96, 168, 336, 504, 672, 840, 1008, and 1344 h.

Anion and cation release through PGP dissolution were measured using ion chromatography (IC) and atomic absorption (AA), respectively. IC (DX-100 Ion chromatograph, Dionex) was used in order to measure phosphate anion (PO_4^{3-}) release. An Ionpac® AS14 anion exchange column was used to elute the polyphosphates. An eluent of 3.5 mM Na_2CO_3/0.1 mM $NaHCO_3$ was used with a flow rate of 0.1 ml/min. The sample run time was 15 min. Sodium phosphate tribasic (Na_3PO_4) (Sigma, Canada) was used to prepare standard solutions. A 1000 ppm working solution was prepared from which serially diluted 10, 20, and 50 ppm standard solutions were obtained. AA

(AA240FS, Varian) was used to investigate the release of Ca^{2+}, Fe^{3+}, and Si^{4+} cations. The instrument was calibrated using certified AA standard solutions.

The weight change of the composites was investigated by removing the specimens from DW, blot drying, weighing and replacing in fresh DW. Weight loss was measured in terms of percentage of original weight. The final dry weight on day 56 was measured by first incubating the specimens at 37 °C until an equilibrium weight was reached. The pH of the DW was also measured using a pH meter (Accumet Excel 20, Fisher) at each time point.

4.3.2.2. Morphological investigations using scanning electron microscopy (SEM)

SEM (JSM 6100, JEOL, Tokyo, Japan; S-3000N, Hitachi) was used to investigate the morphology of the composites before and after ageing in DW for 20 and 56 days. Both secondary electron (SE) and back scattered electron (BSE) modes with accelerating voltages of 4 and 10 kV, respectively, were used. The samples were cryo-fractured and the resulting fracture surfaces were coated with gold/palladium using sputter coaters.

4.3.2.3. Composite initial mechanical properties and as a function of time in PBS

Three-point bend flexural mechanical analysis was used to measure the mechanical properties of the composites. The effect of PG formulation on composite mechanical properties was investigated through changes in flexural strength, Young's modulus, and strain at maximum stress. Tests were performed on initially produced and PBS (Sigma Aldrich, CA) aged specimens stored at 37 °C and tested on days 7 and 28. Mechanical testing was carried out on specimens in the dry state and the extent of their weight loss after PBS ageing was measured. At least three repeat specimens were tested with a cross-head speed of 1 mm min^{-1} using a 1 kN load cell and according to ASTM D 790-95a:1996 (aspect ratio > 16) in an Instron mechanical testing instrument 5582.

4.3.2.4. Molecular weight determination

Gel permeation chromatography (Water Breeze) was used to investigate the molecular weight (M_w) of PCL both after composite fabrication and on day 56 in DW. The GPC was equipped with both ultraviolet (UV 2487) and differential refractive index

(RI 2410) detectors and three Water Styragel HR columns (HR1 with molecular weight measurement in the range of 10^2-5×10^3 g.mol^{-1}, HR2 with molecular weight measurement range of 5×10^2-2×10^4 g.mol^{-1}, and HR4 with molecular weight measurement range of 5×10^3 - 6×10^5 g.mol^{-1} and a guard column. The columns were kept at 40 °C. Tetrahydrofuran (THF) flowing at a rate of 0.3 ml.min^{-1} was used as the mobile phase. Each sample dissolved in THF was filtered through a 0.2 μm syringe filter (Anotop25, Fisher) to remove PGP prior to injection into the module.

4.3.2.5. Fourier transform infrared spectroscopy (FTIR)

FTIR spectroscopy was used to investigate the structural changes in the PCL matrix due to its potential interactions with PGP when processed at high temperature. Polymer and composite films (Table 4.2) were first prepared through solvent casting (low temperature) and then heated while spectra were collected. Composite films of approximately 75 μm thicknesses were prepared by first dissolving 1 g of PCL pellets in 23.5 ml of chloroform, then the appropriate amounts of PGP were added to the solution and ultrasonicated for 5 min.

FTIR spectroscopy was carried out using a Perkin Elmer Spotlight 400 FTIR microscope connected to a Spectrum 400 infrared beam source (Perkin Elmer Instruments, Canada) on disk-shaped specimens (nominal diameter 13 mm) mounted on a KBr disk (N9302615, Perkin Elmer). The microscope was used in transmission mode in the mid infrared region (4000-650 cm^{-1}) with a resolution of 8 cm^{-1} and number of scans 8. A heating chamber was used (BriskONE, BriskHeat Corp.) to increase the temperature from 25 to 60 °C, with a hold for 10 min, then again to 100 °C, with a hold for 60 min, at 25 °C min^{-1}. The system was then cooled down to room temperature for 30 min. The Spectrum Timebase v2.0 software (Perkin Elmer) recorded spectra every 20 s. Since the film was thin enough for the Beer-Lambert law to be valid, changes in the IR spectrum during the thermal processing are an indication of chemical modification. The kinetics of PCL degradation at 100 °C were investigated as proposed by Blaker *et al.* [188].

4.3.2.6. Conditioning in simulated body fluid (SBF)

Three repeat specimens (10×10×1.6 mm) of each composite were placed in vials containing 60 ml of SBF, which had inorganic ion concentrations similar to those of human extracellular fluid, and incubated at 37 ˚C. The ionic concentrations of SBF solution, prepared according to Kokubo *et al.* [251], were (in mM): Na^+, 142; K^+, 5; Mg^{2+}, 1.5; Ca^{2+}, 2.5; Cl^-, 147.8; HCO_3^-, 4.2; HPO_4^{2-}, 1; SO_4^{2-}, 0.5; pH: 7.4. The SBF was replaced every 3 days. Briefly, the SBF was prepared by dissolving respective amounts of NaCl, $NaHCO_3$, KCl, $K_2HPO_4.3H_2O$, $MgCl_2.6H_2O$, $CaCl_2$, and Na_2SO_4 in DW. The pH was adjusted to 7.4 using 1.0 M Tris-buffered HCl. The containers were removed from the incubator on days 7, 14, and 28. Precipitates formed on the surface of the composites were analysed using SEM (Hitachi S-4700) and X-Ray powder diffraction (XRD) (Bruker D8). Composite weight change and SBF pH were also measured at regular time intervals.

4.3.2.7. Statistical Analysis

Statistical analyses were performed to test the significance in the difference between two mean values by using Student's *t*-test, which was used to determine *p* values at a significance level of 0.05.

4.4. Results

4.4.1. Ageing in DW

4.4.1.1. Anion release (PO_4^{3-})

Figure 4.1a shows PO_4^{3-} ion release as a function of time. There was an increase in PO_4^{3-} ion release with an increase in Si10 glass content in the composites. Rapid release of PO_4^{3-} was observed for PCL-PGP 1 in the first 24 h. The rate of PO_4^{3-} ion release decreased considerably on substituting Si10 for Fe10; however, there was a continuous release of PO_4^{3-} ions over time for PCL-PGP 2-5.

4.4.1.2. Cation release (Ca^{2+}, Fe^{3+}, Si^{4+})

Figure 4.1b shows Ca^{2+} ion release as a function of time. Initially the rate of Ca^{2+} ion release was higher with increasing Si10 content in the composites. Interestingly,

however, on day 56 PCL-PGP 2, PCL-PGP 3 and 4 appeared to release more Ca^{2+} ions than PCL-PGP 1 and PCL-PGP 5 ($p<0.05$). As expected, the greatest Si^{4+} ion release (Figure 4.1c) was observed for PCL-PGP 1. The other composites showed similar release profiles up to approximately the 200 h time point, after which continual release of Si^{4+} was observed for the duration of the study. Interestingly, more Fe^{3+} ions were released as the Si10 content increased (Figure 4.1d).

4.4.1.3. Weight loss measurements

The weight change of the composites in DW is shown in Figure 4.1e in terms of percentage of original weight versus time. A rapid weight loss was observed for both PCL-PGP 1 and 2 (up to 168 h) which was followed by a much slower rate of weight loss, reaching approximately 42% in PCL-PGP 1. PCL-PGP 3 showed a similar profile, however, with a lower rate of weight loss that was continual up to day 56, whilst PCL-PGP 4 displayed an even slower rate of weight loss, reaching 17%. PCL-PGP 5, on the other hand, showed a weight gain on day 4, which was followed by a slow and continual weight loss up to day 56. Neat PCL demonstrated no weight loss over the entire ageing period.

Table 4.3 gives the final dry weight of the composites on day 56. The data revealed that there was no residual glass left in PCL-PGP 1 and PCL-PGP 2. The residual glass in PCL-PGP 3, PCL-PGP 4, and PCL-PGP 5 were approximately 12%, 44%, and 67%, respectively, demonstrating intermediate dissolution levels based on the percentages of Si10 and Fe10.

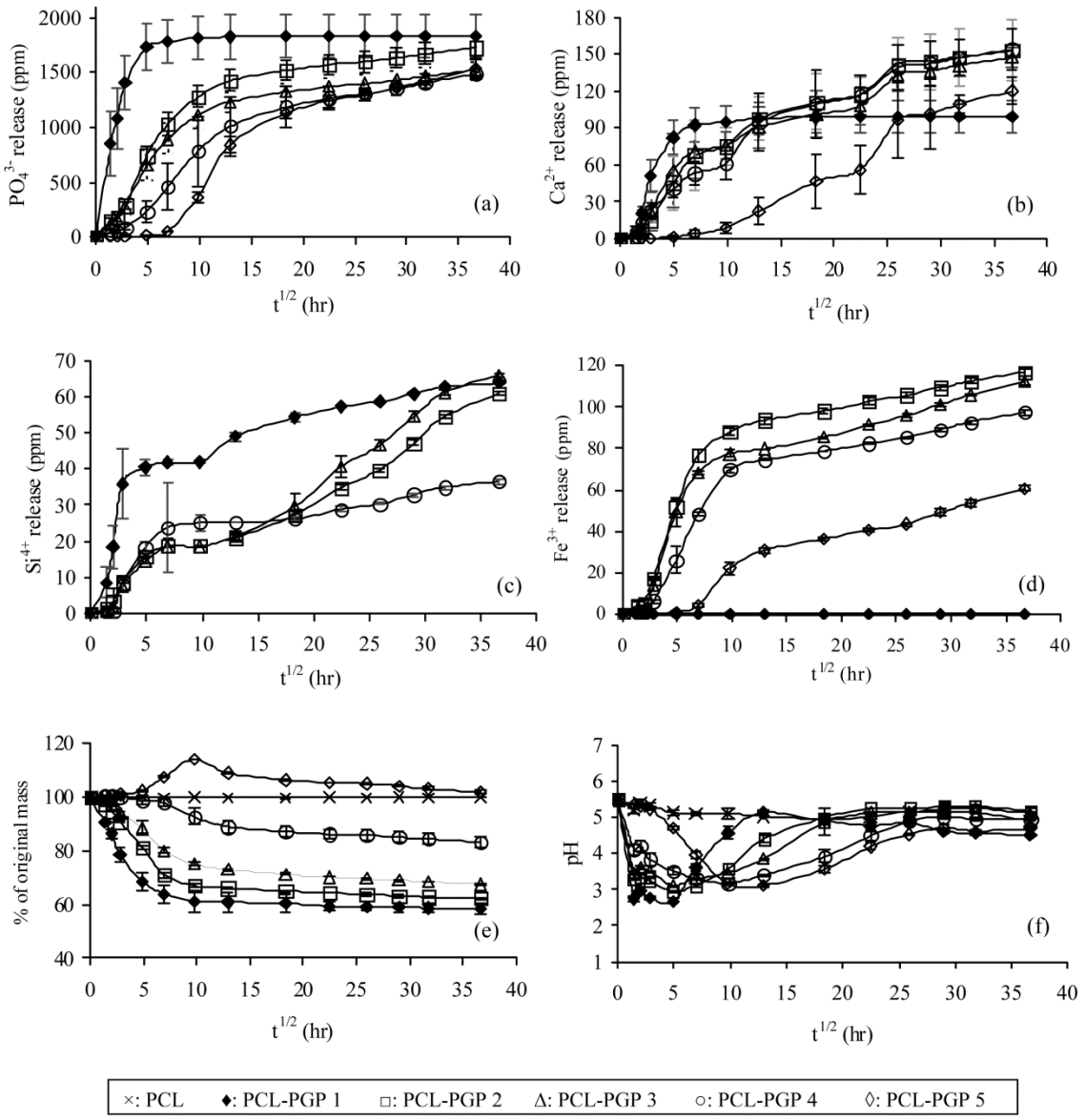

Figure 4.1 Ageing of PCL and PCL-PGP composites in DW incubated for up to 56 days at 37 ºC. (a) PO_4^{3-} (b) Ca^{2+} (c) Si^{4+} and (d) Fe^{3+} ion release from PCL-PGP composites. Anion and cation release increased with increasing Si10 content. (e) Weight loss measurements and (f) pH changes. An initial decrease was observed for composites containing Si10 which increased with Si10 content in the composites. Error bars indicate the standard deviation.

4.4.1.4 pH change

The associated changes in the pH of DW were measured at each time point for all materials and are shown in Figure 4.1f. The pH values of PCL-PGP 1 dropped significantly at early time points and then increased rapidly to the initial pH value,

indicating that all the glass had dissolved. All other composites demonstrated similar behaviours, with the exception of PCL-PGP 5, which showed a delayed decrease in pH. Overall, a slower rate of pH reduction was seen with increasing Fe10 content. The pH of neat PCL remained relatively constant.

Table 4.3 Weight loss and residual glass of the samples in the final dry weight of the specimens after 56 days. There was no residual glass in the composites containing high amount of Si10 glass and low amount of Fe10. The percentage of remaining glass increased with an increase in the amount of Fe10.

Material	% of original mass	Remaining glass (%)
PCL	99.39 ± 0.06	-
PCL-PGP 1	34.91 ± 3.02	0
PCL-PGP 2	40.25 ± 0.12	0
PCL-PGP 3	46.53 ± 1.12	12
PCL-PGP 4	65.33 ± 2.82	44
PCL-PGP 5	81.66 ± 1.07	67

4.4.2. Morphological investigations

Figure 4.2a1 shows a SEM micrograph of an as prepared PCL sample. Figure 4.2a2-a4 shows examples of glass particle distribution within the polymer matrix for as-processed PCL-PGP 5, PCL-PGP 3 and PCL-PGP 1, respectively. Figure 4.2b1 reveals no difference in the morphology of neat PCL after ageing in DW. Figure 4.2b2 shows the structure of PCL-PGP 5 on day 20 in DW, with most of the glass particles still present in the composite. Figure 4.2b3 and b4 shows SEM micrographs of PCL-PGP 3 on day 20 and 56, respectively, in DW, showing that on day 56 in DW both glass particles and pores were present in this composite. The porosity was attributed to the rapid dissolution of Si10 glass particles, as EDS analysis revealed that the remaining PGP comprised Fe10 (data not shown). SEM micrographs of PCL-PGP 1 on day 20 and 56 can be seen in Figure 4.2b5 and b6. No glass particles were observed in PCL-PGP 1 on day 20. These images corroborate the weight loss data given in Table 4.3.

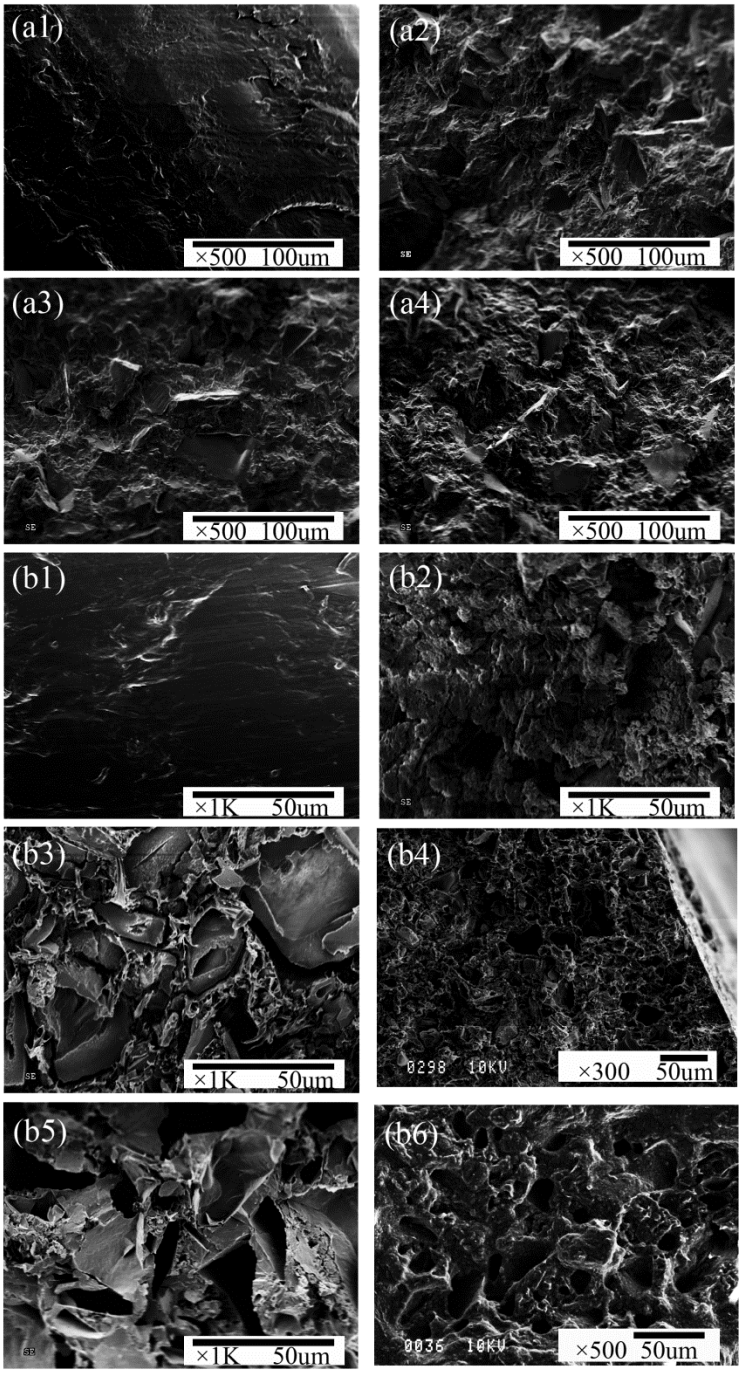

Figure 4.2 (a) SEM micrographs of as-processed cryo-fractured specimens: (a1) PCL; (a2) PCL-PGP 5; (a3) PCL-PGP 3 and (a4) PCL-PGP 1. (b) SEM micrographs after immersion in DW: (b1) PCL (20 days); (b2) PCL-PGP 5 (20 days); (b3) PCL-PGP 3 (20 days); (b4) PCL-PGP 3 (56 days); (b5) PCL-PGP 1 (20 days); (b6) PCL-PGP 1 (56 days). As-processed composites showed well dispersed and attached PGP on the PCL matrix. While all Si10 PGPs underwent dissolution in PCL-PGP 1 at day 20, there were residual Fe10 PGPs in the composites.

4.4.3. Mechanical property changes in PBS

Figure 4.3a shows the weight loss of composites aged in PBS and demonstrates a similar weight loss effect to that seen in DW. The final dry weight of PCL-PGP 1 confirmed that all the glass particles had dissolved. In contrast, PCL-PGP 5 resulted in a 7% weight loss on day 28, with other composites demonstrating intermediate levels. Initial mechanical analysis (Figure 4.3b-d) of the composites revealed that the flexural strength of PCL-PGP 1 was significantly lower ($p<0.05$) compared with the other composites tested. PGP incorporation resulted in a significant increase in Young's modulus which was composition dependent and tended to increase with Si10 content. The modulus values ranged from 0.3 ± 0.03 to 1.5 ± 0.20 to 3 ± 0.78 GPa for PCL, PCL-PGP 5 and PCL-PGP 1, respectively. In parallel, the strain at maximum stress decreased significantly ($p<0.05$) by increasing the Si10 content.

The mechanical properties of neat PCL did not change significantly on ageing in PBS, while those of PCL-PGP decreased progressively, with the composites with higher Si10 contents demonstrating a more rapid decrease. For example, on day 7 in PBS, while the strength of PCL-PGP 2 and PCL-PGP 5 had decreased by 85% and 26%, respectively, the properties of PCL-PGP 1 could not be measured due to loss of integrity. On day 28 in PBS, the Young's modulus values of PCL-PGP 2 and PCL-PGP 5 had decreased by 90% and 28%, respectively, while flexural strain underwent a similar significant decrease for these composites (83% and 69% for PCL-PGP 2 and PCL-PGP 5, respectively).

4.4.4. Molecular weight determination

Figure 4.4a shows the molecular weight of PCL in the various composites. There was a slight change in PCL M_w in PCL-PGP with no or low Si10 content (PCL-PGP 4 and PCL-PGP 5). However, PCL M_w decreased dramatically in PCL-PGP with higher Si10 contents. For example, PCL M_w in PCL-PGP 1 decreased to 14,000 g mol^{-1}. PCL-PGP composites containing both Fe10 and Si10 showed intermediate M_w values. PCL M_w did not appear to be significantly affected by DW conditioning (Figure 4.4a). The polydispersity index of the PCL-PGP did not vary from that of neat PCL and was not affected by the PGP formulation (Figure 4.4b).

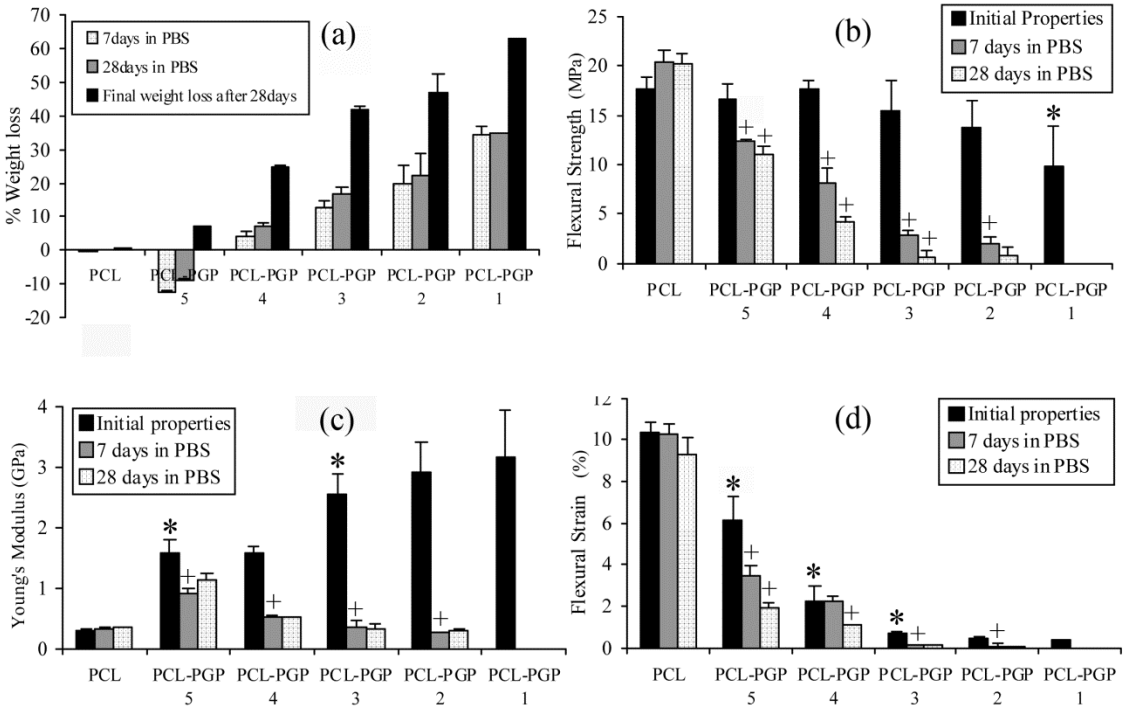

Figure 4.3 Mechanical property changes in PBS. (a) Weight loss of PCL and PCL-PGP composites after 7 and 28 days ageing in PBS (wet) and after 28days dry. As-processed and post PBS conditioning flexural mechanical properties of PCL and PCL-PGP composites: (b) flexural strength, (c) Young's modulus, and (d) strain at maximum stress. Initial flexural strength remained almost constant on addition of PGP except for PCL-PGP 1, for which a statistically significant ($P<0.05$) decrease was observed. Increasing the Si10 content significantly increased the Young's modulus and decreased the strain at maximum stress. After ageing in PBS, the decrease in mechanical properties was considerably greater for high Si10 composites compared with high Fe10 composites. *Statistically significant differences compared with the previous material at the same time point ($p<0.05$), $^{+}$ Statistically significant difference compared with the previous time point for the same material ($p<0.05$).

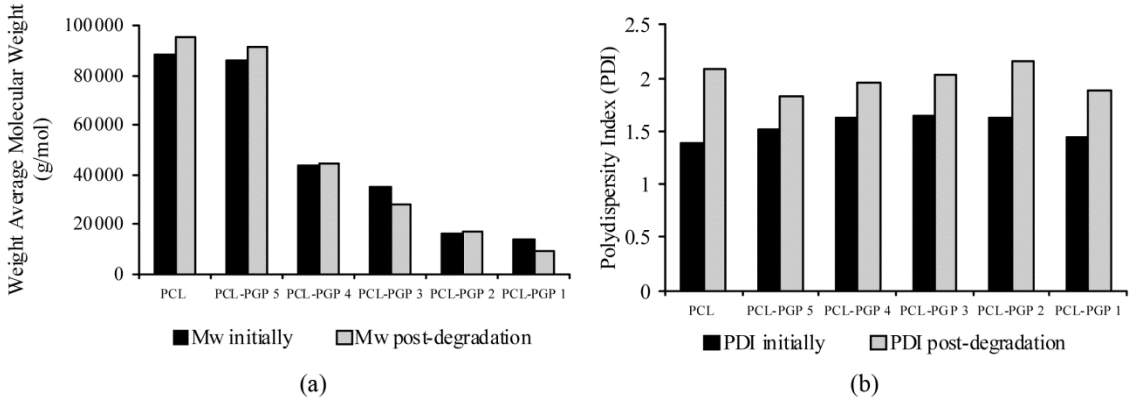

Figure 4.4 (a) Molecular weight and (b) polydispersity index of neat PCL and PCL in the composites, as-processed and post conditioning in DW. There was no difference in the molecular weight of PCL (M_w) in the Fe10 containing composites when compared with neat PCL. However, there was a decrease in PCL M_w with increasing Si10 content. There was no change in PCL M_w in all systems as a consequence of conditioning in DW. Similarly, the polydispersity index remains almost constant.

4.4.5. FTIR analysis

The fractional absorbance (ϕ) change of the carbonyl peak (1728 cm^{-1}), expressed as ϕ_{1728}, for PCL and PCL-PGP composites is shown in Figure 4.5a. PCL-PGP 5 did not show any change when compared with neat PCL. However, there was a considerable increase in ϕ_{1728} for PCL-PGP 1 and PCL-PGP 3 with thermal treatment time at 100 °C, indicating greater changes in absorbance and the fractional absorbance change derivate ($d\phi/dt$) with higher Si10 content. Therefore, a greater and more rapid reduction in PCL M_w would be expected with higher Si10 content. The full spectrum of PCL-PGP 1 before and after thermal treatment is presented in Figure 4.5b. There was a reduction in the absorbance of the carbonyl peak and the appearance of a carboxylate peak at 1634 cm^{-1}. While formation of a carboxylate peak was not observed in PCL and PCL-PGP 5, it became more apparent as the Si10 content increased, as in the case of PCL-PGP 3 and PCL-PGP 1 (Figure 4.5c). In addition, reduction of the ester absorbance peaks for asymmetric C-O-C stretching (1240 cm^{-1}), OC-O stretching (1190 cm^{-1}), and the symmetric C-O-C stretching (1170 cm^{-1}) were observed.

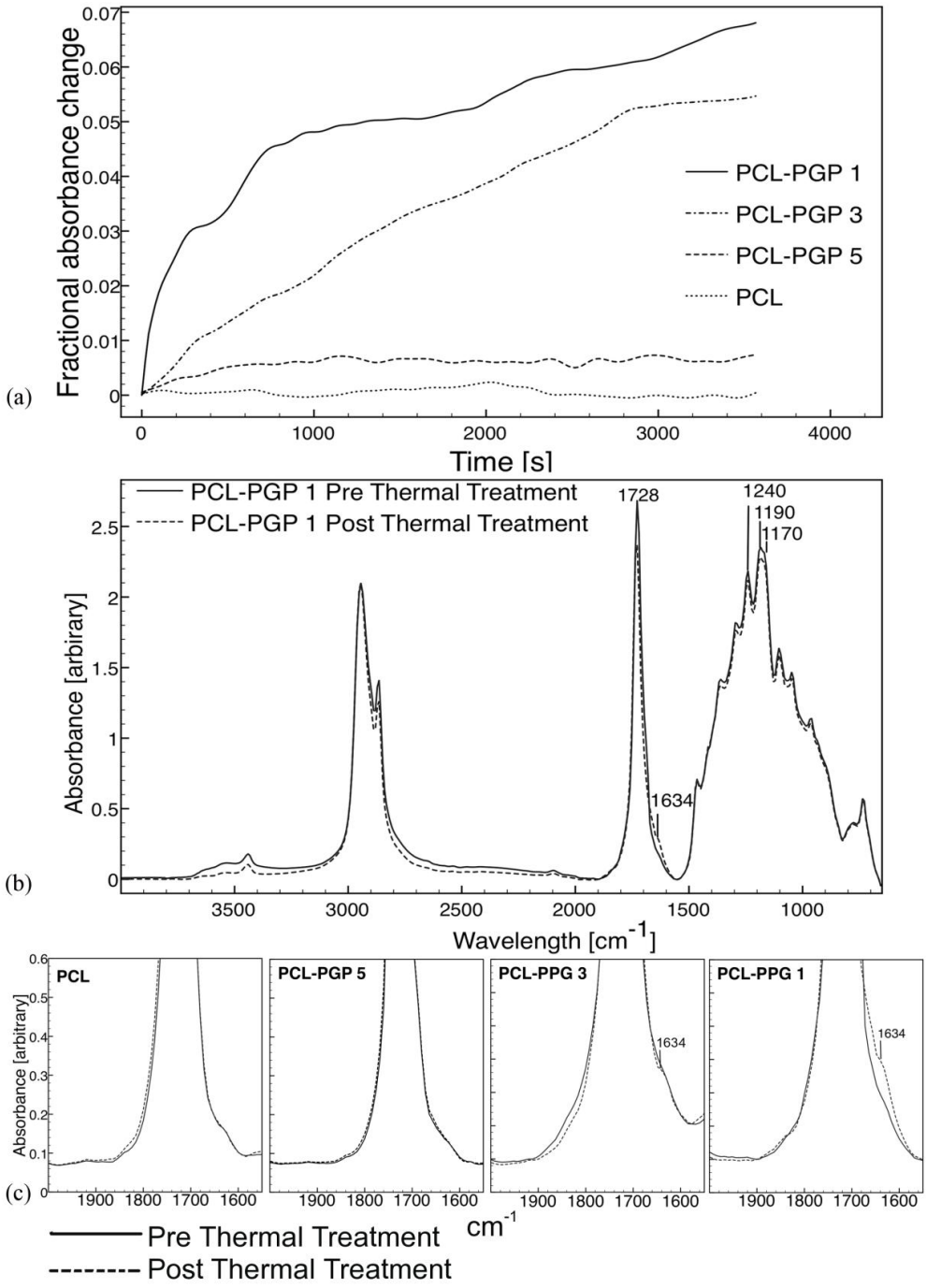

Figure 4.5 FTIR analyses. (a) The fractional absorbance change of the carbonyl peak (1728 cm^{-1}) for PCL and PCL-PGP composites. There was a considerable increase in ϕ_{1728} for PCL-PGP 3 and PCL-PGP 5 during thermal treatment at 100°C. (b) FTIR spectra of PCL-PGP 1 before and after the thermal treatment. There was a reduction in the absorbance of the C=O peak at 1728 cm^{-1} and the concomitant appearance of a carboxylate peak at 1634 cm^{-1}. (c) Comparison of carboxylate peak formation for PCL and PCL-PGP composites. The carboxylate peak became more apparent as the Si10 content in the composites increased, as shown for PCL-PGP 3 and PCL-PGP 1. Neat PCL and PCL-PGP 5 displayed no carboxylate peaks.

4.4.6. Conditioning in SBF

The weight changes of the composites in SBF are shown in Figure 4.6a in terms of the percentage of original weight versus time. Rapid initial weight loss was seen for PCL-PGP 1 (up to 168h), which remained constant thereafter. PCL-PGP 2 and PCL-PGP 3 showed similar behaviours, however, with slower rates of weight loss. A weight gain was observed for PCL-PGP 4 and PCL-PGP 5 in the first 48 and 168 h, respectively, followed by a slow rate of continuous weight loss. No weight loss of neat PCL occurred.

The associated changes in pH of the SBF up to 1 week are shown in Figure 4.6b. While no change in the pH of SBF medium was observed for neat PCL, the pH in the presence of all the composites decreased significantly over time to below 4, the rate of which increased with Si10 content.

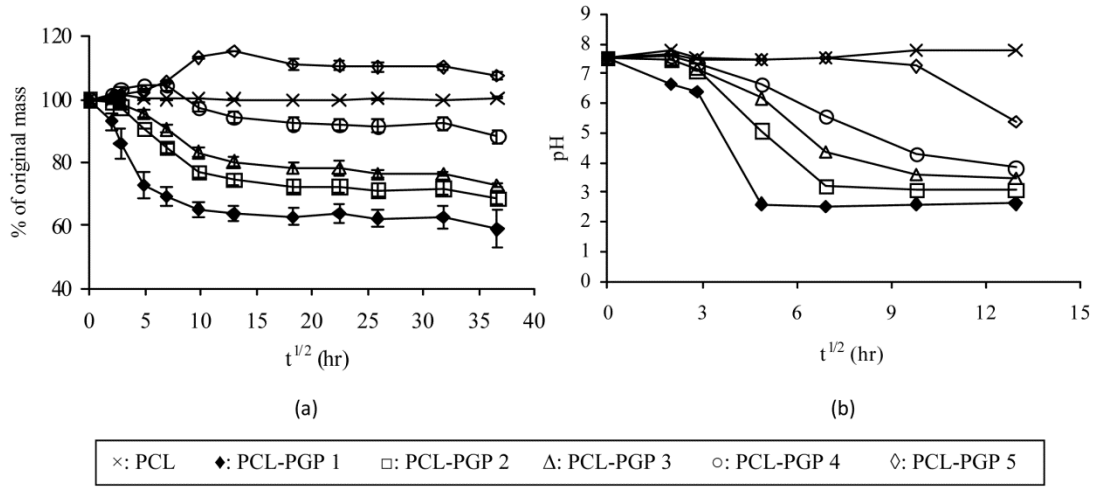

Figure 4.6 (a) Weight loss of PCL and PCL-PGP composites through conditioning in SBF. A significant weight loss was observed for high Si10 containing composites. (b) pH changes obtained for PCL and PCL-PGP composites up to 1 week in SBF. While there was a prompt reduction in the pH to below 4, the required time for this reduction increased with Fe10 content.

Figure 4.7a-e shows the images (on days 7, 14 and 28), SEM micrographs (on day 28), EDS analyses and XRD patterns of the precipitates formed on conditioning in SBF for PCL-PGP 5, PCL-PGP 3 and PCL-PGP 1. Precipitates were observed on the surfaces of PCL-PGP 2 PCL-PGP 3, PCL-PGP 4 and PCL-PGP 5. In contrast, no precipitates were found on PCL-PGP 1. EDS analysis confirmed the presence of calcium, phosphorous and oxygen. The XRD patterns of PCL-PGP 3 are presented in Figure 4.7d,

initially and after 14 and 28 days in SBF. These revealed the formation of brushite (dicalcium phosphate dihydrate, DCPD) precipitates on the surface of the specimens at the latter time point. Figure 4.7e compares the XRD patterns of the surfaces of PCL-PGP 1, PCL-PGP 3 and PCL-PGP 5 on day 28. While the pattern of PCL-PGP 1 confirmed no brushite formation, the pattern of PCL-PGP 5 suggested potential brushite formation; however, the latter could not be confirmed as one of the main peaks for brushite (at 20.8^{o}) was missing.

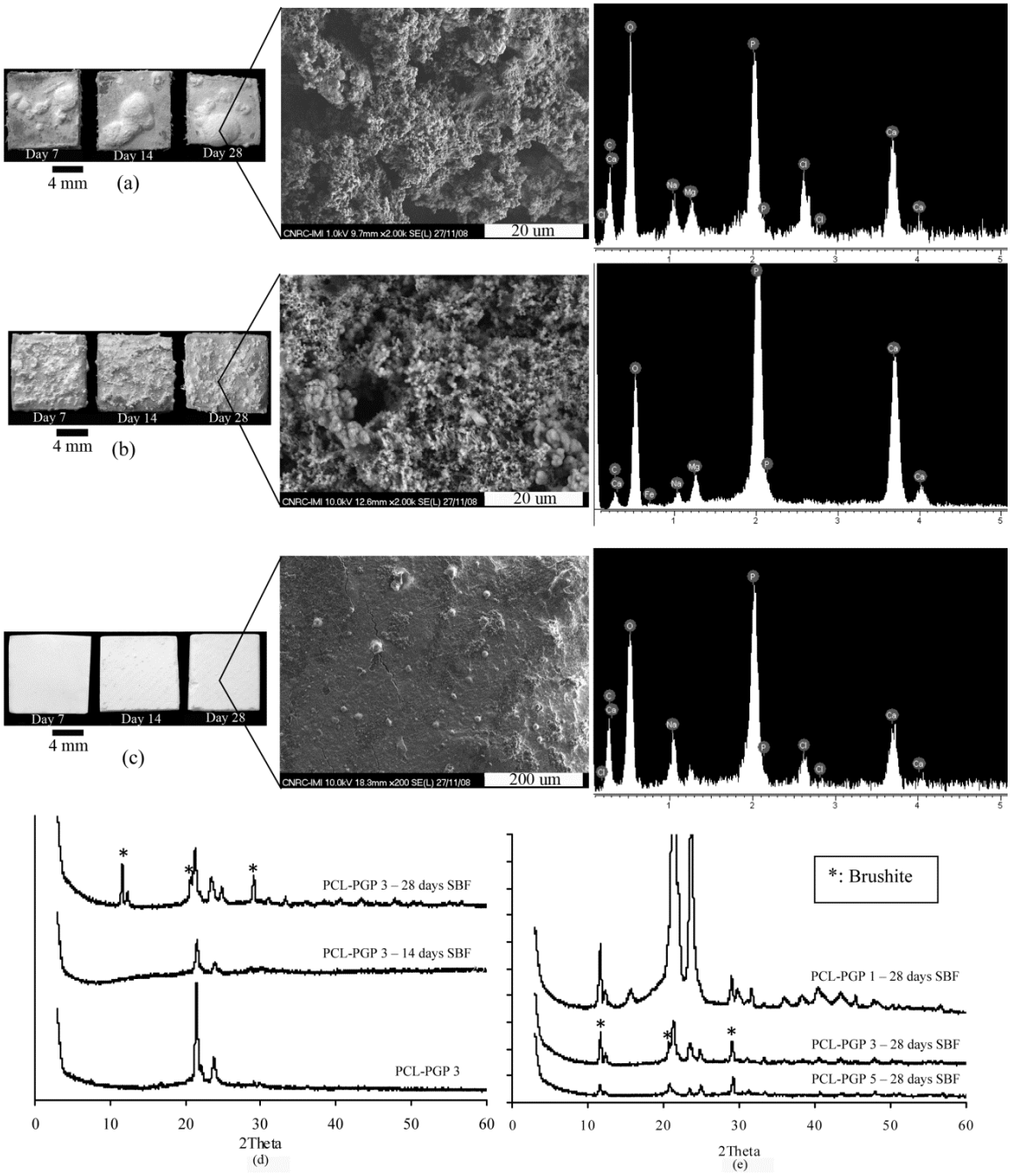

Figure 4.7 Analyses of the precipitates formed on PCL-PGP composites on conditioning in SBF. Images on days 7, 14 and 28, SEM micrographs and EDS spectra on day 28 of (a) PCL-PGP 5, (b) PCL-PGP 3, and (c) PCL-PGP 1. XRD patterns of (d) PCL-PGP 3 as made and on days 14 and 28 in SBF and (e) PCL-PGP 5, PCL-PGP 3 and PCL-PGP 1 after 28 days in SBF.

4.5. Discussion

In this study, particulates of two different PG formulations were incorporated into PCL to potentially produce biodegradable composites of tailored properties for their intended applications in bone augmentation and regeneration. While the reinforcement was kept at 40 vol.%, the glass composition was varied between two ternary based formulations ranging from a high content of SiO_2 to a high content of Fe_2O_3. PG glasses are soluble in aqueous media and upon dissolution can deposit calcium phosphates (depending on formulation) that may prove to be bioactive. However, to achieve such a goal, solubility and its effect on composite properties, e.g. structure and mechanics, must be tailored. The ultimate challenge in bone regeneration is a balance between the rate of tissue growth and that of biomaterial degradation. Therefore, by incorporating two different PG formulations with varying solubilities in a degradable polymer matrix, degradable composites with diverse properties could be produced. By doping PG glasses with Fe, cross-linking between the glass polyphosphate chains is strengthened [99, 119], resulting in a higher glass stability (and low solubility). On the other hand, Si can break down the phosphate glass network, leading to higher solubility [13].

Ageing in DW showed that the rate of weight loss of the composites was dependent on Si10 content. As previously reported by Ahmed *et al.* [112], the release rates of PO_4^{3-} and Ca^{2+} ions were in line with the rate of glass dissolution. While Si^{4+} release is dependent on Si10, interestingly, Fe^{3+} showed a similar dependency. The latter can be explained by the dependence of the rate of ion release on water uptake. With increasing Si10 content, water ingress led to porosity and greater exposure of Fe10 glass particle to water, leading to their dissolution and an increase in Fe^{3+} release. The inclusion of PGPs, which can be of high surface energy, leads to ingress of water, particularly at the filler matrix interface. In the case of PCL-PGP 5, Fe^{3+} release was delayed and coincided with a weight gain in these composites by day 4, indicating the two simultaneous mechanisms: water uptake occurring in the matrix and at the filler-matrix interface with eventual dissolution of PGP resulting in weight loss. Since the solubility of Fe10 glasses is relatively low, weight gain is dominant at early time points. Once the polymer matrix is saturated, weight loss becomes predominant due to glass dissolution [190]. This initial weight gain will be associated with slight dimensional

changes (although not measured here), which is an important consideration in the development of biomaterials.

As a consequence of higher solubility, a rapid reduction in pH was observed in PCL-PGP composites containing Si10. The higher release rate of the phosphate species led to an acidic medium through the formation of phosphoric acid [118, 190]. However, by substituting a Fe10 PGP for the Si10 PGP, the rate of release of phosphate species and pH change was reduced. Rapid changes in pH of the medium due to the PGP dissolution can potentially affect normal proliferation and differentiation of osteogenic cells and may even lead to cell death [23]. Indeed, the significant drop in pH associated with the degradation by-products poses potential cytotoxic issues that need to be addressed. Nevertheless, the modulation effect of reinforcement blends may be translated into more durable quaternary based glasses.

In Fe10 containing composites, glass particles were still present on day 56 in DW. Thus, in composites containing blended glass formulations, pores, formed by rapid dissolution of the Si10 PGP and remnants Fe10 PGP were observed. By controlling the initial glass particle size and their dissolution, defined pore sizes could be created. one advantage of such a structure, *in vivo*, would be that if the pores were designed to be interconnected, an increase in the potential for nutrient and oxygen perfusion and cell migration and growth would be achieved, while favourable ionic species would still be released. In addition, the newly formed porous composite maintained its mechanical properties for longer time periods. In addition, the time-dependent porosities generated by PGP dissolution may also contribute to further controlled porosities within pre-fabricated foamed scaffolds. The generation of these new pores would depend on glass chemistry, size and aspect ratio. The relatively slow degradation rate of PCL ensures that the architectural support that accommodates cell functionalities such as extra cellular matrix production and its mineralization is maintained.

Flexural mechanical analyses were performed to measure the mechanical properties of the various composites, initially and after ageing in PBS. Initially, there was no significant change in the flexural strength of the composites relative to neat PCL except for the PCL-PGP composites containing Si10. On the other hand, the Young's modulus of the PCL-PGP composites was significantly higher than that of PCL, which

increased with increasing Si10 PGP content. Ahmed *et al.* [111] studied the flexural properties of PCL reinforced with binary PG fibres ($50P_2O_5$-50CaO) and showed that there was no significant change in strength. However, the modulus displayed a five-fold increase from 0.5 to 2.4 GPa at 18 vol.%. Previously, Georgiou *et al.* [190] demonstrated a significant increase in the storage modulus of PLA composites incorporating PGP at 20 wt.%. It is worth mentioning that the ultimate compressive strength of trabecular bone from human mandibles ranges from 0.22 to 10.44 MPa [41]. The strength values for vertebra, tibia and femur range from 0.85 to 5.83 MPa, with modulus values in the range 1-3.2 GPa [42]. The mean jaw bone modulus of elasticity in bending varies from 3.93 to 5.53 GPa, and the failure strain from 3.0% to 4.1 % [252]. While the ductility of PCL at ambient and physiological temperatures gives the material a low modulus, since it is above its glass transition temperature, it is interesting to note that the initial values of both the flexural strength and modulus of the composites were within the range of trabecular bone (approximately 20 MPa and 3 GPa for strength and modulus, respectively). Current work by the authors is considering alternative biodegradable α-hydroxy acid ester polymers such as poly($_{D,L}$-lactides) that are less ductile than PCL at physiological temperature.

In this study, the increase in modulus was accompanied by a significant decrease in the strain at maximum stress. These effects indicated a higher level of particle-matrix interaction that resulted in more stress transfer between the particles and the matrix, thus leading to a higher modulus and reduced matrix ductility in the vicinity of the particles with lower strain at maximum stress. Given that all inclusions were at 40 vol.%, it was hypothesised that an interfacial interaction between PGP and PCL occurred during their processing, which increased with increasing Si10 content. It has previously been reported that SGs [188] can cause polyester chain scission (reduction in M_w) when processed at elevated temperatures. In this study, PCL M_w determination revealed similar results, with a dramatic decrease in M_w with increasing PGP Si10 content, which was not demonstrated with PGP with a high Fe10 content. In turn, this affected the mechanical properties of the as prepared composites [188, 253, 254]. Ageing of the composites showed no significant change in PCL M_w, thus confirming that the changes were due to the glass particle dissolution.

As the change in weight in real time is a consequence of water uptake and glass dissolution, the mechanical behaviour of the composites in the wet state may be more representative of the *in vivo* environment. In this study, however, the changes in mechanical properties due to PGP dissolution were carried out in dry state, in order to eliminate the additional plasticising effect of water uptake. Ageing of PCL-PGP containing Si10 in PBS caused a dramatic decrease in its mechanical properties. The rate of decrease was considerably less in composites of increasing Fe10 content. This was in line with the weight loss behaviour and the potential for pore generation due to Si10 dissolution. Since the solubility of Fe10 was relatively low, materials with higher Fe10 contents retained their mechanical properties for longer periods of time. These differences support the hypothesis that the mechanical properties of these composites may be controlled by altering the PGP blend. The relative changes in the magnitude of reduction in the mechanical properties of the various composites induced by reinforcement with different PGP formulations suggest that the properties of these composites may be controlled and optimized for bone regeneration, in particular by using other formulations that have a slower rate of dissolution.

ATR-FTIR on the composites revealed an increase in the fractional absorbance change at 1728 cm^{-1}, *i.e.* a decrease in the absorbance of the C=O bond peak, in the presence of the Si10, while no such reduction occurred in neat PCL or PCL-PGP 5 (supplementary data). Increasing the amount of Si10 content in the composites increased the extent of these changes, which occurred at a faster rate. Moreover, formation of a carboxylate peak (1634 cm^{-1}) became evident in the presence of Si10 and did not occur with neat PCL and predominantly Fe10 composites. This and accompanying changes in the ester data suggest that Si containing glasses reacted with ester bonds due to the high processing temperatures involved. This reaction breaks down the ester bonds and leads to the formation of carboxylate by-products, resulting in the formation of lower molecular weight polymers, as was proposed by Blaker *et al.* [188] for SGs (e.g. Bioglass®). The incorporation of silica into PGP may lead to an increase in the presence of hydroxyl groups at the glass surface. These in turn react with the ester linking group in PCL at the processing temperature of the composite (with PCL being in the melt), leading to carboxylate salts such as calcium carboxylate. The carboxylate peaks indicate the

potential for PCL chain scission and the formation of oligomeric fragments, as confirmed by the reduction in matrix molecular weight.

Weight loss in SBF displayed a similar trend to that in DW, however, to a lower extent due to the presence of ions in SBF. The pH of SBF fell to below pH 4, which was controlled by Fe10 content (i.e. the higher the Fe10 content the lower the dissolution). SBF conditioning resulted in the formation of brushite on the surface of PCL-PGP 3 by day 28. According to the calcium phosphate phase diagram, several calcium phosphates can form with well-defined solubilities, among which only one can be most stable [255]. Therefore, in true thermodynamic equilibrium, phases with greater solubility exist in metastable equilibrium. Ultimately, the metastable phosphates will transform to stable compounds via intermediate phases. The composition of the solution is fixed at a singular point where the isotherms for two phosphates cross over and the position at which the solubility of the salts interchange. The singular point for brushite ($CaHPO_4.2H_2O$) and HA [$Ca_{10}(PO_4)_6(OH)_2$] is at pH 4.3 at 25 °C [255]. Brushite and HA, respectively, are stable below and above this pH [255].

It is recognised that PGs have a lower *Bioactivity Index* compared with SGs such as Bioglass®. Previously, Franks *et al.* [98] suggested that formation of a brushite precipitate is an indication of the bioactivity of PG, with brushite a possible precursor to the formation of apatite [98, 256]. Abou Neel *et al.* [28] showed that in the case of PG based on $50P_2O_5$-(15-20)Na_2O-30CaO-(0-5mol%)TiO_2, no evidence of apatite formation was observed on day 14 in SBF, despite favourable cell response and gene up-regulation. In this study, evidence of brushite formation was only observed on day 28 for mixed glass formulations, indicating that longer times were required for calcium phosphate precipitate formation on the surface of these glasses, as in the case of PCL-PGP 3. PCL-PGP 1 showed no precipitation, which was probably due to the very rapid dissolution of Si10, with a dramatic increase in the amount and rate of PO_4^{3-} ion release in the first 24 h. In contrast, the rate of dissolution PCL-PGP 5 was very slow. Therefore, the use of mixed glass formulations could control the amount and rate of ion release, with a significant effect on the potential for calcium phosphate precipitation. The rate of resorption and associated ion release of bone graft substitutes has been highlighted as an important factor in their successful application [257]. Future studies will focus on the

biological properties of the composites of mixed reinforcements through their interactions with osteoblastic cells.

4.6. Conclusions

The effect of mixed phosphate glass fillers with different formulations on the properties of PCL composites was investigated. Whilst no weight loss was observed for PCL alone over the course of this study, incorporating high and low solubility phosphate-based glass formulations into a composite resulted in a wide range of weight loss rates, from very high for 40%Si10-0%Fe10 to very low for 0%Si10-40%Fe10. Blends of Si10 and Fe10 showed intermediate weight loss rates. As a consequence, high Si10 PGP led to the formation of porosities while high Fe10 PGP remained in the composites for longer time periods. A correlation was observed between the Si10 content and ions released, with the release of PO_4^{3-}, Ca^{2+}, Fe^{3+}, and Si^{4+} ions increasing significantly with increasing Si10 content.

Composite mechanical properties were also affected by glass formulation, both initially and as a function of time in PBS. An increase in Si10 content led to a reaction between PG and PCL matrix when processed at high temperature, causing chain scission and a concomitant reduction in PCL molecular weight. These effects resulted in an initial increase in the Young's modulus and a reduction in the flexural strength and strain values of the composites with increasing Si10 content. Reinforcement with mixed glass formulations resulted in a slower decrease in mechanical properties on ageing in PBS. On day 28 in SBF, brushite formation was indicated on the surfaces of the composites of mixed glass formulations. Therefore, incorporation of mixed phosphate glass fillers within degradable polymer matrices may be effective in tailoring the properties required for bone repair and regeneration.

4.7. Acknowledgements

This work was funded by the Canadian Natural Sciences and Engineering Research Council, Le Fonds Québécois de la Recherche sur la Nature et les Technologies, a Hatch Faculty Fellowship and the Canadian Foundation for Innovation: Leaders Opportunity Fund. Funding for Maziar Shah Mohammadi and Benedetto Marelli

was also partly supported by McGill Engineering Doctoral Awards and the Werner Group, respectively. The authors thank Monique Riendeau, Saurav Mohapatra, Christoph Stähli, Jason Betram and Hye-Lim Choi for their assistance in this work. Milan Maric's group in the Department of Chemical Engineering, McGill University is thanked for GPC analysis. The authors also thank the Composites Research Group at the University of Nottingham for their support. Showan Nazhat is a member of the Centre for Bone and Periodontal Research.

4.8. Appendix: Supplementary data

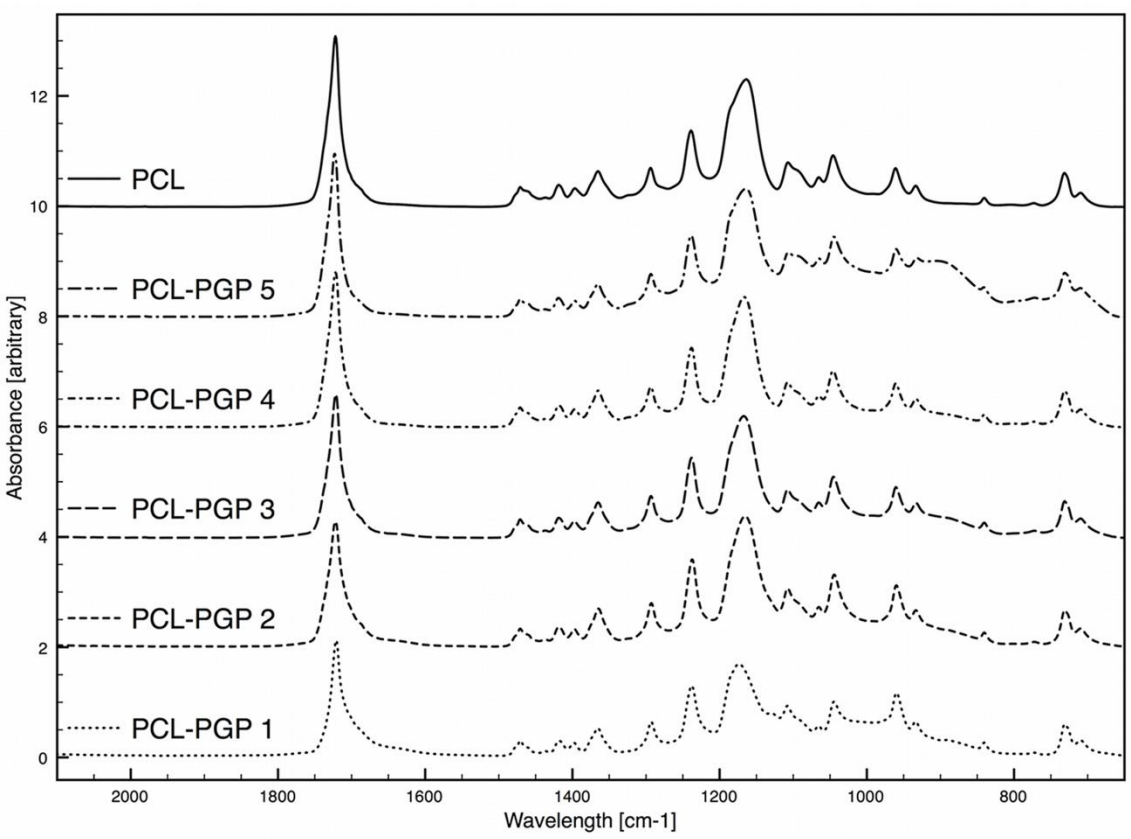

Supplementary Figure 4.1 ATR-FTIR spectra of as-processed PCL and PCL-PGP composites.

CHAPTER 5

Si AND Fe DOPED CALCIUM PHOSPHATE GLASS FIBRES REINFORCED POLYCAPROLACTONE BONE ANALOGOUS COMPOSITES

Along with the advantageous properties of phosphate-based glasses (PGs), such as controllable degradation, when compared to silicate-based glasses (SGs) or other calcium phosphates such as hydroxyapatite, PGs also have the ability to be easily drawn into fibres due to their polymeric structure. Phosphate-based glass fibres (PGFs) could result in a mechanical reinforcing effect when incorporated into a polymer matrix. Furthermore, the degradation of PGFs would result in the formation of channels thus facilitating the oxygen and nutrients perfusion as well as cells migration within the structure.

In the previous study, blends of ternary PG formulations containing SiO_2 or Fe_2O_3 were incorporated into PCL. The results suggested that the composite properties; e.g. weight loss, ion release, bioactivity and mechanical properties, could be modulated by using mixed PG formulation. However, this largely depended on the incorporated amount of each composition. For example, the composite weight loss and ions release increased significantly with increasing amounts of PG containing SiO_2. Composite mechanical

properties were also affected by glass formulation, both initially and as a function of time in phosphate buffered saline. An increase in PG doped SiO_2 content, led to a reaction between PG and PCL matrix when processed at high temperature, causing chain scission and a concomitant reduction in matrix molecular weight.

With the aim of developing a degradable bone analogous composite, in the present study, the effect of doping calcium containing PGs with Si and Fe on the properties of the glass alone and when incorporated into PCL as randomly orientated fibres was investigated. The objectives were to: (i) investigate the effect of Si and Fe doping on PG properties alone when incorporated into PCL for bone repair and regeneration applications. (ii) investigate the effect of PG composition (ternary and quaternary, instead of only ternary in Chapter 4) as well as surface area (fibres instead of particulates) on the composite properties. Quaternary PGs, doped with metal oxides, are more stable compared to the ternary formulation leading to more controlled degradation. To investigate these objectives, a series of parameters were used to characterise the properties of the various composites, as produced and as a function of degradation time. The capacity for calcium phosphate formation and pre-osteoblastic cell cytocompatibility were also investigated.

A manuscript based upon these research findings has been published in the peer-reviewed journal, *Acta Biomaterialia*.

Effect of Si and Fe doping on calcium phosphate glass fibre reinforced polycaprolactone bone analogous composites

Maziar Shah Mohammadi[a], Ifty Ahmed[b], Naser Muja[a], Sergio Almeida[a], Christopher D Rudd[b], Martin N. Bureau[c,a], Showan N. Nazhat[a]

[a] *Department of Mining and Materials Engineering, McGill University, Montreal, QC, H3A 2B2, Canada*

[b] *Division of Mechanics, Materials and Structures, University Park Campus, University of Nottingham, NG7 2RD, U.K.*

[c] *Industrial Materials Institute, National Research Council Canada, QC, J4B 6Y4, Canada*

Key words: Phosphate-based glass fibres, biodegradable composites, bioactivity, pre-osteoblast, tissue engineering

5.1. Abstract

Reinforcing biodegradable polymers with phosphate-based glass fibres (PGFs) is of interest for bone repair and regeneration. In addition to increasing the mechanical properties, PGFs can also release bioinorganics as they are water soluble, a property that may be controllably translated into a fully degradable composite. Herein, the effect of Si and Fe on the solubility of calcium containing PGs in the system ($50P_2O_5$-40CaO-(10-x)SiO_2-xFe_2O_3, where x = 0, 5 and 10 mol. %) were investigated. By replacing SiO_2 with Fe_2O_3, there was an increase in the glass transition temperature and density of the PGs suggesting greater cross-linking of the phosphate chains. This significantly reduced the dissolution rates of degradation and ion release.

Two PG formulations; $50P_2O_5$-40CaO-$10Fe_2O_3$ (Fe10) and $50P_2O_5$-40CaO-$5Fe_2O_3$-$5SiO_2$ (Fe5Si5), were melt drawn into fibres and randomly incorporated into polycaprolactone (PCL). Initially, the flexural strength and modulus significantly increased with PGF incorporation. In deionised water, PCL-Fe5Si5 displayed a significantly greater weight loss and ion release compared to PCL-Fe10. In simulated body fluid, brushite was formed only on the surface of PCL-Fe5Si5. Dynamic mechanical analysis in phosphate buffered saline (PBS) at 37 °C revealed that PCL-Fe10 storage modulus (*E'*) was unchanged up to day 7, whereas the onset of PCL-Fe5Si5 *E'* decrease occurred at day 4. At longer term ageing in PBS, PCL-Fe5Si5 flexural strength and modulus decreased significantly. MC3T3-E1 pre-osteoblasts seeded onto PCL-PGFs grew for up to day 7 in culture. PGF can be used to control the properties of biodegradable composites for potential applications as bone fracture fixation devices.

5.2. Introduction

Composites based on biodegradable polymers and bioactive ceramics have been extensively considered as bone analogous materials [8]. As alternatives to metals, they present the potential for reduced stress shielding, and would negate additional surgical intervention [9]. Degradable synthetic polymers such as poly(α-hydroxy-acid esters), e.g. poly(lactic acid) (PLA), poly(glycolic acid) (PGA) and their copolymers (PLGA) [183], as well as polycaprolactone (PCL) [250] have been considered as matrices. Aside from their lack of bioactivity, these polymers do not have the capacity to withstand certain load bearing conditions. In order to overcome these limitations, bioactive calcium phosphate particulates have been incorporated into these polymeric matrices [190, 258].

It is well recognised that the addition of bioactive glasses and ceramics into a polymeric matrix should improve the properties of the composites. However, while particulate composites are easily manufactured, fibre reinforced composites have been shown to result in a greater increase in their mechanical properties. For example, Jiang *et al.* [186] investigated bioactive glass fibre incorporated PCL and showed an improvement in the flexural strength and modulus of the composites. Foams of hydroxyapatite (HA) short fibre reinforced PLGA have also shown enhanced compressive yield strength [187]. Furthermore, since the composition, content and solubility of the filler component are parameters that can influence composite properties, their tailoring is essential for bone repair and regeneration. However, not all calcium phosphate materials (e.g. silicate-based glasses or HA) provide controlled solubility properties with either the bone regeneration rate or degradation of the matrix.

Phosphate-based glasses (PGs) may be a potential alternative inorganic phase for the purpose of producing composites of controllable degradation [11, 12]. The solubility of PGs can be predicted and controlled through their chemistry [13, 14, 98]. In addition, their structural polymeric nature allows them to be easily drawn into fibres [19], which could result in a mechanical reinforcing effect when incorporated into a polymer matrix. It has been shown that PCL-PGF ($50P_2O_5$-50CaO) composites yielded flexural strength and modulus values approaching 30 MPa and 2.5 GPa, respectively, which were comparable to human trabecular bone [111]. Furthermore, the high surface area to volume ratio of fibres can significantly affect the glass fibre degradation and release of

bioactive ions, which is critical in the biological properties of the composites. PGF reinforced poly(ε-caprolactone/L-lactide) and poly(ortho ester) have been shown to be non-toxic composites with no inflammatory response [196]. Implanted PGF-PCL was also well tolerated with minimal inflammation [197].

In the aim to develop a degradable bone analogous composite, this study investigated the effect of doping calcium containing PGs with Si and Fe on the properties of the glass alone and when incorporated into the PCL matrix as randomly orientated fibres. Fe and Si have been reported to have contrasting roles in PGs. The addition of Fe_2O_3 has been hypothesised to strengthen the cross-linking between the glass polyphosphate chains, which results in higher glass stability [119]. In contrast, Si disrupts the PG network, leading to lower glass stability, thus higher degradation rates [13]. Herein, a series of parameters were used to characterise the properties of the various composites, as produced and as a function of degradation time. The capacity for calcium phosphate formation and pre-osteoblastic cytocompatibility were also investigated.

5.3. Experimental

5.3.1. Phosphate based glass production

Three melt derived PG compositions (Table 5.1) were prepared using P_2O_5, $CaHPO_4$, Fe_2O_3, and SiO_2 (Sigma Aldrich) as starting materials. The precursors were dry blended, poured into a Pt/10%Rh crucible (Birmingham Metal Company), and heated to 400 °C in order to remove moisture. The crucible was then transferred to a second furnace and melted at 1150 °C for 90 min. The molten glass was then cast into a cylindrical shape mould (10 mm in diameter), annealed at 350 °C for 1 h to remove any residual stresses and cut into discs, or poured onto a steel plate and cooled to room temperature to make the bulk glass.

Table 5.1 Glass compositions and coding

Glass Code	Components (mol.%)			
	P_2O_5	CaO	SiO_2	Fe_2O_3
Si10	50	40	10	-
Fe5Si5	50	40	5	5
Fe10	50	40	0	10

Continuous fibres were produced utilising a melt-draw spinning methodology via a specially built in-house facility for the following formulations; $50P_2O_5$-40CaO-$10Fe_2O_3$ (Fe10) and $50P_2O_5$-40CaO-$5Fe_2O_3$-$5SiO_2$ (Fe5Si5). A Pt crucible containing the glass formulation was heated until glass melt flow was initiated through a nozzle at the base of the crucible. The temperature was then adjusted to obtain the appropriate viscosity of the glass. PGFs were guided onto a rotating drum at 1600 rpm to produce fibres in the range of ~10 - 20 μm diameter. The fibres were then removed from the drum and annealed to alleviate any processing induced stresses, which has been shown to increase their resistance to degradation [19]. The heat treatment consisted of heating the fibres up to 200 °C at 20 °C.min^{-1}, then heating to 505 °C at 1 °C.min^{-1} and holding for 90 min, cooling to 300 °C at 0.25 °C.min^{-1} and finally cooling to room temperature at 1 °C.min^{-1}. Once annealed overnight, the fibres were cut to lengths of 10 mm.

5.3.2. PCL-PGF composite production

PGFs (3 g of 10 mm lengths) were dispersed into a 4 L solution of distilled water and Cellosize (Univar Ltd) for 10 min. The fibre-cellulose solution was then poured into a second container consisting of a straining mesh. After ensuring that all fibre aggregates were evenly dispersed, the mesh strainer was extracted from the solution. The resulting random fibre mats were then rinsed with distilled water to remove any residual binder and vacuum-dried at 50°C overnight. PCL pellets (5g, Average M_w ~ 65000, Sigma Aldrich) were heated to 100 °C and pressed at 3 bar for 30 s (J.R. Dare Ltd., heated press) to produce PCL films of ~0.2 mm thickness. The films were cooled under pressure to room temperature using a cold press (Daniels Upstroke Press). Six dried random fibre mats were placed in an alternating sequence with seven PCL films into a metal shim, shielded by two poly(tetrafluoroethylene) sheets, and placed in the hot press (J.R. Dare Ltd) at 100 °C and maintained for 30 min to allow the PCL to melt, then pressed for 30 min at 38 bar and finally cooled in a second press (Daniels Upstroke) to room temperature for 30 min, at 38 bar. Using this procedure, PCL-PGF composites with ~18% fibre volume fraction were produced (Table 5.2). The volume fractions of the composites were calculated using the matrix burn-off method (ASTM D2584-94 [259]). A PCL only

plaque (also 1.6 mm thick) was also produced by melt pressing PCL for 30 min at 38 bar and cooling in the cold press to room temperature for a further 30 min at 38 bar.

Table 5.2 Composite compositions and coding

Composite code	Components (vol.%)		
	PCL	Fe10	Fe5Si5
PCL	100	0	0
PCL-Fe10	82	18	0
PCL-Fe5Si5	82	0	18

5.3.3 Phosphate glass characterization

5.3.3.1. Differential thermal analysis

Differential thermal analysis (DTA, TA Instruments SDT Q600) was conducted to identify the glass transition (T_g), crystallisation (T_c) and melting temperatures (T_m) of the glasses investigated. Analysis was carried out on powdered glass (50 mg) from 25 to 1200 °C at a heating rate of 10 °C.min^{-1} under nitrogen purge. An empty crucible was used as a reference.

5.3.3.2. Density measurements

Density measurements were carried out using Archimedes' principle (n=3). An analytical balance (Mettler Toledo, AB265-S/FACT) with an attached density kit was used. Due to the soluble nature of the PGs in aqueous media, ethanol was used as the submersion liquid for these measurements.

5.3.3.3. Ageing in deionised water

PG discs (Φ=10 mm, n=3) were placed into polypropylene vials containing 10 ml of ultra-pure deionised water (DW, 18.2 MΩ cm resistivity) and incubated for up to 28 days at 37 °C. Ion release, weight loss, and pH of the ageing environment were measured at 6, 24, 72, 168, 336, 504 and 672 hours.

Individual solutions were analysed using an inductively coupled plasma/optical emission spectrophotometer (ICP-OES) (Thermo Jarrell Ash – TRACE SCAN) in order to quantify the released cations (Ca^{2+}, Si^{4+} and Fe^{3+}) as well as the total amount of

phosphate anions. Nitric acid (4%) was added to all samples in order to stabilise the iron ions in their higher oxidation state (3+). Standard solutions (also containing 4% nitric acid) were prepared by serially diluting certified standards to 100, 50, 10, 5 and 1 ppm. The data was plotted as the cumulative ion release as a function of time.

The weight loss of the glass was investigated by removing the specimens from DW, blot drying, weighing and replacing in fresh DW. The surface area of each glass disc was calculated at each time point by measuring the dimensions using a calliper (DURATOOL DC150) as the weight loss rate can be affected by the surface area. The data was plotted as weight loss/surface area (SA) as a function of time in order to calculate the weight loss rate as $mg.mm^{-2}.h^{-1}$.

The pH of the deionised water was also measured using a pH meter (Accumet Excel 20, Fisher) at each time point.

5.3.4. Characterisation of the PCL-PGF composites

5.3.4.1. Ageing in deionised water

PCL-PGF composites were aged in DW for up to 56 days by placing 10×10×1.6 mm^3 specimens (n=3) into vials containing 25 ml of ultra-pure deionised water (18.2 MΩ.cm resistivity) and incubating at 37 °C. Ion release, composite weight loss, and pH of the ageing environment were measured at 14 different time points 0, 2, 4, 8, 24, 48, 96, 168, 336, 504, 672, 840, 1008, and 1344 h.

Anions and cations released via composite degradation were measured using ion chromatography (IC) and atomic absorption (AA), respectively. IC (Dionex, DX-100 Ion chromatograph) was used in order to measure phosphate anion (PO_4^{3-}) release. An Ionpac AS14 anion exchange column was used to elute the polyphosphates. An eluent of 3.5 mM Na_2CO_3/0.1 mM $NaHCO_3$ was used with a flow rate of 0.1 ml min^{-1}. The sample run time was 15 min. Sodium phosphate tribasic (Na_3PO_4) (Sigma, Canada) was used to prepare standard solutions. A 1000 ppm working solution was prepared from which serially diluted 10, 20, and 50 ppm standard solutions were obtained. AA (VARIAN AA240FS) was used to investigate the release of Ca^{2+}, Fe^{3+}, and Si^{4+} cations. The instrument was calibrated using certified AA standard solutions.

The weight change of the composites was investigated by removing the specimens from DW, blot drying, weighing and replacing in fresh deionised water. Weight loss was measured in terms of percentage of original weight. The final dry weight at day 56 was measured by first incubating the specimens for 6 days at 37 °C until an equilibrium weight was reached.

The pH of the deionised water was also measured using a pH meter (Accumet Excel 20, Fisher) at each time point.

5.3.4.2. Morphological investigations

Scanning electron microscopy (SEM, JEOL JSM 6100, Tokyo, Japan and Hitachi S-3000N) was used to investigate the morphology of the composites before and after ageing in DW. The samples were cryo-fractured and the resulting fracture surfaces were sputter-coated with gold/palladium before being analysed using a back scattered electron mode with accelerating voltages of 10 kV.

5.3.4.3. Composites conditioning in simulated body fluid

Three specimens ($10\times10\times1.6$ mm^3) of each composite were placed into vials containing 60 ml of simulated body fluid (SBF) and incubated at 37 °C. The SBF solution was prepared according to Kokubo *et al.* [251] and replenished every 3 days. Briefly, the SBF was prepared by dissolving respective amounts of reagent chemicals including NaCl, $NaHCO_3$, KCl, $K_2HPO_4.3H_2O$, $MgCl_2.6H_2O$, $CaCl_2$, and Na_2SO_4 into DW to generate ionic concentration of Na^+: 142, K^+: 5 , Mg^{2+}: 1.5, Ca^{2+}: 2.5, Cl^-: 147.8, HCO_3^-: 4.2, HPO_4^{2-}: 1, SO_4^{2-}: 0.5 (in mM) and pH: 7.4. The pH was adjusted to physiological pH (7.4) using 1.0M HCl and buffered by Tris. The containers were removed from the incubator at days 7, 14, and 28. Precipitates formed on the surface of the composites were analysed using SEM (Hitachi S-4700) and X-Ray powder diffraction (XRD, Bruker D8). Composite weight change and SBF pH were also measured at regular time intervals.

5.3.4.4. Composite initial mechanical and viscoelastic properties and as a function in PBS

Three-point bend flexural mechanical analysis was used to measure the mechanical properties of the composites. The effect of PG formulation on composite mechanical properties was investigated through changes in Young's modulus, flexural strength and strain at maximum stress. Tests were performed on as produced and PBS conditioned specimens stored at 37 °C and tested at days 7, 14, and 28. Mechanical testing was carried out on specimens in the dry state and the extent of their weight loss after PBS ageing was measured. Weight loss upon PBS conditioning was measured prior to mechanical testing, by first drying the specimens in an incubator (37 °C). Specimen weight was repeatedly monitored for up to six days until equilibrium. Three independent specimens were tested with a cross-head speed of 1 mm/min using a 1 kN load cell in accordance to ASTM D 790-95a:1996 (aspect ratio = 16) in an Instron mechanical testing instrument 5582 (Instron Ltd).

Dynamic Mechanical analysis (DMA 8000, Perkin-Elmer) was performed to evaluate the changes in storage modulus (E') of PCL-PGF composites as a function of temperature. Rectangular specimens (n=3, 1.5×4×30 mm^3) were analysed from -100 to 50 °C at a heating rate of 2 °C/min. A dynamic strain control of 0.003% was applied. DMA tests were also conducted whilst composite specimens were immersed in a PBS bath at 37 ^oC for up to 7 days. The applied dynamic strain in this experiment was 0.0001% for both composites. The test could not be conducted for neat PCL due to the soft rubbery nature of PCL at 37 ^oC being unsuitable for flexural analysis.

5.3.4.5. Cytocompatibility study: Cell culture, seeding, and detection of cell viability

Murine MC3T3-E1 pre-osteoblasts (subclone 14) from American Type Culture Collection (CRL-2594 ATCC) were purchased from Cedarlane Labs and maintained in alpha modified Minimum Essential Medium (α-MEM, HyClone Laboratories Inc.) supplemented with 2 mM L-Glutamine (Invitrogen), 10% Newborn Calf Serum (HyClone Laboratories Inc.) and 1% penicillin/streptomycin (Invitrogen) at 37 °C in humidified atmosphere at of 5% CO_2. Prior to cell seeding PCL, PCL-PGF composites (PCL-Fe10 and PCL-Fe5Si5), and glass slide fragments, each with a surface area of 1

cm^2, were disinfected by immersion in absolute EtOH for 2 hrs. Specimens were then transferred to cell growth medium and conditioned overnight in a tissue culture incubator. MC3T3-E1 pre-osteoblasts were detached from tissue culture flasks (0.05% trypsin /0.02% EDTA), collected by centrifugal rotation (80xg, 5 min) and seeded onto PCL and PCL-PGF composites at a density of 1.0×10^4 cells/cm^2. After either 1, 4, or 7 days in cultured cells were detected by confocal laser scanning microscopy (CLSM, LSM 5, Carl Zeiss). To assess cell viability, cells were labelled using 1 mM calcein AM and 0.1 mM ethidium bromide homodimer-1 (LIVE/DEAD®, Invitrogen) in α-MEM for 30 minutes. Opaque materials were gently inverted (i.e. cell growth surface facing the microscope objective) onto a 50 mm Pelco glass bottom Petri dish (Ted Pella Inc., Redding, CA) and fluorescent-labelled cells were imaged using laser excitation (488 and 543 nm laser lines) and a baseline confocal z-stack was acquired at 1 Airy unit using a 20X EC Plan-Neofluar objective (0.5 N.A.). Maximum intensity projections were generated and analyzed using NIH ImageJ v1.43 software.

5.3.4.6. Statistical Analysis

Statistical analysis was performed to test the significance in the difference between two mean values using the Student's *t*-test which was used to determine *p*-values at a significance level of 0.05.

5.4. Results

5.4.1. Phosphate-based glass characterisation

5.4.1.1. Density and thermal analysis

Figure 5.1 shows representative DTA thermograms of the PG formulations. There was an increase in T_g by substituting SiO_2 with Fe_2O_3 in the glass formulation. T_c on the other hand showed no statistically significant differences among the glass composition. Two T_m peaks were visible for all formulations. T_{m1} and T_{m2} values were 889±5, 877±2 and 857±10 °C, and 913±8, 911±1, and 887±24 °C for Si10, Fe5Si5 and Fe10, respectively. There were no statistically significant differences between the T_m values. However, there was a concomitant increase in T_g and density of the glasses with Fe_2O_3 incorporation (Supplementary Figure 5.1).

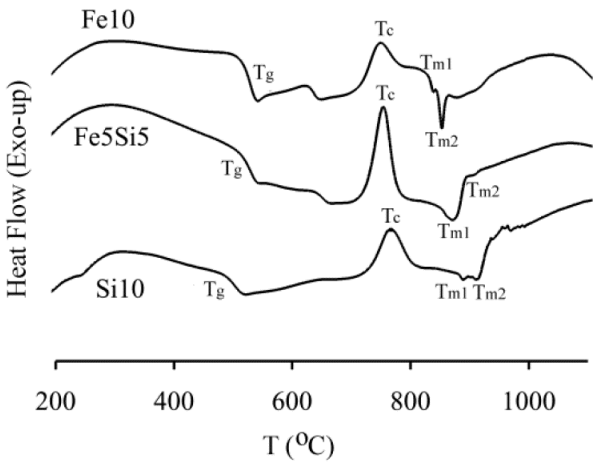

Figure 5.1 Representative DTA thermograms of the PG formulations.

5.4.1.2. Ion release, weight loss, and pH change upon ageing in deionised water

Figure 5.2a shows the total phosphorous release which is apparently in the form of polyphosphates. In the case of Si10 glass, there was a prompt release of phosphorous in solution which decreased significantly (230-fold) when substituting SiO_2 with Fe_2O_3. A similar composition dependent effect was also observed in the case of Ca, Si and Fe ion release as shown in Figures 5.2b, c and d, respectively. It was interesting to note that more Fe ions were released in Fe5Si5 compared to Fe10 due to the higher degradation rate of Fe5Si5. The weight loss of the different glass formulations is illustrated in Figure 5.2e, which also demonstrated a 230-fold reduction in the weight loss rate by substituting SiO_2 with Fe_2O_3. Table 5.3 summarises the ion release and weight loss rates which were linear with time. Reduction in pH compared favourably with solubility and release of phosphate species into the medium which was lower as Fe_2O_3 content increased (Figure 5.2f).

5.4.2. PCL-PGF Composite Characterization

5.4.2.1. Composite ageing in deionised water

5.4.2.1.1. Measurement of ion release

PCL-PGF composites were aged in DW for up to 56 days to determine the extent of ion release due to PG degradation. At day 7 in DW, PO_4^{3-} release was approximately 10-fold higher in PCL-Fe5Si5 when compared to PCL-Fe10 (Figure 5.3a). Ca^{2+} release

showed similar behaviour (Figure 5.3b). In the case of Fe^{3+}, release was greater in PCL-Fe5Si5 than PCL-Fe10 (Figure 5.3c). In contrast to other ion species, which showed a 2 day delay in release, Si^{4+} release occurred within 8 hr (Figure 5.3d). Supplementary Table 1 summarises the ion release rates from the composites, calculated from the linear incline portion of the curves.

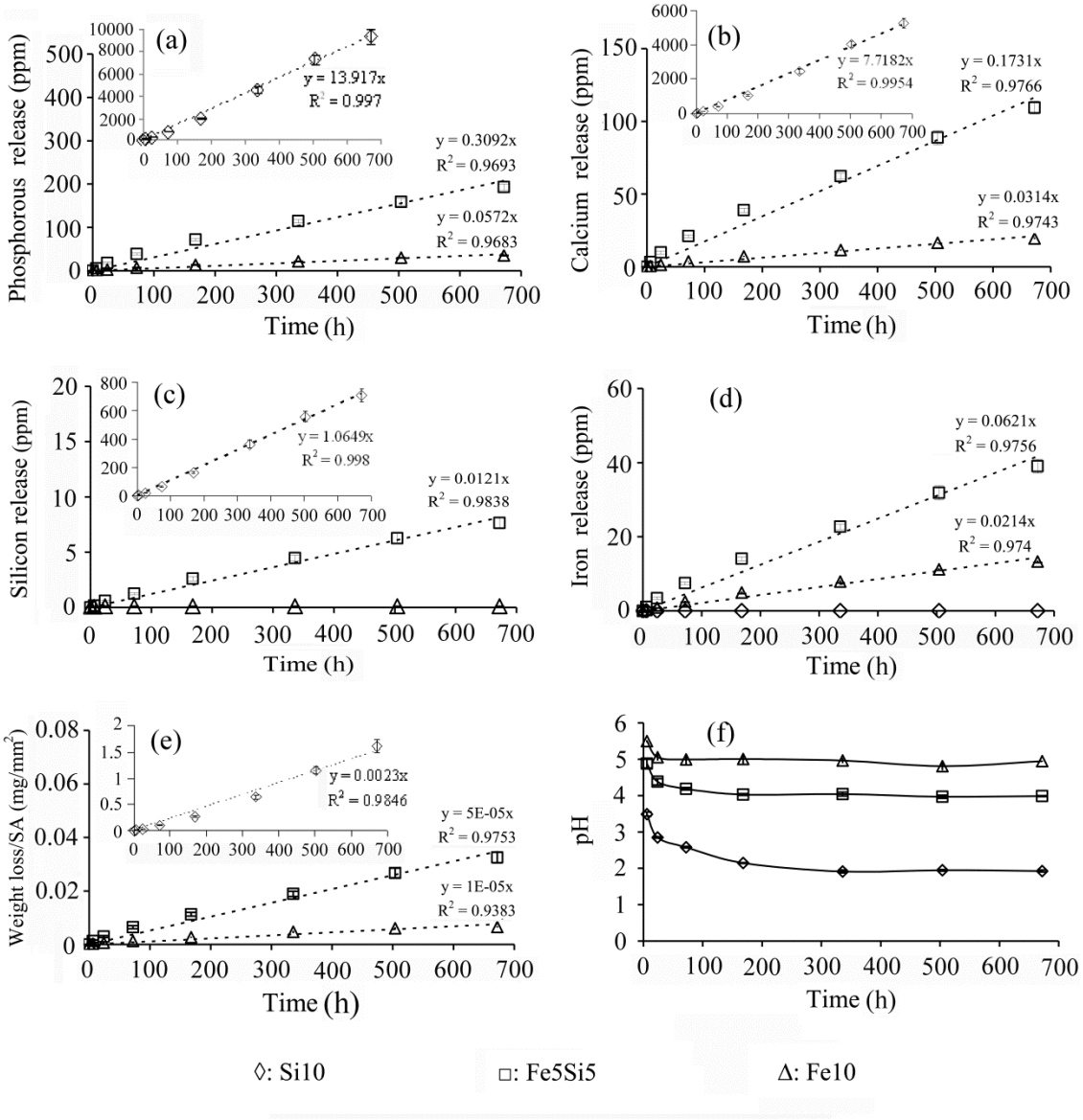

Figure 5.2 Ageing of PGs in DW incubated for up to 28 days at 37 ºC. Cumulative ion release for: (a) total phosphorous, (b) calcium, (c) silicon and (d) iron. (e) Corresponding glass weight loss, and (f) pH change of the immersion environment. Panel insets represent ion release and weight loss for Si10 which was several orders of magnitude greater than Fe5Si5 and Fe10, respectively. The rate of ion release (a-d) and weight loss (e) as well as the linearity over time are indicated by the relative equation and R^2, respectively.

Table 5.3 Cumulative degradation and ion release rates calculated from the slope of the linear fit against time for the PG formulations

Glass code	Degradation ($mg.mm^{-2}.h^{-1}$)	Phosphorous release ($ppm.h^{-1}$)	Ca^{2+} release ($ppm.h^{-1}$)	Si^{4+} release ($ppm.h^{-1}$)	Fe^{3+} release ($ppm.h^{-1}$)
Si10	$23\times10^{-4} \pm 10^{-4}$	13.92 ± 0.94	7.72 ± 0.39	1.06 ± 0.07	-
Fe5Si5	$5\times10^{-5} \pm 3\times10^{-6}$	0.31 ± 0.01	0.17 ± 0.01	$0.01 \pm 8\times10^{-4}$	0.06 ± 0.003
Fe10	$1\times10^{-5} \pm 7\times10^{-7}$	$0.06 \pm 8\times10^{-4}$	$0.03 \pm 9\times10^{-4}$	-	0.02 ± 0.005

5.4.2.1.2. Weight change

Initially in DW, PCL-Fe10 demonstrated a slight weight gain, which was followed by a slow reduction rate (Figure 5.3e). In contrast, PCL-Fe5Si5 showed a much faster weight loss rate between days 4 and 14. Neat PCL demonstrated no weight loss in the entire ageing period. Final dry weight revealed an approximate 9 wt.% loss in PCL-Fe10 in comparison to 73 wt.% for PCL-Fe5Si5 (Table 5.4).

5.4.2.1.3. pH change of deionised water

The pH of DW remained relatively unchanged in the presence of PCL and PCL-Fe10 (Figure 5.3f). In contrast, the pH of DW began to decrease at day 2 exposure to PCL-Fe5Si5, which became increasingly acidic (~pH 3.5) up to day 14. Beyond then, the pH of DW started to recover as the medium was replaced at each time interval.

5.4.2.1.4. Morphological investigation of PCL-PGF composites as-processed and following ageing in deionised water

Figure 5.4a shows SEM micrographs of as prepared PCL-PGF composites at different magnifications as an example of the random fibre distribution within the PCL matrix. At day 56 in DW, both remaining fibres and channel formation attributable to PGF dissolution were observed in PCL-Fe10 (Figure 5.4b). In contract, at the same time point, most of the fibres in PCL-Fe5Si5 had dissolved. Higher magnification images showed residual precipitates within the channels formed (Figure 5.4c).

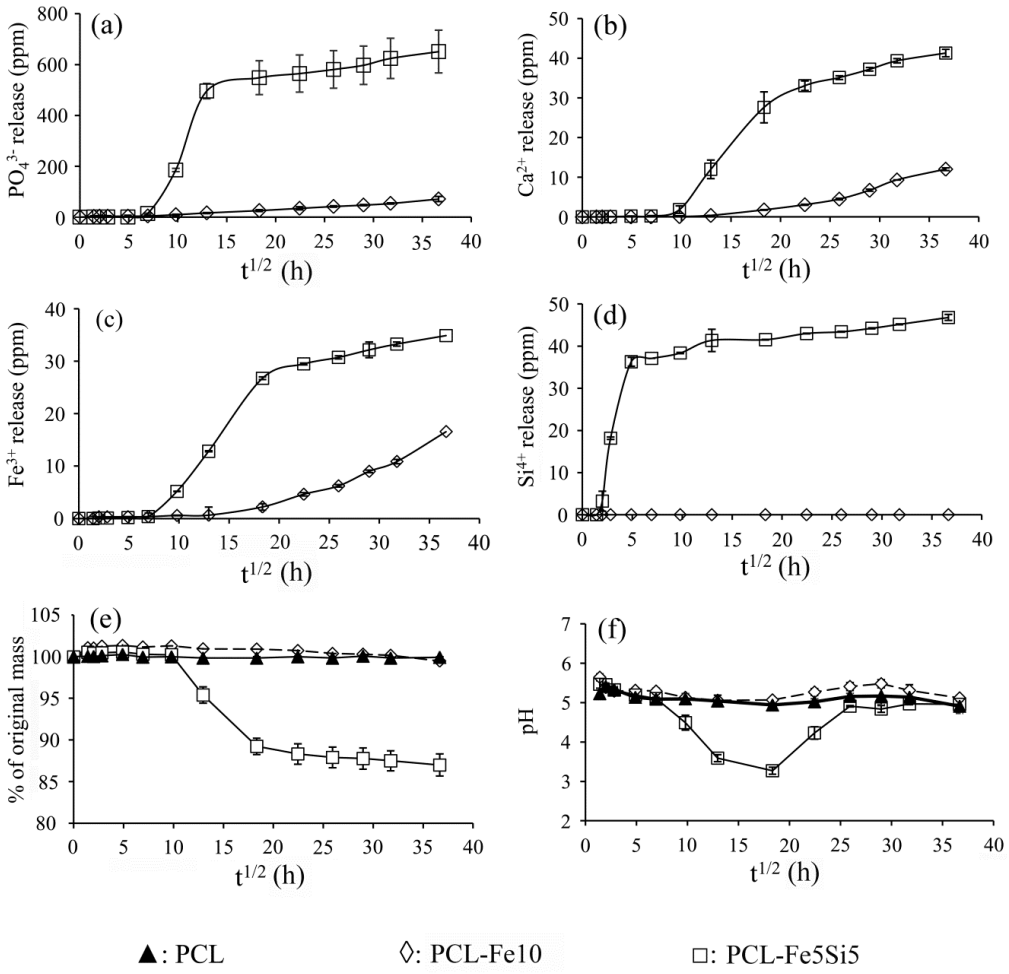

Figure 5.3 Conditioning of PCL and PCL-PGF composites in DW incubated for up to 56 days at 37 ºC. (a) PO_4^{3-}, (b) Ca^{2+}, (c) Fe^{3+}, and (d) Si^{4+} ion release from PCL-PGF composites. Anion and cation release was higher in PCL-Fe5Si5 compared to PCL-Fe10. (e) Weight loss, and (f) pH change of the immersion environment.

Table 5.4 PCL and PCL-PGF composite weight loss and residual fibre content of the composites at day 56 in deionised water.

Material	% of original mass	Remaining Glass (Wt. %)
PCL	99.39 ± 0.06	-
PCL-Fe10	96.95 ± 0.16	91
PCL-Fe5Si5	79.20 ± 2.40	27.54

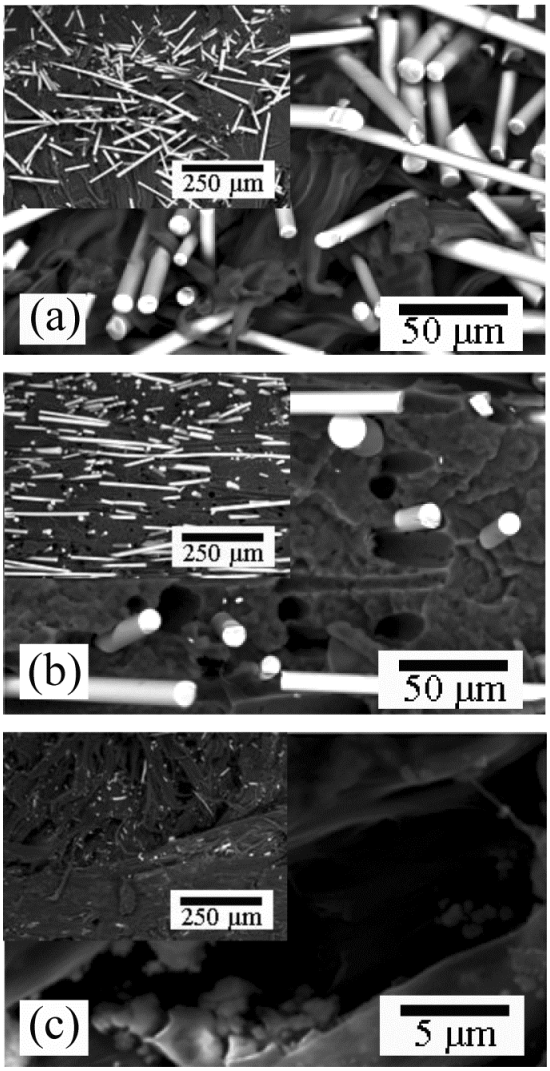

Figure 5.4 Morphological assessment of the PCL-PGF composites as-processed, and at day 56 in DW. (a) SEM micrographs of as-processed cryo-fractured PCL-PGF composites at different magnifications showing randomly dispersed and attached glass fibres within the PCL matrix, (b) PCL-Fe10 at day 56 in DW at different magnifications, and (c) PCL-Fe5Si5 at day 56 in DW at different magnifications. Low magnification images are inserted in the respective higher magnification. A majority of the fibres remained in the microstructure of PCL-Fe10, whereas most of the fibres were dissolved in PCL-Fe5Si5. Fibre dissolution resulted in channel formation within the composite microstructure.

5.4.2.2. Conditioning of PCL and PCL-PGF composites in SBF

In order to investigate the potential of calcium phosphate deposition, PCL and PCL-PGF composites were conditioned in SBF which mimics the *in vivo* physiological ionic composition. PCL-Fe10 demonstrated a slight weight increase up to 1008 h where

the decrease in weight started up to 1344 h whereas PCL-Fe5Si5 demonstrated a slower rate of reduction in weight. No weight loss occurred for the neat PCL sample (Supplementary Figure 5.2a). The associated change in pH of the SBF was also measured at each time point which remained constant for PCL and PCL-Fe10, whereas pH values of PCL-Fe5Si5 dropped considerably within the first week (Supplementary Figure 5.2b).

No precipitates were observed on the surfaces of neat PCL and PCL-Fe10 at days 7, 14 and 28 conditioning in SBF. However, precipitates were observed on the surface of the PCL-Fe5Si5 specimens at days 14, and 28 (Supplementary Figure 5.3). Figure 5.5a shows the SEM micrograph of the precipitates on the surface of PCL-Fe5Si5 at day 28 and EDS analysis confirmed the presence of calcium, phosphorous, and oxygen (Figure 5.5b). Figure 5.5c shows the XRD pattern of the PCL-Fe5Si5 surface initially, and at day 28 in SBF, revealing the formation of brushite.

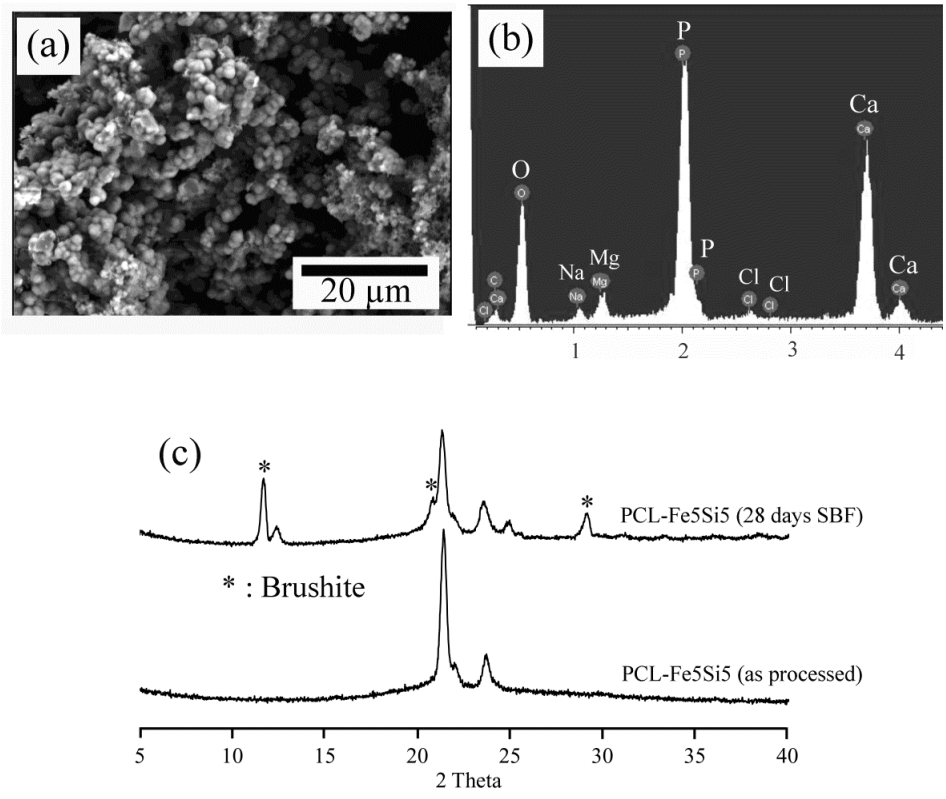

Figure 5.5 Conditioning of PCL and PCL-PGF composites in SBF incubated for up to 28 days. SEM micrograph (a) and EDS spectrum (b) of the precipitates formed on the surface of PCL-Fe5Si5 at day 28, respectively. (c) XRD patterns of PCL-Fe5Si5 as-processed and at day 28 in SBF. Peaks corresponding to the presence of brushite ($CaHPO_4.2H_2O$) are indicated by *.

5.4.2.3. Mechanical properties of PCL and PCL-PGF composites as-processed and upon conditioning in PBS

The weight loss of the composites aged in PBS (Figure 5.6a) demonstrated a similar weight loss effect observed in DW. At day 28, final dry weight revealed there was a 1.2 wt.% loss in PCL-Fe10 in comparison to 9 wt.% in PCL-Fe5Si5. Flexural analysis revealed that the initial flexural strength and modulus of the composites were significantly higher as compared to neat PCL (Figure 5.6b, c, respectively).

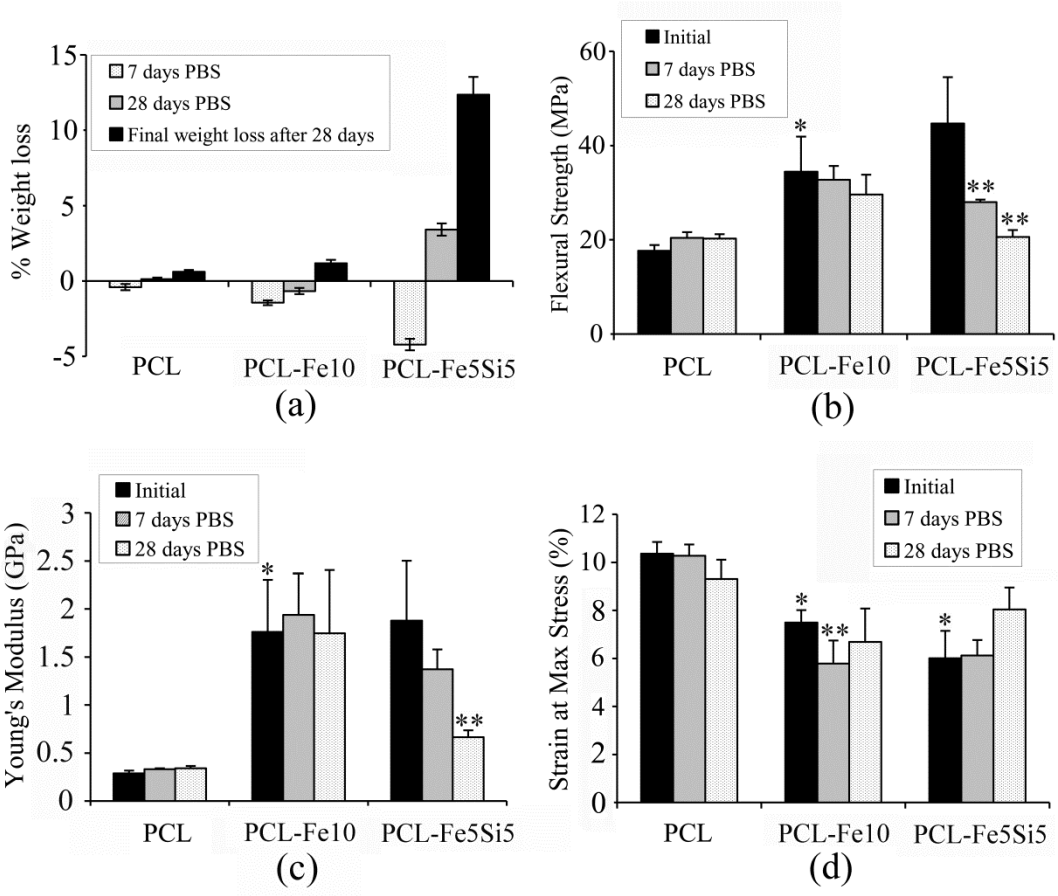

Figure 5.6 Mechanical property changes of PCL and PCL-PGF composites in PBS over the course of 28 days: (a) Weight loss at days 7 and 28, and final dry weight at day 28. (b) flexural strength, (c) flexural modulus, and (d) strain at maximum stress. Initial flexural strength and modulus increased significantly ($p<0.05$) via the addition of PGF. Initial strain at maximum stress decreased with addition of PGF. After ageing in PBS, the decrease in mechanical properties was considerably higher for Fe5Si5 containing composites compared to Fe10 containing composites. * Statistically significant difference for same time point compared with previous sample ($p<0.05$). ** Statistically significant difference for same sample compared to previous time point ($p<0.05$).

However, the strain at maximum stress decreased considerably with PGF incorporation. At days 7 and 28 in PBS, the decrease in flexural strength of PCL-Fe10 was not statistically significant. In contrast, PCL-Fe5Si5 demonstrated a 38 and 54% reduction in flexural strength at days 7 and 28, respectively. Similarly, while the modulus of PCL-Fe10 showed no statistically significant changes with immersion time, the modulus of PCL-Fe5Si5 showed a statically significant reduction at day 28. Although there was a decrease in the strain at maximum stress at day 7 for PCL-Fe10, no statistically significant difference was seen for the samples between day 7 and 28 for both composites.

Figure 5.7a shows representative storage modulus for PCL and PCL-PGF composites as a function of temperature. By incorporating PGF into the polymer, storage modulus increased. In order to monitor in real time, the change in composite modulus upon PGF degradation in physiologic solutions, DMA was conducted on specimens immersed in PBS at 37 ^{o}C (Figure 5.7b). While PCL-Fe10 *E'* remained constant through the course of the study up to day 7, a decrease in PCL-Fe5Si5 *E'* was seen which initiated at day 4.

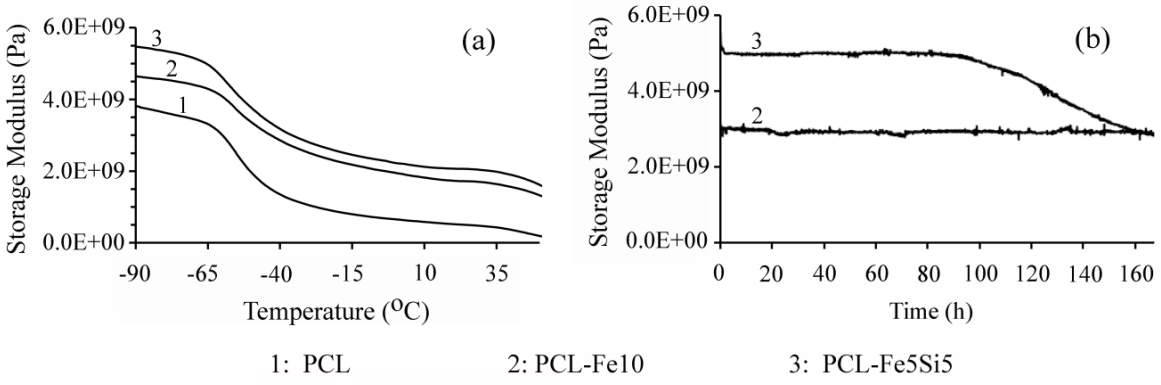

Figure 5.7 DMA of the PCL and PCL-PGF composites: (a) Storage modulus as a function of temperature. (b) Storage modulus of PCL-PGF composites over time while immersed in phosphate buffered saline at 37 ^{o}C.

5.4.2.4. Pre-osteoblast adhesion and viability on PCL and PCL-PGF composites

To assess the cytocompatibility of PCL-PGF composites, the viability of MC3T3-E1 pre-osteoblasts grown on PCL-Fe10 and PCL-Fe5Si5 was compared to cells grown on either PCL or microscope glass slides. Maximum intensity projections of z-stacks obtained by CLSM revealed calcein-AM labelled MC3T3-E1 cells attached to the surfaces of the PCL, PCL-PGF composites and microscope glass slides at days 1, 4 and 7 in culture (Figure 5.8). At day 1, live MC3T3-E1 pre-osteoblasts were attached to the surface of all samples. PCL and PCL-PGF composites showed a similar extent of MC3T3-E1 pre-osteoblast attachment and a predominantly spindle-shaped pattern of cell spreading whereas cell adhesion and spreading onto microscope glass slides was approximately 2-fold greater. At day 4, the number of live cells increased similarly on the surface of all materials. At day 7, MC3T3-E1 cells grown on PCL, PCL-Fe10, and PCL-Fe5Si5 remained viable and approached confluence as compared to cells grown on microscope glass slides. A very low number of necrotic/apoptotic cells were detected on PCL and PCL-PGF composite scaffolds on days 4 and 7.

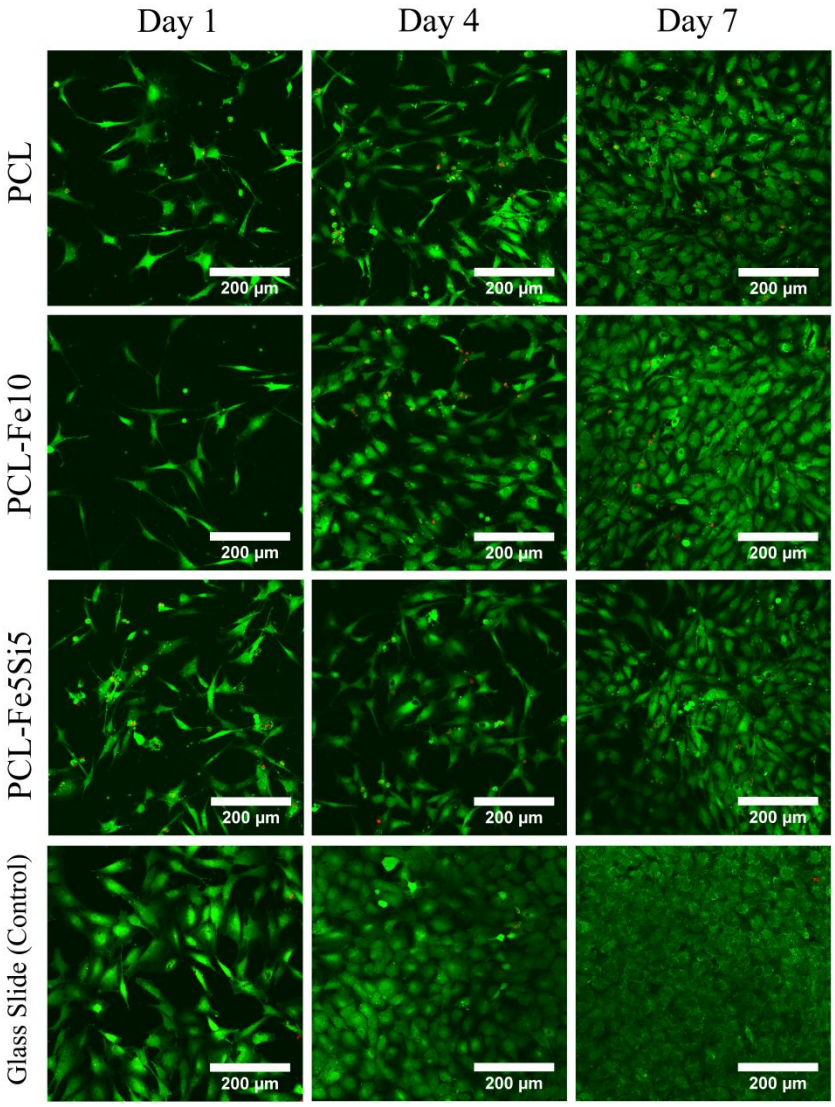

Figure 5.8 MC3T3-E1 pre-osteoblasts stained using calcein-AM (green) and ethidium bromide homodimer-1 (red) after either 1, 4, or 7 days of growth, and fluorescence was detected by CLSM. PCL and the PCL-PGF composites showed a similar extent of MC3T3-E1 pre-osteoblast attachment and a predominantly spindle-shaped pattern of cell spreading on day 1, while cell adhesion and spreading onto microscope glass was approximately 2-fold greater. The number of live cells increased similarly on the surface of all tested specimens after 4 days in culture. PCL, PCL-Fe10 and PCL-Fe5Si5 showed high level of cell viability and approached a level of confluence that was comparable to cells grown on microscope glass after 7 days.

5.5. Discussion

The controllable degradation of PGs has led to various compositions being developed and investigated for their use in biomedical applications [13, 14, 19, 29, 98-101, 109, 118]. It is also increasingly recognised that the properties of PGs can be translated into composites with the aim of producing a fully degradable system. This study investigated the properties of Si and Fe doped PGs alone and when incorporated as randomly orientated fibres into PCL, in order to assess the potential of composites with tailored properties for intended applications in bone augmentation and regeneration.

The concomitant increase in both T_g and density of the PGs with increasing Fe_2O_3 content suggested an increase in the cross-linking density between the phosphate chains [195], possibly due to the formation of P-O-Fe bonds. As a consequence, the degradation rate decreased with increasing Fe_2O_3 content, which was indicated by a reduction in weight loss and ion release. The release rates of PO_4^{3-} and Ca^{2+} ions were in line with the rate of glass dissolution [112].

PGF composition dictated the rate of weight loss of the composites. The weight loss of PCL-Fe5Si5 in DW was significantly higher compared to that of Fe10. A slight weight gain was observed for the PCL-Fe10 composites up to day 4 before the onset of weight loss indicating two simultaneous mechanisms: water uptake occurring in the matrix and at the fibre-matrix interface with eventual dissolution of the fibres resulting in overall weight loss. Since the solubility of Fe10 glasses is relatively low, the weight gain is dominant at early time points. After polymer matrix saturation occurs [190], weight loss becomes more prominent due to glass dissolution.

Ion release measurements were in line with weight loss. Fe^{3+} release also increased in the presence of Si in the PG formulation, which can be attributed to the rate of ion release dependence on water uptake in the composites. Ion release rates of the PCL-Fe5Si5 composite, extracted from the linear part of their release profile, were greater than from Fe5Si5 glass discs (Supplementary Table 5.1), attributable to the significantly greater surface area of the PGFs within the composite. It has been speculated that due to SiO_2 incorporation, the bonds formed within a SiO_2-P_2O_5 network could be more sensitive to hydraulic activity which results in faster dissolution in aqueous media hence higher ion release [11]. Interestingly however, the release rates of

PCL-Fe10 composite and Fe10 disc did not show a considerable difference. It has been shown that the incorporation of Fe_2O_3 into PGs decreased the overall surface energy due to the decrease in polar or acid/base component [118]. In addition, incorporation of Fe_2O_3 into PGs is known to create P-O-Fe bonds which increase hydration resistance [260]. Therefore, it can be concluded that the PG composition is a dominant factor in ion release rate of the composites. These results also indicate that degradation and ion release behaviour of the PGs can be transferred into a composite system.

Longer term ageing of PCL-PGF composites led to an almost complete dissolution of Fe5Si5 fibres whilst relatively minor amounts of Fe10 fibres dissolved. The extensive dissolution of Fe5Si5 fibres led to the creation of channels in the microstructure of the composites. Using the weight and density of the polymer and glasses, porosities of 1.6 and 11.1 vol.% were predicted for PCL-Fe10 and PCL-Fe5Si5, respectively. These would also allow for the creation of interconnectivity within the structure and facilitate the release of ionic species from residual glass fibres [198].

As a consequence of the higher degradation rate, a more rapid rate of pH reduction was observed in PCL-Fe5Si5 composites while the pH remained almost constant in PCL-Fe10. The higher release rate of the phosphate species led to an acidic medium through the formation of phosphoric acid [118]. Therefore, by day 28 conditioning in SBF, brushite ($CaHPO_4.2H_2O$), a possible precursor to the formation of apatite [98, 256] precipitated on the surface of the PCL-Fe5Si5 composites. Phases such as brushite (dicalcium phosphate dehydrate) and octacalcium phosphate are often found in more acidic solutions. Even under ideal HA precipitation conditions, the precipitates are generally non-stoichiometric which suggests the formation of calcium-deficient HA [255]. In contrast, PCL-Fe10 showed no precipitation, a consequence of the low dissolution rate of Fe10. Therefore, tailored amounts of Fe and Si in the glass formulation could control the amount and rate of ion release where there is a significant effect on the potential for calcium phosphate precipitation. Resorption and associated ion release rates of bone graft substitutes have been highlighted as important factors in their successful application [257].

The interest of using PG in PCL lies also in the modulation of mechanical properties, both initially and upon degradation. The results of this study showed that

incorporating PGFs into PCL led to considerable improvements in the flexural properties (up to 250 and 650% increase in strength and modulus, respectively). This reinforcement effect of fibres achieved at 18 vol.% was higher than previously reported for 40 vol.% PG particulates in PCL [94]. This can be directly attributed to the higher fibre aspect ratios leading to greater stress transfer levels to the matrix, as expected from Cox's shear lag model [261] and on the linear shear stress transfer at the fibre-matrix interface [262]. Similar effects on the modulus have been reported in PCL-PGFs ($50P_2O_5$-50CaO) [111], but not in the strength suggesting a lower fibre-matrix adhesion levels were achieved in the latter system. In addition, previously, more than 20 vol.% Si10 particulates resulted in PCL matrix degradation at the processing temperature (100 ºC). Fourier transform infrared spectroscopy (FTIR) indicated a reduction in the absorbance of ester bond at 1722 cm^{-1}, and the formation of a carboxylate bond at 1634 cm^{-1}. In addition, gel permeation chromatography (GPC) confirmed a reduction in PCL molecular weight [94]. In this study, the potential adverse effect of Si-doped PG on PCL was prevented by using: (i) a lower filler content, (ii) fibres instead of particulates thus reducing the surface area, and (iii) a quaternary glass formulation (Fe5Si5) instead of a ternary glass formulation (Si10). FTIR showed no reduction in the intensity of C=O peak at 1722 cm^{-1} in PCL-Fe5Si5 (Supplementary Figure 5.4-a and b). In addition, there was no statistically significant difference between the ratio of 1722 cm^{-1}/1634 cm^{-1} of PCL and PCL-PGF composites (Supplementary Figure 5.4-c). GPC confirmed that PCL molecular weight and polydispersity remained unchanged after PGF incorporation (Supplementary Figure 5.5-a and b).

It is interesting to note that the initial values of both the flexural strength and modulus of the composites were within the range of trabecular bone (approximately 40 MPa and 2 GPa for strength and modulus, respectively) [41, 42, 252]. The mechanical properties of composite samples immersed for 7 and 28 days in PBS, were found to remain within the range of trabecular bone. Post ageing in PBS, the reduction in mechanical properties was higher for PCL-Fe5Si5 compared to PCL-Fe10. This was in line with the weight loss which was 7-fold greater for PCL-Fe5Si5. DMA on composites immersed in PBS indicated that there was no statistically significant change in the storage modulus of PCL-Fe10, and a corresponding weight increase of 1% at day 7. In contrast,

there was a significant reduction in the storage modulus of PCL-Fe5Si5. The onset of this reduction occurred on day 4 which also coincided with the time for PGF dissolution in DW. There was also a 3% increase in weight of PCL-Fe5Si5 at day 7 in PBS. This increase in water uptake is associated with PGF dissolution creating channels within the composites. Therefore, additional water uptake is due to the penetration of water into the newly formed porous structure and at the fibre/matrix interface. The plasticizing effect of water on polymer properties is well known and has been demonstrated through changes in the thermal properties [263]. However, while it has also been shown that hydration levels of up to 1% would not have a plasticizing effect on PCL [264], thermal profiles obtained through differential scanning calorimetry on dry and wet specimens suggested a decrease in the melting temperature of PCL-PGF upon hydration (Supplementary Figure 5.6). Therefore, the reduction in PCL-Fe5Si5 *E'* was due to a combination of the plasticization effect of water and PGF degradation. Consequently, since the solubility of Fe10 was very low, PCL- Fe10 could retain its mechanical properties for a much longer period of time. The degradation rate of PCL is slower than PGA and PLA [170], e.g. Sun *et al.* [265] showed that PCL capsules remained intact in shape when implanted up to 24 months. Based on the PCL-Fe10 weight loss in DW, total degradation of Fe10 PGFs may be estimated to occur within 20 months, which could coincide with that of PCL. Therefore, the PCL-Fe10 may be suitable for longer-term applications such as bone fixation devices. On the other hand, a predicted total degradation time of 2.5 months for Fe5Si5, and in combination with calcium phosphate precipitation within 4 weeks, make PCL-Fe5Si5 more suitable for potential applications in bone tissue engineering when converted to porous scaffolds.

The addition of PGFs into PCL did not alter the pre-osteoblastic cytocompatibility of the materials. MC3T3-E1 cells remained viable and approached confluence on PCL, PCL-Fe10, and PCL-Fe5Si5. Similar study using MG63 cell line on PLA-PG composites has shown cell attachment and viability yet to a lower extent compared to this study [191]. Biocompatibility study of PLA-PG composite foams using human foetal bone cells by Georgiou *et al.* [190] showed that their proliferation rate was similar to PLA foams with either HA or β-tricalcium phosphate (β-TCP). No adverse effects on the cell viability were observed by incorporating PGFs in this study; in addition, these PGFs may

also have a positive influence on cell proliferation and differentiation which requires further investigation.

5.6. Conclusions

While no weight loss in DW was observed for PCL alone over the course of this study, incorporating Fe5Si5 glass fibres into a PCL matrix resulted in composites with a considerable mass loss rate. Si containing PGFs resulted in significantly increased release of PO_4^{3-}, Ca^{2+}, Fe^{3+}, and Si^{4+}. The higher solubility of Fe5Si5 PGFs led to the formation of channels upon degradation while Fe10 PGFs remained in the microstructure for a much longer time period which resulted in maintenance of the mechanical properties over time in physiological fluids. SBF conditioning revealed that brushite precipitates formed on the surface of PCL-Fe5Si5. In addition, MC3T3-E1 pre-osteoblasts showed that the investigated composites were cytocompatible. Therefore, by tailoring the Si and Fe content in the glass composition, the properties of PCL-PGF composites can be controlled to potentially be used as bone analogous materials in applications such as bone fracture fixation devices or, in the case of a porous structure, scaffolds for bone tissue engineering.

5.7. Acknowledgements

This work was funded by the Canadian Natural Sciences and Engineering Research Council, le Fonds Québécois de la Recherche sur la Nature et les Technologies, McGill University Faculty of Engineering Hatch Faculty Fellowship, and Canada Foundation for Innovation: Leaders Opportunity Fund. Funding for Maziar Shah Mohammadi was also partly supported by a McGill Engineering Doctoral Award. The authors thank Saurav Mohapatra, Hye-Lim Choi, Christoph Stähli and Jason Bertram for their assistance in this work. Martin N. Bureau is a member of the Groupe de Recherche en Sciences et Technologies Biomédicales (Fonds de recherche en santé du Québec).

5.8. Appendix A: Supplementary data

Supplementary Table 5.1 Ion release rates calculated from the slope of the linear incline of the graphs in Figure 5.3 for the investigated composites. Ion release rate was greater from PCL-Fe5Si5 compared to PCL-Fe10 due to the faster degradation rate of FE5Si5 PGFs than Fe10.

Composite code	PO_4^{3-} release ($ppm.h^{-1}$)	Ca^{2+} release ($ppm.h^{-1}$)	Si^{4+} release ($ppm.h^{-1}$)	Fe^{3+} release ($ppm.h^{-1}$)
PCL-Fe10	0.05 ± 0.006	0.01 ± 0.0009	-	0.013 ± 0.001
PCL-Fe5Si5	1.6 ± 0.3	0.11 ± 0.01	0.33 ± 0.03	0.09 ± 0.007

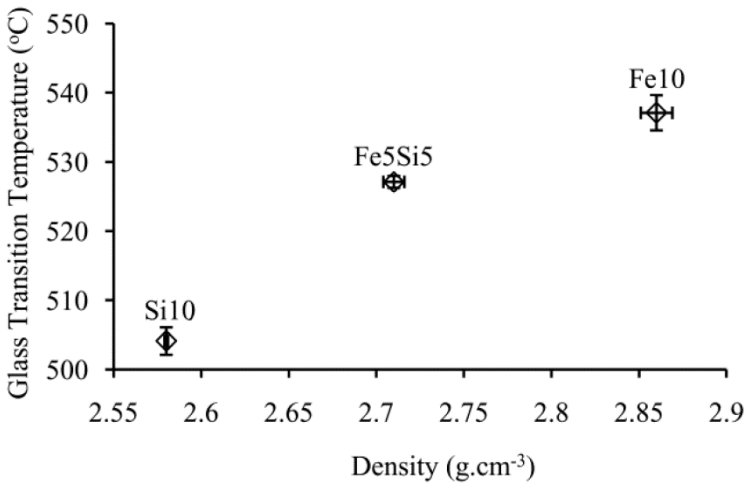

Supplementary Figure 5.1 Glass transition temperature (T_g) versus density for different PG formulations. A correlated increase in T_g and density was observed by substituting silica with iron oxide in the PG formulations.

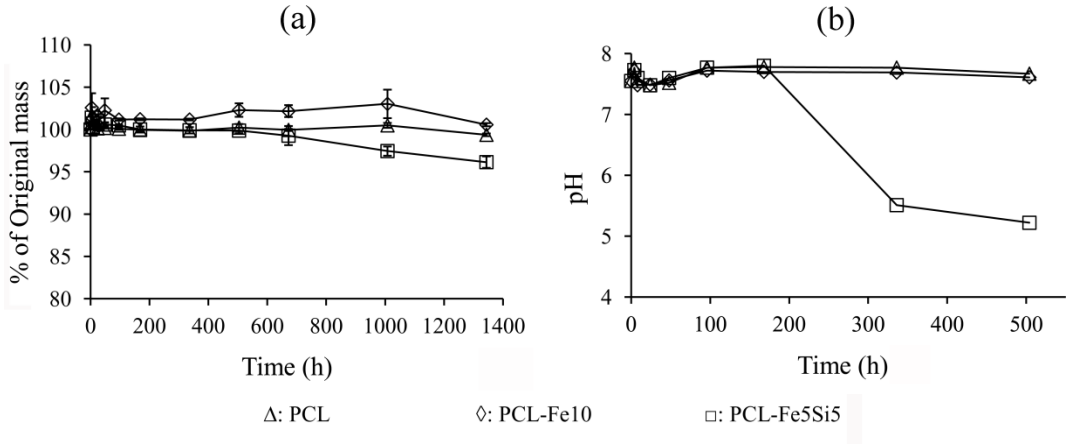

Supplementary Figure 5.2 Conditioning of PCL and PCL-PGF composites in SBF incubated for up to 28 days. (a) Weight loss of PCL and PCL-PGF composites. Weight loss was higher for PCL-Fe5Si5 compared to PCL-Fe10. (b) pH change of the SBF environment following immersion of PCL and PCL-PGF composites. While there was relatively no change for PCL, and PCL-Fe10, the pH decreased considerably for PCL-Fe5Si5 after 168 h.

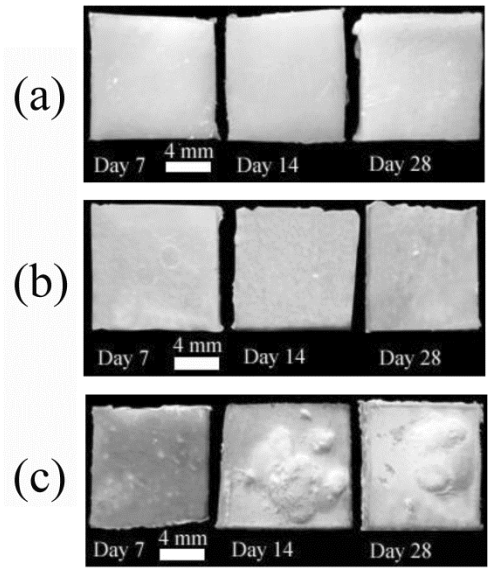

Supplementary Figure 5.3 Photographic images of the precipitates formed on the surface of (a) PCL, (b) PCL-Fe10, and (c) PCL-Fe5Si5 at days 7, 14, and 28 in SBF.

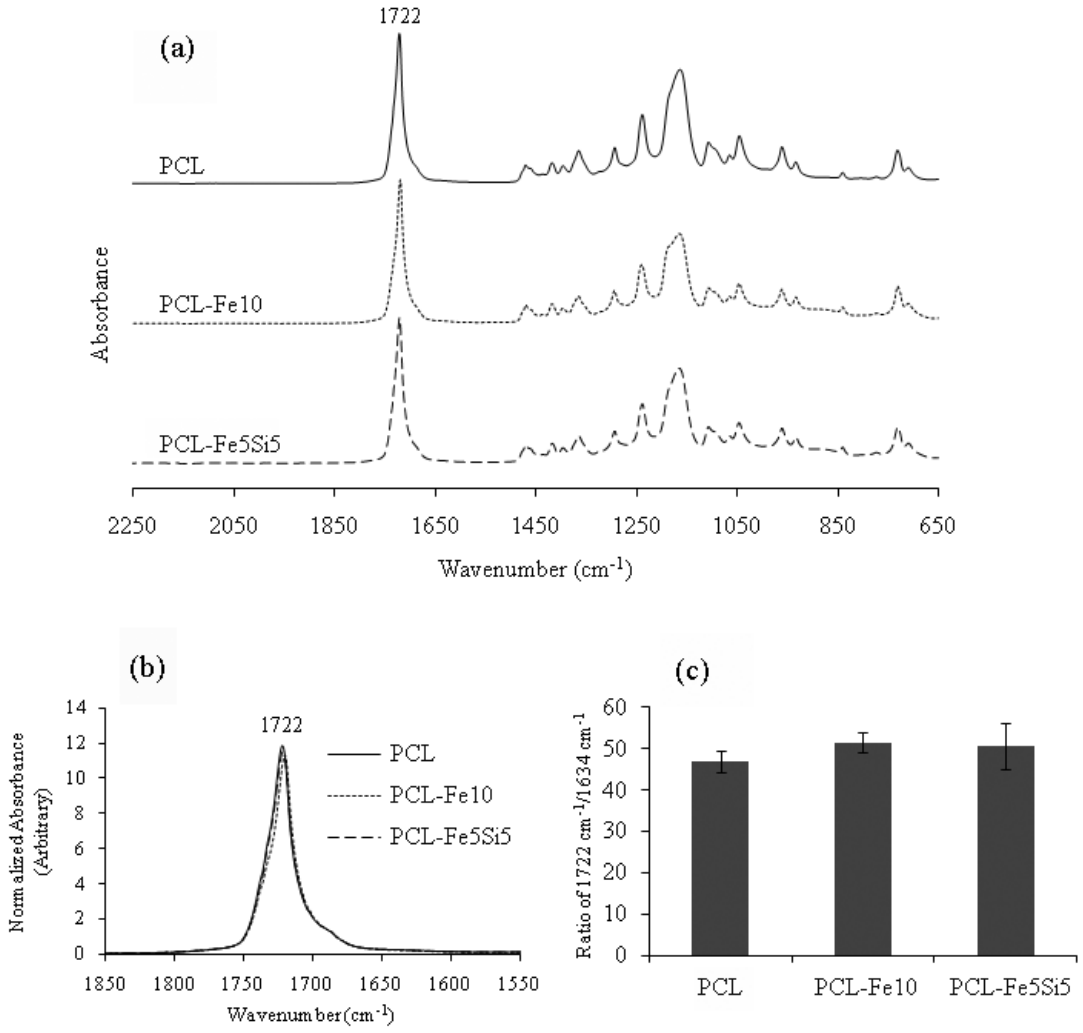

Supplementary Figure 5.4 ATR-FTIR spectra of as-processed PCL and PCL-PGF composites (a). The absorbance of the carbonyl peak at 1722 cm^{-1} remained unchanged in as-processed PCL-PGF composites compared to PCL (b). The absorbance ratio of 1722 cm^{-1}/1634 cm^{-1} did not show a statistical difference in PCL and PCL-PGF composites (c). A reduction in this ratio has been shown to be related to the formation of carboxylate by-products resulting in a reduction in the molecular weight of the polymer matrix [34], which was not observed in this study.

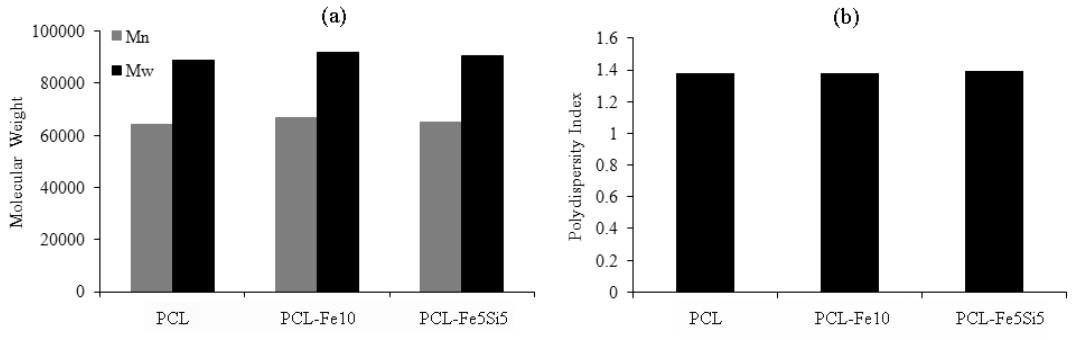

Supplementary Figure 5.5 Molecular weight (a) and polydispersity index (b) of PCL and PCL in PCL-PGF composites measured using gel permeation chromatography. The molecular weight and polydispersity remained unchanged in as-processed PCL-PGF composites compared to PCL.

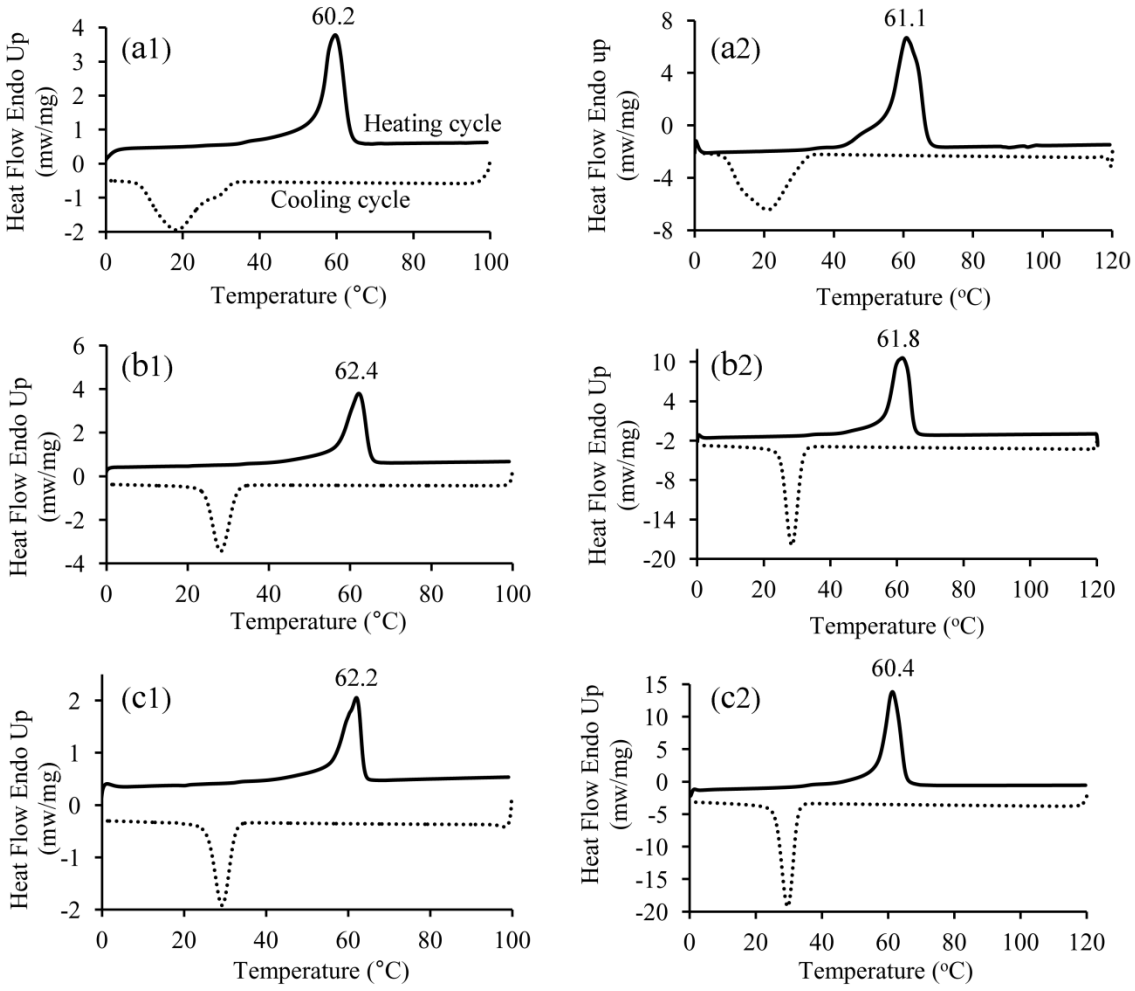

Supplementary Figure 5.6 DSC profiles of PCL and PCL-PGF composites in dry and hydrated states. (a1) PCL dry, (a2) PCL hydrated; (b1) PCL-Fe10 dry, (b2) PCL-Fe10 hydrated; (c1) PCL-Fe5Si5) dry and (c2) PCL-Fe5Si5 hydrated. The test was carried out under a flow of nitrogen purge with a heating rate of 20 ^{o}C min^{-1}on samples of approximately 5 mg. The tests were conducted on as-processed (dry state) and hydrated samples (7 days in DW, which were in line with the time of the DMA experiments). No difference was observed in the thermal profiles of PCL, dry and wet. Slight reductions in the melting temperature of dry and wet PCL-PGF composites were observed.

5.9. Appendix B: Additional information

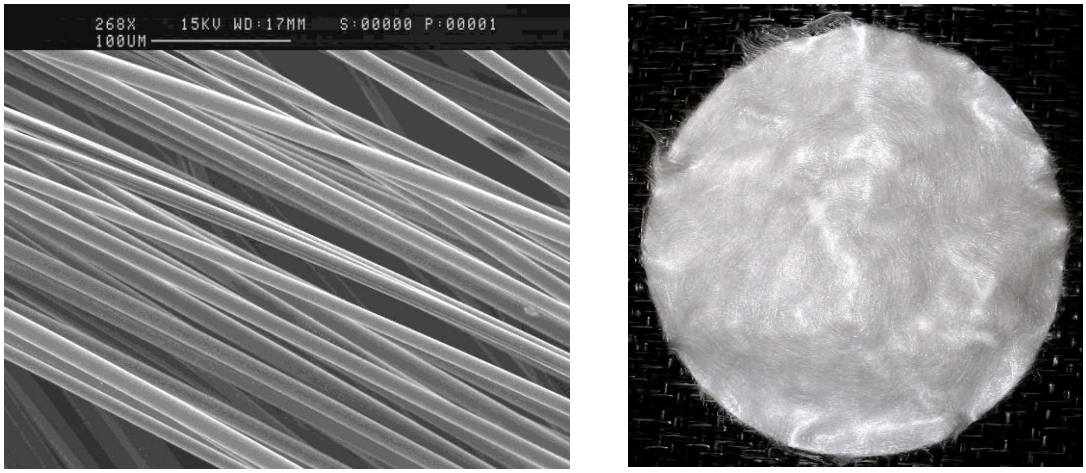

(a) (b)

Supplementary Figure 5.7 SEM micrograph of the pulled PGFs (a); and an example of a non-woven random fibre mat (b).

CHAPTER 6

PHOSPHATE-BASED GLASS SURFACE PROPERTIES INFLUENCE POLYESTER MATRIX COMPOSITE PROPERTIES

It has been reported that bioactive silicate-based glasses (SGs) can cause a reaction with the ester bond in polyesters when processed at elevated temperature that may degrade the polymer leading to a reduction in the molecular weight and a decline in mechanical properties. The addition of different modifiers into phosphate-based glasses (PGs) changes the surface properties such as surface energy and hydrophilicity. These properties have a significant effect on the hydrolysis of the glass which affects the solubility and ion release rates. In addition, the hydrophilicity and surface energy of the PG would affect its interaction with the composite matrix at the interface.

In Chapter 4, the potential reaction between the Si-doped PG and the ester bond was confirmed PCL-PGP composites. This reaction led to creation of carboxylate by-products resulting in a lower molecular weight of the polymer matrix. Since filler composition, volume fraction, morphology and distribution have considerable effects on the filler/matrix interface and composite properties, the aim of this study was to investigate the effect of Si and Fe doped PG fibres on poly(lactic acid) (PLA) matrix and

eventually composite properties. This was carried out by investigating the effect of PG composition on the glass surface energy which was correlated with its solubility and reactivity with the polymer matrix. This reaction occurs at elevated processing temperatures. Since the PGFs used in the previous study (Chapter 5) did not affect the PCL molecular weight at processing temperature of 100 ^{o}C, PLA was selected in this study to investigate whether increasing the processing temperature to above 200 ^{o}C would accelerate the filler/matrix reaction.

A manuscript based upon these research findings has been published in the peer-reviewed journal, *Journal of Materials Science: Materials in Medicine*.

Effect of phosphate-based glass fibre surface properties on thermally produced poly(lactic acid) matrix composites

Maziar Shah Mohammadi[a], Ifty Ahmed[b], Naser Muja[a], Christopher D Rudd[b], Martin N Bureau[c,a], Showan N Nazhat[a]

[a] *Department of Mining and Materials Engineering, McGill University, Montreal, QC, H3A 2B2, Canada*

[b] *Division of Mechanics, Materials and Structures, University Park Campus, University of Nottingham, NG7 2RD, U.K.*

[c] *Industrial Materials Institute, National Research Council Canada, QC, J4B 6Y4, Canada*

Key words: Phosphate-based glass fibres, poly(lactic acid), biodegradable composites, degradation, pre-osteoblasts

6.1. Abstract

Incorporation of soluble bioactive glass fibres into biodegradable polymers is an interesting approach for bone repair and regeneration. However, the glass composition and its surface properties significantly affect the nature of the fibre-matrix interface and composite properties. Herein, the effect of Si and Fe on the surface properties of calcium containing phosphate based glasses (PGs) in the system ($50P_2O_5$-40CaO-(10-x)SiO_2-xFe_2O_3, where x = 0, 5 and 10 mol.%) were investigated. Contact angle measurements revealed a higher surface energy, and surface polarity as well as increased hydrophilicity for Si doped PG which may account for the presence of surface hydroxyl groups.

Two PG formulations, $50P_2O_5$-40CaO-$10Fe_2O_3$ (Fe10) and $50P_2O_5$-40CaO-$5Fe_2O_3$-$5SiO_2$ (Fe5Si5), were melt drawn into fibres and randomly incorporated into poly(lactic acid) (PLA) produced by melt processing. The ageing in deionised water (DW), mechanical property changes in phosphate buffered saline (PBS) and cytocompatibility properties of these composites were investigated. In contrast to Fe10 and as a consequence of the higher surface energy and polarity of Fe5Si5, its incorporation into PLA led to increased inorganic/organic interaction indicated by a reduction in the carbonyl group of the matrix. PLA chain scission was confirmed by a greater reduction in its molecular weight in PLA-Fe5Si5 composites. In DW, the dissolution rate of PLA-Fe5Si5 was significantly higher than that of PLA-Fe10. Dissolution of the glass fibres resulted in the formation of channels within the matrix. Initial flexural strength was significantly increased through PGF incorporation. After PBS ageing, the reduction in mechanical properties was greater for PLA-Fe5Si5 compared to PLA-Fe10. MC3T3-E1 pre-osteoblasts seeded onto PG discs, PLA and PLA-PGF composites were evaluated for up to 7 days indicating that the materials were generally cytocompatible. In addition, cell alignment along the PGF orientation was observed showing cell preference towards PGF.

6.2. Introduction

Composites of biodegradable polymers and bioactive ceramics have been developed for bone repair and regeneration [181, 190, 258, 266-268]. The incorporation of inorganic fillers such as silicate based bioactive glasses (e.g. Bioglass®) and hydroxyapatite into degradable polymers (e.g. poly(lactic acid) (PLA), poly(glycolic acid) (PGA), their copolymers (PLGA) and polycaprolactone (PCL) [183, 250]) has been shown to enhance the Young's modulus, flexural strength and osteoconductivity of the composites [186, 187, 249]. Also, in an effort to tailor the degradation properties of composites, phosphate-based glasses (PGs) have emerged as inorganic fillers [11, 12]. PGs provide several advantages: (i) their solubility can be predicted and easily controlled through their composition [13, 14, 98]; (ii) their polymeric nature allows for some formulations to be drawn into fibres [19]; and (iii) the high surface area to volume ratio of PG fibres (PGFs) can significantly affect their degradation and the release of potentially therapeutic ions, which can influence the biological properties of the composites. Thus, by doping calcium-PGs with various amounts of modifying oxides, the solubility and ion release rate can be controlled for bone regeneration approaches, as well as tailoring the composite mechanical properties.

Glass network modifying oxides not only change the bulk properties of PGs, but also their surface properties such as surface energy and hydrophilicity. These properties significantly affect the hydrolysis of the glass. Since P_2O_5 is chemically unstable due to easily hydrolysable P-O-P bonds, the addition of glass modifying metal oxides, such as Fe_2O_3, increases the PG stability by creating P-O-Fe bonds that are generally less hydrolysable. Abou Neel *et al.* [118] investigated the synergy between composition and surface properties of PGs and its effect on the degradation and ion release of iron containing PGFs and showed that, in the P_2O_5-CaO-Na_2O-Fe_2O_3 system, the polar interactions occurring on the glass surfaces diminished with increasing Fe_2O_3 content. There was a reduction in the overall surface energy with an increase in Fe_2O_3 content which was attributed to the decrease in polar or acid/base component. The hydrophilicity and surface energy of the PG could also influence its interfacial interaction with the polymer matrix. It has previously been shown that thermally produced composites of PCL filled with particulates of Si doped PG resulted in a reduction of PCL matrix

molecular weight as a consequence of a reaction between the glass particulates and the ester bonds, which created carboxylate by-products [94]. Matrix degradation increased with increasing Si content. In terms of PG degradation, it has been shown that the addition of Si disrupts the phosphate network leading to a higher dissolution rate of the glass in aqueous environments [13].

Blaker *et al.* [188] also demonstrated that the inclusion of Bioglass® particles caused a reaction at the filler-poly(D,L-lactide) interface when processed at elevated temperatures. This in turn degraded the polymer matrix leading to a reduction in the mechanical properties of the composite. Therefore, along with the composition and volume fraction of the filler and its solubility, processing conditions are also critical for composite properties [188]. Bioglass® has a high surface energy [140] and creates Si-OH groups on the surface by absorbing water which will subsequently hydrolyse the ester bond causing matrix chain-scission [188].

Therefore, since the surface properties of glasses can have a considerable effect on the filler/matrix interface and composite properties, the aim of this study was to investigate the effect of Fe and Si doped PG fibres on PLA matrix composite properties, when thermally produced. The surface energy of PGs of the system $50P_2O_5$-40CaO-(10-x)SiO_2-xFe_2O_3, where x = 0, 5 and 10 mol.% was measured. The degradation and morphological changes of properties of PLA-PGF was investigated in deionised water for up to 56 days, the mechanical properties of the composites were investigated initially and when aged in phosphate buffered saline (PBS) for up to 28 days. In addition, the cytocompatibility of the glasses and composites was assessed using MC3T3-E1 pre-osteoblasts to investigate their potential application in bone repair and regeneration.

6.3. Experimental

6.3.1. Phosphate glass (PG) production

Three melt derived PG compositions (Table 6.1) were prepared using P_2O_5, $CaHPO_4$, Fe_2O_3, and SiO_2 (Sigma Aldrich) as starting materials. The precursors were dry blended, poured into a Pt/10%Rh crucible (Birmingham Metal Company), and heated to 400 °C in order to remove moisture. The crucible was then transferred to a second furnace and melted at 1150 °C for 90 min. The molten glass was then cast into a

cylindrical shape mould (10 mm in diameter), annealed at 350 °C for 1 h to remove any residual stresses and cut into discs, or poured onto a steel plate and cooled to room temperature to make the bulk glass.

Table 6.1 Glass compositions and coding

Glass code	Components (mol.%)			
	P_2O_5	CaO	SiO_2	Fe_2O_3
Si10	50	40	10	-
Fe5Si5	50	40	5	5
Fe10	50	40	0	10

A specialist in house fibre-drawing rig was used to produce glass fibres utilising a melt drawn technique from the following ternary and quaternary formulations; $50P_2O_5$-$40CaO$-$10Fe_2O_3$ (Fe10) and $50P_2O_5$-$40CaO$-$5Fe_2O_3$-$5SiO_2$ (Fe5Si5). PGFs were guided onto a rotating drum at 1600 rpm to produce fibres in the range of 10 - 20 μm in diameter. The fibres were removed from the drum and annealed by heating up to 200 °C at 20 °C.min^{-1}, then heating to 505 °C at 1 °C.min^{-1} and holding for 90 min, cooling to 300 °C at 0.25 °C.min^{-1} and finally cooling to room temperature at 1 °C.min^{-1}. Once annealed overnight, the fibres were cut to lengths of 10 mm to prepare the random fibre mats.

6.3.2. PLA-PGF composite production

PGFs (3 g of 10 mm length) were dispersed into a 4 L solution of distilled water and Cellosize (Univar Ltd) for 10 min. The fibre-cellulose solution was then poured into a second container consisting of a straining mesh. After ensuring that all fibre aggregates were evenly dispersed, the mesh strainer was extracted from the solution. The resulting random fibre mats were then rinsed with distilled water to remove any residual binder and vacuum-dried at 50 °C overnight. PLA pellets (5 g, Resin 3051-D, Natureworks®, molecular weight ~91,000 confirmed by GPC) were heated to 210 °C and pressed at 3 bar for 30 s (J.R. Dare Ltd., heated press) to produce PLA films of ~0.2 mm thickness. The films were cooled under pressure to room temperature using a cold press (Daniels

Upstroke Press). Six dried random fibre mats were placed in an alternating sequence with seven PLA films into a metal shim, shielded by two poly(tetrafluoroethylene) sheets, and placed in the hot press (J.R. Dare Ltd), set at 210 °C. This stack of PLA films and random fibre mats were then heated at 210 °C for 15 min followed by pressing for 15 min at 38 bar, and finally cooled in another press (Daniels Upstroke) for a further 15 min, at 38 bar. Using this procedure, PLA-PGF composites with ~18 vol.% PGF were produced (see Table 6.2). The volume fractions of the composites were calculated using the matrix burn-off method (ASTM D2584-94 [259]). A PLA plaque was also produced following the same film stacking technique.

Table 6.2 Composite compositions and coding

Composite code	Components (vol.%)		
	PLA	Fe10	Fe5Si5
PLA	100	0	0
PLA-Fe10	82	18	0
PLA-Fe5Si5	82	00	18

6.3.3. Bulk and surface characterisation of PGs

6.3.3.1. X-ray diffraction of the crystallised PG

X-ray diffraction (XRD) was used to identify the phases present within the crystalline state of the glasses. PGs were crystallised for 3 h at 775 °C. XRD was conducted using a Bruker diffractometer (Bruker AXS Inc.) in flat plate geometry from $2\Theta = 6^{o}$ to 86^{o}, with Ni-filtered Cu k_{α} radiation, and using a Philips diffractometer (PW1710) from $2\Theta = 5^{o}$ to 100^{o} with a step size of 0.02 and a count time of 0.1 s. The patterns were analysed using the EVA software package.

6.3.3.2. Wettability and surface free energy of the PG

Surface properties of PGs were measured through their wettability and surface free energy. Glass discs from each composition were abraded against silicon carbide paper (1200/4000, Struers) using ethanol as the lubricant. Prior to testing, the specimens were ultrasonicated in ethanol for 20 min and allowed to dry. The static contact angle was

measured with a contact angle system OCA (Future Digital Scientific) and ultrapure water and diiodomethane (DII) were used to represent polar and non-polar characteristics, respectively. Droplets (5 µl) were placed on the glass surface via a syringe and the drop profile was recorded for 10 sec. The contact angle was calculated after 2 sec from the time the droplet was in contact with the surface. The measurements were carried out on triplicate samples. The surface free energy was calculated using the OWRK (Owens, Wendt, Rable and Kaelble) method via SCA20 software.

6.3.4. Structural characterisation of the PLA-PGF composites

Attenuated total reflectance-Fourier Transform Infrared spectroscopy (ATR-FTIR) was used to investigate the structural changes in the PLA matrix due to its potential interactions with PGF after thermal processing. Spectra were obtained from neat PLA and as-processed composites using a PerkinElmer 400 FTIR. This study was conducted in the 600-3500 cm^{-1} range with a 4 cm^{-1} resolution, and number of scans of 32. All the spectra were normalised to the peak at 1453 cm^{-1}.

Gel permeation chromatography (GPC, Water Breeze) was used to investigate the molecular weight (M_w) of PLA after composite fabrication. The GPC was equipped with both ultraviolet (UV 2487) and differential refractive index (RI 2410) detectors and three Water Styragel HR columns (HR1 with molecular weight measurement in the range of 100-5,000 $g.mol^{-1}$, HR2 with molecular weight measurement range of 500-20,000 $g.mol^{-1}$, and HR4 with molecular weight measurement range of 5,000-600,000 $g.mol^{-1}$ and a guard column. The columns were kept at 40 °C. Tetrahydrofuran (THF) flowing at a rate of 0.3 $ml.min^{-1}$ was used as the mobile phase. Each sample dissolved in THF was filtered through a 0.2 µm syringe filter (Anotop25, Fisher) to remove PGF prior to injection into the module.

6.3.5. Ageing of composites

6.3.5.1. Ion release and weight loss in deionised water

PLA-PGF composites were aged in deionised water (DW) for up to 56 days by placing specimens (n=3, 10×10×1.6 mm^3) into vials containing 25 ml of ultra-pure deionised water (18.2 MΩ.cm resistivity) and incubating at 37 °C. Ion release, weight

loss, and pH of the ageing environment were measured at 14 different time points (0, 2, 4, 8, 24, 48, 96, 168, 336, 504, 672, 840, 1008, and 1344 h).

Anions and cations released via composite degradation were measured using ion chromatography (IC) and atomic absorption (AA), respectively. IC (Dionex, DX-100 Ion Chromatograph) was used in order to measure phosphate anion (PO_4^{3-}) release. An Ionpac AS14 anion exchange column was used to elute the polyphosphates. An eluent of 3.5 mM Na_2CO_3/0.1 mM $NaHCO_3$ was used with a flow rate of 0.1 ml/min with sample run time of 15 min. Sodium phosphate tribasic (Na_3PO_4) (Sigma, Canada) was used to prepare standard solutions. A 1000 ppm working solution was prepared from which serially diluted 10, 20, and 50 ppm standard solutions were obtained. AA (VARIAN AA240FS) was used to investigate the release of Ca^{2+}, Fe^{3+}, and Si^{4+} cations. The instrument was calibrated using certified AA standard solutions.

The weight change of the composites was investigated by removing the specimens from DW, blot drying, weighing and replacing in fresh deionised water. Weight loss was measured in terms of percentage of original weight. The final dry weight at day 56 was measured by first incubating the specimens for 6 days at 37 °C until an equilibrium weight was reached.

The pH of the deionised water was also measured using a pH meter (Accumet Excel 20, Fisher) at each time point.

6.3.5.2. Morphological investigations

Scanning electron microscopy (SEM, Hitachi S-3000N) was used to investigate the morphology of the cryo-fractured surface of the composites before and after ageing in DW. Back scattered electron mode with accelerating voltages of 20 kV was used.

6.3.6. Composite initial mechanical properties and as a function of time in PBS

Flexural (three-point bend) mechanical test was used to measure the mechanical properties of the composites. The effect of PG formulation on composite mechanical properties was investigated through changes in flexural strength, Young's modulus, and strain at maximum stress. Tests were performed on initially produced and PBS (Sigma Aldrich) conditioned specimens stored at 37 °C and tested at days 7, 14, and 28.

Mechanical testing was carried out on specimens in the dry state and the extent of their weight loss after PBS ageing was measured prior to mechanical testing, by first drying the specimens. Three repeat specimens were tested with a cross-head speed of 1 mm/min using a 1 kN load cell in accordance to ASTM D 790-95a:1996 (aspect ratio = 16) in an Instron mechanical testing instrument 5582 (Instron Ltd).

6.3.7. Cytocompatibility study: Cell culture, seeding, and detection of cell viability

Murine MC3T3-E1 pre-osteoblasts (subclone 14) from American Type Culture Collection (CRL-2594 ATCC) were purchased from Cedarlane Labs and maintained in alpha modified Minimum Essential Medium (α-MEM, HyClone Laboratories Inc.) supplemented with 2 mM L-Glutamine (Invitrogen), 10% Newborn Calf Serum (NBCS, HyClone Laboratories Inc.) and 1% penicillin/streptomycin (Invitrogen) at 37 °C in humidified atmosphere at of 5% CO_2. Both PG glass discs and PLA-PGF composites were assessed. Prior to cell seeding, PG glass discs (1 cm in diameter), PLA, PLA-Fe10 and PLA-Fe5Si5 and glass slide fragments (positive control), each with a surface area of 1 cm^2, were sterilised by immersion in absolute EtOH for 2 h. Specimens were then transferred to cell growth medium and conditioned overnight in a tissue culture incubator. MC3T3-E1 pre-osteoblasts were detached from tissue culture flasks (0.05% trypsin/0.02% EDTA), collected by centrifugal rotation (80 xg, 5 min) and seeded onto the samples at a density of 1.0×10^4 cells/cm^2. After 1, 4 and 7 days in culture, cells were detected by confocal laser scanning microscopy (CLSM, LSM 5, Carl Zeiss). To assess cell viability, cells were labelled using 1 mM calcein AM and 0.1 mM ethidium bromide homodimer-1 (LIVE/DEAD®, Invitrogen) in α-MEM for 30 minutes. Opaque materials were gently inverted (i.e. cell growth surface facing the microscope objective) onto a 50 mm Pelco glass bottom Petri dish (Ted Pella Inc.) and fluorescent-labelled cells were imaged using laser excitation (488 and 543 nm laser lines) and a baseline confocal z-stack was acquired at 1 Airy unit using a 20x EC Plan-Neofluar objective (0.5 N.A.). Maximum intensity projections were generated and analysed using NIH ImageJ v1.43 software.

6.3.8. Statistical analysis

A Student's *t*-test was used to determine significant differences between two means using statistical significant level of $p<0.05$.

6.4. Results

6.4.1. Glass characterisation

6.4.1.1. Determination of crystalline phases in PG using X-ray diffraction

Table 6.3 presents the identified phases from the crystalline state of the PGs. Calcium phosphate (α-(CaP_2O_6), ICCD No. 11-0039 and α-$Ca(PO_3)_2$, ICCD No. 17-0500) was identified as the main phase of all the three PG formulations. Wollastonite ($CaSiO_3$, ICCD No. 3-0626) was also identified in Fe5Si5. In the case of Fe10, calcium iron oxide ($CaFe_2O_4$, ICCD No. 3-0040) was identified in addition to the calcium phosphate phases.

Table 6.3 Identification of phases in the crystallized Si and Fe doped PG formulations using X-ray diffraction.

Glass code	Phase 1	Phase 2	Phase 3
Si10	α-(CaP_2O_6)	α-$Ca(PO_3)_2$	
Fe5Si5	α-$Ca(PO_3)_2$	α-(CaP_2O_6)	α-$CaSiO_3$
Fe10	α-(CaP_2O_6)	α-$Ca(PO_3)_2$	$CaFe_2O_4$

6.4.1.2. Surface properties of PGs

Table 6.4 summarises the mean contact angles for water and DII, polar, non-polar, and total surface energy, as well as the surface polarity of the PGs. Si10 glass showed the lowest water contact angle which increased with Fe_2O_3 content. In contrast, the DII contact angle was not significantly affected by the different compositions. While the polar surface energy and hence the surface polarity decreased by substituting SiO_2 with Fe_2O_3, the dispersive surface energies remained statistically unchanged. Consequently, the total surface energy increased with increasing amounts of SiO_2.

6.4.2. Structural characterization of as prepared PLA-PGF composites

ATR-FTIR spectra of PLA and PLA-PGF composites are presented in Figure 6.1a. The band originating from stretching vibrations of C=O is situated at 1745 cm^{-1} for PLA, which decreased in PLA-Fe5Si5 compared to PLA and PLA-Fe10 (Figure 6.1b). Differences between the spectra of PLA-Fe10 and PLA-Fe5Si5 can also be seen in the 1050-1250 cm^{-1} range attributed to C-O and C-O-C stretching vibrations. The absorbance ratio of the peak at 1745 cm^{-1}:1600 cm^{-1} decreased by 50% in PLA-Fe5Si5 compared to PLA and PLA-Fe10 (Figure 6.1c).

Table 6.4 Contact angle measurements with ultrapure water (CA^{H2O}) and diiodomethane (CA^{DII}), Total surface energy (SE^t) with the dispersive (SE^d) and polar (SE^p) parts of different phosphate glass compositions according to the OWRK method, and surface polarity ($X^p = SE^p/SE^t$). Si10 glass showed the lowest CA^{H2O} which increased significantly by substituting SiO_2 with Fe_2O_3 in the glass formulation; whereas, the contact angle for DII was unchanged. On the other hand, SE^t decreased significantly by substituting SiO_2 with Fe_2O_3. In addition, the substitution of SiO_2 with Fe_2O_3 resulted in reduced surface polarity.

Sample	CA^{H2O} (°)	CA^{DII} (°)	SE^t (mN/m)	SE^d (mN/m)	SE^p (mN/m)	X^p
Si10	10.37 ± 5.99	38.42 ± 3.19	71.97 ± 1.02	28.88 ± 1.66	43.1 ± 2.54	0.60 ± 0.02
Fe5Si5	* 22.85 ± 1.2	37.77 ± 2.04	* 68.43 ± 0.55	29.78 ± 0.81	* 38.71 ± 0.86	* 0.56 ± 0.01
Fe10	** 42.85 ± 1.72	37.2 ± 1.7	** 58.54 ± 0.73	31.91 ± 0.98	** 26.62 ± 1.53	** 0.45 ± 0.02

* Statistically significant compared to Si10 ($p<0.05$)

** Statistically significant compared to Fe5Si5 ($p<0.05$)

The effect of PGF incorporation on the molecular weight of PLA was investigated using GPC. While the M_w of neat PLA was considerably reduced after processing, which could be associated with thermal degradation at the processing temperature (210 °C, 30 minutes, and 38 bar), a 4-fold reduction in PLA M_w was observed in PLA-Fe5Si5 compared to as received PLA, which was also much greater than that in PLA-Fe10 (Figure 6.1d). However, the polydispersity index of all the tested materials was not significantly changed.

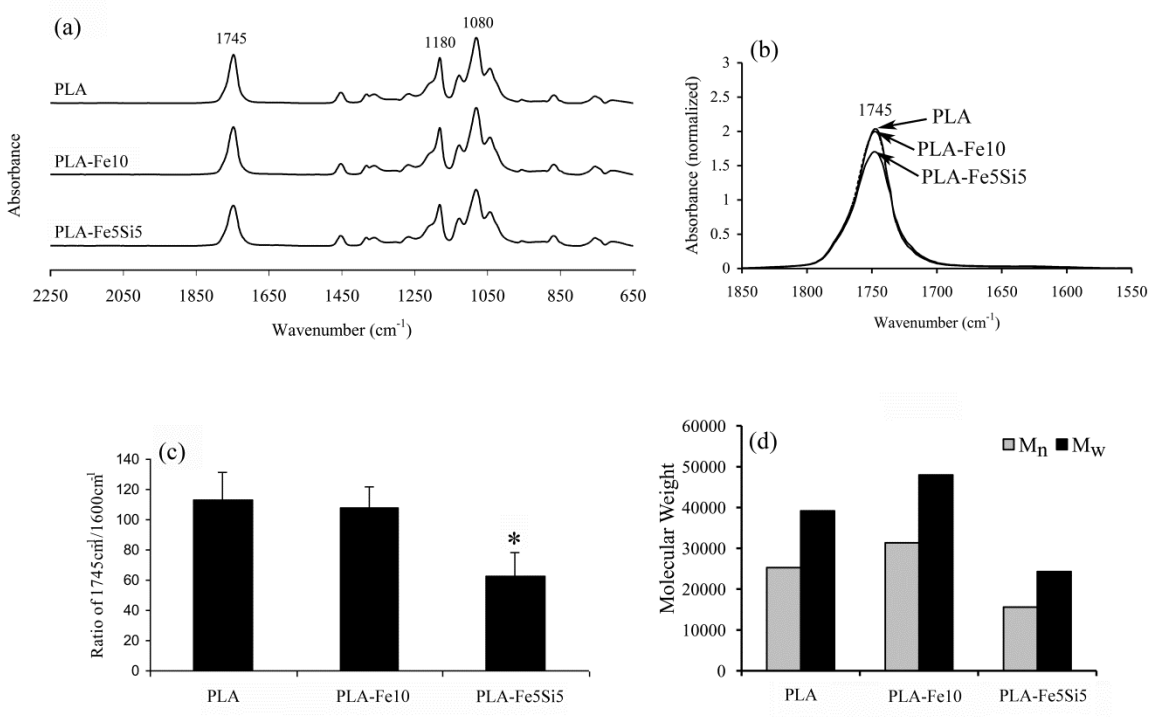

Figure 6.1 ATR-FTIR analysis: (a) ATR-FTIR spectra of as-processed PLA and PLA-PGF composites. PLA-Fe5Si5 showed a decrease in the absorbance of the peaks at 1745 (C=O stretching), 1080 and 1180 cm^{-1} (C-O/C-C stretching). (b) The superimposition of the peak at 1745 cm^{-1} indicating the reduction in its intensity in the case of PLA-Fe5Si5 when compared to PLA and PLA-Fe10. (c) The absorbance ratio of 1745 cm^{-1}/1600 cm^{-1}; there was a statistically significant reduction in this ratio in the case of PLA-Fe5Si5 ($p<0.05$). (d) Gel permeation chromatography: Number (M_n) and weight (M_w) average molecular weight of PLA and PLA in PLA-PGF composites. There was a greater reduction of the molecular weight of as-processed PLA-Fe5Si5 relative to PLA and PLA-Fe10.

6.4.3. Ageing of PLA-PGF composites in DW

Figure 6.2 shows the ion release, percentage of original mass, and pH change as a function of time in DW. At day 4 in DW, PO_4^{3-} and Ca^{2+} release was approximately 10-fold higher in PLA-Fe5Si5 compared to PLA-Fe10 (Figure 6.2a, b, respectively). Fe^{3+} release (Figure 6.2c) showed a similar trend but at a lower extent and greater amount was released from PLA-Fe5Si5 compared to PLA-Fe10. Si^{4+} release occurred within 8 h, which was more rapid compared to the other ionic species which indicated a 48 to 72 h delay prior to release (Figure 6.2d).

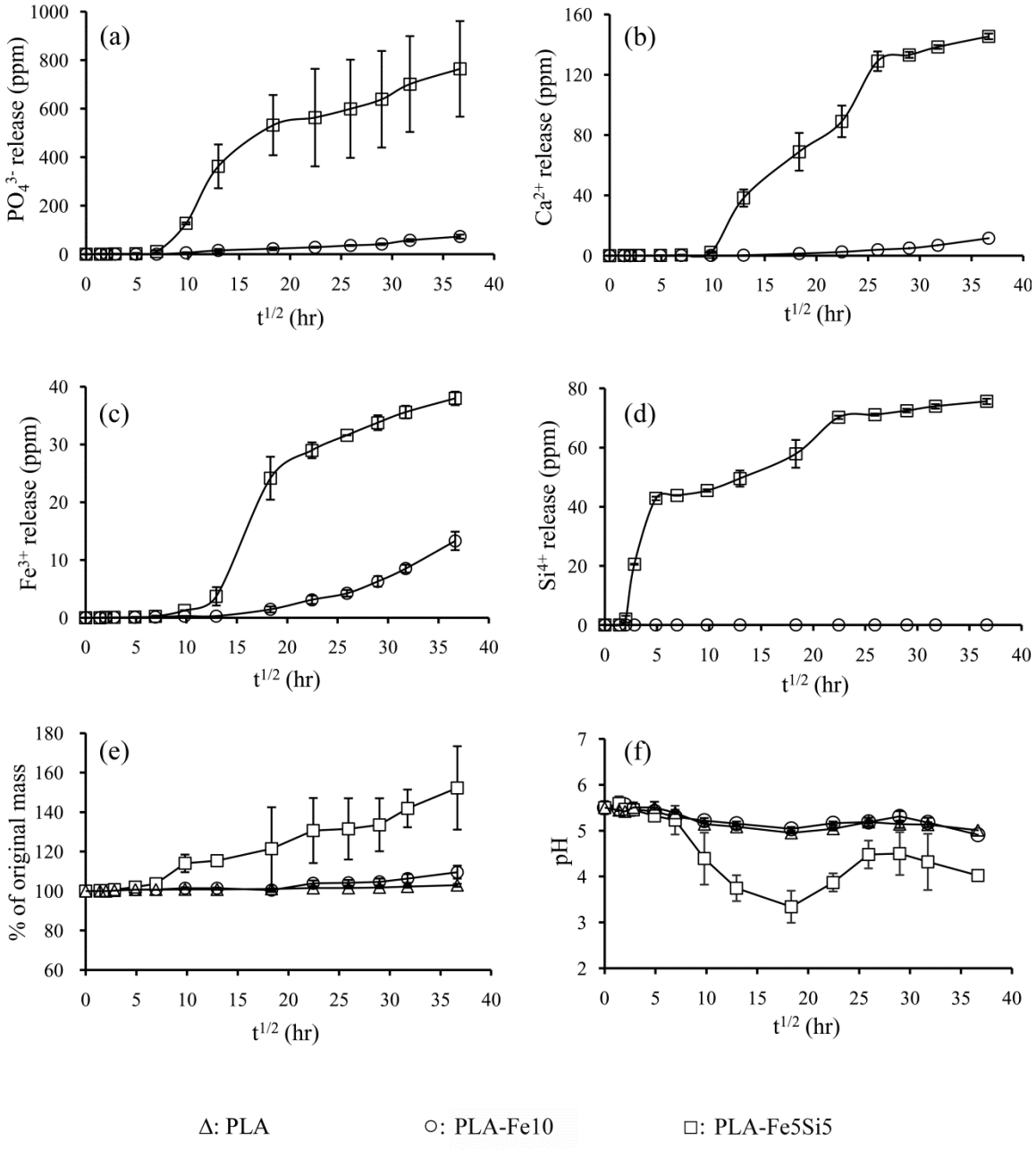

Figure 6.2 Ageing of PLA and PLA-PGF composites in DW incubated for up to 56 days at 37 ºC. (a) PO_4^{3-}, (b) Ca^{2+}, (c) Fe^{3+}, and (d) Si^{4+} ion release. Anion and cation release was higher in PLA-Fe5Si5 compared to PLA-Fe10. (e) Weight loss, and (f) pH change of the immersion environment. PLA-Fe5Si5 composites underwent a significantly higher increase in weight relative to PLA-Fe10 and PLA. There was a relatively greater reduction in the pH of DW in the case of PLA-Fe5Si5

While neat PLA demonstrated no weight change across the entire conditioning period in DW, PLA-Fe10 demonstrated a minor degree of weight gain (<10%) by day 56

(Figure 6.2e). In contrast, after 48 h, there was a significant weight gain in PLA-Fe5Si5 which increased by up to 50% by day 56. The delay in weight gain coincided with the delay in ionic release (Figure 6.2a-c). Based on the final dry weight of the composites at day 56 (Table 6.5), there was a 2.23 and 23.41 % weight loss for PLA-Fe10 and PLA-Fe5Si5, respectively. Residual glass was estimated at 93.36 and 26.17 wt. % for PLA-Fe10 and PLA-Fe5Si5, respectively.

The pH of DW remained relatively unchanged in the presence of PLA and PLA-Fe10 (Figure 6.2f). In the case of PLA-Fe5Si5, there was a decrease in pH, which initiated after 48 h. The pH became increasingly acidic (~pH 3.5) up to 336 h after which, it started to recover (back towards neutral) due to medium replacement at each time interval and reductions in phosphate release (Figure 6.2a).

Table 6.5 Weight loss and residual glass fibres of the samples in the final dry weight of the specimens after 56 days incubation in DW at 37 ^{o}C. At day 56, there were ~7 and 74 wt.% reduction of Fe10 and Fe5Si5, respectively.

Material	% of original mass	Remaining glass (wt.%)
PLA	99.91 ± 0.07	-
PLA-Fe10	97.77 ± 0.73	93.36
PLA-Fe5Si5	76.59 ± 4.23	26.17

6.4.4. Morphological characterisation

SEM micrographs of the morphology of as-processed PLA-PGF composites demonstrated the random distribution of PGFs within the PLA matrix (Figure 6.3a, b). After 56 days immersion in DW, both channels and residual glass fibres were observed in PLA-Fe10 (Fig. 6.3c, d). As a consequence of the increased solubility of Fe5Si5 PGF, PLA-Fe5Si5 demonstrated fewer remaining fibres. In addition there was a substantial presence of matrix associated voids (Figure 6.3e, f).

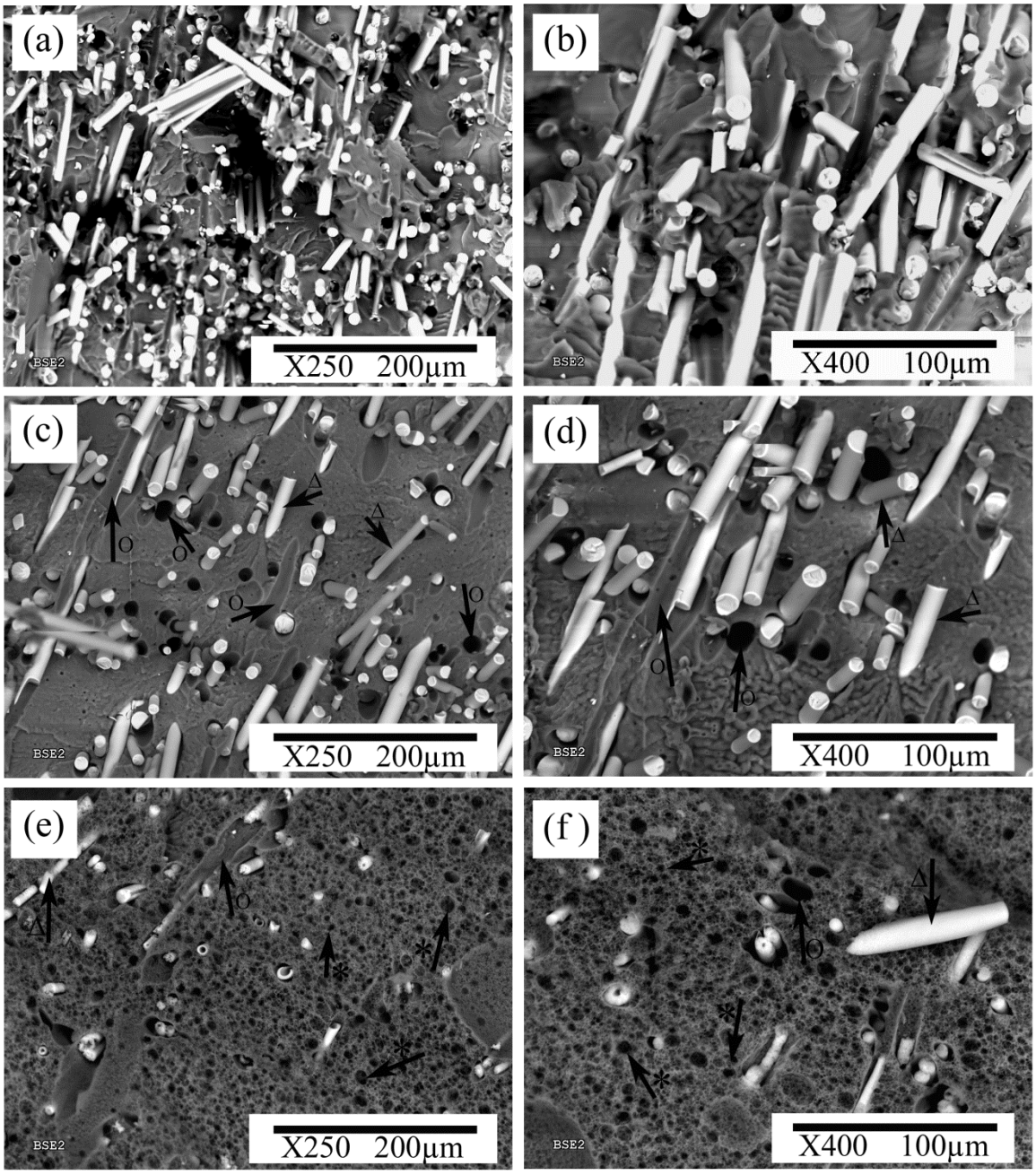

Figure 6.3 Morphological characterisation: SEM micrographs of cryo-fractured specimens as-processed and after conditioning in DW at different magnifications: (a and b) as-processed PLA-PGF composites, (c and d) PLA-Fe10 at day 56 days and (e and f) PLA-Fe5Si5 after 56 days. As-processed composites showed randomly dispersed and attached glass fibres in the polymeric matrix. After 56 days of immersion in DW, a majority of the PGF remained in the microstructure of PCL-Fe10 due to very low degradation rate of Fe10 glass fibres, and channel formation can also be seen as a result of dissolved fibres. In contrast, most of the glass fibres were dissolved in PCL-Fe5Si5 due to considerably higher degradation rate of Fe5Si5 glass fibres. Void formation was observed in the PLA matrix in PLA-Fe5Si5. (Arrows with Δ: PGF, Arrows with O: Channels, Arrows with *: Voids).

6.4.5. Mechanical property changes in PBS

Figure 6.4a shows the weight change in the composites as a function of immersion time in PBS. At Day 28, there was a loss of 11.69 wt.% in the final dry weight of PLA-Fe5Si5, compared to 0.84 wt.% for PLA-Fe10. Mechanical characterisation of as-processed composites demonstrated 2.5- and 2.2-fold increases in the initial flexural strength and modulus through reinforcement with PGF (Figure 6.4b, c). The strain at maximum stress (Figure 6.4d) did not show a statistically significant difference.

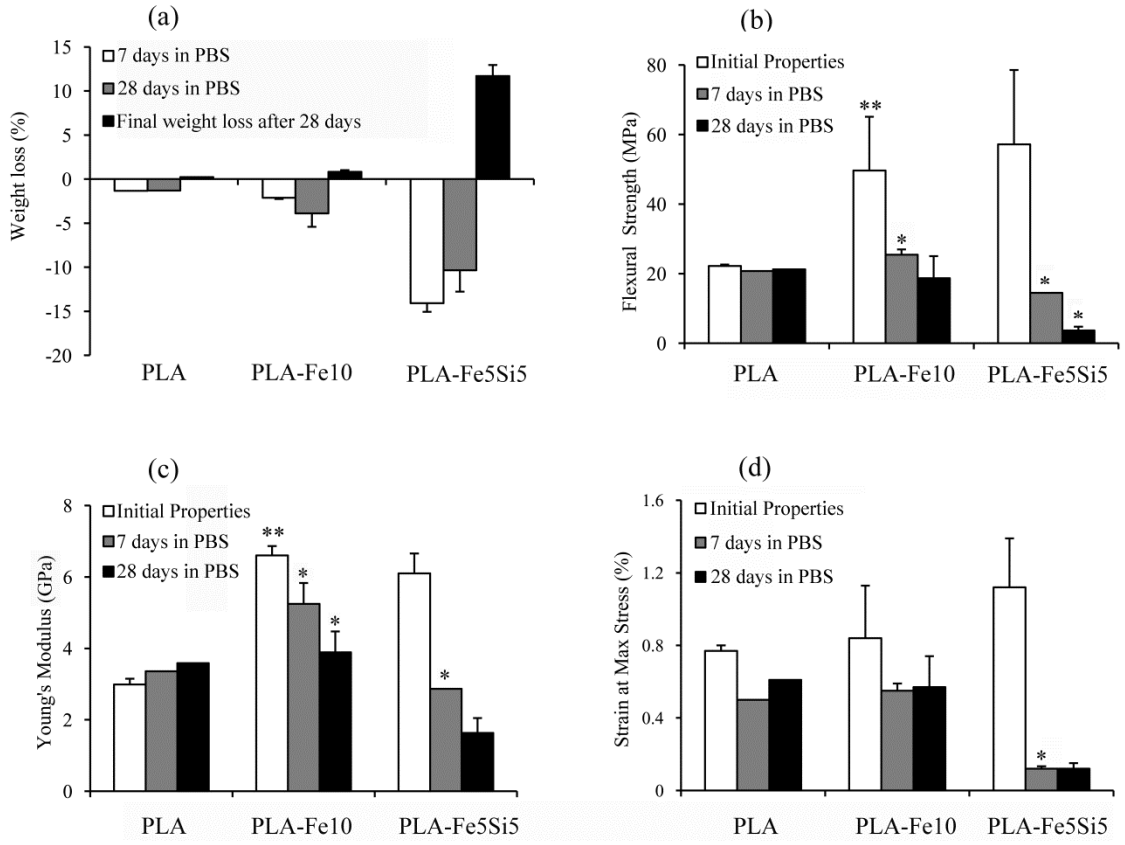

Figure 6.4 Mechanical properties and weight loss over the course of 28 days in PBS: (a) Weight loss of PLA and PLA-PGF composites at days 7 and 28, and final dry weight at day 28. (b) flexural strength (c) flexural modulus, and (d) strain at maximum stress of PLA and PLA-PGF composites as produced and post PBS conditioning. Initial flexural strength increased significantly ($p<0.05$) via the addition of PGF. While flexural modulus increased significantly ($p<0.05$), there was no significant change in strain at maximum stress. After ageing in PBS, the decrease in mechanical properties was considerably higher for Fe5Si5 containing composites compared to Fe10 containing composites. * Statistically significant difference for same time point compared with previous sample ($p<0.05$). ** Statistically significant difference for same sample compared to previous time point ($p<0.05$).

At days 7 and 28 in PBS, the flexural strength of the PLA-PGF composites decreased significantly ($p<0.05$). The reduction was greater in PLA-Fe5Si5 (75 and 94% at days 7 and 28, respectively) compared to PLA-Fe10 (49 and 62% at days 7 and 28, respectively). There was a similar trend in the reduction of the Young's modulus of the composites. Strain at maximum stress of PLA-Fe10 remained relatively unchanged with immersion time whereas that of PLA-Fe5Si5 decreased significantly at day 7. There was no statistically significant difference in the strain at maximum stress between day 7 and 28 for both PLA-Fe10 and PLA-Fe5Si5.

6.4.6. Cytocompatibility assessment of PG and PLA-PGF composites

To assess the cytocompatibility of PG and PLA-PGF composites, the viability of MC3T3-E1 pre-osteoblasts grown on PG glass discs, PLA-Fe10 and PLA-Fe5Si5 was compared to cells grown on either neat PLA or microscope glass slides. After days 1, 4 or 7, cells were stained using calcein-AM (green fluorescent cells) and ethidium bromide homodimer-1 (red fluorescent cell nuclei) and Live/Dead® fluorescence staining was detected by CLSM. Maximum intensity projections of z-stacks obtained by CLSM revealed viable, calcein-AM labelled MC3T3-E1 cells attached to the surfaces of the PG discs (Figure 6.5) as well as PLA, PLA-PGF composites (Figure 6.6) and microscope glass slides at days 1, 4 and 7 in culture. At day 1, live MC3T3-E1 pre-osteoblasts attached to the surface of each of the samples. Fe10 and Fe5Si5 showed a slightly greater extent of MC3T3-E1 pre-osteoblast attachment compared to the control (Figure 6.5). The number of necrotic/apoptotic dead cells, indicated by EtBr-1 nucleic binding, was very low and comparable for each condition. At day 4, as the centre of the PG glass discs was covered by cells (data not shown), confocal images were captured on the edge to reveal the growing cells (Figure 6.5). Cells were viable on the surfaces of Fe10 and Fe5Si5, with a limited number of dead cells observed on the PG glass discs compared to the control. However, at day 7 the cells completely covered the surfaces of both compositions. PLA and the PLA-PGF composites showed a similar extent of MC3T3-E1 pre-osteoblast attachment whereas cell adhesion and spreading onto the microscope glass slide was greater (Figure 6.6). Unlike PLA and microscope glass slide, cell alignment was detected along the PGF within PLA-PGF composites. After 4 days of cell growth, the number of

live cells increased and approached confluence, whilst only a few necrotic/apoptotic cells were detected. At day 7, the surface of all the tested specimens was covered by living cells, and the cell alignment effect of the PGF was still evident within the PLA-PGF composites compared to neat PLA and microscope glass slide.

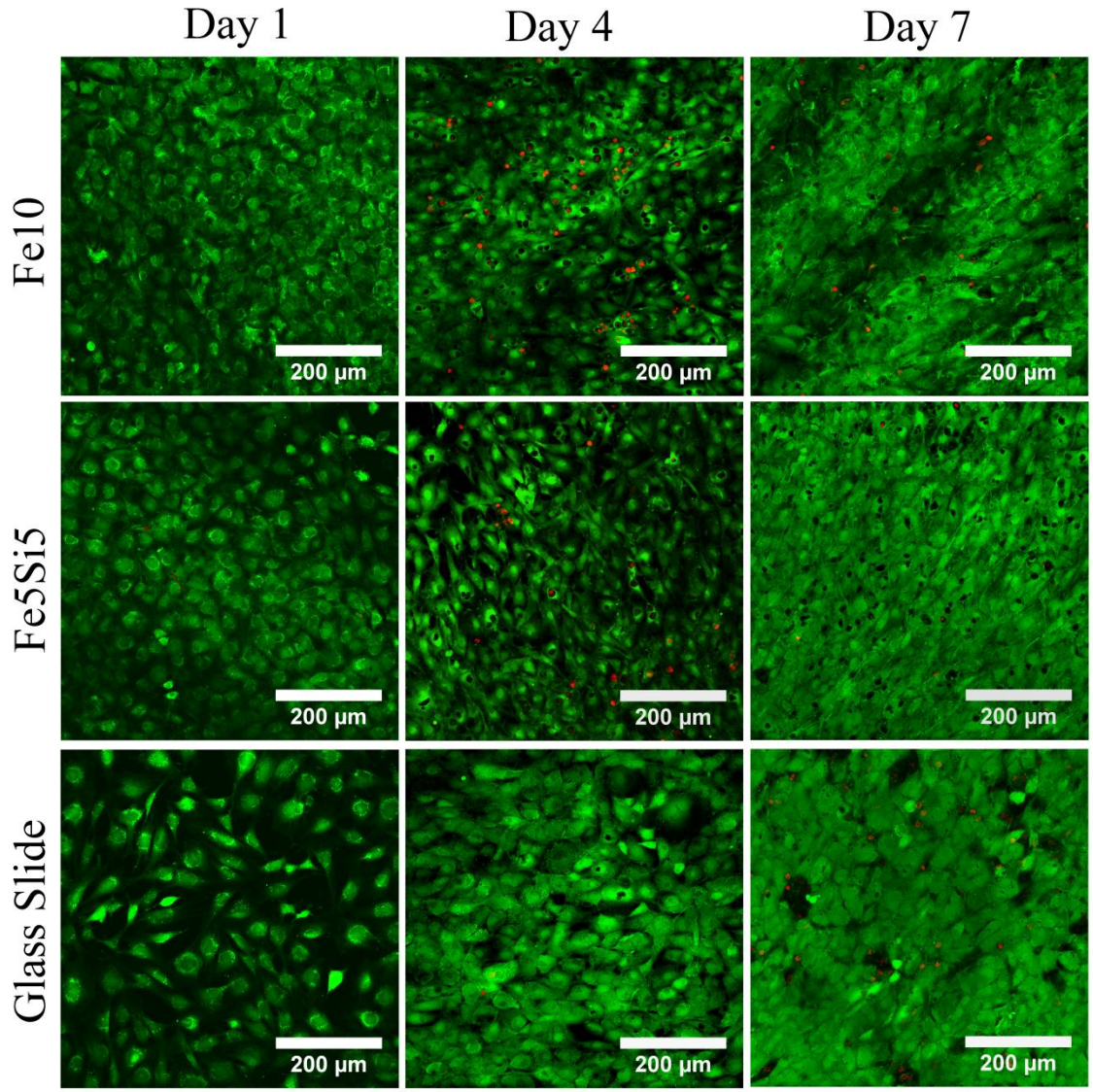

Figure 6.5 Live/Dead® staining of MC3T3-E1 pre-osteoblasts seeded on PG discs: Cells were stained using calcein-AM (green) and ethidium bromide homodimer-1 (red) at days 1, 4 and 7, and fluorescence was detected by CLSM. Fe10 and Fe5Si5 PG discs showed a similar extent of MC3T3-E1 pre-osteoblast attachment higher than the microscope glass on day 1. Since the center of the specimen was covered by cells, day 4 images were captured on the edge of the samples showing the growing cells. The growing cells completely covered the surface of the specimens at day 7.

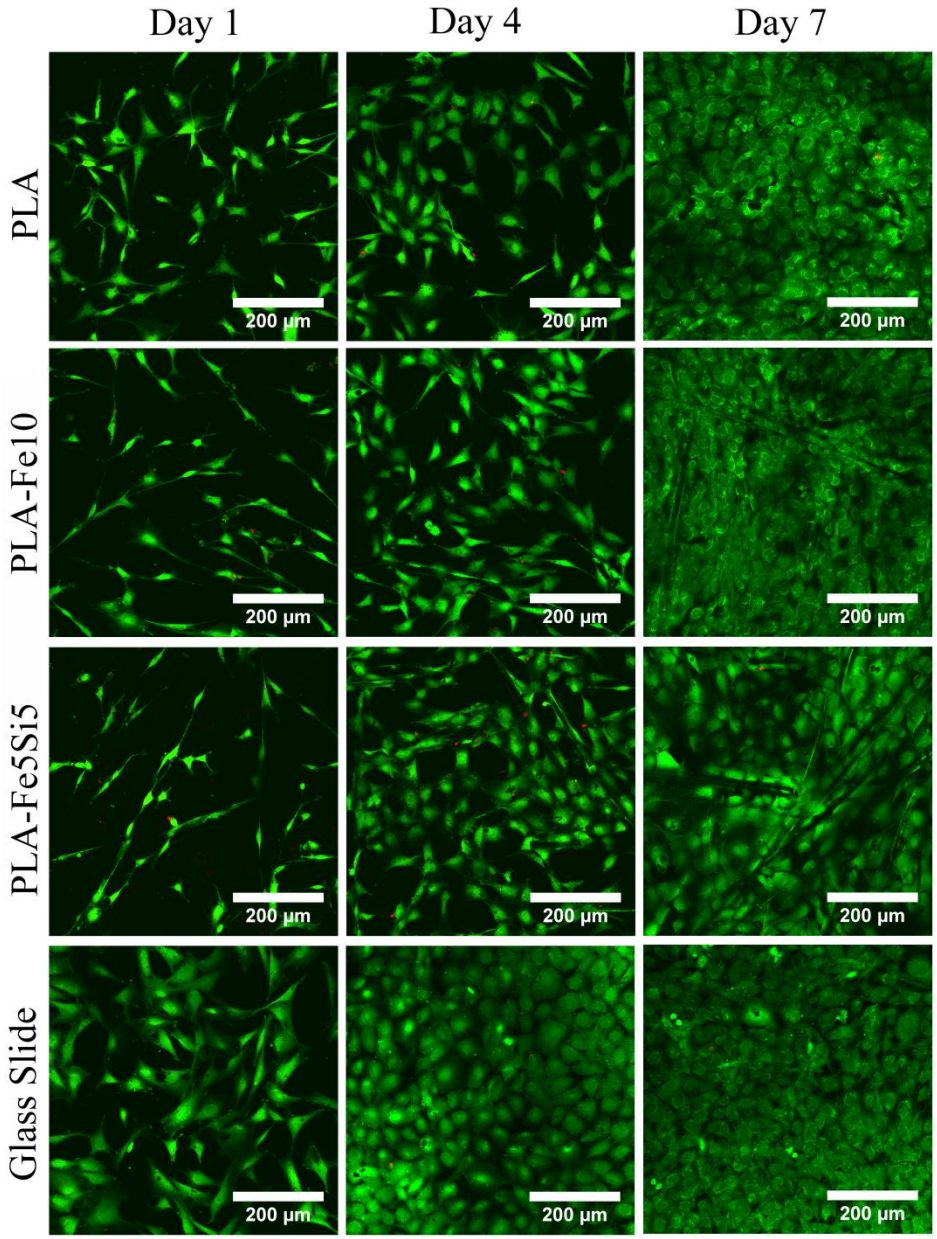

Figure 6.6 Live/Dead® staining of MC3T3-E1 pre-osteoblasts seeded on PLA-PGF composites: Cells were stained using calcein-AM (green) and ethidium bromide homodimer-1 (red) at days 1, 4 and 7, and fluorescence was detected by CLSM. PLA and the PLA-PGF composites showed a similar extent of MC3T3-E1 pre-osteoblast attachment on day 1, while cell adhesion and spreading onto microscope glass was greater. However, cell alignment along the PGF was observed on PLA-PGF composites indicating tendency of the cells towards the PGF. The number of live cells increased and approached confluence similarly on the surface of all tested specimens after 4 and 7 days in culture.

6.5. Discussion

Biodegradable composites of tailored properties for applications in bone augmentation and regeneration could be produced using soluble PGFs and biodegradable polymers, such as PLA. PG composition dictates its degradation characteristic. For example, it has been demonstrated that the presence of Fe_2O_3 strengthens the cross-linking between the glass polyphosphate chains producing hydration resistant bonds, which results in higher glass stability [13, 119]. In contrast, Si breaks down the PG network, lowering the stability and increasing the degradation rates [13]. In addition, the polar interactions at the glass surface are influenced by the composition. It has been shown that Fe_2O_3 incorporation resulted in reduced surface polarity, and hence surface energy [118]. Since SiO_2 disrupts the network, and can form hydroxyl groups (Si-OH) at the surface of PG, the aim of this study was to investigate the effect of Fe_2O_3 and SiO_2 incorporation on the surface properties of PG. Glass surface properties also impacts the nature of interfacial interaction of fibre and matrix, which affects composite properties. Therefore, this study also investigated the influence of incorporating Fe and Si doped PGFs on PLA-PGF composite properties.

X-ray diffraction revealed the presence of calcium phosphate (α-(CaP_2O_6) and α-$Ca(PO_3)_2$) as the main phase of the crystallised PGs. $CaSiO_3$ and $CaFe_2O_4$ were also identified in Fe5Si5 and Fe10 PGs, respectively. Although these phases are present in the crystalline state of the PG, the formation of different phases could be an indication of structural difference which affects the bulk properties.

By altering the composition, the hydrophilicity as well as surface energy of the glasses can be controlled, which significantly affect the hydrolysis driven solubility of PGs, as well as their interactions with the polymer matrix. This study has shown that lower contact angles were obtained on the surface of Si10 and Fe5Si5 compositions when using water as the test liquid due to the polar characteristic of PGs, which can be attributed to the P-O-P bonds [120]. However, substitution of SiO_2 with Fe_2O_3 in the glass formulation significantly increased the contact angle of water, while it decreased the total surface energy, as well as the polar characteristic of the PG. This may be attributable to the reduction in the concentration of hydroxyl groups at the surface of the PG with a decrease in SiO_2. The surface energies of Si10 and Fe5Si5 was 72 and 68.4

mN/m, respectively, which are greater than what has been reported for Bioglass® (54.7 mN/m [147]) and within the range reported for iron containing PGs in the P_2O_5-CaO-Na_2O-Fe_2O_3 systems with 0 to 5 mol.% Fe_2O_3 (61.2 to 76 mN/m) [118]. However, the surface polarity of Si10 and Fe5Si5 compositions were 0.60 and 0.56, respectively, which were higher than that of these PGs (0.43 to 0.51) [118] indicating the effect of SiO_2 on increasing surface polarity. The greater hydrophilicity of Si10 and Fe5Si5 PGs increases their wettability and water adsorption leading to an increase in the concentration of Si-OH groups at the surface.

Hydroxyl group formation at the surface of PGs through SiO_2 incorporation increased the potential for interfacial interaction between the fibres and PLA matrix. As an indication of PLA degradation in the as prepared composites, FTIR spectra of PLA-Fe5Si5 revealed a reduction in the absorbance of the carbonyl peak at 1745 cm^{-1} compared to PLA; whereas, it did not change for PLA-Fe10. Reductions were also observed in the peaks around 1080 and 1180 cm^{-1} which are attributed to C-O/C-C stretching peaks. A previous study [94] also demonstrated similar behaviour with Si doped PG particulates in PCL, where a potential reaction took place between Si10 and the ester bond in the polyester at elevated temperature causing chain-scission and forming carboxylate by-products, which decreased the matrix molecular weight. The high surface energy of Si10 composition, as measured in this study, combined with particulate surface area enhanced the reaction with the PCL ester bond [94]. While carboxylate by-products were not indicated in this study, possibly due to the presence of SiO_2 in the quaternary system (Fe5Si5) with lower surface energy and polarity compared to Si10, combined with the relatively lower surface area of the fibres than particulates, the reduction in the ratio of 1745 cm^{-1}:1600 cm^{-1} indicated PLA chain scission. The reduction in PLA M_w, particularly in the case of PLA-Fe5Si5 confirmed matrix degradation, which was greater than that in neat PLA and PLA-Fe10. Blaker *et al.* [188] confirmed the induction of polyester degradation through silicate-based bioactive glasses incorporated at elevated temperatures. A reduction in the M_w of the matrix by incorporation of bioactive glass particles into poly(ε-caprolactone-co-DL-lactide) has also been reported [8].

The influence of glass surface properties and PLA matrix degradation on the ageing behaviour of the composites was demonstrated through ion release and weight

loss in deionised water. PLA-Fe5Si5 was found to have a significantly greater anion and cation release compared to PLA-Fe10 as reflected by their ion release rates (Supplementary Table 6.1). As previously reported, the release rates of PO_4^{3-} and Ca^{2+} ions were in line with the rate of glass dissolution [112]. While Si^{4+} release was due to the presence of Fe5Si5 fibres, Fe^{3+} also showed a similar dependency on the presence of Si in the formulation. The latter can be explained by the rate of ion release dependence on water uptake. The addition of Si increased the glass solubility and water ingress due to channel formation. The greater exposure of glass fibres to water resulted in greater dissolution and an increase in Fe^{3+} ion release. Since neat PLA did not gain weight, it can be assumed that the water uptake occurred at the fibre-matrix interface and within the degraded matrix, particularly in the case of PLA in PLA-Fe5Si5. Water uptake was higher in PLA-Fe5Si5 compared to PLA-Fe10 due to higher hydrophilicity and surface energy of Fe5Si5. In addition, in the case of PLA-Fe5Si5, matrix degradation may have resulted in the formation of voids upon ageing in DW leading to more water ingress. The voids may be due to the leaching of low molecular weight species produced through PLA matrix degradation. SEM images of PLA-Fe5Si5 after immersion in water displayed void formation within the PLA matrix, which were not observed in either neat PLA (data not shown) or in PLA-Fe10. SEM micrographs confirmed that after 56 days ageing, a much greater amount of the Fe5Si5 fibres dissolved compared to Fe10 fibres. The extensive dissolution of Fe5Si5 fibres led to the creation of channels in the microstructure of the composites, which may also provide interconnectivity within the structure, and allow the release of ionic species from residual glass fibres. Higher degradation rate in Fe5Si5 containing composites led to a more rapid rate of pH reduction compared to PLA-Fe10. The higher release rate of the phosphate species led to an acidic medium through the formation of phosphoric acid [118].

Flexural mechanical analysis showed that incorporating PGF into PLA led to a considerable increase in the flexural strength and Young's modulus, resulting in values within the ranges found for trabecular bone [41, 42, 252] (approximately 40 MPa and 2 GPa for strength and modulus, respectively). These increases were attributed to the higher levels of stress transfer expected from fibre reinforcement, in comparison to particulate reinforcement. Both the length-to-diameter ratio as well as the larger shear

surface of individual reinforcements, led to a higher modulus and reduced ductility. In contrast, Si and Fe doped PG particulates did not increase the strength when incorporated into PCL [94]. It has also been shown that incorporation of various SiO_2 bioactive glass particulates into poly(α-hydroxyesters) at elevated temperatures resulted in a reduction in the strength and modulus and increased degradation of the composite matrices [8, 188, 253].

As a consequence of ageing in PBS, the reduction in mechanical properties was greater for PLA-Fe5Si5 compared to PLA-Fe10, which can be attributed to greater weight loss and channel generation, as well as PLA matrix degradation in PLA-Fe5Si5. The lower solubility rate of Fe10 was reflected by the greater retention of the mechanical properties of PLA-Fe10 (~ 22 MPa and 4.2 GPa for strength and modulus, respectively, at day 28), which were still within the range for trabecular bone.

The cytocompatibility of PGs has been demonstrated to be dependent on their solubility rate [113, 269, 270]. For example, Skelton *et al*. [23] showed that as a consequence of their rapid dissolution, PGs of the system $50P_2O_5$-(50-x)CaO-xNa_2O, x = 2 to 10 mol.% adversely affected the viability of osteoblasts. PGs with lower degradation rates demonstrated better cytocompatibility, viability, and proliferation, and early differentiation was only observed at higher CaO content (48 mol.%). However, the incorporation of metal oxides, such as TiO_2 and Fe_2O_3, has been shown to improve biocompatibility by controlling the glass degradation and ionic release rates hence maintaining the appropriate pH favoured by the osteoblasts [28, 269]. Bitar *et al.* [269] investigated the biological response of PGs in the $50P_2O_5$-46CaO-xNa_2O-yFe_2O_3 (y = 0-3 mol.%) system using primary human osteoblasts and fibroblasts. Replacing Na_2O with Fe_2O_3 resulted in significant improvement in cell viability, proliferation and differentiation. In addition, the positive effect of Si on bone metabolism has been demonstrated, and its substitution into calcium phosphate ceramics, e.g. hydroxyapatite (HA) or tricalcium phosphate, has demonstrated enhanced biological responses [241]. However, the direct influence of Si on osteoblastic cells is still under question due to the lack of evidence of therapeutic release of Si from these calcium phosphates [257]. The incorporation of Si into soluble PGs can also control the release of phosphorous and calcium ions which may affect the biological behaviour of osteoblasts. For example, the

release of phosphorous and calcium ions from HA coatings has been shown to influence osteoblast responses, where enhanced osteoblast differentiation was observed with additional calcium concentration; while additional phosphorous was suggested to slow down the differentiation and mineralisation [271]. In this study, MC3T3-E1 cells remained viable and approached confluency on Fe10 and Fe5Si5 PG discs compared to cells grown on microscope glass slides. The addition of Si and Fe containing PGF into PLA altered the pre-osteoblastic cytocompatibility of the materials and cell alignment along the PGF was observed indicating the tendency of pre-osteoblasts towards PGF. This could be due to the release of favourable ions from the PGF which needs further investigations. Similar study using MG63 cell line on PLA-PGF ($50P_2O_5$-40CaO-$5Na_2O$-$5Fe_2O_3$) composite have shown cell attachment and viability yet to a lower extent compared to this study [191].

6.6. Conclusions

PG composition can greatly influence its bulk and surface properties, which would also affect composite properties when incorporated as fillers. In this study, the effect of SiO_2 and Fe_2O_3 doping on PG surface properties, and its influence on the composite properties when incorporated into PLA as PGF were investigated. The addition of SiO_2 in the PG formulation resulted in higher hydrophilicity, surface energy, and surface polarity. Increased surface energy and polarity increased the interaction between the Fe5Si5 and the polymer matrix reducing the molecular weight of the PLA matrix by chain-scission, which did not occur in PLA-Fe10 (SiO_2 free PGF). Increased hydrophilicity resulted in more rapid hydrolysis of the glass resulting in higher degradation and ion release in the composite system, as well as increased water uptake. Initially, PGF incorporation increased the strength and modulus of the composites by 2.5- and 2.2-fold, respectively, compared to neat PLA. The reduction in mechanical properties after ageing in PBS was higher for PLA-Fe5Si5 compared to PLA-Fe10 due to higher degradation rate of Fe5Si5 fibres. In addition, MC3T3-E1 pre-osteoblasts showed that the investigated composites were cytocompatible and cells preferably aligned along the phosphate glass fibres in PLA-PGF composites.

6.7. Acknowledgements

This work was funded by the Canadian Natural Sciences and Engineering Research Council, le Fonds Québécois de la Recherche sur la Nature et les Technologies, McGill University Faculty of Engineering Hatch Faculty Fellowship, and Canada Foundation for Innovation: Leaders Opportunity Fund. Funding for Maziar Shah Mohammadi was also partly supported by a McGill Engineering Doctoral Award. The authors thank Saurav Mohapatra and Hye-Lim Choi for their assistance in this work. Martin N. Bureau is a member of the Groupe de Recherche en Sciences et Technologies Biomédicales (Fonds de recherche en santé du Québec).

6.8. Appendix: Supplementary data

Supplementary Table 6.1 Ion release rates calculated from the slope of the linear incline of the graphs in Figure 6.2 for the investigated composites. Ion release rate was greater from PLA-Fe5Si5 compared to PLA-Fe10 due to the higher degradation rate of Fe5Si5 PGFs than Fe10.

Composite code	PO_4^{3-} release ($ppm.h^{-1}$)	Ca^{2+} release ($ppm.h^{-1}$)	Si^{4+} release ($ppm.h^{-1}$)	Fe^{3+} release ($ppm.h^{-1}$)
PLA-Fe10	0.04 ± 0.009	0.009 ± 0.003	-	0.011 ± 0.004
PLA-Fe5Si5	2.96 ± 0.3	0.2 ± 0.026	1.85 ± 0.025	0.1 ± 0.019

CHAPTER 7

Si AND Ti DOPED CALCIUM PHOSPHATE-BASED GLASSES FOR BONE TISSUE ENGINEERING APPLICATIONS

There is a large demand for bioresorbable biomaterials in tissue regeneration that can stimulate controlled cellular responses that would be replaced by the natural tissue as they degrade. In phosphate-based glasses (PGs), this may be achieved by tailoring the glass composition.

In previous studies, Si and Fe incorporation into PG was attempted in order to modify the PG properties. It was shown that while Si increased the glass solubility by disrupting the phosphate network, Fe reduced the dissolution rate cross-linking the glass network. Therefore, PGs with various degradation rates from 2.3×10^{-3} to 1×10^{-5} $mg.mm^{-2}.h^{-1}$ were produced. Composites of biodegradable polymers incorporating these PG formulations were characterised in terms of weight loss, ion release, pH change, mechanical properties initially and post conditioning in physiological fluids, bioactivity ad cytocompatibility.

The present study developed sodium-free PG formulations doped with SiO_2 and TiO_2 in order to tailor the properties of PGs for potential application in bone tissue engineering. This was performed by substituting Fe_2O_3 as the network modifier in previous studies with TiO_2. Hence, $50P_2O_5$-40CaO-xSiO_2-(10-x)TiO_2, where x = 10, 7, 5, 3 and 0 mol.%, formulations were developed and investigated.

A manuscript based upon these research findings is under preparation to be submitted for peer-review.

Effect of silica and titania doping on sodium-free calcium phosphate-based glass properties for bone tissue engineering

Maziar Shah Mohammadi[a], Florencia Chicatun[a], Christoph Stähli[a], Naser Muja[a], Martin N Bureau[b], Showan N Nazhat[a]

[a] *Department of Mining and Materials Engineering, McGill University, Montreal, QC, H3A 2B2, Canada*

[b] *Industrial Materials Institute, National Research Council Canada, QC, J4B 6Y4, Canada*

Key words: Calcium phosphate-based glass, silica, titania, degradation, ion release, tissue engineering

7.1. Abstract

Soluble phosphate-based glasses (PGs) are of potential interest for bone tissue engineering applications as their dissolution and ionic release rates can be controlled by their composition. Silicate-based glasses have been extensively investigated for bone applications, and Si has been shown to improve osteoblastic response in calcium phosphates. TiO_2 incorporation has also demonstrated enhanced biological response of PGs. Furthermore, the addition of Na_2O as a modifying oxide, which has been a major component of the majority of PG formulations that have been investigated to date, may not be required. Therefore, this study developed and investigated the properties of Na-free PGs doped with both SiO_2 and TiO_2. The structural and chemical properties, as well as degradation, ion release, and osteogenic potential of PGs with the formulation $50P_2O_5$-40CaO-xSiO_2-(10-x)TiO_2, where x = 10, 7, 5, 3, and 0 mol.%, were investigated.

Substituting SiO_2 with TiO_2 resulted in a concomitant increase in density and glass transition temperature, indicating the cross-linking effect of Ti in the glass network and resulted in significantly lower degradation rates. X-ray diffraction revealed the presence of $Ti(P_2O_7)$ in crystallized TiO_2-containing PGs, and nuclear magnetic resonance showed an increase in Q^1 phosphate species with increasing TiO_2 content suggesting an increase in P-O-Ti bonds. Contact angle measurements showed that the substitution of SiO_2 with TiO_2 resulted in reduced hydrophilicity and surface energy. The incorporation of TiO_2 significantly increased MC3T3-E1 pre-osteoblasts viability, metabolic and alkaline phosphatase (ALP) activities. However, the increased ionic release from the PG, attributable to the presence of SiO_2 in the TiO_2-doped formulations, led to an up-regulation in ALP activity. While incorporating 3 mol.% TiO_2 stabilised the PG network against degradation in aqueous environments, ALP activity was higher in PGs with 5 to 7 mol.% SiO_2. Thus, a combination of Si and Ti doping may be required for optimum control of ion release and osteoblastic response. Doping PGs with SiO_2 and TiO_2 showed promising tailored properties for potential bone tissue engineering applications.

7.2. Introduction

In recent decades, the interest in biomaterials science has altered from developing inert materials with a passive interface to materials that interact with living tissues without compromising their natural biological procedure [28]. There is a large demand for bioactive and bioresorbable biomaterials in bone tissue engineering that stimulate controlled osteoblastic responses [3], which should be replaced by the regenerating bone as they degrade [272].

The positive effect of Si on bone metabolism has been recognized [241, 243], and silicate-based glasses (SGs) have been extensively investigated for bone applications [241]. In particular, Bioglass® (45S5) is Food and Drug Administration approved as bone grafting material for intraoral applications [273]. Xynos *et al.* [274] have shown the positive effect of the ionic products of bioactive glass dissolution on the proliferation of human osteoblasts, induction of insulin-like growth factor II, and protein synthesis. In their study, the analysis of the bioactive glass-conditioned medium showed an 88-fold higher Si concentration with also changes in the P^{5+} and Ca^{2+} concentrations relative to control, and suggested that solutions containing high Si concentrations are mitogenic for bone cells as had previously been reported by Keeting *et al.* [275]. In addition, there has been much research interest in Si-containing bone graft substitutes leading to the development of Si-substituted calcium phosphates [276, 277]. Si-substituted hydroxyapatite or tricalcium phosphate have shown that cells are positively influenced through the release of Si ions during material resorption [241]. Gupta *et al.* [278] demonstrated increased osteoblastic differentiation through the effect of exogenous P and Si at the interface of an Si-rich calcium phosphate where Si was shown to up-regulate osteocalcin and osteopontin expression. In addition, dissolved Si has been demonstrated to increase collagen-I synthesis and enhance osteoblastic differentiation [279]. However, such studies have been questioned since there is not enough evidence of therapeutic release of Si from these calcium phosphates. Moreover, it has not been clearly demonstrated whether the positive biological response of Si-substituted calcium phosphates is due to Si ion release, or other effects such as change in material properties; e.g. topographical effect, or release of Ca^{2+} ions [257]. In addition to Si, dissolved P and Ca can either positively or negatively affect the function of osteoblasts depending on

their concentration in media. For example, exposure to Ca^{2+} has been shown to enhance osteoblastic function [271]. Moreover, the presence of phosphorous in the media can act as a specific signal for the expression of osteopontin and protein synthesis by osteoblast-like cells [280]. However, elevated P^{5+} concentration was suggested to slow down osteoblastic differentiation and mineralisation [271, 281]. Therefore, the controlled release of ionic products from ceramic or glass dissolution plays a key role in stimulating and enhancing bone-cell function [278].

Owing to their soluble nature in aqueous environments, phosphate-based glasses (PGs) have emerged as potential bioinorganics for bone tissue engineering [11, 12]. These glasses are soluble due to the hydrolysis of the P-O-P bonds and their solubility and ionic release can be predicted and controlled through their chemistry, specifically by the addition of modifying oxides [13, 14, 98]. Various PG formulations have been developed and investigated for biomedical applications, mainly based on P_2O_5-CaO-Na_2O systems [19, 29, 99-101, 109, 110, 112, 118, 119]. Na_2O is deemed important to be a major component of the SGs in order to reduce the high network connectivity and increase the surface reactivity [20]. However, PGs are readily soluble in aqueous environments due to their lower network connectivity and may not require Na_2O as a modifying oxide. In addition, the positive effect of Na^+ ions on cells has been questioned [22, 23]. The addition of CaO, on the other hand, has been shown to increase the stability of PGs since the divalent cationic nature of Ca ionically cross-links the phosphate chains [138]. In addition, high Ca containing metaphosphate glasses have elicited a better cellular proliferation compared to those of the low calcium content [110]. Moreover, the incorporation of titania (TiO_2) into PGs has been attempted to control their degradation rate and improve their biological response [28, 29, 120, 134, 282]. A reduction in degradation rate was obtained by incorporation of up to 5 mol.% TiO_2 into P_2O_5-CaO-Na_2O system which was attributed to the formation of strong P-O-Ti bonds. Moreover, addition of TiO_2 enhanced the MG63 cells attachment and viability [29]. In contrast, the incorporation of SiO_2 into PGs has been shown to increase the degradation rate by disrupting the glass network [13, 94]. It has been stated that the bonds formed in SiO_2-P_2O_5 network may be more sensitive to hydrolytic activity [13]. Therefore, Si substitution

may be a suitable alternative to Na_2O containing PGs for releasing controlled amounts of bioinorganics for bone applications.

In order to assess the influence of Si on the properties of bioinorganic releasing glasses, this study developed Na-free PGs doped with a combination of silica and titania. The physico-chemical, surface, dissolution and ionic release characteristics as well as osteogenic potential of the glasses were investigated, in order to tailor the properties of PGs for potential application in bone tissue engineering.

7.3. Experimental

7.3.1. Phosphate glass production

P_2O_5, $CaHPO_4$, SiO_2 (Alfa Aesar), and TiO_2 (Sigma Aldrich) precursors were used to produce melt derived PG compositions given in Table 7.1. The precursors were dry blended, poured into a Pt/10%Rh crucible (Kitco Inc.) and placed into a furnace (Carbolite RHF1500, Ancansco) at 350 °C for 20 min in order to remove the moisture. The precursors were then melted at the various temperatures and times (Table 7.1). The melt was cast in a pre-heated cylindrical shape graphite mould (10 mm in diameter), and annealed to remove the residual stresses (Table 7.1). The glass rods were then cut into approximately 2 mm thick discs using a diamond blade cutting machine (Buehler, IsoMet®).

Table 7.1 Glass compositions, coding, and processing conditions.

Glass code	Glass composition (mol.%)				Processing temperature	
	P_2O_5	CaO	SiO_2	TiO_2	Melting	Annealing
					T (^{o}C)/t (h)	T (^{o}C)/t (h)
Si10	50	40	10	0	1150/1.5	450/2
Si7Ti3	50	40	7	3	1350/3.5	450/2
Si5Ti5	50	40	5	5	1350/3.5	450/2
Si3Ti7	50	40	3	7	1500/3.5	550/2
Ti10	50	40	0	10	1500/3.5	550/2

7.3.2. Characterization of the glass bulk and surface properties

7.3.2.1. Density measurements

Density measurements were carried out using Archimedes' principle (n=3) through a density kit attached to an analytical balance (Mettler Toledo, AB265-S/FACT). Ethanol was used as the submersion liquid.

7.3.2.2. Differential thermal analysis

Differential thermal analysis (DTA, TA Instruments SDT Q600) was conducted to identify the three main thermal parameters: glass transition temperature (T_g), crystallization temperature (T_c) and melting temperature (T_m). The test was carried out on powdered glass samples of approximately 50 mg from 25°C up to 1200 °C at a heating rate of 10 °C/min under nitrogen purge. An empty crucible was used as a reference.

7.3.2.3. X-ray diffraction of the crystallised PG

X-ray diffraction (XRD) was used to identify the phases that are present in the crystalline state of the glasses. The glass compositions were crystallized at the temperatures obtained from DTA for 3 h. The test was conducted on a Bruker Diffractometer (Bruker AXS Inc.) in flat plate geometry from $2\Theta = 6^o$ to 86^o, with Ni-filtered Cu k_α radiation, and a Philips (PW1710) from $2\Theta = 5^o$ to 100^o with a step size of 0.02 and a count time of 0.1 s. The patterns were analysed using the EVA software package.

7.3.2.4. Nuclear magnetic resonance (NMR)

^{31}P MAS spectra were obtained at a frequency of 161.8 MHz on a Varian VNMRS400 spectrometer. Samples were placed in 4 mm rotors and spun at 12500 Hz. A 30^0 pulse was applied every 5 s and typically 128 scans were accumulated. Spinworks software was used for deconvolution of the spectra and calculating different species fractions.

7.3.2.5. Wettability and surface free energy of the PG

Glass discs from each composition were abraded against silicon carbide paper (1200/4000, Struers) using ethanol as the lubricant. Prior to the test, the samples were

ultrasonicated in ethanol for 20 min and allowed to dry. The static contact angle was measured with a contact angle system OCA (Future Digital Scientific) and ultrapure water (UW) and diiodomethane (DII) were used to represent both polar and non-polar characteristics, respectively. Droplets (5 µl) were placed on the glass surface via a syringe and the drop profile was recorded for 10 sec. The contact angle was calculated after 2 sec from the time the droplet was in contact with the surface. The measurements were carried out in triplicates. The surface free energy was calculated using the Owens, Wendt, Rable and Kaelble (OWRK) method via SCA20 software.

7.3.3. Ageing in deionised water

PG discs (Φ=10 mm, n=3) were placed in polypropylene vials containing 10 ml of ultra-pure deionised water (DW, 18.2 MΩ cm resistivity) and incubated for up to 28 days at 37 °C. Ion release, weight loss, and pH of the ageing environment were measured at 6, 24, 72, 168, 336, 504 and 672 hours.

Individual solutions were analysed using an inductively coupled plasma-optical emission spectrophotometer (ICP-OES) (Thermo Jarrell Ash – TRACE SCAN) in order to quantify the released cations (Ca^{2+}, Si^{4+} and Fe^{3+}) as well as the total amount of phosphorous atoms present in phosphate species. Nitric acid (4%) was added to all samples in order to stabilise the iron ions in their higher oxidation state (3+). Standard solutions (also containing 4% nitric acid) were prepared by serially diluting certified standards to 100, 50, 10, 5 and 1 ppm. The data was plotted as the cumulative ion release as a function of time.

The weight loss of the glass was investigated by removing the specimens from DW, blot drying, weighing and replacing in fresh DW. The surface area of each glass disc was calculated at each time point by measuring the dimensions using a calliper (DURATOOL DC150), as the weight loss rate can be affected by the surface area. The data was plotted as weight loss/surface area (SA) as a function of time in order to calculate the weight loss rate as $mg.mm^{-2}.h^{-1}$.

The pH of the deionised water was also measured using a pH meter (Accumet Excel 20, Fisher) at each time point.

7.3.4. *In vitro* biological assessment using MC3T3-E1 pre-osteoblasts

7.3.4.1. Cell viability

Cell viability was assessed on all PG compositions and compared to that on microscope glass (positive control). $50P_2O_5$-40CaO-$5Na_2O$-$5TiO_2$ (Na5Ti5), published elsewhere [136], was also produced and tested to compare the effect of having SiO_2 instead of Na_2O in the glass composition on the biological response. Murine MC3T3-E1 pre-osteoblasts (ATCC subclone 14, Cedarlane Laboratories) were maintained in Minimum Essential Medium (MEM, Gibco-Invitrogen) containing 1 % Penicillin/streptomycin (Gibco), 2 mM L-glutamine (Gibco), 0.225 mM aspartic acid (Sigma), and 10 % v/v of fetal bovine serum (Hyclone) at 37 °C in a 5% CO_2 humidified atmosphere. Prior to cell seeding, PG discs (φ = 1 cm) and glass slide fragments, each with a surface area of 1 cm^2, were abraded against silicon carbide paper (1200/4000, Struers) using ethanol as a lubricant, ultrasonicated in ethanol for 20 min, and allowed to dry. The samples were sterilised by dry heating at 120^oC for 1 h. Specimens were then transferred to cell growth medium and conditioned overnight in a tissue culture incubator. MC3T3-E1 pre-osteoblasts were detached from tissue culture flasks (0.05% trypsin/0.02% EDTA), collected by centrifugal rotation (80xg, 5 min) and seeded onto the samples at a density of 1.0×10^4 cells/cm^2. After 1, 4 and 7 days in culture, cells were labelled using 1 mM calcein AM and 0.1 mM ethidium bromide homodimer-1 (LIVE/DEAD®, Invitrogen) in αMEM for 30 min. Fluorescent labeled cells were imaged using confocal laser scanning microscopy (CLSM, LSM 5, Carl Zeiss, Oberkochen, Germany; laser excitation 488 and 543 nm) and a baseline confocal z-stack was acquired at 1 Airy unit using a 20x EC Plan-Neofluar objective (0.5 N.A.). Opaque materials were gently inverted (i.e. cell growth surface facing the microscope objective) onto a 50 mm Pelco glass bottom Petri dish (Ted Pella Inc., Redding, CA). Maximum intensity projections were generated and analyzed using NIH ImageJ v1.43 software.

7.3.4.2. Cell proliferation assay

The metabolic activity of MC3T3-E1 pre-osteoblast cells was evaluated for up to 2 weeks in the presence of the PG extracts using the AlamarBlue™ assay (Biosource). PG extracts were prepared by dissolving respective amounts of PG particulates in

medium and incubated at 37 ^{o}C to mimic the release of each formulation at day 3. The values were calculated using the PG weight loss profile. The solutions were then used to treat the cells and investigate the effect of PG dissolution by-products on cell proliferation. Each medium was exchanged every 2 days. At days 1, 4, 7, 10 and 14, the culture medium was replaced with MEM containing 10% by volume AlamarBlue^{TM} reagent and incubated at 37 °C for 4 h. Aliquots (100 μL) of the supernatants (n=3) of each well were pipetted into 96-well plates and the resulting fluorescence was read with a spectrofluorometer (Mithras LB 940, Berthold technologies) with excitation and emission at 570 nm and 585 nm.

7.3.4.3. Alkaline phosphatase quantification

Alkaline phosphatase (ALP) activity of MC3T3-E1 pre-osteoblast cells was evaluated for up to 2 weeks in the presence of the PG extracts using the ALP kit (SIGMAFAST™, Sigma). The solutions described in section 7.3.4.2 were used to treat the cell cultures in 24-well plates. Three controls (growth medium) were used: non-treated (NT), with ascorbic acid (AA), and with AA and β-glycerophosphate (AA+GP). The cultures were washed thoroughly with phosphate-buffered saline and solubilised in 10 mM Tris, pH 7.4, 0.2% Igepal (Sigma) and 2 mM phenylmethylsulfonyl fluoride for 10 min on ice, and detached from the culture dish with a cell scraper. After 30s (2x) sonication and 10 min centrifugation at 2000 rpm at 4 ^{o}C, the supernatant was extracted and used for measuring ALP activity and protein concentration (micro BCA protein kit, Pierce) at days 1, 7 and 14 in culture. ALP activity was determined colorimetrically by mixing 10 μL supernatant (n=3) with 200 μL of a freshly prepared substrate solution (SIGMAFAST™ p-nitrophenyl phosphate and Tris buffer tablets, Sigma). After 30 min incubation in the dark at 37 °C, 0.5 M NaOH was added to stop the reaction and an absorbance reading was taken at 405 nm using a microplate reader (Mithras LB 940, Berthold technologies). Protein content was measured by mixing an equal volume of working solution and sample, and incubating for 1 h at 60 °C, before reading the absorbance at 562 nm. Albumin (BSA) was used as a standard. Calf intestinal ALP (Sigma) was used as a standard. ALP activity was normalized to cellular protein content.

7.3.5. Statistical analysis

Student's *t*-test was used to determine the significance in the difference between two mean values, which was used to determine *p*-values at a significance level of 0.05. Regarding the biological response experiments (cell proliferation and differentiation), statistically significant differences among groups were determined using one-way ANOVA with a Tukey-Kramer's post-hoc multiple comparison of means. The level of statistical significance was set at $p = 0.05$.

7.4. Results

7.4.1. Density and thermal properties of PGs

Figure 7.1 shows representative DTA thermograms of the PG formulations. There was an increase in T_g by substituting SiO_2 with TiO_2 (from 542±1.7 °C for Si10 to 603±1.9 °C for Ti10). The density of the PGs increased significantly ($p<0.05$) by substituting SiO_2 with TiO_2.

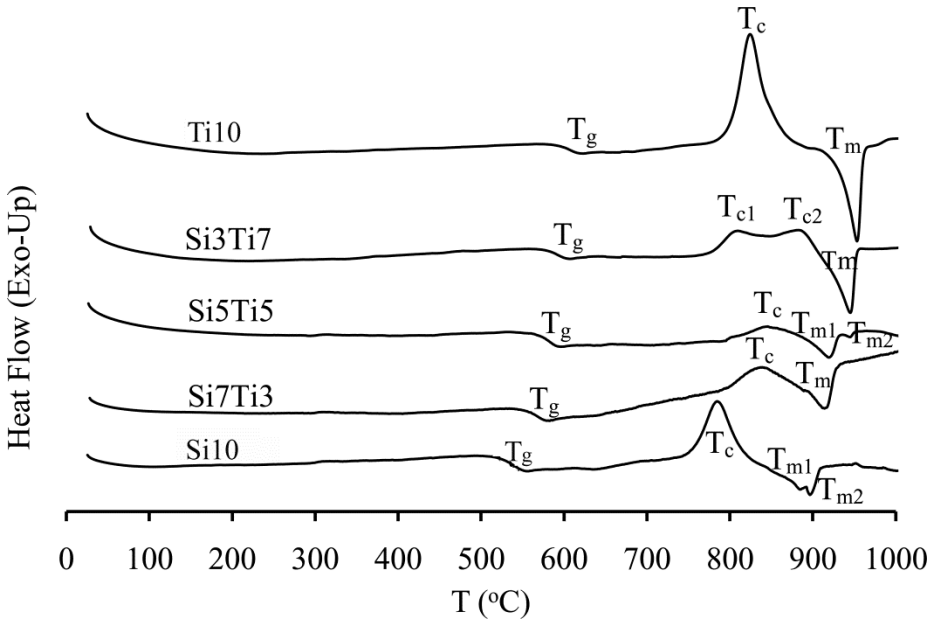

Figure 7.1 Representative DTA thermograms of investigated Si and Ti-doped PGs showing glass transition temperature (T_g), glass crystallization temperature (T_c), and melting temperature (T_m). T_g and T_m of the PGs increased by substituting SiO_2 with TiO_2. Tc was observed in the range of 780-890 °C for all the PG formulations.

Crystallization peaks were observed in the range of 780-890 °C, which were used to crystallize the glass samples to identify their crystalline phases through XRD. Si3Ti7 exhibited two crystallisation temperatures at 820±10.2 °C and 885.8±2.9 °C. Except for Si10 and Si5Ti5 that indicated a second melting temperature (T_{m2}) at 909.3±14 °C and 949.8±3.4 °C, respectively, the T_{m1} increased gradually by substituting SiO_2 with TiO_2 from 894.8±10.5 °C for Si10 to 952.6±2.8 °C for Ti10. There was a concomitant increase in the density of the PGs by substituting SiO_2 with TiO_2 (from 2.48±0.01 g.cm^{-3} for Si10 to 2.65±0.01 g.cm^{-3} for Ti10) (Figure 7.2).

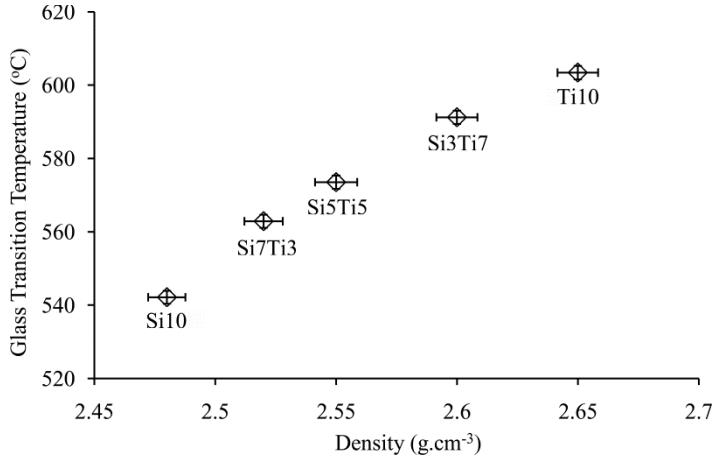

Figure 7.2 T_g versus density for investigated Si and Ti doped PGs. There was a concomitant increase in T_g and density with TiO_2 content in the PG formulations.

7.4.2. Determination of phases in the crystallized PG using X-ray diffraction

Table 7.2 presents the phases identified in the crystallized state of the PGs. Calcium phosphate was identified as the main phase of all formulations. The dominant calcium phosphate phase was α-(CaP_2O_6) (ICCD No. 11-0039) for Si10, α-$Ca(PO_3)_2$ (ICCD No. 17-0500) for Si7Ti3, Si5Ti5, and Si3Ti7, and $Ca_2P_2O_7$ (ICCD No. 01-071-2123) in the case of Ti10. α-$Ca(PO_3)_2$ was also detected for Si10. In the glass formulations containing more than 3 mol.% TiO_2, titanium phosphate TiP_2O_7 (ICCD No. 01-070-9482) was identified as the second phase.

Table 7.2 Identification of phases in the crystallized Si and Ti-doped PG formulations using X-ray diffraction.

Glass code	Phase 1	Phase 2
Si10	α-(CaP_2O_6)	α-$Ca(PO_3)_2$
Si7Ti3	$Ca(PO_3)_2$	
Si5Ti5	$Ca(PO_3)_2$	$Ti(P_2O_7)$
Si3Ti7	$Ca(PO_3)_2$	$Ti(P_2O_7)$
Ti10	$Ca_2P_2O_7$	$Ti(P_2O_7)$

7.4.3. NMR Spectroscopy

Figure 7.3a shows the ^{31}P MAS NMR spectra of the glasses. In order to examine the different peak constituents, the frequency scale was expanded to remove the spinning sidebands (Figure 7.3b).

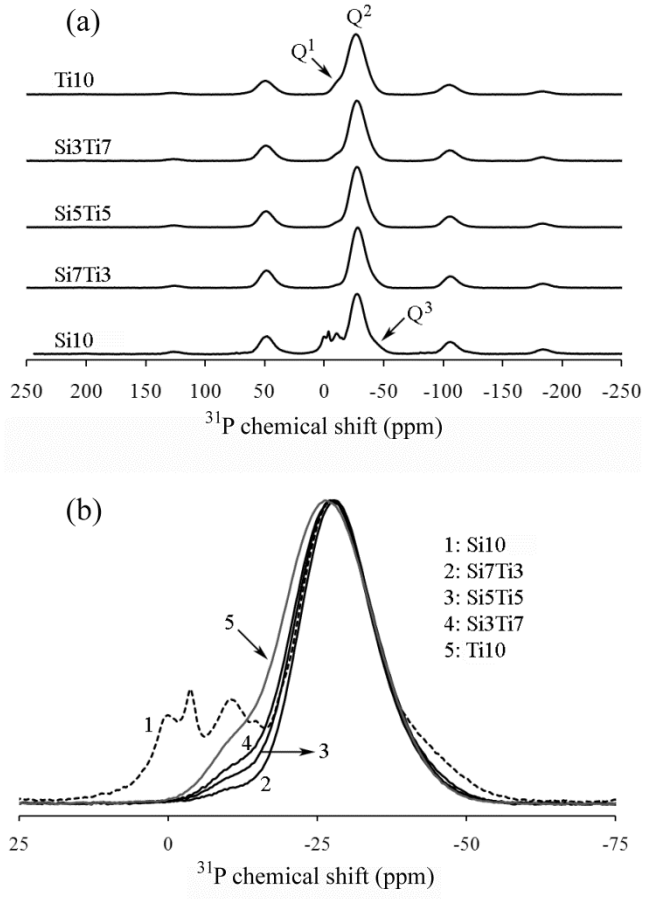

Figure 7.3 (a) ^{31}P MAS NMR spectra of PGs. (b) Spectra without the sidebands focusing on different Q^n species that were present in the PGs structure. The majority of the phosphorous is sited as Q^2 species.

Considering the Q^n notation of the phosphate structure, where n refers to the number of bridging oxygen atoms (P-O-P linkages) in the PO_4 tetrahedron [283], the majority of the phosphates was present as Q^2 species (at a chemical shift of approximately -27 ppm) [100, 284]. This is expected from a metaphosphate stoichiometry since the glass compositions consist of 50 mol.% P_2O_5 [94]. A slight chemical shift to less negative frequencies was observed with increasing TiO_2 content. The line-width increased with increasing TiO_2 content in the PG formulations which has been interpreted as increased irregularity in the phosphate network (Figure 7.3b) [121]. In addition, a shoulder peak formation (at approximately -10 ppm) was observed with the substitution of SiO_2 with TiO_2, as an indication of the formation Q^1 species. Si10 spectrum was different in the range of -15 to 10 ppm compared to other PG compositions. Table 7.3 presents the Q^1, Q^2 and Q^3 fractions. By substituting SiO_2 with TiO_2, the Q^1 and Q^2 fractions increased while the Q^3 fraction decreased. However, combination of the overlap and broadness of Q^2 and Q^3 make the determination of their area relatively inaccurate. Therefore, the sum of Q^2 and Q^3 is reasonably well determined and showed a monotonic decrease by increasing TiO_2 content.

Table 7.3 Q^n fractions for various Si and Ti doped PG formulations investigated in this study. The majority of the phosphorous sited as Q^2 species which increased by substituting SiO_2 with TiO_2.

Glass code	Q^1 fraction	Q^2 fraction	Q^3 fraction	(Q^2 + Q^3) fraction
Si10	0.001	0.661	0.117	0.778
Si7Ti3	0.018	0.863	0.118	0.982
Si5Ti5	0.034	0.859	0.107	0.966
Si3Ti7	0.059	0.810	0.131	0.941
Ti10	0.063	0.903	0.033	0.936

7.4.4. Surface properties of PG

Table 7.4 summarizes the mean contact angle measurements for UW and DII, the polar, non-polar, and total surface energy, as well as surface polarity of the PGs. Si10 glass indicated the lowest contact angle for UW which increased with TiO_2 substitution and content. In contrast, the contact angle for DII was not significantly different between the various compositions. While there was no difference ($p>0.05$) between the dispersive

energy values for all the PG formulations, the polar surface energy of Si10 was greater than that of the TiO_2-doped glasses. Moreover, the total surface energy and surface polarity decreased by incorporating TiO_2 into the PG formulation.

Table 7.4 Contact angle measurements with ultrapure water (CA^{H2O}) and diiodomethane (CA^{DII}), Total surface energy (SE^t) with the dispersive (SE^d) and polar (SE^p) parts of different PG compositions according to the OWRK method, and surface polarity ($X^p = SE^p/SE^t$). Si10 glass showed the lowest CA^{H2O} which increased significantly by substituting SiO_2 with TiO_2 in the glass formulation whereas the contact angle for DII was unchanged. On the other hand, SE^t decreased significantly by substituting SiO_2 with TiO_2. In addition, the substitution of SiO_2 with TiO_2 resulted in reduced surface polarity.

Glass code	CA^{H2O} (°)	CA^{DII} (°)	SE^t (mN/m)	SE^d (mN/m)	SE^p (mN/m)	X^p
Si10	10.4 ± 6.0	38.4 ± 3.2	72.0 ± 1.0	28.9 ± 1.7	43.1 ± 2.5	0.60 ± 0.02
Si7Ti3	* 31.8 ± 3.5	36.3 ± 3.7	* 63.6 ± 4.0	30.7 ± 2.0	* 32.9 ± 2.0	* 0.51 ± 0.02
Si5Ti5	$^{\Delta}$* 38.6 ± 1.5	40.4 ± 4.1	* 59.7 ± 1.8	29.9 ± 1.8	* 29.8 ± 0.8	* 0.50 ± 0.02
Si3Ti7	$^{\Delta}$* 37.3 ± 0.9	40.6 ± 2.8	* 60.9 ± 0.1	29.6 ± 1.4	* 31.3 ± 1.2	* 0.51 ± 0.01
Ti10	$^{\Delta}$* 39.8 ± 2.2	45.2 ± 5.2	* 58.7 ± 2.1	27.5 ± 2.5	* 31.2 ± 1.0	* 0.53 ± 0.03

* Statistically significant compared to Si10 ($p<0.05$)

$^{\Delta}$ Statistically significant compared to Si7Ti3 ($p<0.05$)

7.4.5. Ion release, weight loss, and pH change upon ageing in deionised water

Figure 7.4a shows the total phosphorous release upon ageing in DW. There was a rapid release of phosphorous in the case of Si10 glass which decreased significantly (450-fold) by replacing SiO_2 with TiO_2 at 10 mol.% in the glass composition. The ionic release profiles from Si10 were plotted separately as they were several orders of magnitude higher compared to those of the PGs doped with TiO_2. Calcium, silicon and iron release profiles are shown in Figures 7.4b, c and d, respectively, where a similar trend was observed, and ion release decreased by substituting SiO_2 with TiO_2. The weight loss of the different glass formulations, which was linear with time, is illustrated in Figure 7.4e. The weight loss was consistent with the ion release where Si10 showed the highest rate of dissolution, which decreased with increasing TiO_2 content in the glass formulation. There was a 375-fold reduction in the weight loss rate by substituting SiO_2 with TiO_2 at 10 mol.% (Table 7.5). There was a higher pH reduction with higher SiO_2 content. The pH

reduction controllably decreased by substituting SiO_2 with TiO_2 in the PG formulation (Fig. 7.4f).

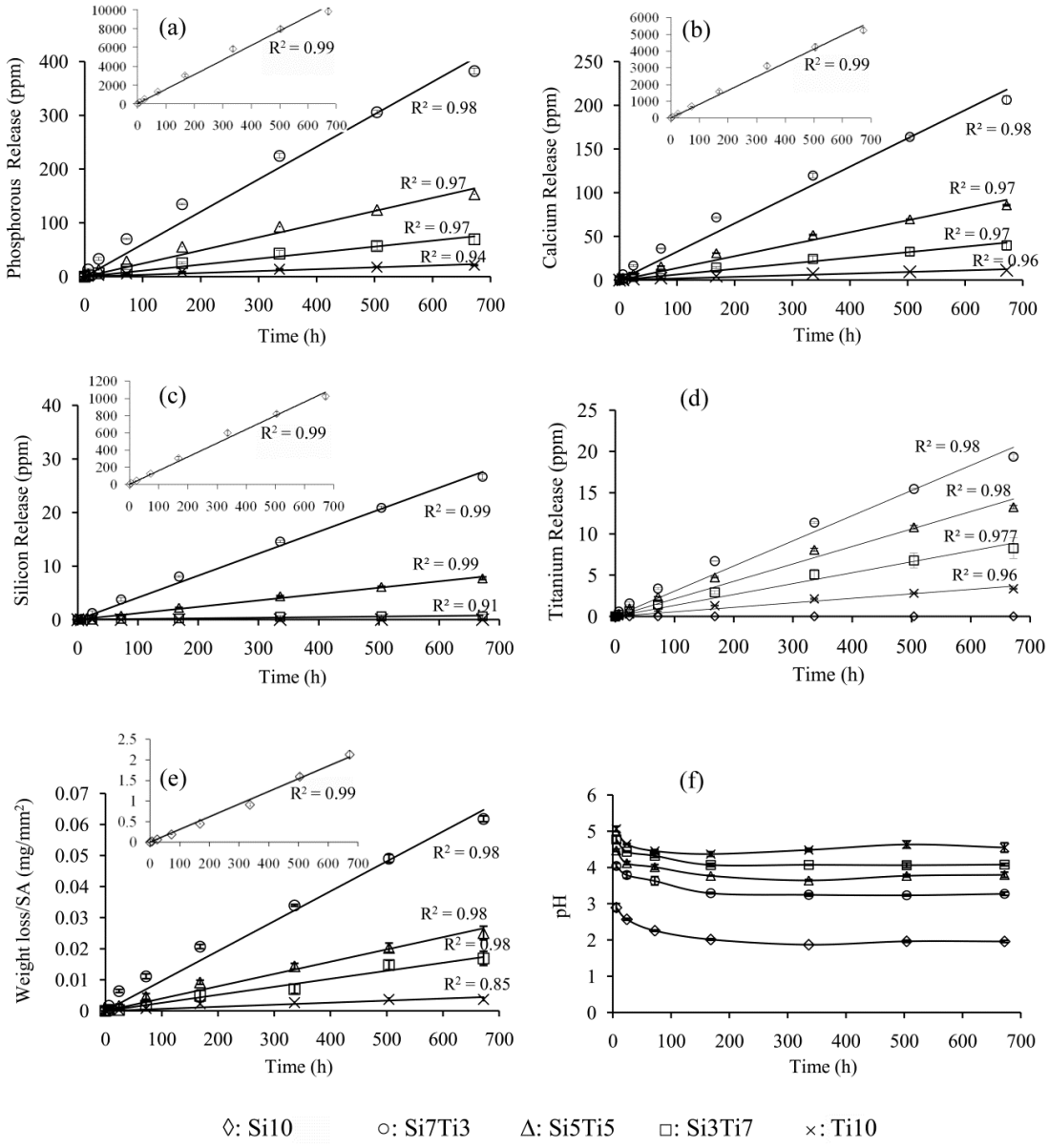

Figure 7.4 Ageing of PGs in DW incubated for up to 28 days at 37 ºC. Cumulative ion release for: (a) phosphorous, (b) calcium, (c) silicon and (d) titanium. (e) Corresponding weight loss per surface area (SA), and (f) pH change of DW. Panel insets represent the results for Si10 which was several orders of magnitude greater than TiO_2-doped PGs. Ion release increased linearly (indicated by R^2 value) over time and decreased significantly by substituting SiO_2 with TiO_2. Weight loss was in line with ion release and increased linearly over time (indicated by R^2 value) and decreased significantly by substituting SiO_2 with TiO_2. As a consequence of higher degradation, the pH reduction was considerably higher in Si10 than TiO_2-doped PGs.

Table 7.5 Weight loss ($mg.mm^{-2}.h^{-1}$) and ion release ($ppm.h^{-1}$) rates as calculated from the slope of the linear fit against time for the PG formulations. The degradation and ion release rates significantly decreased by substituting SiO_2 with TiO_2.

Glass code	Weight loss	Phosphorous	Calcium	Silicon	Titanium
Si10	$3.1\times10^{-3} \pm 1.1\times10^{-4}$	15.45 ± 0.59	8.24 ± 0.31	1.78 ± 0.05	-
Si7Ti3	$9.6\times10^{-5} \pm 1.6\times10^{-6}$	0.58 ± 0.05	0.32 ± 0.01	$0.04 \pm 4\times10^{-4}$	$0.036 \pm 3\times10^{-4}$
Si5Ti5	$3.9\times10^{-5} \pm 3.2\times10^{-6}$	0.24 ± 0.002	$0.14 \pm 5\times10^{-4}$	$0.013 \pm 3\times10^{-4}$	$0.025 \pm 3\times10^{-4}$
Si3Ti7	$2.7\times10^{-5} \pm 1.1\times10^{-5}$	0.11 ± 0.015	0.06 ± 0.01	$0.001 \pm 6\times10^{-4}$	0.013 ± 0.002
Ti10	$6.7\times10^{-6} \pm 1.1\times10^{-6}$	0.035 ± 0.001	$0.02 \pm 7\times10^{-4}$	-	$0.005 \pm 1\times10^{-4}$

7.4.6. *In vitro* assessment of pre-osteoblastic cells with PGs and their ionic products

7.4.6.1. Cell viability

The viability of MC3T3-E1 pre-osteoblasts seeded on the PG discs was assessed to indicate their cytocompatibility (Figure 7.5). At days 1 and 4, live MC3T3-E1 pre-osteoblasts were attached on the surfaces of all formulations. At day 7, cells remained viable and approached confluence on the surfaces of all TiO_2 doped PGs. However, necrotic/apoptotic cells were detected on Si10.

7.4.6.2. Metabolic activity

There were no significant differences in the metabolic activity of MC3T3-E1 cells seeded on the various glasses compared to the positive control, except in the case of Si10 which was significantly ($p<0.05$) lower (Figure 7.6). There was a significant increase in the metabolic activity at day 4 for all the TiO_2 doped PGs, which was in contrast to Si10, where no significant increase in metabolic activity was observed. At day 7, all PGs showed an increase compared to day 4. Proliferation continued to increase up to day 10; however, a significant reduction was observed for Si10. Cell metabolic activity gradually increased up to day 14 in TiO_2-doped PGs.

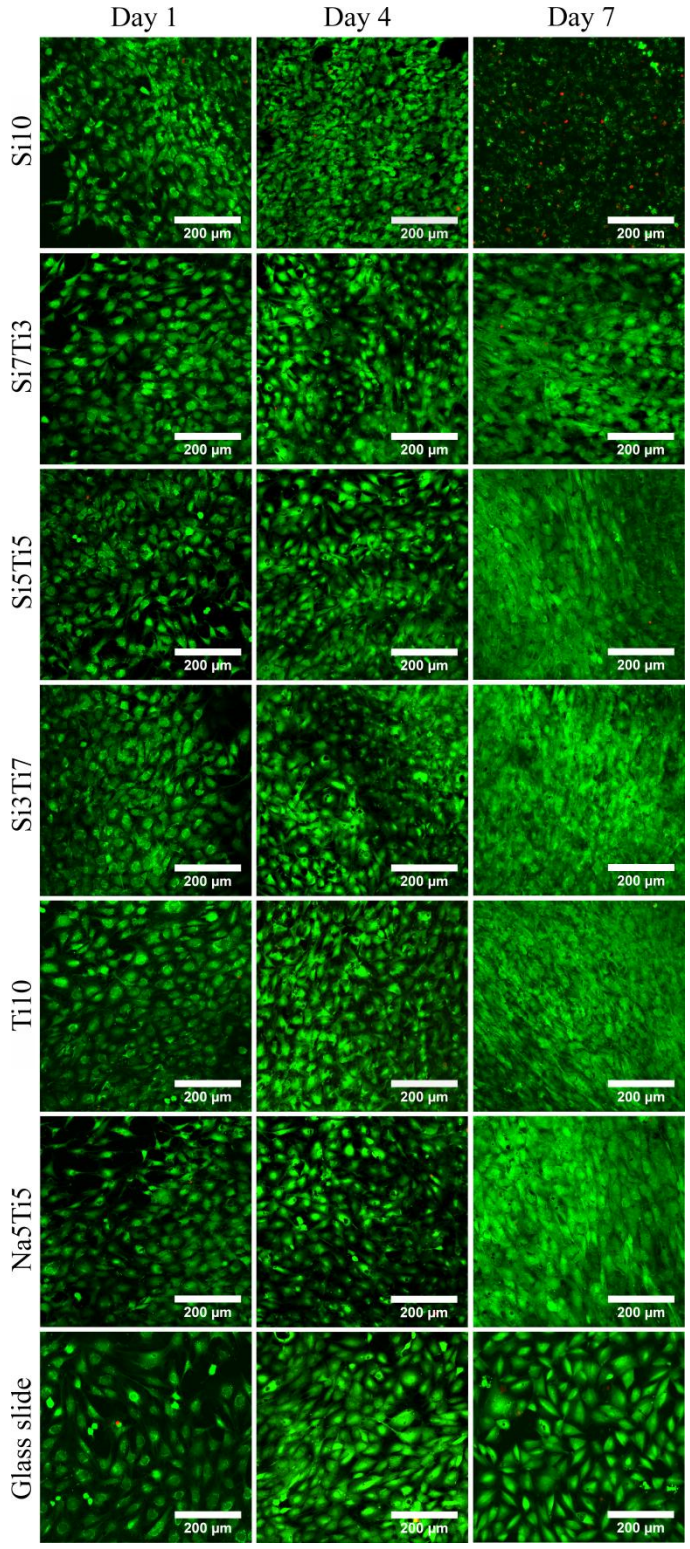

Figure 7.5 Confocal laser scanning microscopy of MC3T3-E1 pre-osteoblasts stained with calcein-AM (green) and ethidium bromide homodimer-1 (red) at days 1, 4 and 7 in culture.

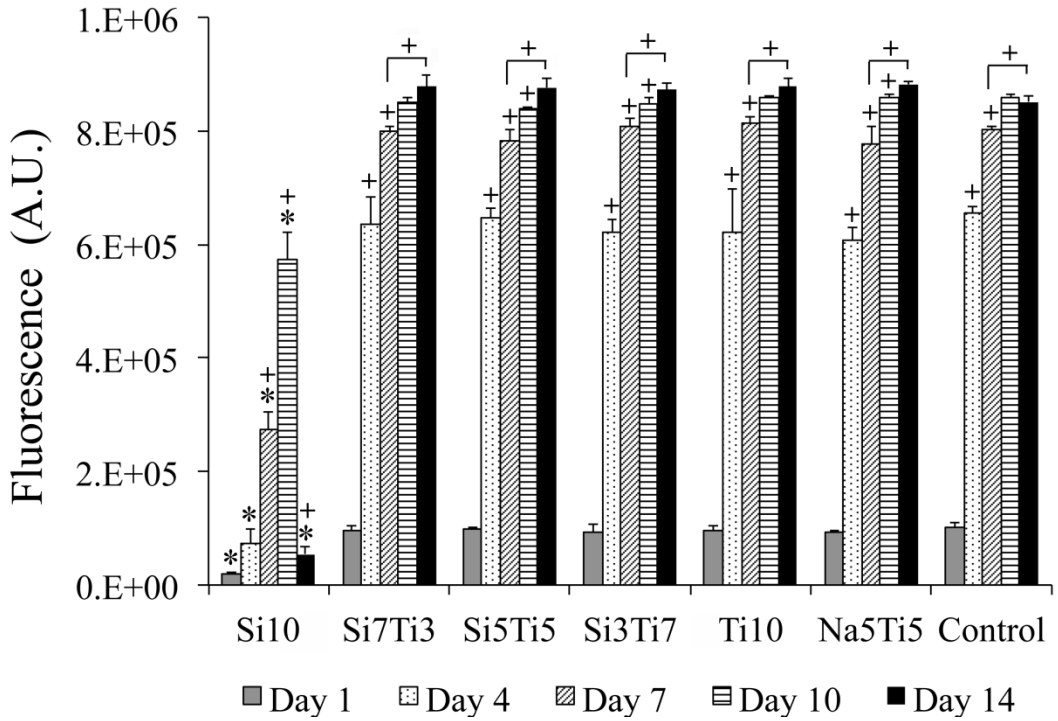

Figure 7.6 Effect of ionic release of PGs (at day 3) on MC3T3-E1 metabolic activity (AlamarBlue™ assay). There were no significant differences in cell metabolic activity between all PG compositions and the positive control (growth medium) except for Si10 which maintained significantly lower metabolic activity relative to all other conditions. * Statistically significant compared to control; + Statistically significant compared to previous time point.

7.4.6.3. ALP production

Figure 7.7 shows the ALP activity levels of MC3T3-E1 cells exposed to the ions released from all PGs as well as controls at days 1, 7, and 14 of culture. Cells exposed to Si10 extracts presented very low ALP levels which can be correlated with lower metabolic activity (Figure 7.6). There was a significant increase in ALP levels by substituting SiO_2 with TiO_2. At day 1, all formulations showed similar ALP activities compared to controls except for Ti10 which exhibited a higher value compared to the controls and other PG formulations. At day 7, there was a significant ($p<0.05$) increase in the ALP activity of MC3T3-E1 cells exposed to the ions released from all the TiO_2-doped PGs compared to the control (growth medium) with AA and with AA+GP. The NT control (growth medium) showed a significantly ($p<0.05$) lower value compared to AA and AA+GP controls. At day 14, Si7Ti3 maintained its ALP level which was statistically higher than those of the controls, as well as Si5Ti5, Si3Ti7, Ti10, and Na5Ti5. Other

TiO_2-doped PGs presented a reduction in the ALP activity at day 14 compared to day 7 with similar values as the AA+GP control, which were higher than NT and AA controls. The Na5Ti5 composition exhibited a statistically lower ALP level than Si7Ti3 and Si5Ti5, but similar to Si3Ti7 and Ti10.

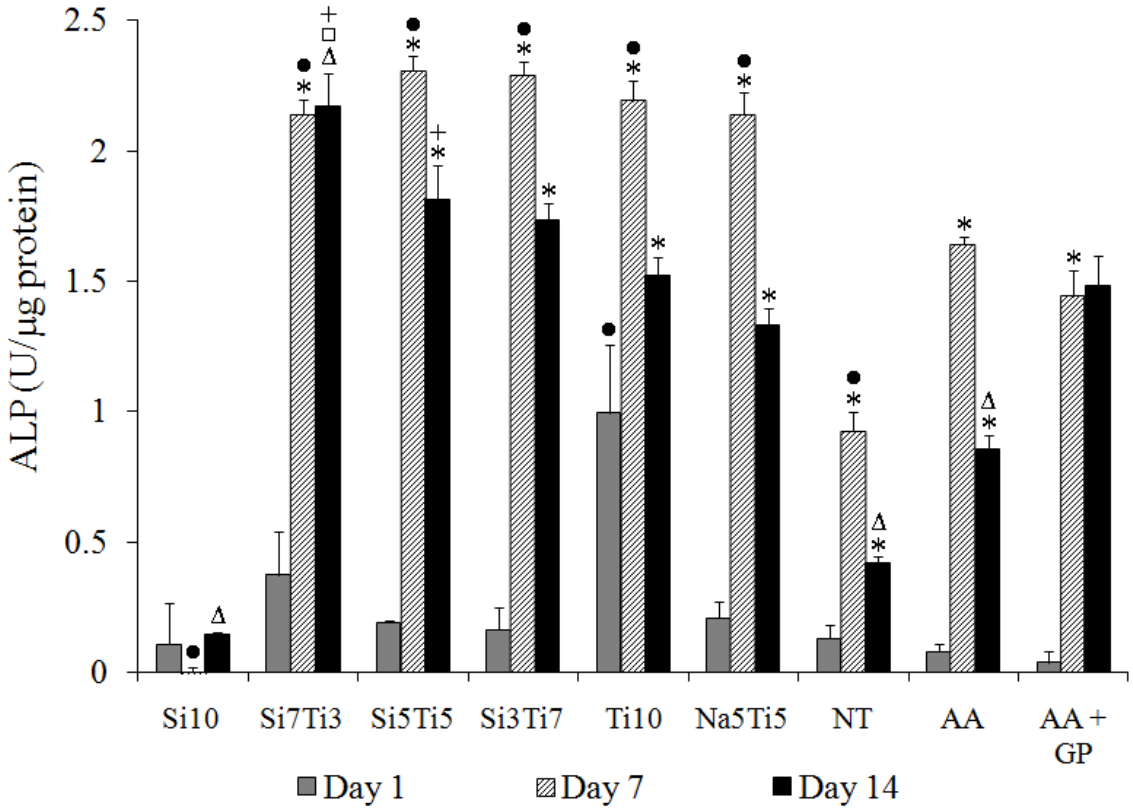

Figure 7.7 Osteogenic differentiation. Effect of PG extracts (at day 3) on MC3T3-E1 alkaline phosphatase activity (ALP assay). NT: Non-Treated control (growth medium); AA: Control with ascorbic acid (AA); AA+GP: Control with AA and β-glycerophosphate (GP). * Statistically significant for same sample compared to previous time point; • Statistically significant for same time point compared to AA control; Δ Statistically significant for same time point compared to AA+GP control; + Statistically significant compared to Na5Ti5 control; □ Statistically significant compared to Si3Ti7, Ti10, Si10 and Na5Ti5.

7.5. Discussion

The aim of this study was to develop Na-free PGs with tailored properties for bone repair and regeneration by doping silica and titania into the glass composition. The incorporation of Si into PGs has been shown to increase degradation and ion release rates by disrupting the phosphate network [13]. On the other hand, the incorporation of Ti increases PG stability resulting in lower degradation and ion release rates [29]. The controlled release of ionic products from materials has been shown to significantly influence the function of bone cells [278], and therefore impacts bone tissue engineering. PGs have the potential for bone repair and regeneration applications since they are controllably degradable and can be produced in diverse geometries and compositions [28]. However, a highly degradable surface and degradation products adversely affect cell attachment and function [23, 110]. Hence, the main challenge is to produce PGs with tailored physico-chemical and biological properties to support cells for new tissue formation at a rate that should ultimately match that of the degrading glasses. In addition, the ionic release products due to PG dissolution are vital for cellular functions [136].

PG volumetric density increased by substituting SiO_2 with TiO_2.T_g has been considered as an indication of the cross-link density between the phosphate chains in PG [120]. A concomitant increase in T_g and volumetric density suggested a cross-linking effect of TiO_2 in the phosphate chains which is possibly due to the formation of P-O-Ti bonds [121]. Ionic cross-linking between the non-bridging oxygens of two different chains strengthens the glass structure. XRD analysis confirmed the formation of Ti(P_2O_7) phase in the crystallized PGs with more than 3 mol.% addition of TiO_2. ^{31}P MAS NMR confirmed that the majority of the phosphate structure consisted of the Q^2 species. An increase in the line-width of Q^2 resonance with increasing TiO_2 content indicated a more disordered phosphate network due to the higher field strength and cross-linking potential of Ti which leads to a wider distribution of bond angles and lengths [121]. Si10 showed a number of additional peaks in the range of -15 to 10 ppm compared to the Ti-doped PG compositions. One of the peaks observed in that range could be attributed to the Q^0 formation since the Si significantly disrupted the phosphate network resulting in the reduced connectivity of the phosphate structure. In addition, since SiO_2 is also a glass former, there is a possibility that a silicate network was formed within the glass structure

of Si10. In this case, phosphorous atoms could act as network modifiers which may account for the formation of the additional peaks at -15 to 10 ppm in the NMR spectrum. For the TiO_2 containing glasses, the fraction of Q^1 species increased with TiO_2 content while the sum of Q^2 and Q^3 decreased. This effect indicates higher abundance of phosphate chain endings along with fewer linear chain segments (P-O-P) and branching units which can be explained by the higher field strength of Ti compared to Si resulting in increased phosphate chain cleavage. Therefore, more P-O-M bonds are present (where M is a metallic cation) which lead to higher chemical stability compared to P-O-P bonds [138].

An important challenge in bone regeneration is the balance between the rate of tissue growth and that of biomaterial degradation. The degradation and ion release rates of the PGs in deionised water were dependent on the glass formulation. The cumulative weight loss per surface area was linear with time and decreased by substituting SiO_2 with TiO_2. The degradation rate was significantly higher for Si10 compared to TiO_2–doped PGs, and decreased significantly by complete substitution of SiO_2 with TiO_2. The addition of Si to PG breaks down its network, leading to higher solubility [13]. In contrast, the reduction in degradation rate with higher TiO_2 content can be attributed to the formation of more hydrolysis resistant P-O-Ti bonds, which corroborates the DTA and NMR results. Ti was found to have a greater effect on stabilizing the PG network compared to Fe, where the degradation rate was increased an order of magnitude from 6.7×10^{-6} $mg.mm^{-2}.h^{-1}$ for Ti10 to 1×10^{-5} $mg.mm^{-2}.h^{-1}$ for previously published Fe10 ($50P_2O_5$-40CaO-$10Fe_2O_3$) [285].

The addition of different modifiers into the glass network changes the surface properties such as surface energy and hydrophilicity of the material. Surface properties are important in bioactive and bioresorbable glasses since they have a significant effect on the solubility and ion release rates [118]. The dissolution mechanism of PGs is also susceptible to changes in the hydrophilicity and surface energy of the glasses [120]. Furthermore, these glass surface properties are critical in determining cellular interactions such as adhesion, motility, and signalling [23]. Although UW has a higher surface tension than DII, lower contact angles were obtained for UW than DII on the surface of the PGs as a consequence of the polar characteristic which can be attributed to the P-O-P bonds

[286]. However, the addition of glass modifiers can significantly affect the polar characteristic of PGs [118]. Si10 showed the lowest contact angle value which considerably increased by substituting with TiO_2. The contact angle values for DII (a non-polar liquid) were in contrast to those observed in the case of water (a polar liquid). There was no statistically significant difference for DII contact angle values among all tested PGs. Therefore, neither SiO_2 nor TiO_2 affected the non-polar characteristic of PGs. The ratio of the polar to dispersive parts also increased, indicating that the polar characteristic increased with SiO_2 in the glass composition which may be due to the concentration of hydroxyl groups (Si-OH) at the surface of the PG. Si10 showed a statistically greater total surface energy and polarity compared to all the TiO_2-doped PGs. No statistical differences were observed among all TiO_2 containing PGs.

Ion release upon PG degradation was in line with their weight loss, which demonstrated a linear increase with time. There was a significant reduction in the rates of release of P and Ca ions (up to 400-fold) between Si10 and Ti10. Si release rate also decreased significantly by substituting SiO_2 with TiO_2. However, the Ti release was more dependent on the dissolution rate rather than the TiO_2 content; for example, Si7Ti3 showed a 7-fold increase in Ti release compared to Ti10. The biocompatibility of TiO_2-containing glasses has been associated with Ti release [28, 29]. Higher degradation and ion release rates of Si10 led to greater pH reduction compared to other compositions. The pH reduction may be due to hydrolysis of phosphate chains as the cleavage of two adjacent phosphates involves the release of two protons [287]. The reduction in pH considerably decreased by substituting SiO_2 with TiO_2 attributed to controlled degradation rate of TiO_2-doped PGs. While deionised water was used for ease of released ion detection, the change in pH is expected to be smaller in a cell culture medium since it is highly concentrated with ions and buffers [121].

The incorporation of TiO_2 has been shown to improve the biocompatibility of PGs by controlling the glass degradation and ion release rates, thus; maintaining the appropriate pH favoured by the osteoblasts [28]. The glass surface should initially be able to facilitate cell attachment, which will be followed by proliferation and differentiation [288]. MC3T3-E1 cells attached, remained viable, and approached confluency on the surface of all tested PG discs compared to cells grown on microscope glass, except for

Si10, where necrotic/apoptotic cells were detected at day 7. Cell viability improved significantly by substituting SiO_2 with TiO_2 at 3 mol.%, and at day 7 MC3T3-E1 cells completely covered the surface of 5, 7, and 10 mol.% TiO_2 PGs. At day 7, the low level of cell viability for Si10 could be attributed to the high degradation and ion release rates, especially phosphates, making it difficult to have a controlled pH under static cell culture. Cells were also viable and approached confluency on Na5Ti5 at day 7.

Cell metabolic activity increased compared to the positive control except for Si10 which exhibited lower levels relative to all materials. Dissolution of Si10 formulation in the medium for the proliferation and ALP experiments resulted in medium colour change from pink to yellow (pH reduction) due to the presence of phenol red (pH indicator) in the medium. Precipitation in the medium was observed for this composition which could potentially be the consequence of supersaturation of ions due to significant ionic release from Si10. Therefore, lower metabolic and ALP activities were observed for Si10 compared to TiO_2-doped formulations. Abou Neel *et al.* [136] investigated the proliferation of human osteosarcoma cells in the presence of glass extracts for up to 5 days for Na-containing PGs doped with up to 5 mol.% TiO_2. Their study showed that while Ti-free formulation led to lower cell numbers compared to Ti-doped formulations at day 1, all tested specimens exhibited a similar trend of increasing cell number with time compared to the positive control (growth medium) at days 3 and 5. In the present study, Na5Ti5 composition from [136], was selected and used as a Si-free control, and to compare Na5Ti5 to Si5Ti5 in order to investigate the effect of replacing Na_2O with SiO_2 in the PG formulation. Although the metabolic activity was similar for Na5Ti5 and Si/Ti-doped formulations, the ALP activity was higher for Si7Ti3 and Si5Ti5 compared to Na5Ti5 and other formulations. This could be attributed to higher ionic release rates of Si7Ti3 and Si5Ti5 compared to Si3Ti7 and Ti10, as well as the release of Si as compared to the Si-free formulation, Na5Ti5.

It has been demonstrated that PGs release inorganic PO_4^{3-} (Pi) and polyphosphates such as $P_2O_7^{4-}$ (PPi), $P_3O_9^{3-}$, and $P_3O_{10}^{5-}$ [112]. Inorganic polyphosphates are prevalent in mammalian cells, especially in human osteoblasts, facilitating bone formation [289]. In calcifying tissues, PPi exists extracellularly, and has been found to have an important inhibitory effect on the formation of hydroxyapatite crystals *in vivo* [290]. Extracellular

PPi levels are regulated by several cell membrane proteins such as ALP, ectonucleotide pyrophosphatase phosphodiesterase 1, and mouse progressive ankylosis [291]. ALP is responsible for cleaving the inhibitor PPi to generate Pi [292]. Matrix mineralisation occurs as a result of ALP upregulation which reduces the extracellular PPi level [293]. Different phosphate sources can serve as ALP substrates to induce mineral deposition, such as PPi, β-GP, adenosine 5'-triphosphate, and pyridoxal-5'-phosphate in combination with other enzymes (e.g. transglutaminase 2) [294]. In order to study the effect of PGs on the differentiation of MC3T3-E1 pre-osteoblasts, ALP activity was measured as an early marker of osteoblastic differentiation [288]. All TiO_2-doped PGs showed a significant increase in ALP activity at day 7 compared to day 1 and all the controls, suggesting that PGs may induce higher osteoblastic expression. At day 14, all TiO_2-doped PGs showed greater ALP levels than the NT and AA controls. Si7Ti3 showed similar behaviour to the AA+GP control and maintained its ALP level up to day 14. However, other PGs ($\geq$ 5 mol. % TiO_2) showed similar behaviour to AA control and presented a reduction in ALP at day 14. This reduction can be related to their lower degradation and ion release rate compared to Si7Ti3. It was found that there was a linear increase in ALP production with increasing rate of phosphorus release from PGs, or the amount of dissolved phosphorous in the medium by dissolving respective amounts of PGs (Supplementary Figure 7.1). Consequently, higher content of polyphosphates was present in Si7Ti3 which may contribute to the higher ALP levels at day 14. Expected ionic concentrations from the dissolved PGs in the growth medium (calculated theoretically) are presented in supplementary Table 7.1. Ionic concentrations were significantly high for Si10, which decreased significantly with TiO_2 content. Si7Ti3 provided concentrations of 49.91 and 25.76 ppm for P and Ca ions, respectively, which were 2-fold higher than Si5Ti5 composition having concentrations of 25.01 and 12.91 ppm for P and Ca, respectively. These values were higher than other compositions with lower SiO_2 content. Therefore, higher ALP values for Si7Ti3 and Si5Ti5 at day 14 compared to other compositions could be attributed to the presence of higher P and Ca ions. P and Ca concentrations for Na5Ti5 composition (Si-free composition with 5 mol.% TiO_2) were similar to Si3Ti7, and showed similar behaviour to Si3Ti7 and Ti10. Therefore, these results suggested that

5 to 7 mol.% SiO_2 incorporation up-regulated the ion concentrations to the point of inducing higher ALP levels.

7.6. Conclusion

Doping PGs with SiO_2 and TiO_2 resulted in modified structure, and provided tailored properties for bone tissue engineering such as degradation, ionic release and cellular responses. TiO_2-free composition (Si10) showed significantly greater degradation rates. The level of ion release from Si10 was too high and impaired the growth and proliferation of MC3T3-E1 pre-osteoblasts. However, by substituting SiO_2 with TiO_2, a concomitant increase in PG density and T_g suggested a cross-linking effect of Ti in the phosphate network which led to increased stability, and resulted in lower degradation rates. This effect was also supported by XRD showing the formation of $Ti(P_2O_7)$ in crystallized TiO_2-containg PGs, and by NMR which indicated an increased amount of Q^1 species. The substitution of SiO_2 with TiO_2 also resulted in reduced hydrophilicity and surface energy. The addition of TiO_2 resulted in a significant improvement in MC3T3-E1 pre-osteoblasts viability, proliferation, and differentiation compared to Si10. Si7Ti3 maintained higher level of ALP up to day14 compared to other formulations attributed to higher release of phosphate and calcium ions. ALP activity of Si5Ti5 was also higher than that of Na5Ti5 at day 14. It was found that the incorporation of 3 mol.% TiO_2 was sufficient for stabilising the PG network; however, 5 to 7 mol. % SiO_2 resulted in higher ALP activity compared to Si-free compositions (Ti10 and Na5Ti5), AA and AA+GP controls at day 14 in culture. Therefore, doping PGs with SiO_2 and TiO_2 could be a promising route to tailor PG properties for potential bone tissue engineering applications.

7.7. Acknowledgements: This work was funded by the Canadian Natural Sciences and Engineering Research Council, le Fonds Québécois de la Recherche sur la Nature et les Technologies, McGill Faculty of Engineering, Hatch Faculty Fellowship, and Canadian Foundation for Innovation: Leaders Opportunity Fund. Funding for Maziar Shah Mohammadi, Florencia Chicatun and Christoph Stähli was also partly supported by a McGill Engineering Doctoral Award. Showan N. Nazhat is a member of the Centre for

Bone and Periodontal Research. Martin N. Bureau is a membre of the Groupe de Recherche en Sciences et Technologies Biomédicales (Fonds de recherche en santé du Québec). The authors thank Dr. Frederick Morin and Pierre Vermette for their assistance in this work.

7.8. Appendix: Supplementary Data

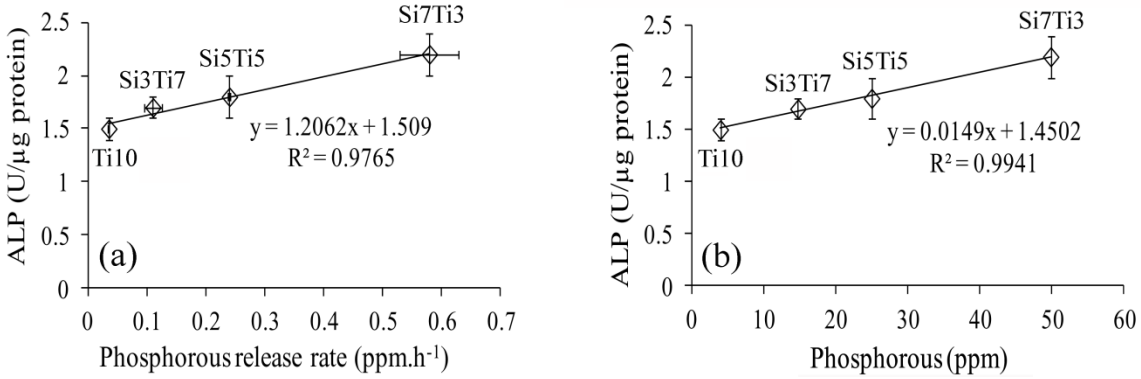

Supplementary Figure 7.1 (a) ALP versus phosphorous release rate in DW; (b) ALP versus the amount of dissolved phosphorous in medium (calculated theoretically). There was a linear increase in ALP production by increasing rate of phosphorus release from PGs, or the amount of dissolved phosphorous in the medium by dissolving respective amounts of PGs.

Supplementary Table 7.1 Theoretically calculated weight of PG powder (according to 72 h dissolution in DW) dissolved in 10 ml of growth medium, and expected ionic concentrations.

Glass code	Weight (mg)	Phosphorous (ppm)	Calcium (ppm)	Silicon (ppm)	Titanium (ppm)
Si10	48.38	1509	779	136	-
Si7Ti3	1.61	49.91	25.76	3.15	2.32
Si5Ti5	0.81	25.01	12.91	1.13	1.94
Si3Ti7	0.48	14.76	7.62	0.4	1.6
Ti10	0.13	3.97	2.05	-	0.61
Na5Ti5	0.43	13.26	6.84	-	1.03

CHAPTER 8

SOLID-STATE FOAMING USING CARBON DIOXIDE: A TECHNIQUE TO PRODUCE PDLLA-PG COMPOSITE FOAMS

Polymer-PG composite systems developed in this dissertation show promising results for applications in bone repair and regeneration; such as bone fracture fixation devices or tissue engineering (TE) scaffolds. As a suitable scaffold for TE, these materials should have the ability to be converted into a porous structure with controlled morphology in terms of pore size and interconnectivity. Therefore, the aim of this study was to investigate the foamability of these composite systems.

The $50P_2O_5$-40CaO-$10TiO_2$ glass formulation, developed and investigated in Chapter 7, was selected and incorporated into poly(D,L-lactic) acid (PDLLA) to produce biocompatible composites for foaming, through solid-state CO_2 gas foaming. Amorphous polymers foam more easily than the crystalline polymers because of increased gas dissolution in less organised morphologies. Therefore, amorphous PDLLA was selected for this study to remove the adverse effect of crystallinity on foaming and investigate the effect of PG filler on the foamability of the composites.

A manuscript based upon these findings is under preparation to be submitted for peer-review.

Calcium phosphate glass particulate-reinforced poly(D,L-Lactic) acid composite foams through solid-state foaming using carbon dioxide

Maziar Shah Mohammadi[a], Jason Bertram[a], Benedetto Marelli[a], Richard Gendron[2b], Showan N Nazhat[a], Martin N Bureau[b,a]

[a] *Department of Mining and Materials Engineering, McGill University, Montreal, QC, H3A 2B2, Canada*

[b] *Industrial Materials Institute, National Research Council Canada, QC, J4B 6Y4, Canada*

Key words: Phosphate-based glass particulates, poly(D,L-lactic) acid, biodegradable composites, solid-state foaming, carbon dioxide, tissue engineering

8.1. Abstract

Bone tissue engineering requires degradable scaffolds with an appropriate morphology regarding pore size and interconnectivity to serve as a template for cell proliferation, differentiation, and eventually induction of tissue growth. In this study, a calcium phosphate-based glass (PG) formulation ($50P_2O_5$-40CaO-$10TiO_2$, in mol.%) was produced and incorporated into biodegradable poly(D,L-lactic acid) (PDLLA) at 0, 5, 10, 20, and 30 vol.% as a particulate (PGP) filler. The composites were fabricated by melt extrusion and compression moulding. The composites were then converted into porous structures through solid-state foaming using high pressure gaseous carbon dioxide. Specimens were initially saturated with carbon dioxide at 2.4 MPa for 72 hours at room temperature. Saturated specimens were then removed from the autoclave to atmospheric pressure followed by a temperature increase to induce phase separation, and generate the foams. Physico-mechanical properties as well as morphological investigations were carried out on both composites and foams. PGP incorporation resulted in enhanced strength and modulus (up to > 2-fold) in both composites and foams compared to both unfoamed and foamed neat PDLLA respectively, due to appropriate distribution of PGPs and filler/matrix interface. Neat PDLLA foam showed 92% porosity while PDLLA-PGP composites had a porosity ranging from 79 to 91% depending on PGP content. Incorporation of PGPs resulted in reduced pore size, with further reduction in pore size observed at higher PGP content. Pore size remained in the 200-500 μm range for all the composite foam systems, therefore within the acceptable range for bone tissue engineering applications. The presence of PGPs led to the formation of pore windows, inter-pore openings. The fraction of open pores increased significantly with increasing PGP content (up to 78% at 30 vol.% PGP). The approach used in this study for fabrication of PDLLA-PGP composite foams showed interesting and promising foam morphologies for intended applications in bone tissue engineering.

8.2. Introduction

Tissue engineering is a promising alternative to current surgical techniques used to treat severely damaged tissues [61]. Bone repair has been considered to be one of the major applications of tissue engineering. The general concept of bone tissue engineering (BTE) includes the use of a construct to promote the regeneration of the damaged tissue [295]. This construct is composed of a scaffold, viable cells and biologically active agents (e.g. growth factors) [295, 296]. An ideal scaffold for tissue engineering applications should have biodegradability, biocompatibility, interconnected porosity with appropriate pore size, and appropriate mechanical properties to be able to stand the applied forces [55, 156, 157, 200].

Current scaffolds in BTE are made either of polymers or ceramics. Because of the inherent properties of the base materials, the use of these scaffolds is often limited due to their brittleness when made of ceramics or their low mechanical strength when made of polymers. To overcome this issue, porous structures based on composites have been developed for bone repair applications. In the latter, the mechanical properties of the polymer matrix are improved through particle reinforcement. Due to their bioactivity, the use of bioceramics has been shown to improve the overall biological response of the construct [297, 298]. Poly(α-hydroxy-acid esters), e.g. poly(lactic acid) (PLA), poly(glycolic acid) (PGA) and their copolymers (PLGA) [183], as well as polycaprolactone (PCL) [250], have been considered as degradable synthetic polymers for matrices of BTE scaffolds. Calcium phosphate ceramics and glasses, such as hydroxyapatite (HA) and silicate-based glasses (e.g. Bioglass®) incorporated into biodegradable polymers have been extensively studied for BTE applications [183, 247, 249]. Phosphate-based glasses (PGs) may be a potential alternative inorganic phase for the purpose of producing composites of controllable degradation characteristics since the solubility of PGs in aqueous environments can be predicted and controlled by altering their composition [13, 14, 98]. A variety of binary, ternary, and quaternary PG compositions have been developed for biomedical application mainly based on P_2O_5-CaO and P_2O_5-CaO-Na_2O systems, with or without the addition of several modifying oxides [19, 99, 100, 112, 118]. For example, the incorporation of titanium dioxide (TiO_2) into

PGs has been proven to control their degradation rate and improve their biological response for BTE [28, 29, 120, 134].

Several techniques have been reported for the preparation of three-dimensional (3D) scaffolds [299] including solvent casting-particle leaching [300], thermally induced phase separation (TIPS) [301], freeze drying-particle leaching [302], extrusion [303], compression moulding [304], injection moulding [305], wet spinning [306], and electrospinning [307]. The selection of the scaffolding technique can have a critical effect on the properties of the *in vivo* performance. For many of the aforementioned techniques, the use of large amount of organic solvents is the main disadvantage; while for others, high temperatures involved often lead to thermal degradation of thermo-liable components (e.g. pharmaceutical drugs and bioactive agents) [308].

Batch foaming using atmospheric gases such as carbon dioxide (CO_2) and nitrogen has been developed to produce highly porous foams avoiding the use of organic solvents. CO_2 is usually the preferred candidate and acts as a porogen to create 3D polymeric structures to be used as scaffolds [221]. Batch foaming using CO_2 is frequently performed above the critical temperature (T_c = 30.95 ^oC) and pressure (P_c = 7.38 MPa) of CO_2, and this process is often referred as supercritical foaming [227].

In the batch foaming process, the first step consists of dissolving the gas in the polymer sample using a high pressure autoclave. Concentration of the gas is dictated by the temperature and pressure conditions chosen. Foaming occurs through the thermodynamic instability induced either by a rapid depressurisation or a temperature increase. In the first case, depressurization leads to the supersaturation of the CO_2 dissolved in the polymer matrix. Consequently, nucleation of the cells take place [309], followed by cell growth. However, this technique is effective for amorphous polymers or semi-crystalline polymers with low glass transition temperature (T_g) [308]. For example, Georgiou *et al*. [190] produced and investigated PLA-phosphate glass ($50P_2O_5$-46CaO-$4Na_2O$) composite foams for BTE by using supercritical CO_2 ($scCO_2$) (T=195 ^oC and P_{sat} = 15-25 MPa). Foaming occurred by sudden release of gas with depressurisation rate of 2.5-5.5 $bar.s^{-1}$, and a cooling rate of 2-6 $^oC.s^{-1}$ which stabilised the foam. PG content was 0, 5, 10, and 20 wt.%. It was shown that the glass content affected the foam morphology, and smaller pores were created with increasing amounts of glass content. The addition of

fillers increased the foam densities. However, the required level of porosity for BTE remained above 75%. Cytocompatibility study with human foetal bone cells showed similar results compared to foams of PLA with HA or β-TCP. However, their foaming process was not efficient, and did not result in significant void formation for PLA-20 (wt.%) PG.

The technique based on temperature increase is solid-state foaming (SSF). The gas-charged sample is removed from the autoclave and its solid state at room temperature prevents foaming. Expansion is obtained after the polymer is taken above its T_g. This method is directly related to the plasticizing properties of CO_2. The dissolution of CO_2 lowers the T_g of amorphous polymers due to a thermodynamic effect of intermolecular interactions between CO_2 and the polymer. As the temperature is increased above the momentarily T_g resulting from the remaining gas dissolved in the polymer, nucleation and growth can occur. The final temperature is usually set above the T_g of the neat polymer, in order to maximize the efficiency of the gas being dissolved. If the level of plasticization is such that the resulting T_g is well below the room temperature, e.g. by using very high pressure CO_2, the foaming technique can be performed at room temperature during the depressurization step. Mooney *et al*. [238] developed this technique by foaming poly(D,L-lactic-co-glycolic acid). The samples were exposed to high pressure CO_2 (5.5 MPa) for 72 hours at room temperature followed by a pressure drop to atmospheric levels. Large pores (~100 μm) and porosity up to 93% could be produced using this technique.

In this study, poly(D,L-lactic acid)-PGP composites were developed with 5, 10, 20 and 30 wt.% PGP content. A PG formulation ($50P_2O_5$-$40CaO$-$10TiO_2$) was produced and used as particulate reinforcement. Amorphous poly(D,L-lactic acid) (PDLLA) was selected as the polymer matrix to facilitate the foaming procedure and remove the effect of crystallinity. The composites were foamed using SSF method. The specimens were first exposed to high pressure CO_2 at room temperature followed by a temperature rise to induce cell nucleation and foaming. Physico-mechanical properties as well as morphology of the composites were characterised prior to foaming. Morphological properties of the foams were then investigated in terms of distribution of PG particulates

within the cells, porosity, interconnectivity and pore size. Compressive mechanical properties of the foams were also investigated.

8.3. Experimental

8.3.1. Phosphate glass production

P_2O_5, $CaHPO_4$, SiO_2 (AlfaAesar, Canada), and TiO_2 (Sigma Aldrich, Canada) precursors were used to produce a melt derived phosphate-based glass (PG) composition ($50P_2O_5$-40CaO-$10TiO_2$ (in Mol.%)). The precursors were dry blended, poured into a Pt/10%Rh crucible (Kitco Inc., Canada). The crucible was placed into a furnace (Carbolite RHF1500, Ancansco, Canada), heated to 350 °C, and kept for 20 min in order to remove the moisture. The precursors were then melted at 1500 °C for 3.5 h, and quickly poured onto a steel plate to quench the melt and produce solid amorphous glass. The bulk glass was then pulverized for 45 seconds to produce glass particulates. The particle size distribution analyzer (Horiba LA-920, Japan) was used to measure the PG particle size, which revealed d50 of 50 μm.

8.3.2. Polymer-PGP composite fabrication

Biodegradable poly(D,L-lactic acid) (Purasorb® PDL 05, Purac Biochem, Goerinchem, Netherlands) with a density of 1.26 $g.cm^{-3}$, an inherent viscosity of 1.58 $dL.g^{-1}$, and M_w of 60 kDa was used as the matrix. The T_g of this PDLLA was 65 ^oC. This polymer was fully amorphous and used without further purification. PDLLA pellets were mixed with 0, 5, 10, 20 or 30 vol.% PGPs in dry conditions and dried overnight under vacuum at 45 °C. A micro-compounder (Thermo Scientific HAAKE MiniLab, Germany) with two conical co-rotating screws of reduced capacity (5 cm^3) was used to melt extrude the PDLLA-PG composites. Melt extrusion was performed at 110 °C, with a screw rotation speed of 100 rpm and an overall residence time of 4 min. The process was performed under a flow of nitrogen to limit polymer degradation. The extruded composite rods were cut into small pieces (for homogeneity of the bulk composite) and were dried overnight under vacuum at 45 °C prior to compression moulding. Compression moulding was carried out with a closed mould using a Carver Laboratory Press (Model M, United States) by applying a pressure of 2 MPa at 160 °C for 10 min.

The composites were then cooled to room temperature under pressure in the same press. Material codes and compositions used in this study are presented in Table 8.1.

Table 8.1 Material codes and compositions.

Material code	PDLLA (vol.%)	PGP ($50P_2O_5$-40CaO-$10TiO_2$) (vol.%)
PDLLA	100	-
PDLLA-5PGP	95	5
PDLLA-10PGP	90	10
PDLLA-20PGP	80	20
PDLLA-30PGP	70	30

8.3.3. Polymer-PG composite foaming

PDLLA and PDLLA-PG composites were cut into 10×10×2.6 mm^3 specimens. SSF process was used to foam the specimens. The samples were saturated with CO_2 in an autoclave (E3000, Quorum Technologies) attached to a CO_2 cylinder. Prior to foaming experiments, CO_2 solubility in PDLLA at different pressures and times at room temperature was determined using initial slope method (extrapolation) when the sample was removed from the autoclave. This step enabled the determination of the adequate conditions and concentration of CO_2. The chosen CO_2 pressure for the SSF experiments was finally set to 2.4 MPa, and the samples were kept at this pressure for at least 3 days to ensure that the CO_2 content was 5 wt.%. The specimens were then retrieved from the pressure vessel and brought to atmospheric pressure. Foaming was conducted through an abrupt temperature rise using an oven which was set at 80 ^oC. Heat exposition for 1 to 2 min was sufficient for the samples to be foamed.

8.3.4. PDLLA-PG composite characterisation

8.3.4.1. Density measurement

Archimedes' Principle was used to experimentally measure the density of the composites. A balance (Sartorius BP 110 S) with an appropriate hydrostatic weighing apparatus was used for this purpose. Due to the hygroscopic nature of the composites, isopropanol (A416-20, Fisher Chemical) was used as the submersion liquid for these

measurements. The results were then compared to the theoretical densities calculated using the rule of mixtures.

8.3.4.2. Polymer burn-off

True weight percentages of PGP were obtained by polymer burn-off. Samples were placed in pre-weighted ceramic crucibles and then weighted once more. They were then heated in a furnace at 650 °C for 1 hour, removed and left to cool under fume hood for 10 minutes. The crucibles were again weighted, and the weight measurements were used to experimentally verify the amount of PGP in each composite system, with comparison to nominal expected weight percentages.

8.3.4.3. Morphological characterisation

Scanning electron microscopy (SEM) analysis of the cryo-fractured surfaces was conducted to study the morphology of the PDLLA-PG composites using a Hitachi S-4700 field emission scanning electron microscope. Samples were mounted on brass studs and coated using an Emitech K575X *Peltier Cooled* platinum coater (under argon) before being analysed using a back scattered electron mode with accelerating voltages of 2 kV.

8.3.4.4. Molecular weight investigation of the polymer matrix

The molar masses of pure PDLLA (both starting granules and after compression moulding) and the PDLLA polymer within the composites (after both extrusion and compression moulding) were measured with a gel permeation chromatograph (GPC, Viscotek-TDAMax) at 25 °C, using tetrahydrofuran (THF) as eluent and polystyrene (PS 99K) as the standard reference. PG particles were removed from the dissolved mixture using 0.22 μm filters. The molar mass was analyzed and recorded before and after processing to determine whether the inclusion of Ti-doped PG had a degradative effect on the PDLLA polymer matrix at the processing conditions.

8.3.4.5. Composite mechanical properties

Three-point bend flexural mechanical analysis was used to measure the mechanical properties of the composites. The effect of PG formulation on composite

mechanical properties was investigated through changes in flexural strength and modulus. Three independent specimens were tested with a cross-head speed of 1 mm/min using a 1 kN load cell in accordance to ASTM D 790-95a:1996 (width-to-depth aspect ratio = 16) in an Instron mechanical testing instrument 5582 (Instron Ltd).

8.3.5. PDLLA-PG foam characterisation

8.3.5.1. Morphological characterisation using SEM

Cryo-fractured surfaces of the foams were investigated to study the morphology of the cells in PDLLA-PGP foams using the same method as described in Section 8.3.4.3.

8.3.5.2. Morphological characterisation using micro-CT

MicroCT analysis was performed with a SkyScan 1172 (SkyScan, Kontich, Belgium), adapting a previously developed protocol [310]. In brief, freeze-cut samples (20×20×8 mm^3) were analysed with a resolution of 9.7 µm through a 360° flat-field corrected scan at 67 kV and 178 µA, and then reconstructed (NRecon software, SkyScan) with a beam hardening correction of 10, a ring artefact correction of 20 and an "auto" misalignment correction. The intensity of the CT scan 8bit images generated was dependent on the density of air, PDLLA and PGP. The 2D and 3D analyses of pore size, total porosity and percentage of open pores (software CTAn, SkyScan) were carried out using a grayscale intensity range of 10 to 255 (8 bit images) in order to remove background noise. The edges of the samples (2 mm thick for each dimension) were not considered in the analysis in order to avoid the artefacts intrinsic to the cutting procedure. Due to the different density of PDLLA and PG, it was possible to differentiate between the two materials using an intensity range of 10 to 30, and a threshold above 30, respectively. This criterion allowed the 3D reconstruction and the visualization of the different phases (CTVol software, Skyscan). PDLLA and PGP phases were pseudo-coloured in grey and red, respectively.

8.3.5.3. Mechanical properties

Due to the small size of the foamed samples, compression mechanical test, instead of flexural test, was performed (Instron 5582) to measure the mechanical properties of the

foams. The effect of PG formulation on composite mechanical properties was investigated through changes in compression strength and Young's modulus. Three independent specimens were tested with a cross-head speed of 10% of thickness per minute using a 1 kN load cell in accordance to ASTM D 1621-00.

8.3.6. Statistical Analysis

Statistical analysis was performed to test the significance in the difference between two mean values by using the Student's *t*-test which was used to determine *p*-values at a significance level of 0.05. Regarding the micro-CT results (pore size, porosity, and open pore fraction of the foams), statistically significant differences were determined using one-way ANOVA with a Tukey-Kramer's post-hoc multiple comparison of means. The level of statistical significance was set at $p = 0.05$.

8.4. Results

8.4.1. PDLLA-PGP composite characterisation

8.4.1.1. Density measurements

Figure 8.1 shows the density of each composite system. The density of the composite increased with increasing PGP content in PDLLA. Experimental values were very close to the nominal values confirming the amount of PG present in the composite systems.

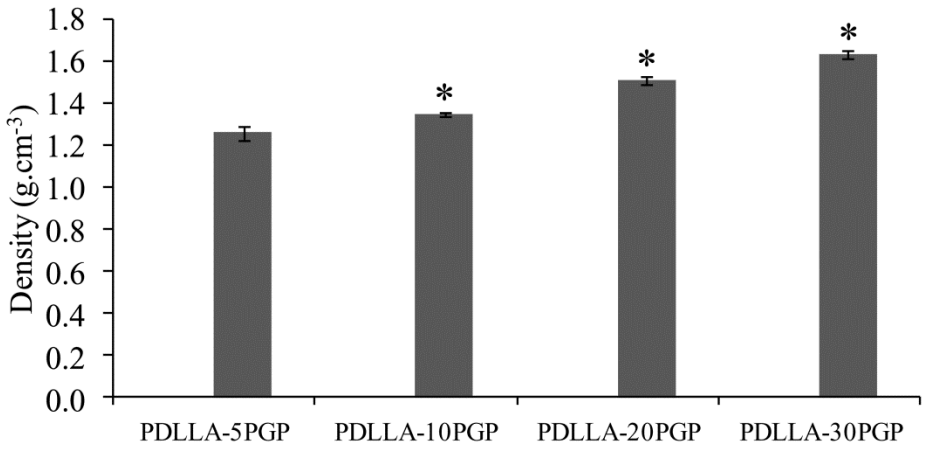

Figure 8.1 Density values of each composite.
* Statistically significant compared to previous material ($p<0.05$)

8.4.1.2. Determination of PGP content from pyrolysis (Polymer burn-off)

Theoretical and experimental weight percentage values of the components for each composite after fabrication are presented in Table 8.2. These results confirmed the amount of PG particulates used to fabricate each composite.

Table 8.2 Theoretical and experimental weight percentage values of the components for each composite after fabrication.

Material code	Theoretical		Experimental	
	PDLLA (wt.%)	PG (wt.%)	PDLLA (wt.%)	PG (wt.%)
PDLLA-5PGP	90.03	9.97	90.16 ± 0.65	9.84 ± 0.65
PDLLA-10PGP	81.06	18.94	83.53 ± 0.09	16.47 ± 0.09
PDLLA-20PGP	65.54	34.46	67.11 ± 0.08	32.89 ± 0.08
PDLLA-30PGP	52.59	47.41	54.14 ± 0.14	45.86 ± 0.14

8.4.1.3. Morphological characterisation

SEM micrographs of the morphology of as-processed PDLLA-5PGP, PDLLA-10PGP, PDLLA-20PGP and PDLLA-30PGP are shown in Figure 8.2a-d. A uniform distribution of PGPs within the PDLLA matrix was observed. Figure 8.2e and f show the respective morphology of PDLLA-20PGP and PDLLA-30PGP at higher magnifications where well bonded PGPs uniformly distributed within the matrix were observed.

8.4.1.4. Molecular weight investigation of the polymer matrix

The weight-average molecular weight (M_w) of the PDLLA matrix in the various composites is shown in Figure 8.3. No significant difference was observed in the M_w of the PDLLA matrix of the composites. However, when compared to the M_w of the PDLLA granules, PDLLA-10PGP and PDLLA-20PGP showed a statistically ($p<0.05$) lower M_w (respectively 50954 ± 91 Daltons and 49936 ± 13 Daltons compared to 51594 ± 131 Daltons for PDLLA granules). In contrast to thermal degradation often observed in poly(lactic acid), neat PDLLA only showed a slight reduction in this study. With respect to M_w, the PDLLA matrix of the composites did not appear to be considerably affected by PGP incorporation at the processing conditions.

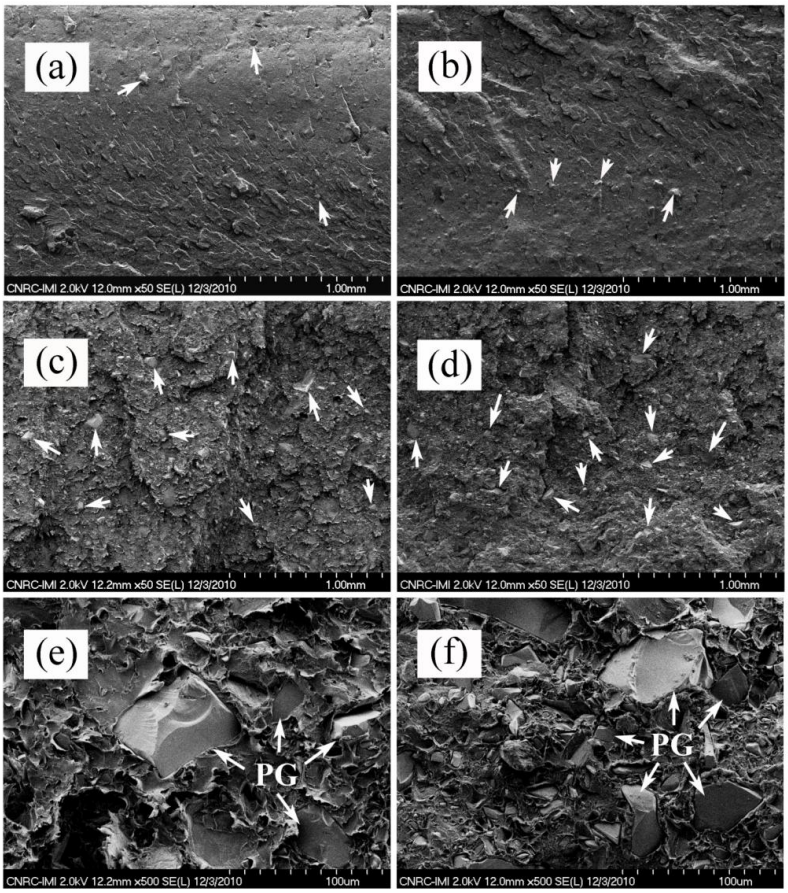

Figure 8.2 SEM micrographs of the composites. (a) PDLLA-5PGP (50x), b) PDLLA-10PGP (50x), (c) PDLLA-20PGP (50x), (d) PDLLA-30PGP (50x), (e) PDLLA-20PGP (500x), and (f) PDLLA-30PGP (500x). The arrows indicate the PG particulates dispersed within the matrix.

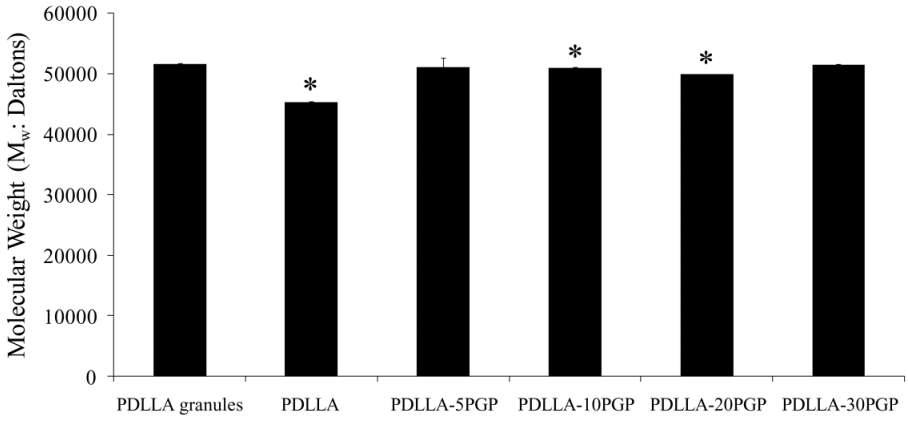

Figure 8.3 Molecular weight (M_w) of PDLLA before (starting granules) and after processing with different PGP content. * Statistically significant compared to PDLLA granules ($p<0.05$)

8.4.1.5. Composite mechanical properties

Flexural mechanical analysis (Figure 8.4a, b) of the composites revealed that the flexural strength and modulus of the PDLLA-PGP composites increased up to ~2-fold at 30 vol.% PGP incorporation when compared to neat PDLLA processed and moulded under similar conditions. The increase in the flexural strength and modulus was not statistically significant at 5 vol.% PGP incorporation. However, mechanical properties improved significantly at 10, 20 and 30 vol.% PGP compared to neat PDLLA ($p<0.05$). Comparing the composite systems, only PDLLA-30PGP showed a statistically significant increase in flexural strength. PDLLA-20PGP and PDLLA-30PGP showed a statistically significant increase in Young's modulus compared to other composites.

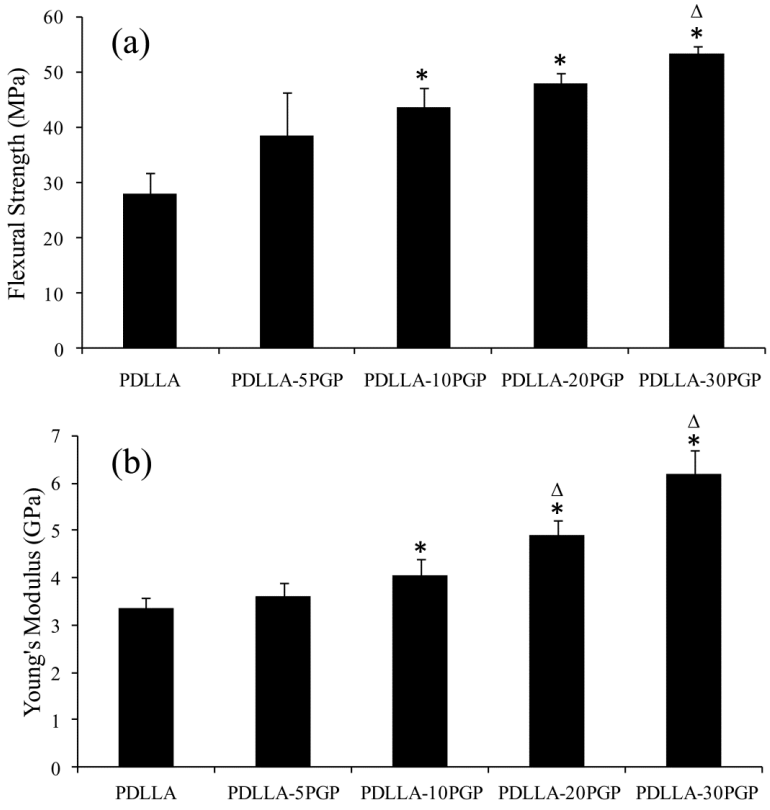

Figure 8.4 Flexural strength (a), and Young's modulus (b) of PDLLA and PDLLA-PGP composites with different PGP content. * Statistically significant compared to PDLLA ($p<0.05$); Δ Statistically significant compared to previous material ($p<0.05$)

8.4.2. PDLLA-PG foam characterisation

8.4.2.1. CO_2 solubility in PDLLA

Several trials were carried out in order to find appropriate processing conditions for composite foaming. CO_2 contents in PDLLA samples at different pressures and exposure times at room temperature are presented in Table 8.3. As expected, CO_2 content generally increased with an increase in pressure. At a specific pressure, CO_2 content increased by increasing the gas exposure time. There appears to be a saturation point however for a specific pressure and time. At pressures below 2 MPa, CO_2 content was not more than 3 wt.% which led to ineffective foaming. For example, CO_2 content was 2.76 wt.% at 1.7 MPa after 164 hours. At higher pressures (e.g. 3.4 MPa), even at shorter soaking times (e.g. 27 h), the samples were soft and sticky, and bubbles formed within them as soon as they were removed from the autoclave to atmospheric pressure. This indicates that the resulting T_g was below room temperature. Knowing that 6.1 wt% of CO_2 was dissolved into the PDLLA sample; this suggests a plasticization level of roughly 6.5 ^oC/wt.% of CO_2. Moderate pressures (~2.4 MPa) were found to be appropriate to obtain sufficient dissolved CO_2 (~ 5 wt.%) for effective foaming leading to uniform expansion and high porosity. However, at least 72 hours was required for saturation of the samples with CO_2. It should be kept in mind that the soaking time is related to the diffusivity of the gas and the thickness of the sample. Diffusivity is slow below T_g and increases rapidly in the rubbery state. This explains the fast dissolution at high pressure such as 3.4 MPa but the very long soaking time required at moderate pressure such that the sample remained in the glassy state.

Table 8.3 CO_2 solubility in PDLLA at different pressures and times at room temperature; Initial slope method was used to determine (extrapolate) initial content of CO_2 when the sample was removed from the autoclave.

Pressure (MPa)	Exposure Time (h)	CO_2 content (wt.%)	Note
1.7	21, 96, 164	1.06, 2.03, 2.76	
2.2	22	2.91	Few bubbles present inside the sample
2.4	72	5.48	Selected for the foaming experiment
3.4	27	6.1	Plasticized at room temperature

8.4.2.2. Morphological characterisation using micro-CT

Figure 8.5 shows 2D and 3D micro-CT images of PDLLA and PDLLA-PGP foams. Pore size, porosity, and percentage of open pores measured by micro-CT analysis are presented in Table 8.4. While large and closed pores were observed in PDLLA foam (Fig. 8.5a), PGP incorporation resulted in reduced pore size, and increased open structure (Figure 8.5b-e). As can be seen, pore size considerably decreased by increasing PGP content from an average of 920 μm for neat PDLLA foam to 190 μm for PDLLA-30PGP. While there was a slight reduction in total porosity, increasing PGP content led to a significant increase in the percentage of open pores, ranging from 7.7% for PDLLA-5PGP to 79% for PDLLA-30PGP.

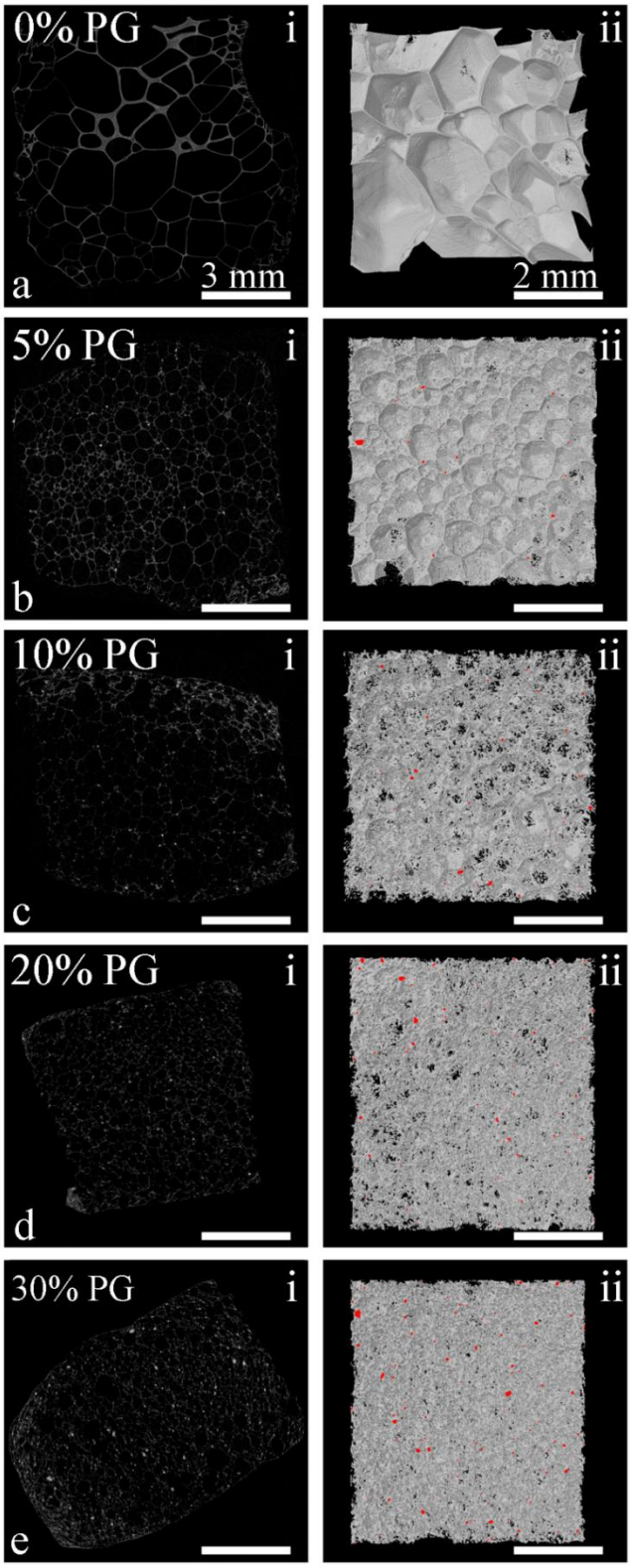

Figure 8.5 Micro-CT images of PDLLA (a), PDLLA-5PGP (b), PDLLA-10PGP (c), PDLLA-20PGP (d), and PDLLA-30PGP (e). i and ii represent 2D and 3D images, respectively.

Table 8.4 Pore size, total porosity and percentage of open pores for PDLLA, and PDLLA-PGP composite foams measured by micro-CT.

Material code	Pore size (μm)	Total porosity (vol.%)	Percentage of open pores
PDLLA	920 ± 640	92.03 ± 1.59	3.75 ± 0.65
PDLLA-5PGP	530 ± 230	87.91 ± 0.44	7.67 ± 1.17
PDLLA-10PGP	270 ± 210	90.99 ± 0.51	21.8 ± 3.47
PDLLA-20PGP	230 ± 140	87.99 ± 0.48	50.45 ± 6.24
PDLLA-30PGP	190 ± 130	78.78 ± 0.35	78.61 ± 0.35

By incorporating PGPs into PDLLA, there were approximately 2, 6, 14, and 21-fold increase in the percentage of open pores at 5, 10, 20, and 30 vol.% PGP content, respectively. As shown in Figure 8.6, the content of open cells was linearly proportional to the glass particulate concentration.

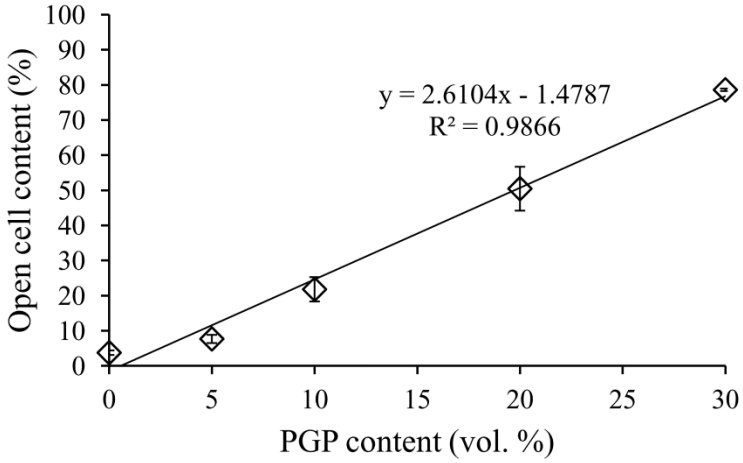

Figure 8.6 Dependency of percentage of open cells on PGP content.

In addition, the reduction in the pore size was increased by increasing the PGP content. The nucleation density is defined by the number of cells per unit volume of the original unfoamed polymer. It was evaluated using the following equation [311]:

$$\beta \cong \frac{6\times 10^{+12}\left[\left(\phi/100\right)/\left(1-\phi/100\right)\right]}{\pi d^{3}} \tag{8.1}$$

where β is the cell nucleation density (cells/cm^3), d the average diameter of the cells (μm), and ϕ the volume porosity (%). Increasing the number of particulates impacted the nucleation density only at the low fractions of fillers, typically less than 10 vol.%, as illustrated below (Figure 8.7). Above this value, the nucleation density is constant at approximately 1×10^6 cells/cm^3 (unfoamed polymer).

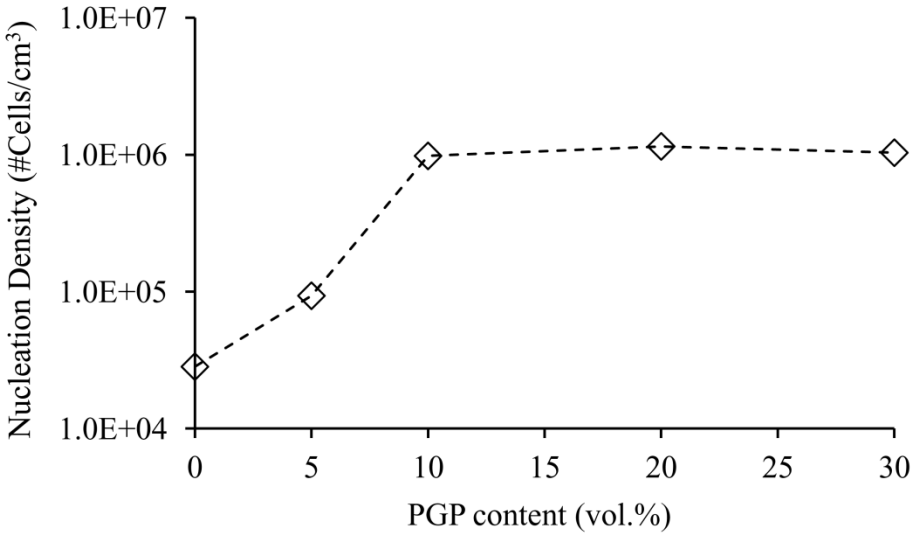

Figure 8.7 Nucleation density versus PGP content for PDLLA-PGP composites with different PGP content.

8.4.2.3. Morphological characterisation

SEM micrograph of PDLLA and PDLLA-PGP composite foams are presented in Figure 8.8. PDLLA foam (Figure 8.8a) exhibed very large pores. The incorporation of 5 vol.% PGP resulted in a reduction in the pores size (Figure 8.8b). At 5 vol.% PGP, the structure appeared to be dominated by closed pores. PGPs were found to be present in the pore walls (data not shown), and energy-dispersive spectrometry (EDS) analysis confirmed the PGP composition used in this study. Increasing the amount of PGP to 10 vol.% resulted in further reduction of the pore size (Figure 8.8c). Well distributed PGP within the porous structure was observed, which were also confirmed by EDS analyses. Increasing the amount of PGP to 20 and 30 vol.% led to further pore size reduction (Figure 8.8d and f). A considerable increase in the amount of open pores and resulting

open windows were observed at higher PGP contents (PDLLA-20PGP and PDLLA-30PGP) (Figure 8.8e, g, h). SEM observations revealed that the PG particles were associated with open pores and resulting open windows.

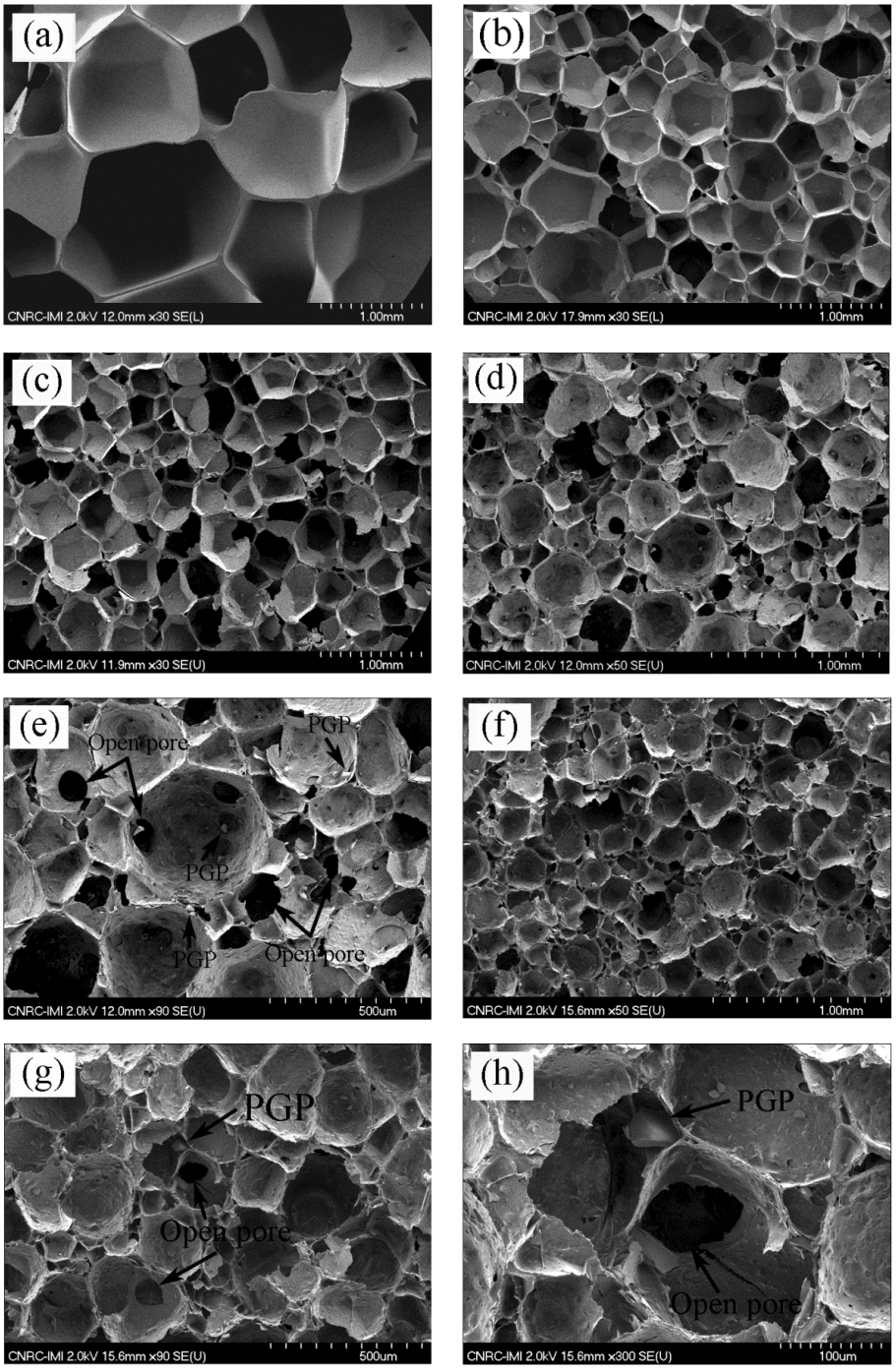

Figure 8.8 SEM micrographs of foamed PDLLA (a), PDLLA-5PGP (b), PDLLA-10PGP (c) PDLLA-20PGP (d), PDLLA-20PGP at higher magnification (e), PDLLA-30PGP (f), and PDLLA-30PGP at higher magnification (g and h).

8.4.2.4. Mechanical properties

Compressive strength and modulus of PDLLA and PDLLA-PGP foams are shown in Figure 8.9 for each material. While a tendency of increasing strength with PGP content was observed (Figure 8.9a) when compared to foamed PDLLA, a significant increase in compressive strength was only observed for foamed PDLLA-30PGP. The same tendency of increasing modulus with PGP content was observed (Figure 8.9b) when compared to foamed PDLLA, but the statistically significant increase in the Young's modulus was observed at 10 vol.% PGP incorporation (PDLLA-10PGP).

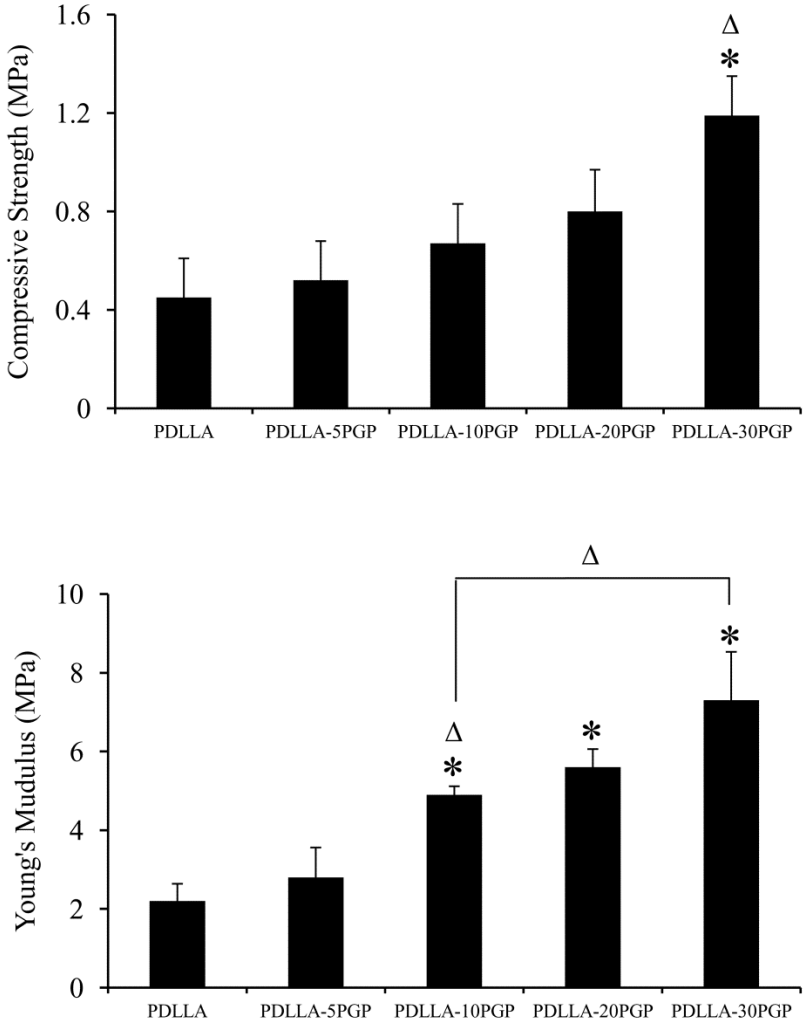

Figure 8.9 Mechanical properties of composite foams. Compressive strength (a) and Young's modulus (b) of PDLLA and PDLLA-PGP foams. * Statistically significant compared to PDLLA ($p<0.05$); Δ Statistically significant compared to previous material ($p<0.05$)

8.5. Discussion

An ideal scaffold for BTE should be biocompatible, fully degradable and porous with an appropriate pore size to serve as a template for cells to proliferate, differentiate and promote tissue growth. Poly(lactic acid) is a commonly used biodegradable polymer for producing porous tissue engineering scaffolds [190]. In addition, PGs have been shown to be appropriate materials for BTE due to their controlled degradation and release of favourable ions such as phosphorous and calcium [100]. Therefore, combining these two materials should lead to a biodegradable composite for potential applications in BTE. In addition, by taking advantage of the solubility of CO_2 in PLA, this composite system could be foamed in order to create a 3D porous structure.

The PG used in this study has been assessed in terms of its degradation, ion release and cytocompatibility using MC3T3-E1 pre-osteoblasts, and showed cell attachment and viability with a confluent growth, as well as proliferation and alkaline phosphatase production (see chapter 7). The incorporation of PG into PDLLA (5, 10, 20 and 30 vol.%) resulted in a significant increase in the density of the composites with PG content. The amount of PG in each composite was verified by polymer burn-off. Appropriate distribution and filler/matrix interface are important characteristics of composites which play a key role in determining composite properties. The composite fabrication technique used in this study resulted in well dispersed PGPs within the PDLLA matrix with an appropriate interface. Previously, it was shown that SiO_2 containing PGs resulted in the degradation of polyester matrix leading to a significant reduction in the matrix molecular weight when processed at elevated temperatures (Chapters 4 and 6). Therefore, in order to investigate whether TiO_2 incorporation in the PG formulation would affect the matrix at the processing conditions used in this study, the PDLLA M_w was measured after processing and compared to that of the initial PDLLA granules. While there was a reduction in M_w of neat PDLLA after compression moulding, PDLLA M_w remained unchanged after extrusion and compression moulding for composites with 5 and 30 vol.% PGPs when compared to neat granules of PDLLA. T-test showed a statistically significant reduction ($p<0.05$) in the M_w of PDLLA-10PGP and PDLLA-20PGP composites after processing compared to M_w of neat PDLLA granules. The M_w of the initial PDLLA granules was measured as 51600 ± 131 Daltons, and that of

all the composite systems showed values between 50000 to 51500 Daltons. Therefore, the incorporation of Ti PGPs into PDLLA at the processing conditions did not considerably change the molecular weight of the matrix.

Flexural analysis was performed to measure the mechanical properties of the various composites. There was a statistically significant increase in the flexural strength compared to neat PDLLA when the PGP content was ≥ 10 vol.%. However, no statistical difference was observed for PDLLA-10PGP, PDLLA-20PGP, and PDLLA-30PGP. Enhancement of Young's modulus of the composites also occurred above 10 vol.% PGP, which was statistically significant at 20, and 30 vol.%. There was an approximately 2-fold increase in the flexural strength and modulus at 30 vol.% PGP compared to neat PDLLA. The strength and modulus of the composites were in the range of 38.5-53 MPa, and 3.6-6.2 GPa, respectively, which were within the range of trabecular bone [41, 42, 252]. The lack of improvement in the mechanical properties of PCL when reinforced with PGP in the previous study [94] was a consequence of polymer matrix degradation due to the presence of Si in the PG composition which was prevented in this study. No significant change in the flexural strength of PCL was reported when reinforced with binary PG fibres ($50P_2O_5$-50CaO) at 18 vol.% [111]. However, the modulus displayed a 5-fold increase from 0.5 to 2.4 GPa, which was lower than the values obtained in this study. Previously, a significant increase in the storage modulus of PGP incorporated PLA composites at 20 wt. % was demonstrated by Georgiou *et al.* [190].

CO_2 solubility in PDLLA was found to be pressure and time dependent at room temperature since it occurs by diffusion. However, appropriate conditions should be considered in order to avoid lack of gas content which leads to ineffective foaming, or too much gas content which plasticises the samples prior to foaming step. Plasticization occurs due to the diffusion of CO_2 into the polymer matrix separating the polymer chains which results in lower resistance to chain rotation. Consequently, a reduction of the T_g occurs. CO_2 content at 5 wt.% was found to be effective for the foaming without plasticization at room temperature. By reducing the CO_2 pressure, the solubility of the gas in the polymer decreases [224] generating nuclei (or bubbles) which then grow to form the pores in the foam. T_g begins to increase again once the CO_2 vacates the polymer making it glassy and the pores can no further grow. Therefore, performing the foaming at

temperatures (80 ^{o}C) above the T_g of the polymer matrix (60 ^{o}C for PDLLA) results in more efficient removal of the gas leading to an effective foaming.

The structure of the composite foams was investigated using micro-CT. Reduced pore size, and increased open pore structure were observed in the 2D images. In addition, 3D images revealed the effect of PGP content and distribution on pore size, and open structure. There was a significant reduction in pore size with PGP content, yet still in the acceptable range for BTE application. It has been reported by Salgado *et al.* [55] that an optimal pore size for BTE should be between 200 to 900 μm. However, according to Karageorgiou and Kaplan [312], it is not possible to suggest an optimal pore size due to the large number of bone features *in vivo*, and the diversity of biomaterials and cells used *in vitro* and *in vivo*. They also reported that, although there is no optimal pore size, larger pore size favours osteogenesis because they allow sufficient nutrient supplies and exchange of metabolic products. However, there is also an upper limit for the pore size due to possible reduction in the mechanical stability of the scaffolds and surface area available for cell attachment. In contrast, pore occlusion by cells will prevent cellular diffusion within the scaffold if the pores are excessively small. Micro-CT analysis also showed that although there was a reduction in total porosity for PDLLA-20PGP and PDLLA-30PGP, down to respectively 88 and 79%, the percentage of open pores increased significantly as the PGP content was increased, which were found to be 50 and 79% for PDLLA-20PGP and PDLLA-30PGP, respectively. The presence of PGPs, especially at higher percentages such as those in PDLLA-20PGP and PDLLA-30PGP, led to the creation of open windows and open pores, which linearly increased by increasing PGP content. In addition, since PGPs are soluble in aqueous environments, their dissolution will increase both porosity and open pore percentage in physiological fluids.

SEM micrographs revealed the distribution of PGPs within the cellular structure and at the vicinity of the pores. EDS analysis indicated the presence of phosphorous, calcium, titanium and oxygen, confirming the presence of the elements used for fabrication of PGPs in this study (P_2O_5-CaO-TiO_2). Neat PDLLA resulted in very large cellular structure. Close examination of this structure indicated an uneven distribution of the polymer in the cell walls, struts and vortices. Despite the presence of few cell walls having a near constant wall thickness which would indicate a homogeneous deformation,

large vortices and necking present in some walls led to rounded smooth cell geometry. Such characteristics have been reported previously [313] and might be associated with the cell growth mechanism involved in SSF. However, the incorporation of PGP into PDLLA resulted in a reduction in the pore size and a more homogeneous cellular structure. Incidentally, once glass particulates have been added to PDLLA, e.g. for 5 vol.% of glass content, the cellular structure improved dramatically. In addition to the increased cell nucleation, the angular shape of the cells is better defined and the thinner cell walls have a much more even thickness. The presence of irregularities on the surface of the cell walls is associated with large glass particulates. The larger cells display intact cell walls, despite the large strains involved with such expansion. This observation is not necessarily in contradiction with the open pore content determined by micro-CT, considering the limited SEM investigation and the rather small value of open cell content reported for this PGP content (7.67% open pores). Increasing the glass content to 10 vol.% led again to an increased nucleation associated with smaller cells. Roughness of the cell walls is predominant and rupture of some of these walls is initiated, as indicated by the presence of circular holes. This cell opening behaviour is magnified at 20 vol.%, with holes present in most of the cells. In addition, the cross section of the walls exhibit also a porosity that should be linked to the loss of adhesion between the glass particulates and the polymer, and the further stretching of the polymer films creating such voids [314]. Although the morphological characterization of the initial composites might suggest good contact between the matrix and the filler particles (also validated through mechanical testing), disassociation at the matrix-particle interface should have occurred during the biaxial stretching of the cell walls. The content of large glass particulates susceptible to weaken the cell walls during expansion is increased and so is the probability of such cell wall rupture. Larger glass particulates are more prone to induce cell opening, with bigger size than the wall thickness estimated as 10-20 μm. While larger glass particulates would obviously lead rapidly to cell wall rupture, for particulates much smaller than the wall thickness, local stress concentrations are such that cracks and lens-like voids will be formed during stretching, weakening locally the film and contributing eventually to the complete rupture of the cell wall. In addition, the cells no longer exhibited angular corners, and became more spherical. Increasing the glass content

further to 30 vol.% had a strong effect on the opening of the cells. However, this increase in open cells probably induced gas loss thus limiting the expansion of the cellular structure. With approximately the same nucleation density as for the composite with 20 vol.%, the total porosity remains below 80% with an average cell diameter of less than 200 µm. In addition, some PGPs could also act as nucleation sites, a more controlled cellular structure would be obtained in their presence.

The incorporation of PGPs into PDLLA led to an improvement in the compressive strength of PDLLA-PGP composite foams only at 30 vol.% PGP content which showed ~ 2.6-fold increase compared to neat PDLLA. Young's modulus of the foams increased at 10 vol.% PGP incorporation, and there was up to ~ 3.3-fold increase at 30 vol.% PGP content. It is well-known that the mechanical properties of foams changes with respect to the change in the relative density. In the actual case, the mechanical properties depend on those of the composite systems. Therefore, a similar dependence of the modulus as a function of the glass content is expected for both dense and foamed composites. For the unfoamed composites, the modulus roughly increased linearly with the glass content. A similar dependency was observed for the foamed composites, except for an abrupt increase in the modulus with an increase in PGP from 5 to 10 vol.%. The morphological variable susceptible to provide a clue to this significant increase might be the cell diameter, which rapidly decreases initially with glass content, then stabilizes around the 200 µm-range. Even though impact of the cell diameter on the mechanical performances has been the subject of many studies and that claims on the high gains associated with microcellular structures are still the object of controversy [315], our results nevertheless presented a two-fold increase in the modulus from the neat unfoamed PDLLA to the 30 vol.% PGP filled composite, while the increase was 3-fold for the foamed composite.

The results obtained with the SSF method are more attractive than those resulting from the batch foaming method based on rapid depressurization in the molten state followed by cooling of the cellular structure. Adopting this last technique, Georgiou *et al.* [190] developed composite foams based on commercial bioresorbable semi-crystalline poly-L-lactic acid and PG formulation. Although PGP content as high as 20 wt.% was investigated, foaming could only be performed for 5 and 10 wt.% PGP, with the porosity

maintained above 75%. The SSF technique used in this study combined with using amorphous PDLLA as the matrix allowed for producing foams with higher PGP content up to 30 vol.% (~ 45 wt.%), and increased porosity and open pore structure.

In addition, the results obtained with the SSF method still compare advantageously with other reviewed techniques such as salt-leaching and TIPS, as evidenced from the following studies. Navarro *et al*. [189] produced composite scaffolds of poly(95L/5DL) lactic acid reinforced with calcium phosphate glass particles ($44.5P_2O_5$-44.5CaO-$6Na_2O$-$5TiO_2$) using salt-leaching technique (94% w/w NaCl particles). Chloroform and distilled water were used for dissolution of the polymer and salt-leaching process, respectively. High salt content resulted in high porosity (as much as 97%); however, compressive mechanical properties were in the range of kPa. In addition to using an organic solvent which is one of the disadvantages of salt-leaching technique, the water used for salt-leaching is detrimental for PGs since they are water sensitive. Therefore, PGP dissolution might have occurred during the 2 days salt-leaching process which could have affected both porosity and mechanical properties of the as-produced foams. Blaker *et al.* [194] used TIPS technique to produce porous microstructures composed of PLGA and silver-doped PGs. Although TIPS process results in high porosity and interconnectivity, the pore size is normally smaller than required for BTE. In their study, porous macro-spheres (up to 2000 μm in diameter) with pores in the range of 30-70 μm were produced. PDLLA-Bioglass® composite foams fabricated by TIPS process resulted in tubular pores of ~100 μm [10].

In this study, a relatively high PGP content could be incorporated into PDLLA and successfully foamed using the SSF method with CO_2. The resulting cellular structures of these foams were adequate for BTE scaffold applications. The use of glass particulates along with the SSF process contribute synergistically to the desired high porosity, average-size cell diameter and open cell structure. In conclusion, three essential functions for the foaming process can be attributed to the glass particulates. Overall, the particulates increase the nucleation and lead to smaller cell walls. Larger particulates (> 20 μm) create the needed pores during late cell growth, and the smaller particulates (< 20 μm) modify the rheological behaviour (increased melt strength) so that homogeneous

deformations occur throughout the cellular structure under expansion, at least in its early stage.

8.6. Conclusions

PDLLA-PGP composites and foams could be successfully produced with up to 30 vol.% PGP content through melt extrusion and compression moulding for composites followed by solid-state gas foaming using CO_2. PGP incorporation did not adversely affect the molecular weight of the polymer matrix hence resulted in enhanced mechanical properties in both composite and foam systems due to appropriate PGP distribution and filler/matrix interface. Solid-state foaming using CO_2 was shown to be an effective route for producing macro-porous structures of PDLLA-PGP composites. Composite foams with approximately 79 to 91% porosity were obtained, based on various PGP contents, compared to 92% porosity in the case of neat PDLLA foam. While large pores were observed in neat PDLLA foams, the incorporation of PGP into PDLLA resulted in reduced pore size due to increased viscosity, PGPs acting as nucleation sites and also barrier against cell growth. Consequently, a more controlled cellular structure was obtained in the presence of PGPs. The pore size decreased with increasing PGP content, yet it remained in the acceptable range for bone tissue engineering applications. In addition, the percentage of open pores increased significantly by increasing PGP content (up to 78% at 30 vol.% PGP). It was hypothesised that the presence of PGPs could lead to creation of open windows which opened up the pores. Moreover, PGPs will increase both porosity and open pore percentage upon dissolution in physiological fluids. PDLLA-PGP foam morphologies obtained in this study were promising for potential applications in bone tissue engineering.

8.7. Acknowledgements: This work was funded by the Canadian Natural Sciences and Engineering Research Council, le Fonds Québécois de la Recherche sur la Nature et les Technologies, Hatch Faculty Fellowship, and Canadian Foundation for Innovation: Leaders Opportunity Fund. Funding for Maziar Shah Mohammadi was also partly supported by a McGill Engineering Doctoral Award. Martin N. Bureau is a membre of

the Groupe de Recherche en Sciences et Technologies Biomédicales (Fonds de recherche en santé du Québec).

CHAPTER 9

SUMMARY OF ACCOMPLISHMENTS AND GENERAL DISCUSSION

9.1. Introduction

This Chapter includes the summary of accomplishments of this research. A general discussion will be provided for each accomplishment by comparing all the PG formulations, and composite systems presented in this dissertation (as separate manuscripts) in order to comprehensively discuss the effect of PG composition, geometry and content on tailoring the properties of PGs, polyester-PG composites and foams for bone repair and regeneration applications.

9.2. Role of SiO_2, Fe_2O_3 and TiO_2 in phosphate-based glasses

Silicate-based glasses (SGs) have been extensively investigated for bone applications, and Bioglass® is Food and Drug Administration (FDA) approved as bone grafting material for intraoral applications [273]. Due to the confirmed positive effect of

Si on the biological properties of ceramics and glasses [241], there has been significant research interest on Si-containing bone graft substitutes; e.g. Si-substituted calcium phosphates such as hydroxyapatite (HA) and tricalcium phosphate (TCP). Although SiO_2 incorporation into phosphate-based glasses (PGs) has been studied by Patel *et al.* [13], the study mainly focused on the degradation properties of $50P_2O_5$-30CaO-(15-x)Na_2O-$5Fe_2O_3$-xSiO_2 (x = 0, 1, 3, and 5 mol.%) system and focused on the effect of Fe on reducing the degradation rate. There is also a general lack of a thorough investigation on the effect of SiO_2 doping into PGs on their properties alone and when incorporated into a composite system. In addition, the majority of PG formulations investigated to date included a respective amount of sodium, as presented in Table 2.3. SGs, of the system SiO_2-CaO-Na_2O-P_2O_5 were developed by Hench and co-workers, and the compositional dependence of their bioactivity and tissue bonding properties have been well reported. This compositional dependence has been demonstrated with the SiO_2-CaO-Na_2O phase diagram [20]. It was found that the glasses in the silica-rich region were almost inert, while those with high NaO_2 content resorbed within 10 to 30 days of implantation. In addition, it was found that sodium has a key role on the surface reactivity of SGs, and the formation of a calcium phosphate layer in physiological fluids, which is initiated by the rapid exchange of sodium ions with H^+ or H_3O^+ from the solution [21]. Therefore, the presence of sodium was deemed to be necessary as a network modifier in order to reduce the high network connectivity of SGs. However, PGs have low network connectivity, and are naturally unstable and readily soluble in aqueous environments. It has been demonstrated that the P_2O_5-CaO-Na_2O system inhibited cell adhesion and proliferation and increased cell death [23]. This could be mediated by the loss of PG surface integrity due to dissolution, and high release of Na^+ and PO_4^{3-} ions affecting the PH of the culture environment. In addition, sodium ions have been reported to be detrimental to cells [22]. These reports question the need of incorporating sodium into the PG formulation. Therefore, this research conducted a thorough investigation on the bulk and surface properties of numerous sodium-free PG formulations doped with or without SiO_2, Fe_2O_3 and TiO_2. For this purpose, this research was initiated by the fabrication of a ternary PG formulation doped with SiO_2 ($50P_2O_5$-40CaO-$10SiO_2$ in mol.%), namely Si10, without the addition of other metal oxides. The partial or whole substitution of SiO_2 by Fe_2O_3 or

TiO_2 was then followed to create either ternary or quaternary systems of SiO_2/Fe_2O_3 or SiO_2/TiO_2 doped PGs. In all formulations P_2O_5 and CaO contents were kept at 50 and 40 mol.%, respectively, and the remaining 10 mol.% was substituted by SiO_2, Fe_2O_3, or TiO_2.

Si10 formulation resulted in PG with rapid dissolution rate in aqueous environments, which was significantly ($P<0.05$) higher than those doped with either Fe_2O_3 or TiO_2. Consequently, rapid dissolution of Si10 occurred within days and large amount of phosphates release resulted in a significant pH reduction. Therefore, doping the PG composition with a metal oxide was found to be necessary for increasing the durability. Doping PGs with Fe_2O_3 or TiO_2 resulted in controlled dissolution and ion release. Figure 9.1 shows the degradation and ion release rates of all the PG formulations investigated in this study.

The rapid degradation of Si10 formulation could be tailored controllably by partially substituting with various amounts of Fe_2O_3 or TiO_2. All the formulations showed statistically significant differences in their degradation and ion release rates. Si-free formulations demonstrated the lowest rates (e.g. 6.7×10^{-6} $mg.mm^{-2}.h^{-1}$, 0.035 $ppm.h^{-1}$ and 0.02 $ppm.h^{-1}$ for weight loss, phosphorous and calcium release of Ti10, respectively). Compared to Fe_2O_3, TiO_2 was found to be more effective in stabilising the PG network since the degradation and ion release rates of Si5Ti5 and Ti10 were statistically ($p<0.05$) lower compared to Fe5Si5 and Fe10, respectively. The effect Fe_2O_3 and TiO_2 on stabilising the PG network by acting as cross-link within the phosphate network was also reflected in physical properties of PGs where a concomitant increase in the glass transition temperature (T_g) was observed by incorporating Fe_2O_3 or TiO_2 into PG composition.

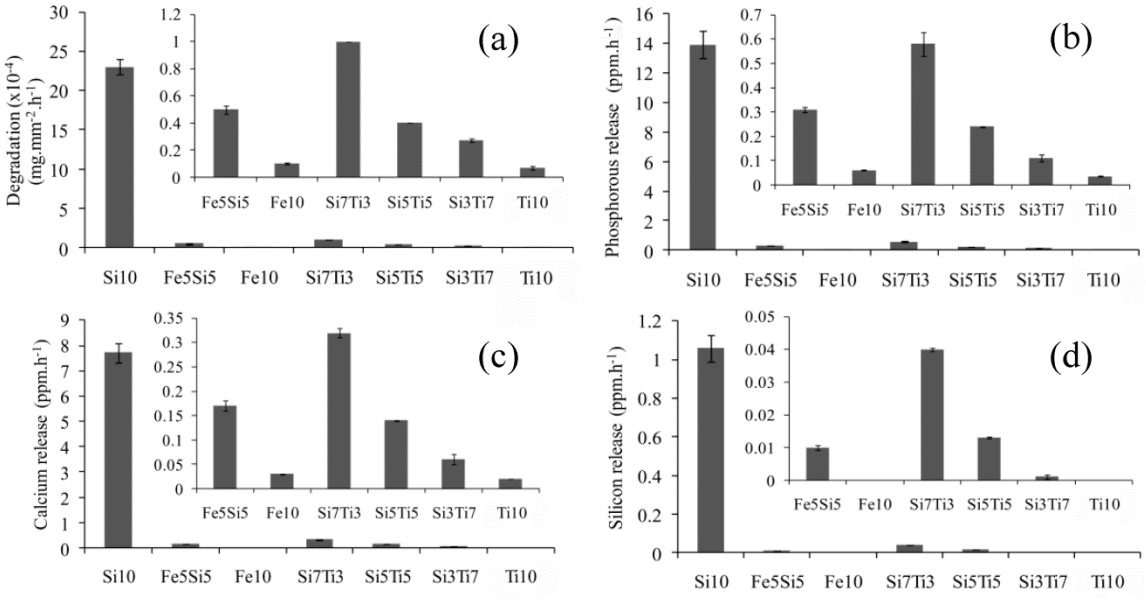

Figure 9.1 Degradation and ion release rates for all the PG formulations investigated in this study. (a) Degradation as measured by weight loss, release rates of (b) Phosphorous, (c) Calcium, and (d) Silicon. Si10 degradation and ion release rates were significantly higher than PGs doped with either Fe_2O_3 or TiO_2.

SiO_2, Fe_2O_3 and TiO_2 incorporation not only influenced the bulk properties of PGs but also their surface properties. Surface energies and polarity of all PG formulations are presented in Figure 9.2. It was found that Si10 formulation showed significantly ($p<0.05$) higher surface energy and polarity compared to all other formulations. This was also valid for hydrophilicity as revealed through contact angle measurements. Increased hydrophilicity, surface energy and polarity of SiO_2 containing PGs could be attributed to the formation of hydroxyl (Si-OH) groups on the surface. Fe10 formulation showed the highest water contact angle (lowest hydrophilicity), and lowest surface energy and polarity among all PG formulations.

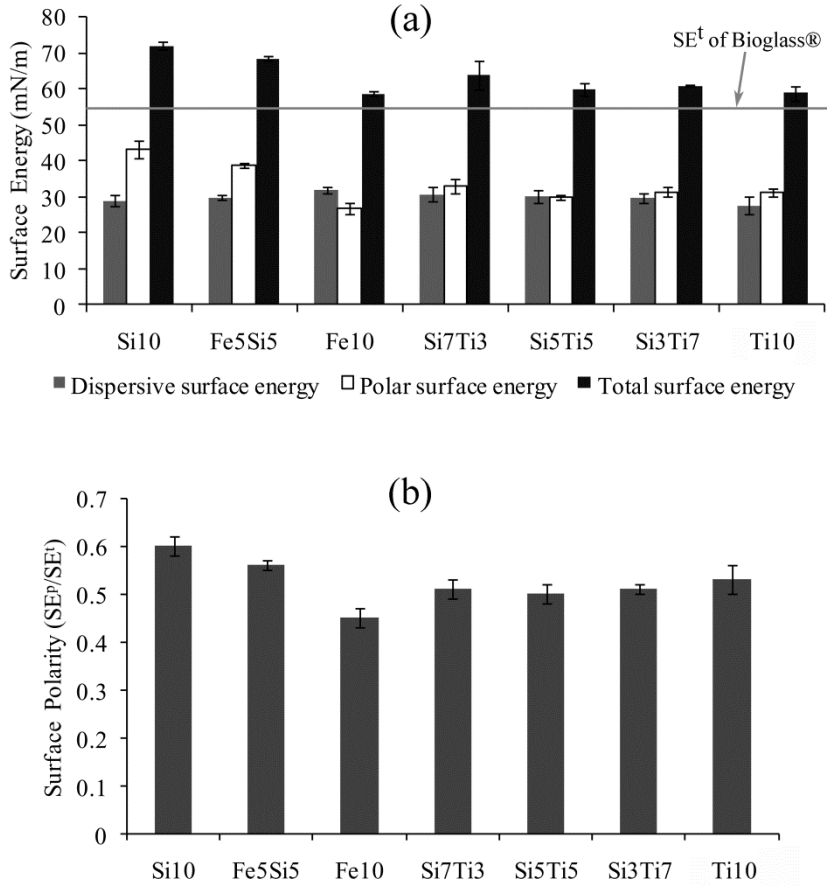

Figure 9.2 Surface properties of all the PG formulations investigated in this study. (a) Dispersive, polar, and total surface energy, (b) Surface polarity. Si10 showed the highest polar and total surface energies, as well as surface polarity. Fe_2O_3 and TiO_2 doping resulted in reduced surface energy and polarity compared to Si10. Total surface energy of Bioglass® [147] has also been indicated with a line for comparison.

Comparing Si-free formulations, although Fe10 and Ti10 show no statistically significant differences between their total surface energy, the polar surface energy and surface polarity of Ti10 were significantly ($p<0.05$) higher than those of Fe10. Therefore, doping PGs with Fe_2O_3 resulted in a greater reduction in hydrophilicity, surface energy and polarity compared to TiO_2; which may be attributed to the ability of Ti in forming functional groups (Ti-OH) on the surface [78], thus leading to enhanced hydrophilicity and surface polarity. It should be noted that there was no statistical significant difference among the dispersive surface energies of all PG formulations investigated in this study. The polar characteristic of PGs is a unique property which results in their wettability and hydrophilicity. For example, the polar surface energy of HA and β-TCP is lower than

their dispersive ones [316]; however, the polar surface energy of most of the PG formulations, especially those doped with SiO_2, was greater than the dispersive surface energy.

Surface properties of PGs play a key role in their bioactivity and biocompatibility [120]. Increased hydrophilicity enhances the hydrolysis mechanism of PG dissolution and hence ion release which controls the calcium phosphate deposition. In addition, attachment and viability of cells significantly depend on the rate of dissolution and ion release occurring at the surface [23]. Cytocompatibility investigations over 7 days revealed that the Si10 formulation was detrimental for pre-osteoblasts due to rapid dissolution and ion release rate which resulted in reduction of pH of the culture medium. However, cytocompatibility was significantly improved by doping PGs with Fe_2O_3 or TiO_2. PGs doped with TiO_2 were found to be more cytocompatible compared to those doped with Fe_2O_3 since less necrotic/apoptotic cells were observed on Ti-doped formulations. A positive effect of doping PGs with Ti has been previously reported [28, 29]. However, a more detailed cytocompatibility study on Si and Ti doped formulations revealed an interesting effect of doping PGs with Si on their potential application in bone tissue engineering (BTE). While Si10 was detrimental for pre-osteoblasts, substituting 3 mol.% SiO_2 with TiO_2 (Si7Ti3) was adequate to achieve controlled dissolution and ion release for obtaining cell attachment, viability, and proliferation. A further increase in TiO_2 content resulted in reduced degradation and ion release rates, and did not significantly change cell attachment, viability and proliferation. However, it was found that the presence of 5 to 7 mol.% SiO_2 resulted in increased alkaline phosphatase (ALP) activity and production. It was hypothesised that doping PGs with SiO_2 would up-regulate ion release (calcium and phosphate species) leading to increased ALP activity.

In conclusion, doping PGs with SiO_2 and a modifying metal oxide (e.g. TiO_2) was found to be promising in producing PGs for potential BTE applications.

9.3. Translation of PG properties into composite systems

Incorporation of PGs into biodegradable polymers is an interesting approach for bone repair and regeneration. The investigated PG formulations in this study were incorporated into biodegradable polyesters to investigate whether the soluble nature of

PGs can be translated into composite systems. Both PG particulates (PGPs) and fibres (PGFs) were incorporated at different volume fractions with the aim of tailoring composite properties.

As a first approach, blends of mixed PGP formulations (Si10 and Fe10) were incorporated into polycaprolactone (PCL) at 40 vol.%. It was found that the soluble nature of PGs can be translated into a composite system. Weight loss and ion release of the composites were dependant on the incorporated PG formulations. For example, composites with greater Si10 content showed higher weight loss and ion release rates compared to composites with greater Fe10 content. In addition, composites with greater Fe10 content demonstrated a delay in weight loss and ion release; e.g. 24 h for PCL-PGP (40 vol.% Fe10), due to the less hydrolysable nature of Fe10 (lower hydrophilicity) compared to Si10. PCL-PGP (40 vol.% Si10) showed no precipitation on its surface upon ageing in simulated body fluid (SBF), which was probably due to the very rapid dissolution rate of Si10 where a dramatic increase in the amount and rate of PO_4^{3-} ion release was observed in the first 24 hours. In contrast, PCL-PGP (40 vol.% Fe10) rate of ion release was very slow. However, the use of mixed glass formulations could control the amount and rate of ion release and showed a significant effect on the potential for calcium phosphate precipitation where brushite, an apatite precursor, was detected on the surface of composites with mixed PG formulations at day 28 in SBF. Another interesting outcome of using mixed PG formulations was observed in the microstructure of the composites upon ageing in aqueous environments. While, rapid dissolution of Si10 PGPs resulted in the formation of pores within the microstructure, Fe10 PGPs remained for longer time periods. Therefore, it was hypothesized that porosities generated through PGP dissolution could result in further controlled pore generation within pre-fabricated foamed scaffolds leading to an increase in the potential for nutrient and oxygen perfusion and cell migration and growth. On the other hand, the newly formed porous composite maintains its mechanical properties for longer time periods due to the presence of slower degrading PGPs. In addition, favourable ionic species would still being released.

The second approach was using PGFs as fillers. Fe10 and Fe5Si5 PGFs (18 vol.%) were incorporated into PCL and poly(lactic acid) (PLA) as randomly oriented fibres. The dependence of weight loss and ion release on PG composition was also

observed where composites reinforced with Fe5Si5 PGFs showed greater weight loss and ion release rates compared to those reinforced with Fe10. In addition, the delay in weight loss and ion release initiation was increased (up to 4 days) compared to PCL-PGP composites. This was probably due to lower surface area of PGFs compared to PGPs, lower volume fraction, and Fe-doped formulations. The ion release rates of PCL-Fe10 and PLA-Fe10 were not significantly different. However, ion release rates of PLA-Fe5Si5 were higher than those of PCL-Fe5Si5. PLA-Fe5Si5 showed significant water ingress upon ageing in deionised water which was later found to be attributed to matrix degradation due to interaction between Si and ester bond at elevated processing temperature. Therefore, more water up-take could lead to faster degradation of PGFs resulting in higher ion release rates. The positive effect of PGF incorporation was also observed in the pre-osteoblastic response where MC3T3-E1 cells preferably aligned along the PGFs which could be attributed to the favourable ionic release. An example of cell alignment on PLA-Fe5Si5 surface is demonstrated in Figure 9.3.

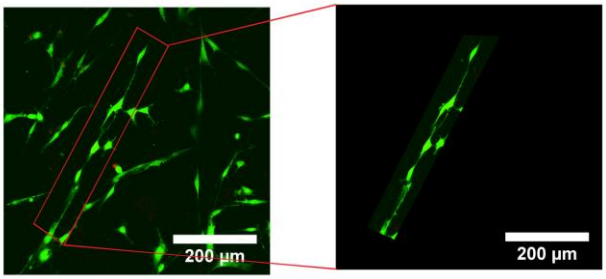

Figure 9.3 MC3T3-E1 pre-osteoblasts alignment along the PGF orientation on the surface of PLA-Fe5Si5 composite at day 1.

The reinforcing effect of PGs was considerably depended on 1) the PG formulation and geometry (particulate or fibre), 2) the polymer matrix and 3) the processing conditions. Figure 9.4 shows the relative flexural strength and modulus to the polymer matrix for all the composite systems investigated in this dissertation. Blends of Si10 and Fe10 PGPs did not increase the flexural strength of PCL, yet significantly increased the modulus. However, a significant increase in the mechanical properties (up to 2.5 fold) was observed when Fe10 and Fe5Si5 formulations were incorporated into both PCL and PLA as PGFs which was attributed to the higher fibre aspect ratios leading to greater stress transfer levels to the matrix. However, the increase in the flexural

strength of PLA-Fe5Si5 was less significant which was found to be attributed to the degrading effect of Si on the PLA matrix at elevated processing temperature, and will be discussed in section 9.3. Incorporating Ti10 formulation into poly (D,L-lactic) acid (PDLLA) resulted in an up to 2-fold increase in the flexural mechanical properties at 30 vol.%. While Si-doped PGPs did not increase the strength but significantly increased the modulus of PCL-PGP composites due to degrading effect of Si, Ti-doped PGPs improved both strength and modulus of PDLLA at controlled processing conditions (temperature, time, and pressure). This could be due to a greater stress transfer between Ti10 PGPs with the matrix, and maintaining the PDLLA matrix molecular weight.

Rate of reduction in the mechanical properties in physiological environments is of importance in the application of degradable materials. It was found that the rate of reduction in the mechanical properties of polymer-PG composites was directly related to the PG dissolution rate. Consequently, composites reinforced with Si-doped PGPs and PGFs showed a greater rate of reduction in the mechanical properties upon conditioning in phosphate buffered saline (PBS) (Figure 9.5). The rate of reduction in mechanical properties was also greater in composites reinforced with PGPs compared to PGFs due to the faster degradation rates of the particulates. For example, PCL-PGP (0Fe10/40Si10) showed the greatest loss in mechanical properties among all the investigated composite systems in PBS, and could not be tested at days 7 and 28; however, PCL-PGF (Fe10) and PCL-PGF (Fe5Si5) maintained their greater strength and modulus compared to neat PCL at days 7 and 28 in PBS. PLA-Fe5Si5 showed the highest rate of reduction in mechanical properties among the polymer-PGF composites due to degraded PLA matrix, as discussed earlier. Degraded matrix resulted in void formation species upon ageing in deionised water observed by SEM.

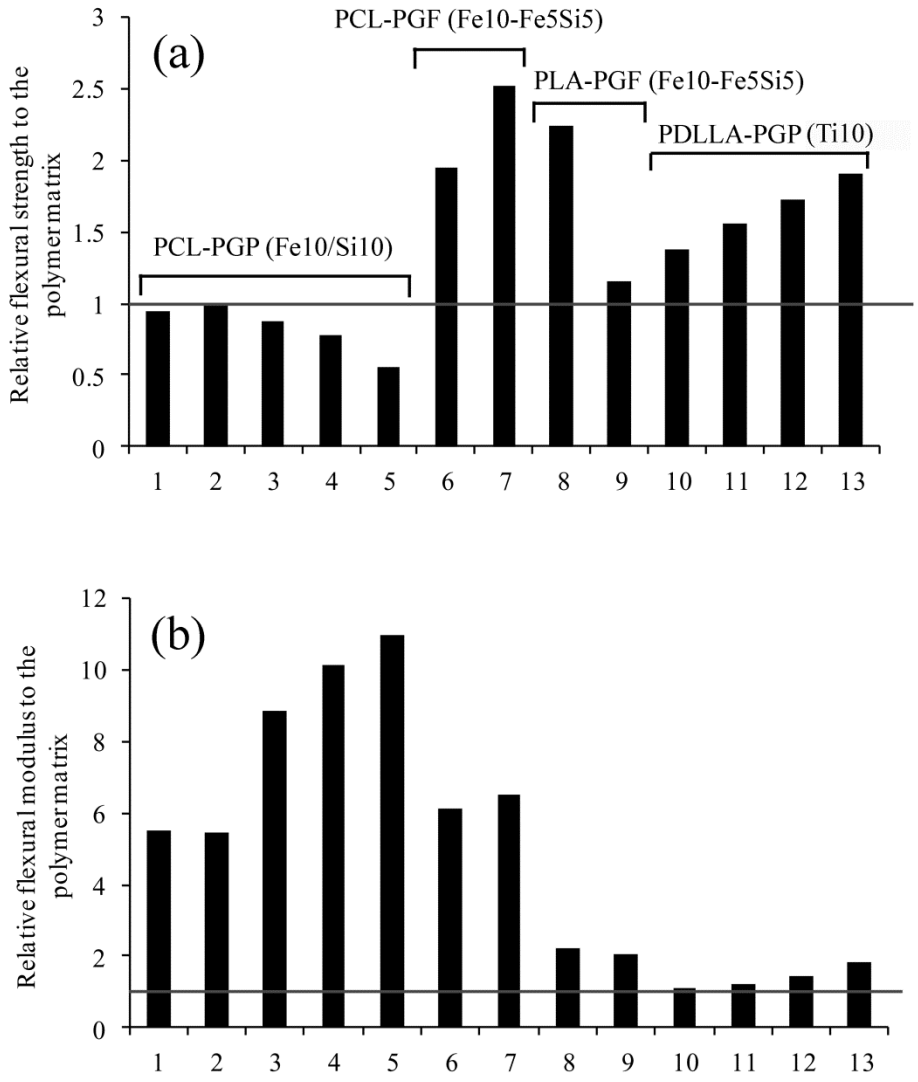

Figure 9.4 Relative flexural strength (a) and modulus (b) of the composite systems to those of the polymer matrix. **1:** PCL-PGP(40Fe10/00Si10), 100 ^{o}C, 30 min, 38 bar. **2:** PCL-PGP(30Fe10/10Si10), 100 ^{o}C, 30 min, 38 bar. **3:** PCL-PGP(20Fe10/20Si10), 100 ^{o}C, 30 min, 38 bar. **4:** PCL-PGP(10Fe10/30Si10), 100 ^{o}C, 30 min, 38 bar. **5:** PCL-PGP(00Fe10/40Si10), 100 ^{o}C, 30 min, 38 bar. **6:** PCL-PGF(18Fe10), 100 ^{o}C, 30 min, 38 bar. **7:** PCL-PGF(18Fe5Si5), 100 ^{o}C, 30 min, 38 bar. **8:** PLA-PGF(18Fe10), 210 ^{o}C, 30 min, 38 bar. **9:** PLA-PGF(18Fe5Si5), 210 ^{o}C, 30 min, 38 bar. **10:** PDLLA-PGP(5Ti10), 110 ^{o}C and 4 min (extrusion), 160 ^{o}C, 10 min, and 16 bar (compression). **11**: PDLLA-PGP(10Ti10), 110 ^{o}C and 4 min (extrusion), 160 ^{o}C, 10 min, and 16 bar (compression). **12:** PDLLA-PGP(20Ti10), 110 ^{o}C and 4 min (extrusion), 160 ^{o}C, 10 min, and 16 bar (compression). **13:** PDLLA-PGP(30Ti10), 110 ^{o}C and 4 min (extrusion), 160 ^{o}C, 10 min, and 16 bar (compression).

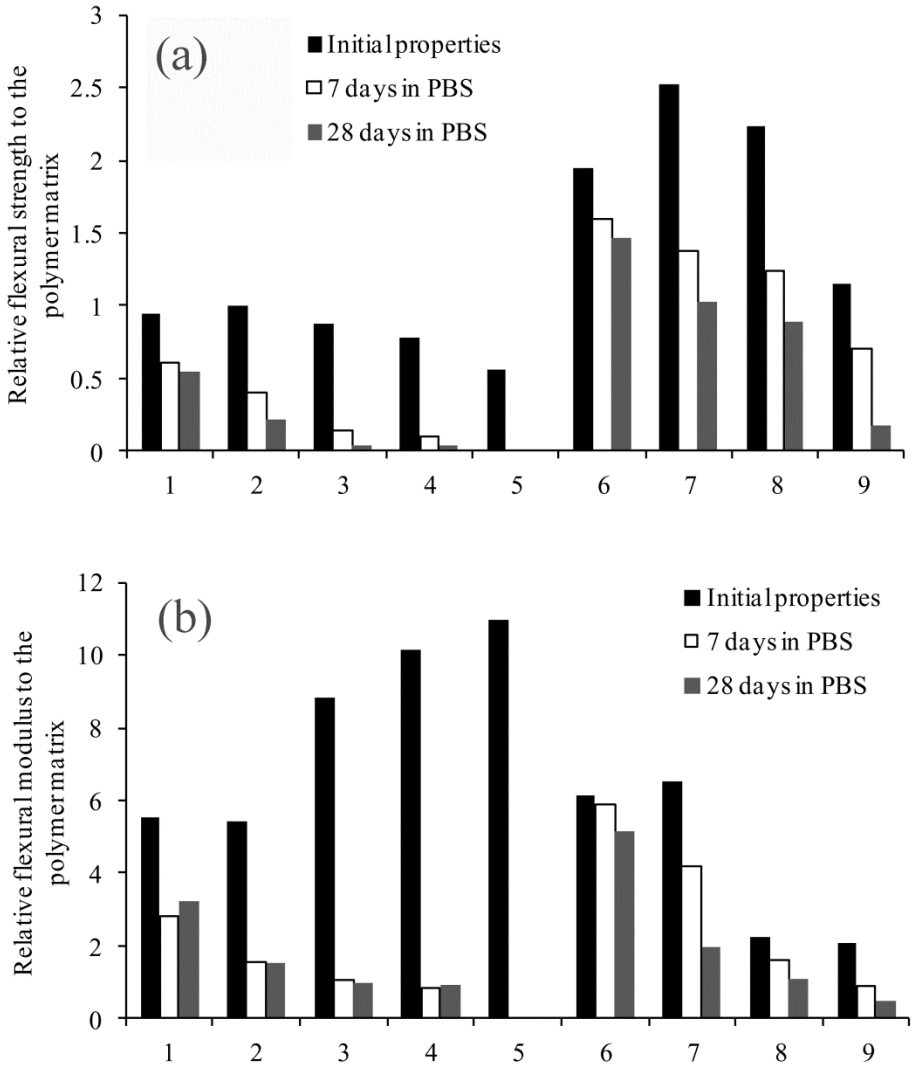

Figure 9.5 Relative flexural strength (a) and modulus (b) of the composite systems to those of the polymer matrix initially and after ageing in PBS for 7 and 28 days. **1:** PCL-PGP(40Fe10/00Si10), 100 ^{o}C, 30 min, 38 bar. **2:** PCL-PGP(30Fe10/10Si10), 100 ^{o}C, 30 min, 38 bar. **3:** PCL-PGP(20Fe10/20Si10), 100 ^{o}C, 30 min, 38 bar. **4:** PCL-PGP(10Fe10/30Si10), 100 ^{o}C, 30 min, 38 bar. **5:** PCL-PGP(00Fe10/40Si10), 100 ^{o}C, 30 min, 38 bar. **6:** PCL-PGF(18Fe10), 100 ^{o}C, 30 min, 38 bar. **7:** PCL-PGF(18Fe5Si5), 100 ^{o}C, 30 min, 38 bar. **8:** PLA-PGF(18Fe10), 210 ^{o}C, 30 min, 38 bar. **9:** PLA-PGF(18Fe5Si5), 210 ^{o}C, 30 min, 38 bar.

Therefore, composite properties could be tailored by incorporating PGs which was dictated by their geometry and composition. Incorporating PGs into biodegradable polymers led to composites with modulated mechanical properties, degradability, ion release, bioactivity, and cytocompatibility.

9.4. Role of PG surface properties and processing conditions on interaction with polyester matrix

The reaction of Bioglass® with poly(α-hydroxy esters) when processed at elevated temperatures has been reported to degrade the polymer matrix [188]. This dissertation investigated whether Si-doped PGs would also demonstrate a similar effect in the composite systems based on PCL and PLA. It was found that there was a potential reaction between Si and the ester bond which led to a reduction in the matrix molecular weight when processed under certain conditions. Figure 9.6 shows the relative M_w of the polymer matrix to the initial polymer pellets after processing with PGs of different geometries and compositions used for composite fabrication. Fe10 formulation as either particulates or fibres did not decrease the PCL M_w when processed at 100 ^oC. However, Si10 incorporation as PGPs resulted in a significant reduction in M_w which increased by increasing Si10 content. Composites containing 40 vol.% Si10 PGPs showed the greatest reduction in M_w (up to 80%) among all composite systems. FTIR analyses also confirmed the formation of carboxylate by-products which leads to the formation of lower M_w polymer. SiO_2 incorporation into PGs can disrupt the phosphate network and also form hydroxyl groups (Si-OH) on the surface by absorbing water which will subsequently hydrolyse the ester bond causing matrix chain-scission. This effect could be correlated with the surface properties of PGs. Glass surface properties impact the nature of interfacial interaction of filler and matrix. Therefore, since doping PGs with Fe_2O_3 resulted in reduced surface energy and polarity due to a reduction in the concentration of hydroxyl groups, PCL degradation was prevented when processed with quaternary Fe5Si5 formulation as PGFs at 100 ^oC. This could also be related to lower surface area of fibres compared to particulates. Therefore, the potential adverse effect of Si-doped PG on PCL could be reduced by using: (i) PG with reduced surface energy; e.g., a quaternary glass formulation (Fe5Si5) instead of a ternary glass formulation (Si10); (ii) lower filler content; and (iii) fibres instead of particulates thus reducing the surface area. However, Fe5Si5 PGFs degraded PLA when processed at 210 ^oC as the PLA M_w was decreased by 75% (Figure 9.6). It should be noted that although there was a 48% reduction in M_w of PLA-Fe10, it was due to thermal degradation as was also observed in neat PLA after processing. Therefore, Fe10 PGFs did not alter the molecular weight in this case. It was

concluded that in addition to the PG composition, processing temperature would also play an important role in the potential interaction between PGs and polymer matrix.

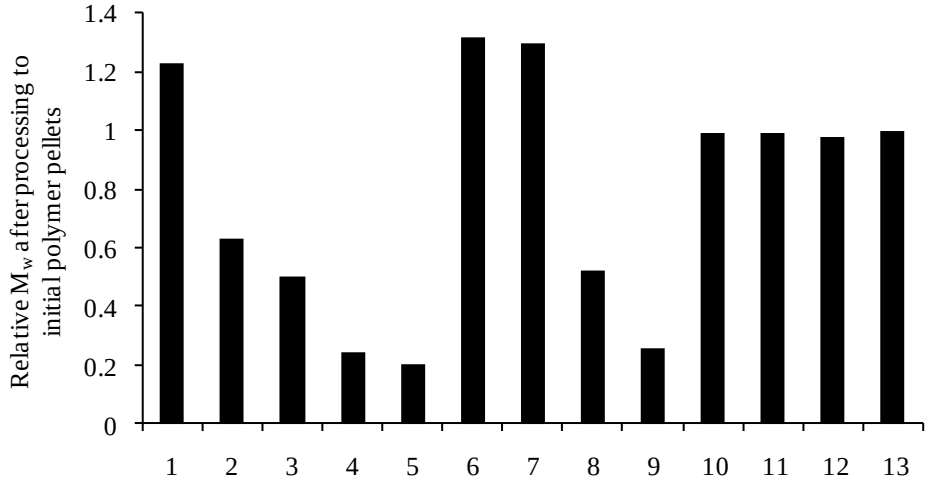

Figure 9.6 Relative M_w of the polymer matrix after thermal processing to initial polymer pellets for composite systems investigated in this study. **1:** PCL-PGP(40Fe10/00Si10), 100 ^{o}C, 30 min, 38 bar. **2:** PCL-PGP(30Fe10/10Si10), 100 ^{o}C, 30 min, 38 bar. **3:** PCL-PGP(20Fe10/20Si10), 100 ^{o}C, 30 min, 38 bar. **4:** PCL-PGP(10Fe10/30Si10), 100 ^{o}C, 30 min, 38 bar. **5:** PCL-PGP(00Fe10/40Si10), 100 ^{o}C, 30 min, 38 bar. **6:** PCL-PGF(18Fe10), 100 ^{o}C, 30 min, 38 bar. **7:** PCL-PGF(18Fe5Si5), 100 ^{o}C, 30 min, 38 bar. **8:** PLA-PGF(18Fe10), 210 ^{o}C, 30 min, 38 bar. **9:** PLA-PGF(18Fe5Si5), 210 ^{o}C, 30 min, 38 bar. **10:** PDLLA-PGP(5Ti10), 110 ^{o}C and 4 min (extrusion), 160 ^{o}C, 10 min, and 16 bar (compression). **11**: PDLLA-PGP(10Ti10), 110 ^{o}C and 4 min (extrusion), 160 ^{o}C, 10 min, and 16 bar (compression). **12:** PDLLA-PGP(20Ti10), 110 ^{o}C and 4 min (extrusion), 160 ^{o}C, 10 min, and 16 bar (compression). **13:** PDLLA-PGP(30Ti10), 110 ^{o}C and 4 min (extrusion), 160 ^{o}C, 10 min, and 16 bar (compression).

Therefore, there is a potential reaction between Si and ester bond in polyesters due to formation of Si-OH groups on the surface leading to increased surface energy and polarity. However, this reaction would also depend on filler surface area, as well as processing conditions. In order to avoid having a potential adverse effect of Si on PDLLA matrix, Ti10 PGP was selected as filler for composite foam fabrication through solid-state gas foaming. Composites were processed through micro-extrusion (at 110 ^{o}C / 4 min) followed by compression moulding (160 ^{o}C / 10 min). GPC showed no reduction in the molecular weight of PDLLA after processing with 5, 10, 20, and 30 vol.% Ti10 PGP (Figure 9.6).

9.5. Solid-state foaming with CO_2: An effective technique for polymer-PG composite foam fabrication

Porous polymer-PG composites have the potential to be used as scaffolds for BTE applications. Previously, PLA-PG composites had been foamed by using supercritical carbon dioxide ($scCO_2$) (T=195 ^oC and P_{sat}=150-250 bar) [190]. However, this foaming process was not efficient, and did not result in significant void formation for 20 wt.% (~12 vol.%) incorporation of PGP. In this study, PDLLA-PGP (up to 30 vol.% PGP content) composites were successfully foamed using solid-state CO_2 foaming. Composites were saturated with CO_2 in an autoclave (p=2.4 MPa) at room temperature for 72 h, followed by increasing the temperature above the T_g of the polymer matrix. While foaming neat PDLLA was not uniform and led to very large pores (~1 mm in diameter), incorporating PGPs into PDLLA resulted in more uniform and controlled foaming. Although the pore size decreased with increasing PGP content (200-500 μm), it was deemed to be in the acceptable range of BTE applications [55]. The reduction in pore size could be due to PGPs acting as nucleation sites. In addition, PGP incorporation increases the viscosity of the polymer matrix which reduces the pore growth rate. PGP incorporation reduced the total porosity from 92% for neat PDLLA to approximately 88% for PDLLA-(5, 10 and 20)PGP and 79% for PDLLA-30PGP. However, there was a significant increase in the percentage of open pores with PGP incorporation. Figure 9.7 shows the total porosity and percentage of open pores for PDLLA and PDLLA-PGP foams with 5, 10, 20 and 30 vol.% PGP content. It was hypothesised that PGP incorporation could lead to the formation of open windows within the pores attributable to the impingment of growing pores with PGPs leading to creation of open windows. Since PGPs are soluble in physiological environments, their dissolution can lead to increased porosity and interconnectivity, when immerssed in an aqeous environment.

PGP incorporation not only resulted in interesting morphologies but also increased the compressive strength (statistically significant at 30 vol.%) and modulus (statistically significant at 10 vol.%) of the composite foams compared to neat PDLLA foam. In addition, there was an increase in the ratio of foam density to cell size with PGP

incorporation. It was found that the compressive strength and modulus of the foams increased as density/cell size increased.

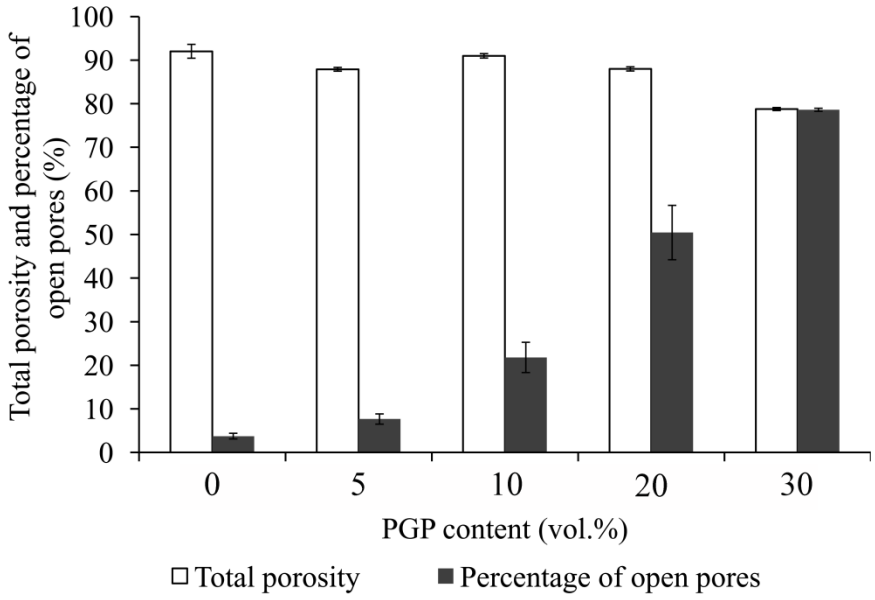

Figure 9.7 Total porosity and percentage of open pores for PDLLA and PDLLA-PGP foams with 5, 10, 20 and 30 vol.% PGP. While PGP incorporation slightly reduced the total porosity, the percentage of open pores increased significantly with increasing PGP content, and was statistically significant ($p<0.05$) for all the composites.

Therefore, solid-state foaming using CO_2 was found to be an effective technique for foaming polymer-PG composite foams. PGP incorporation led to controlled pore size, and increased the percentage of open pores. Foam compressive strength and modulus increased with increasing PGP content. Therefore, polymer-PG composites can be converted to an interesting porous morphology for BTE applications.

CHAPTER 10

CONCLUSIONS, ORIGINAL CONTRIBUTIONS TO KNOWLEDGE AND FUTURE PERSPECTIVES

10.1. Conclusions

The overall conclusions of this dissertation can be summarised as:

- ✓ The degradation rate of phosphate-based glasses (PGs) could be controlled by incorporating SiO_2, Fe_2O_3, or TiO_2 into the glass formulation. SiO_2 incorporation significantly increased the solubility of PG since Si can disrupt the phosphate network. In contrast, the addition of Fe_2O_3, or TiO_2 led to considerable decrease in solubility since Fe and Ti can create cross-links within the phosphate network. Therefore, it was found that by incorporating various contents of SiO_2 and Fe_2O_3 or TiO_2 into the PG, the degradation rate can be controllably tailored.
- ✓ The composition of PG can considerably influence its surface properties. There was an increase in the degradation of the PGs with an increase in the hydrophilicity, surface energy and polarity. Since the ion release from PG is in

line with the dissolution rate, surface properties would also affect the bioactivity and cytocompatibility of PGs.

- ✓ Si10 ($50P_2O_5$-40CaO-$10SiO_2$) composition was detrimental for MC3T3-E1 pre-osteoblasts viability at day 7 due to high ion release rate and hence reduction of pH of the environment. The substitution of SiO_2 with Fe_2O_3 or TiO_2 significantly improved cell viability which was in line with a controlled ion release. TiO_2-doped PGs showed a better response compared to Fe_2O_3-doped PGs possibly attributable to the presence of Ti^{4+} ions.
- ✓ The presence of Si was effective in up-regulating ionic release leading to higher alkaline phosphatase (ALP) activity. For example, while 3 mol.% TiO_2 was sufficient for stabilising the PG network leading to improved cell attachment and viability, compositions with 5 to 7 mol.% SiO_2 showed higher ALP activity compared to other compositions, as well as the controls. Hence, doping PGs with SiO_2 and TiO_2 showed promising tailored properties for potential bone tissue engineering (BTE) applications.
- ✓ The versatility of PG properties were translated to a composite system by incorporation into a degradable polymer (polycaprolactone (PCL) and poly(lactic acid) (PLA)) which largely depended on the glass composition. For example, it was found that the PG composition dictated the rate of weight loss and ion release of the composites.
- ✓ Composite properties could be modulated by incorporating mixed PG formulations. In PCL-PG composites containing blends of glass particulate (PGP) formulations, pores, formed by rapid dissolution of the Si10 PGP and remnants Fe10 PGP were observed. An advantage of such a structure, *in vivo*, would be that if the pores were designed to be interconnected, an increase in the potential for nutrient and oxygen perfusion and cell migration and growth would be achieved, while favourable ionic species would still being released. In addition, the newly formed porous composite maintains its mechanical properties for longer time periods.
- ✓ The higher solubility of Fe5Si5 PG fibres (PGFs) led to the formation of channels upon degradation while Fe10 PGFs remained in the microstructure for a much

longer time period. This resulted in the maintenance of the mechanical properties over time in physiological fluids.

- ✓ Brushite, an apatite precursor, was formed on the surface of the composites of mixed PG formulations, as well as, Fe5Si5 PGF containing composites at day 28 in simulated body fluid as an indication of potential calcium phosphate deposition.
- ✓ It was found that the surface properties of PGs have an important role on composite properties when processed at elevated temperatures. For example, Si doped PGs showed greater surface energy and polarity possibly due to the presence of hydroxyl groups on the surface. Consequently, incorporating these PGs into polyesters showed a potential reaction with the ester bond leading to a lower molecular weight polymer which ultimately affected composite properties. This reaction was found to be dependent on PG composition, filler surface area, and processing conditions (temperature, time and pressure).
- ✓ PGs with different geometries (particulates or fibres) and various degradation times from several weeks to several months were produced. For instance, based on the PCL-Fe10 weight loss, total degradation of Fe10 PGFs could be estimated to occur within 20 months, which may coincide with that of PCL, and may be suitable for longer-term applications such as bone fixation devices. On the other hand, a predicted total degradation time of 2.5 months for Fe5Si5 allows them to be more suitable for BTE applications when converted to porous scaffolds.
- ✓ PDLLA-PGP composites and foams were successfully produced with up to 30 vol.% PGP through melt extrusion and compression moulding for composites followed by solid-state gas foaming using carbon dioxide (CO_2). Solid-state foaming using CO_2 was shown to be an effective route for producing macro-porous structures of PDLLA-PGP composites.
- ✓ Foaming neat PDLLA resulted in large pores (~ 1 mm in diameter); however, PGP incorporation resulted in reduced pore size which was maintained within the acceptable range of BTE (~ 200-500 μm depending on the PGP content). In addition, a porosity range of 79-91% was achieved for various PGP contents.

- ✓ The percentage of open pores in the composite foams increased significantly with PGP content. Therefore, it was hypothesised that the presence of PGPs could lead to creation of open windows within the porous structure.

10.2. Original contributions to knowledge

The original contributions of this research can be summarized as:

- ✓ Development of novel sodium-free PG formulations doped with either SiO_2, Fe_2O_3 or TiO_2 with controllable properties.

- ✓ Investigating the effect of PG composition and geometry on the production and properties of biodegradable polyester-PG composites. The novelty of this part of research can be summarized as:

    - Using blends of mixed PG formulations in order to modulate the composite properties.
    - Development of polyester-PGF composites with different PGF composites and degradation rates to be suitable for different applications such as bone fixation devices or scaffolding material for bone tissue engineering applications.
    - Investigating the potential reaction between PG filler and the polyester matrix, and the parameters that can influence this interaction.

- ✓ Development of polyester-PG composite foams with high PG content and a unique morphology in terms of high porosity and open cell content as well as appropriate pore size suitable for bone tissue engineering scaffolds.

10.3. Future perspectives

It is envisaged that the results generated through this research will serve as a source for future investigations on PGs and polymer-PG composites for bone repair and regeneration. Followings can be considered in order to further expand this research:

- Other PG compositions that can be considered for further investigations. For example, the effect of adding Fe_2O_3 or TiO_2 on the extent of reducing the degradation of PGs was found not to be the same. Therefore, PGs doped with both Fe_2O_3 and TiO_2; e.g. $50P_2O_5$-$40CaO$-$5Fe_2O_3$-$5TiO_2$ (Fe5Ti5) could be a new composition to be investigated.

- The up-regulating effect of SiO_2 on the ionic release of the PGs which showed potential enhancement on the bioactivity and osteogenic properties could be used to improve the antimicrobial properties of PGS if the PG is doped with both SiO_2 and certain metal oxides that provide the antimicrobial properties. PGs doped with certain oxides such as CuO, Ag_2O and Ga_2O_3 have been shown to have anti-microbial properties due to release of copper, silver and gallium ions [124, 126, 130].

- The production of Si and Ti-doped phosphate glass fibres is worth considering as PGFs showed distinct properties compared to PGPs, specially in the enhancement of the mechanical properties of the composites.

- An interesting approach could be the production of composite fibres. In this case, PGPs could be incorporated into a polymer using a spinning process to produce polymer-PG composite fibres. These fibres can then be used to produce scaffolds for BTE applications.

- More biological assessments can be performed in order to further assess the cellular responses to the glasses, composites and foams. For example, the effect of dissolution products of PGs at different time on cell response can be carried out and compared to 72 h release as investigated in this dissertation. In addition, the experiments can be performed in the presence of PGs in the culture medium to investigate the effect of continuous release of bioinorganics form PGs which would better represent conditions *in vivo*. Other differentiation and mineralisation assays are needed to further investigate the osteogenic properties of PGs. These experiments can also be performed with composite systems since ion release rates are different form composite systems compared to PG discs. Composite foams produced in this dissertation showed interesting morphologies with appropriate pore size and open structure. However, the cellular responses to these foams have to be examined, such as cellular migration into the porous structure, and the effect of PGPs on the biological response of the composite foams. Moreover, since these materials were found to be cytocompatible *in vitro*, the biocompatibility assessment through *in vivo* implantation in an animal model would provide an insight towards understanding their biological response.

CHAPTER 11: REFERENCES

1. Stevens MM. Biomaterials for bone tissue engineering. Materials Today. 2008;11(5):18-25.
2. Schieker M, Seitz H, Drosse I, Seitz S, W M. Biomaterials as Scaffold for Bone Tissue Engineering. European Journal of Trauma. 2006;2:114-24.
3. Hench LL, Polak JM. Third-generation biomedical materials. Science. 2002;295(5557):1014-7.
4. Kretlow JD, Mikos AG. Review: Mineralization of synthetic polymer scaffolds for bone tissue engineering. Tissue Eng. 2007;13(5):927-38.
5. Liu CZ, Czernuszka JT. Development of biodegradable scaffolds for tissue engineering: a perspective on emerging technology. Mater Sci Tech-Lond. 2007;23(4):379-91.
6. Boccaccini AR, Maquet V. Bioresorbable and bioactive polymer/Bioglass (R) composites with tailored pore structure for tissue engineering applications. Compos Sci Technol. 2003;63(16):2417-29.
7. Ramakrishna S, Mayer J, Wintermantel E, Leong KW. Biomedical applications of polymer-composite materials: a review. Compos Sci Technol. 2001;61(9):1189-224.
8. Rich J, Jaakkola T, Tirri T, Narhi T, Yli-Urpo A, Seppala J. In vitro evaluation of poly(epsilon-caprolactone-co-DL-lactide)/bioactive glass composites. Biomaterials. 2002;23(10):2143-50.
9. Daniels AU, Chang MKO, Andriano KP, Heller J. Mechanical-Properties of Biodegradable Polymers and Composites Proposed for Internal-Fixation of Bone. Journal of Applied Biomaterials. 1990;1(1):57-78.
10. Klein CPAT, Driessen AA, Degroot K, Vandenhooff A. Biodegradation Behavior of Various Calcium-Phosphate Materials in Bone Tissue. Journal of biomedical materials research. 1983;17(5):769-84.
11. Knowles JC. Phosphate based glasses for biomedical applications. J Mater Chem. 2003;13(10):2395-401.
12. Abou Neel EA, Pickup DM, Valappil SP, Newport RJ, Knowles JC. Bioactive functional materials: a perspective on phosphate-based glasses. J Mater Chem. 2009;19(6):690-701.
13. Patel A, Knowles JC. Investigation of silica-iron-phosphate glasses for tissue engineering. J Mater Sci-Mater M. 2006;17(10):937-44.
14. Gao HS, Tan TN, Wang DH. Effect of composition on the release kinetics of phosphate controlled release glasses in aqueous medium. J Control Release. 2004;96(1):21-8.
15. Taboas JM, Maddox RD, Krebsbach PH, Hollister SJ. Indirect solid free form fabrication of local and global porous, biomimetic and composite 3D polymer-ceramic scaffolds. Biomaterials. 2003;24(1):181-94.
16. Ylinen P, Suuronen R, Taurio R, Tormala P, Rokkanen P. Use of hydroxylapatite/polymer-composite in facial bone augmentation. An experimental study. Int J Oral Max Surg. 2002;31(4):405-9.
17. Rizzi SC, Heath DT, Coombes AGA, Bock N, Textor M, Downes S. Biodegradable polymer/hydroxyapatite composites: Surface analysis and initial

attachment of human osteoblasts. Journal of biomedical materials research. 2001;55(4):475-86.
18. Luklinska ZB, Bonfield W. Morphology and ultrastructure of the interface between hydroxyapatite-polyhydroxybutyrate composite implant and bone. J Mater Sci-Mater M. 1997;8(6):379-83.
19. Ahmed I, Lewis M, Olsen I, Knowles JC. Phosphate glasses for tissue engineering: Part 2. Processing and characterisation of a ternary-based P2O5-CaO-Na2O glass fibre system. Biomaterials. 2004;25(3):501-7.
20. Hench LL. Bioceramics - from Concept to Clinic. J Am Ceram Soc. 1991;74(7):1487-510.
21. Hench LL WJ. An introduction to bioceramics. 2 ed: World Scientific; 1993.
22. Jones JR, Gentleman E, Polak J. Bioactive glass scaffolds for bone regeneration. Elements. 2007;3(6):393-9.
23. Skelton KL, Glenn JV, Clarke SA, Georgiou G, Valappil SP, Knowles C, et al. Effect of ternary phosphate-based glass compositions on osteoblast and osteoblast-like proliferation, differentiation and death in vitro. Acta Biomaterialia. [Article]. 2007;3(4):563-72.
24. Pitt CG, Gratzl MM, Kimmel GL, Surles J, Schindler A. Aliphatic Polyesters .2. The Degradation of Poly(Dl-Lactide), Poly(Epsilon-Caprolactone), and Their Copolymers Invivo. Biomaterials. 1981;2(4):215-20.
25. Kohn IEaJ. Physico-mechanical properties of degradable polyesters used in medical applications: a comparative study. Biomaterials. 1990;12:292-303.
26. P. Christel FC, J.L. Leray, C. Morin and M. Vert. Biodegradable composites for internal fixation In: G.D. Winter DFG, H. Plenk, editor. Biomaterilas. New York: Wiley and Sons; 1980. p. 271-80.
27. Baldwin DF, Shimbo M, Suh NP. The Role of Gas Dissolution and Induced Crystallization during Microcellular Polymer Processing - a Study of Poly(Ethylene-Terephthalate) and Carbon-Dioxide Systems. J Eng Mater-T Asme. 1995;117(1):62-74.
28. Abou Neel EA, Mizoguchi T, Ito M, Bitar M, Salih V, Knowles JC. In vitro bioactivity and gene expression by cells cultured on titanium dioxide doped phosphate-based glasses. Biomaterials. 2007;28(19):2967-77.
29. Abou Neel EA, Knowles JC. Physical and biocompatibility studies of novel titanium dioxide doped phosphate-based glasses for bone tissue engineering applications. J Mater Sci-Mater M. 2008;19(1):377-86.
30. Baron R. In Primer on the Metabolic Bone Diseases and Disorders of Mineral Metabolism. In: Favus MJ, editor. Washington DC: American Society for Bone and Mineral research; 2003. p. 1-9.
31. Sommerfeldt DW, Rubin CT. Biology of bone and how it orchestrates the form and function of the skeleton. Eur Spine J. 2001;10:S86-S95.
32. P. WOZNIAK AH. bone regeneration and repair using tissue engineering. In: A.R. Boccaccini JEG, editor. Tissue engineering using ceramics and polymers. Cambridge: Woudhead publishing; 2007.
33. Barthelat F. Biomimetics for next generation materials. Philos T Roy Soc A. [Article]. 2007;365(1861):2907-19.
34. Beniash E. Biominerals-hierarchical nanocomposites: the example of bone. Wiley Interdisciplinary Reviews: Nanomedicine and Nanobiotechnology. 2011;3(1):47-69.

35. Currey J. The Structure of Bone Tissue. Bones: Structure and Mechanics. Princeton: Princeton University Press; 2002.
36. Weiner S, Wagner HD. The material bone: Structure mechanical function relations. Annu Rev Mater Sci. [Review]. 1998;28:271-98.
37. Weiner S, Traub W, Wagner HD. Lamellar bone: Structure-function relations. J Struct Biol. [Article]. 1999;126(3):241-55.
38. Spense A. Basic Medical Anatomy: Benjamin/Cummings; 1990.
39. Olszta MJ, Cheng XG, Jee SS, Kumar R, Kim YY, Kaufman MJ, et al. Bone structure and formation: A new perspective. Mat Sci Eng R. 2007;58(3-5):77-116.
40. Shea JE, Miller SC. Skeletal function and structure: Implications for tissue-targeted therapeutics. Adv Drug Deliver Rev. 2005;57(7):945-57.
41. Mondrinos MJ, Dembzynski R, Lu L, Byrapogu VKC, Wootton DM, Lelkes PI, et al. Porogen-based solid freeform fabrication of polycaprolactone-calcium phosphate scaffolds for tissue engineering. Biomaterials. 2006;27(25):4399-408.
42. Teo JCM, Si-Hoe KM, Keh JEL, Teoh SH. Correlation of cancellous bone microarchitectural parameters from microCT to CT number and bone mechanical properties. Mat Sci Eng C-Bio S. 2007;27(2):333-9.
43. Zhu WB, Mow VC, Koob TJ, Eyre DR. Viscoelastic Shear Properties of Articular-Cartilage and the Effects of Glycosidase Treatments. J Orthopaed Res. 1993;11(6):771-81.
44. Keaveny TM, Morgan EF, Niebur GL, Yeh OC. Biomechanics of trabecular bone. Annu Rev Biomed Eng. 2001;3:307-33.
45. Goldstein SA, Wilson DL, Sonstegard DA, Matthews LS. The Mechanical-Properties of Human Tibial Trabecular Bone as a Function of Metaphyseal Location. J Biomech. 1983;16(12):965-9.
46. Brown TD, Ferguson AB. Mechanical Property Distributions in the Cancellous Bone of the Human Proximal Femur. Acta Orthop Scand. 1980;51(3):429-37.
47. McCalden RW, McGeough JA, CourtBrown CM. Age-related changes in the compressive strength of cancellous bone - The relative importance of changes in density and trabecular architecture. J Bone Joint Surg Am. 1997;79A(3):421-7.
48. Mosekilde L, Mosekilde L, Danielsen CC. Biomechanical Competence of Vertebral Trabecular Bone in Relation to Ash Density and Age in Normal Individuals. Bone. 1987;8(2):79-85.
49. Morgan EF, Keaveny TM. Dependence of yield strain of human trabecular bone on anatomic site. J Biomech. 2001;34(5):569-77.
50. Keller TS, Mao Z, Spengler DM. Young Modulus, Bending Strength, and Tissue Physical-Properties of Human Compact-Bone. J Orthopaed Res. 1990;8(4):592-603.
51. Hutmacher DW, Schantz JT, Lam CXF, Tan KC, Lim TC. State of the art and future directions of scaffold-based bone engineering from a biomaterials perspective. J Tissue Eng Regen M. 2007;1(4):245-60.
52. National Osteoporosis Foundation. Clinician's Guide to Prevention and Treatment of Osteoporosis. [cited 2011 January 13]; Available from: http://www.nof.org/professionals/clinical-guidelines.
53. Bone Health and Osteoporosis: A Report of the Surgeon General. Washington, DC2004.

54. MJ Yaszemski JO, L Lu, BL Currier. Bone Engineering. 1st ed. Toronto: Em squared; 1994.
55. Salgado AJ, Coutinho OP, Reis RL. Bone tissue engineering: state of the art and future trends. Macromol Biosci. 2004;4(8):743-65.
56. Spitzer RS, Perka C, Lindenhayn K, Zippel H. Matrix engineering for osteogenic differentiation of rabbit periosteal cells using alpha-tricalcium phosphate particles in a three-dimensional fibrin culture. Journal of biomedical materials research. 2002;59(4):690-6.
57. Simon CG, Khatri CA, Wight SA, Wang FW. Preliminary report on the biocompatibility of a moldable, resorbable, composite bone graft consisting of calcium phosphate cement and poly(lactide-co-glycolide) microspheres. J Orthopaed Res. 2002;20(3):473-82.
58. Rose FRAJ, Oreffo ROC. Bone tissue engineering: Hope vs hype. Biochem Bioph Res Co. 2002;292(1):1-7.
59. Petite H, Viateau V, Bensaid W, Meunier A, de Pollak C, Bourguignon M, et al. Tissue-engineered bone regeneration. Nat Biotechnol. 2000;18(9):959-63.
60. Williams D. Bone Engineering. 1st ed. Toronto: Em squared; 1999.
61. Li ST. Biologic biomaterials: tissue-derived biomaterials (collagen). In: Park JB, Bronzino JD, editors. Biomaterials: Principles and Applications. New York: CRC Press; 2002. p. 118-42.
62. DoH. Science. 2000;289:1498-500.
63. Heath CA. Cells for tissue engineering. Trends Biotechnol. 2000;18(1):17-9.
64. Stock UA, Vacanti JP. Tissue engineering: current state and prospects. Annu Rev Med. 2001;52:443-51.
65. Griffith LG, Naughton G. Tissue engineering - Current challenges and expanding opportunities. Science. 2002;295(5557):1009-14.
66. Serpooshan V. Control of dense collagen gel scaffolds for tissue engineering through measuremnet and modelling of hydraulic permeability. Montreal: McGill; 2010.
67. George JHS. Engineering of Fibrous Scaffolds for use in Regenerative Medicine. London: Imperial College London; 2009.
68. Hutmacher DW. Scaffolds in tissue engineering bone and cartilage. Biomaterials. 2000;21(24):2529-43.
69. Vats A, Tolley NS, Polak JM, Gough JE. Scaffolds and biomaterials for tissue engineering: a review of clinical applications. Clin Otolaryngol. 2003;28(3):165-72.
70. Jarcho M. Calcium-Phosphate Ceramics as Hard Tissue Prosthetics. Clin Orthop Relat R. 1981(157):259-78.
71. J Huang SB. Ceramic biomaterials. In: AR Boccaccini JG, editor. Tissue engineering using ceramics and polymers. Cambridge: Woodhead publishing; 2007.
72. Saravanapavan P, Jones JR, Pryce RS, Hench LL. Bioactivity of gel-glass powders in the CaO-SiO2 system: A comparison with ternary (CaO-P2O5-SiO2) and quaternary glasses (SiO2-CaO-P2O5-Na2O). J Biomed Mater Res A. 2003;66A(1):110-9.
73. Gough JE, Notingher I, Hench LL. Osteoblast attachment and mineralized nodule formation on rough and smooth 45S5 bioactive glass monoliths. J Biomed Mater Res A. 2004;68A(4):640-50.

74. Gough JE, Jones JR, Hench LL. Nodule formation and mineralisation of human primary osteoblasts cultured on a porous bioactive glass scaffold. Biomaterials. 2004;25(11):2039-46.
75. Day RM, Boccaccini AR. Effect of particulate bioactive glasses on human macrophages and monocytes in vitro. J Biomed Mater Res A. 2005;73A(1):73-9.
76. Hench LL WJ. Biological applications of bioactive glasses. Life Chemistry Reports 1996;13:187.
77. Delahaye F, Montagne L, Palavit G, Touray JC, Baillif P. Acid dissolution of sodium-calcium metaphosphate glasses. J Non-Cryst Solids. 1998;242(1):25-32.
78. Kokubo T, Kim HM, Kawashita M. Novel bioactive materials with different mechanical properties. Biomaterials. 2003;24(13):2161-75.
79. Hench LL. Bioceramics. J Am Ceram Soc. [Review]. 1998;81(7):1705-28.
80. Sepulveda P, Jones JR, Hench LL. Characterization of melt-derived 45S5 and sol-gel-derived 58S bioactive glasses. Journal of biomedical materials research. 2001;58(6):734-40.
81. Varanasi VG, Saiz E, Loomer PM, Ancheta B, Uritani N, Ho SP, et al. Enhanced osteocalcin expression by osteoblast-like cells (MC3T3-E1) exposed to bioactive coating glass (SiO(2)-CaO-P(2)O(5)-MgO-K(2)O-Na(2)O system) ions. Acta Biomaterialia. 2009;5(9):3536-47.
82. Lao J, Nedelec JM, Jallot E. New strontium-based bioactive glasses: physicochemical reactivity and delivering capability of biologically active dissolution products. J Mater Chem. 2009;19(19):2940-9.
83. Liu X, Huang WH, Fu HL, Yao AH, Wang DP, Pan HB, et al. Bioactive borosilicate glass scaffolds: in vitro degradation and bioactivity behaviors. J Mater Sci-Mater M. 2009;20(6):1237-43.
84. Oki A, Parveen B, Hossain S, Adeniji S, Donahue H. Preparation and in vitro bioactivity of zinc containing sol-gel-derived bioglass materials. J Biomed Mater Res A. 2004;69A(2):216-21.
85. Zehnder M, Soderling E, Salonen J, Waltimo T. Preliminary evaluation of bioactive glass S53P4 as an endodontic medication in vitro. J Endodont. 2004;30(4):220-4.
86. Zamet JS, Darbar UR, Griffiths GS, Burgin W, Newman HN. Particulate bioglass (Perioglas(R)) in the treatment of periodontal intrabony defects. J Dent Res. 1997;76:2219-.
87. Gomez-Vega JM, Saiz E, Tomsia AP, Marshall GW, Marshall SJ. Bioactive glass coatings with hydroxyapatite and Bioglass (R) particles on Ti-based implants. 1. Processing. Biomaterials. 2000;21(2):105-11.
88. Rezwan K, Chen QZ, Blaker JJ, Boccaccini AR. Biodegradable and bioactive porous polymer/inorganic composite scaffolds for bone tissue engineering. Biomaterials. 2006;27(18):3413-31.
89. Xynos ID, Hukkanen MVJ, Batten JJ, Buttery LD, Hench LL, Polak JM. Bioglass (R) 45S5 stimulates osteoblast turnover and enhances bone formation in vitro: Implications and applications for bone tissue engineering. Calcified Tissue Int. 2000;67(4):321-9.
90. Chen QZZ, Thompson ID, Boccaccini AR. 45S5 Bioglass (R)-derived glass-ceramic scaffolds for bone tissue engineering. Biomaterials. 2006;27(11):2414-25.

91. Stoor P, Soderling E, Salonen JI. Antibacterial effects of a bioactive glass paste on oral microorganisms. Acta Odontol Scand. 1998;56(3):161-5.
92. Day RM. Bioactive glass stimulates the secretion of angiogenic growth factors and angiogenesis in vitro. Tissue Eng. 2005;11(5-6):768-77.
93. M. Shah Mohammadi CS, S. N. Nazhat. Bioactive glasses for wound healing. In: Ylanen HO, editor. Bioactive glasses: Materials, properties and applications. Cambridge: Woudhead Publishing; 2011. p. 246-66.
94. Mohammadi MS, Ahmed I, Marelli B, Rudd C, Bureau MN, Nazhat SN. Modulation of polycaprolactone composite properties through incorporation of mixed phosphate glass formulations. Acta Biomaterialia. 2010;6(8):3157-68.
95. Kaneko Y, Thoendel M, Olakanmi O, Britigan BE, Singh PK. The transition metal gallium disrupts Pseudomonas aeruginosa iron metabolism and has antimicrobial and antibiofilm activity. J Clin Invest. 2007;117(4):877-88.
96. Lansdown ABG. Silver. I: Its antibacterial properties and mechanism of action. Journal of wound care. [Historical Article; ; Research Support, Non-U.S. Gov't; Review]. 2002;11(4):125-30.
97. Mcauslan BR, Reilly W. Endothelial-Cell Phagokinesis in Response to Specific Metal-Ions. Experimental Cell Research. 1980;130(1):147-57.
98. Franks K, Abrahams I, Knowles JC. Development of soluble glasses for biomedical use Part I: In vitro solubility measurement. J Mater Sci-Mater M. 2000;11(10):609-14.
99. Ahmed I, Parsons AJ, Rudd CD, Nazhat SN, Knowles JC, Guerry P, et al. Comparison of phosphate-based glasses in the range 50P(2)O(5)-(50-x)CaO-xNa(2)O prepared using different precursors. Glass Technol-Part A. 2008;49(2):63-72.
100. Ahmed I, Lewis M, Olsen I, Knowles JC. Phosphate glasses for tissue engineering: Part 1. Processing and characterisation of a ternary-based P2O5-CaO-Na2O glass system. Biomaterials. 2004;25(3):491-9.
101. Gough JE, Christian P, Scotchford CA, Jones IA. Long-term craniofacial osteoblast culture on a sodium phosphate and a calcium/sodium phosphate glass. J Biomed Mater Res A. 2003;66A(2):233-40.
102. Hoppe U. A structural model for phosphate glasses. J Non-Cryst Solids. 1996;195(1-2):138-47.
103. Walter G, Hoppe U, Baade T, Kranold R, Stachel D. Intermediate range order in MeO-P2O5 glasses. J Non-Cryst Solids. 1997;217(2-3):299-307.
104. Hoppe U, Walter G, Kranold R, Stachel D. Structural specifics of phosphate glasses probed by diffraction methods: a review. J Non-Cryst Solids. 2000;263(1-4):29-47.
105. Brow RK. Review: the structure of simple phosphate glasses. J Non-Cryst Solids. 2000;263(1-4):1-28.
106. Kirkpatrik RJ BR. Nuclear magnetic resonance investigation of the structures of phosphate and phosphate-containing glasses: a review. Solid State Nuclear Magnetic Resonance 1995;5:9-21.
107. Walter G, Hoppe U, Barz A, Kranold R, Stachel D. Intermediate range structure of mixed phosphate glasses by X-ray diffraction. J Non-Cryst Solids. 2000;263(1-4):48-60.

108. Schneider J, Oliveira SL, Nunes LAO, Bonk F, Panepucci H. Short-range structure and cation bonding in calcium-aluminum metaphosphate glasses. Inorg Chem. 2005;44(2):423-30.
109. Gough JE, Christian P, Scotchford CA, Rudd CD, Jones IA. Synthesis, degradation, and in vitro cell responses of sodium phosphate glasses for craniofacial bone repair. Journal of biomedical materials research. 2002;59(3):481-9.
110. Salih V, Franks K, James M, Hastings GW, Knowles JC, Olsen I. Development of soluble glasses for biomedical use Part II: The biological response of human osteoblast cell lines to phosphate-based soluble glasses. J Mater Sci-Mater M. 2000;11(10):615-20.
111. Ahmed I, Parsons AJ, Palmer G, Knowles JC, Walkers GS, Rudd CD. Weight loss, ion release and initial mechanical properties of a binary calcium phosphate glass fibre/PCL composite. Acta Biomaterialia. 2008;4(5):1307-14.
112. Ahmed I, Lewis MP, Nazhat SN, Knowles JC. Quantification of anion and cation release from a range of ternary phosphate-based glasses with fixed 45 mol% P(2)O(5). Journal of Biomaterials Applications. 2005;20(1):65-80.
113. Bitar M, Salih V, Mudera V, Knowles JC, Lewis MP. Soluble phosphate glasses: in vitro studies using human cells of hard and soft tissue origin. Biomaterials. 2004;25(12):2283-92.
114. Knowles JC, Franks K, Abrahams I. Investigation of the solubility and ion release in the glass system K2O-Na2O-CaO-P2O5. Biomaterials. 2001;22(23):3091-6.
115. Franks K, Salih V, Knowles JC, Olsen I. The effect of MgO on the solubility behavior and cell proliferation in a quaternary soluble phosphate based glass system. J Mater Sci-Mater M. 2002;13(6):549-56.
116. Salih V, Patel A, Knowles JC. Zinc-containing phosphate-based glasses for tissue engineering. Biomed Mater. 2007;2(1):11-20.
117. Abou Neel EA, O'Dell LA, Smith ME, Knowles JC. Processing, characterisation, and biocompatibility of zinc modified metaphosphate based glasses for biomedical applications. J Mater Sci-Mater M. 2008;19(4):1669-79.
118. Abou Neel EA, Ahmed I, Blaker JJ, Bismarck A, Boccaccini AR, Lewis MP, et al. Effect of iron on the surface, degradation and ion release properties of phosphate-based glass fibres. Acta Biomaterialia. 2005;1(5):553-63.
119. Ahmed I, Collins CA, Lewis MP, Olsen I, Knowles JC. Processing, characterisation and biocompatibility of iron-phosphate glass fibres for tissue engineering. Biomaterials. 2004;25(16):3223-32.
120. Abou Neel EA, Chrzanowski W, Knowles JC. Effect of increasing titanium dioxide content on bulk and surface properties of phosphate-based glasses. Acta Biomaterialia. 2008;4(3):523-34.
121. Abou Neel EA, Chrzanowski W, Valappil SP, O'Dell LA, Pickup DM, Smith ME, et al. Doping of a high calcium oxide metaphosphate glass with titanium dioxide. J Non-Cryst Solids. 2009;355(16-17):991-1000.
122. Abou Neel EA, Chrzanowski W, Pickup DM, O'Dell LA, Mordan NJ, Newport RJ, et al. Structure and properties of strontium-doped phosphate-based glasses. J Roy Soc Interface. 2009;6(34):435-46.
123. Lakhkar N, Abou Neel EA, Salih V, Knowles JC. Titanium and Strontium-doped Phosphate Glasses as Vehicles for Strontium Ion Delivery to Cells. Journal of Biomaterials Applications. 2011;25(8):877-93.

124. Valappil SP, Ready D, Abou Neel EA, Pickup DM, Chrzanowski W, O'Dell LA, et al. Antimicrobial gallium-doped phosphate-based glasses. Adv Funct Mater. 2008;18(5):732-41.
125. Valappil SP, Ready D, Abou Neel EA, Pickup DM, O'Dell LA, Chrzanowski W, et al. Controlled delivery of antimicrobial gallium ions from phosphate-based glasses. Acta Biomaterialia. 2009;5(4):1198-210.
126. Ahmed I, Ready D, Wilson M, Knowles JC. Antimicrobial effect of silver-doped phosphate-based glasses. J Biomed Mater Res A. 2006;79A(3):618-26.
127. Ahmed I, Abou Neel EA, Valappil SP, Nazhat SN, Pickup DM, Carta D, et al. The structure and properties of silver-doped phosphate-based glasses. J Mater Sci. 2007;42(23):9827-35.
128. Valappil SP, Pickup DM, Carroll DL, Hope CK, Pratten J, Newport RJ, et al. Effect of silver content on the structure and antibacterial activity of silver-doped phosphate-based glasses. Antimicrob Agents Ch. 2007;51(12):4453-61.
129. Mulligan AM, Wilson M, Knowles JC. The effect of increasing copper content in phosphate-based glasses on biofilms of Streptococcus sanguis. Biomaterials. 2003;24(10):1797-807.
130. Abou Neel EA, Ahmed I, Pratten J, Nazhat SN, Knowles JC. Characterisation of antibacterial copper releasing degradable phosphate glass fibres. Biomaterials. 2005;26(15):2247-54.
131. Zhang Y, Santos JD. Crystallization and microstructure analysis of calcium phosphate-based glass ceramics for biomedical applications. J Non-Cryst Solids. 2000;272(1):14-21.
132. Vitale-Brovarone C, Novajra G, Milanese D, Lousteau J, Knowles JC. Novel phosphate glasses with different amounts of TiO(2) for biomedical applications Dissolution tests and proof of concept of fibre drawing. Mat Sci Eng C-Mater. 2011;31(2):434-42.
133. G. Novajra CV-B, JC. Knowles, G. Maina, V. Aina, D. Ghigo, L. Bergandi. Effects of TO2-containing phosphate glasses on solubility and in vitro biocompatibility. J Biomed Mater Res Part A. 2011;99A:295-306.
134. Rajendran V, Devi AVG, Azooz M, El-Batal FH. Physicochemical studies of phosphate based P2O5-Na2O-CaO-TiO2 glasses for biomedical applications. J Non-Cryst Solids. 2007;353(1):77-84.
135. Navarro M, Ginebra MP, Clement J, Martinez S, Avila G, Planell JA. Physicochemical degradation of titania-stabilized soluble phosphate glasses for medical applications. J Am Ceram Soc. 2003;86(8):1345-52.
136. EA. Abou neel WC, G. Georgiou, MJ Dalby, JC. Knowles. In vitro biocompatibility and mechanical performance of titanium doped high calcium oxide metaphosphate-based glasses. Journal of Tissue Engineering. 2010.
137. Sales BC, Boatner LA, Ramey JO. Chromatographic studies of the structures of amorphous phosphates: a review. J Non-Cryst Solids. 2000;263(1-4):155-66.
138. Bunker BC, Arnold GW, Wilder JA. Phosphate-Glass Dissolution in Aqueous-Solutions. J Non-Cryst Solids. 1984;64(3):291-316.
139. Bae BS, Weinberg MC. Oxidation-Reduction Equilibrium in Copper Phosphate-Glass Melted in Air. J Am Ceram Soc. 1991;74(12):3039-45.

140. Blaker JJ, Maquet V, Boccaccini AR, Jerome R, Bismarck A. Wetting of bioactive glass surfaces by poly(alpha-hydroxyacid) melts: interaction between Bioglass (R) and biodegradable polymers. E-Polymers. 2005:-.
141. Wu S. Polymer interface and adhesion. New York: Marcel Dekker; 1982.
142. RJ Good CVO. The modern theory of contact angles and the hydrogen bond components of surface energies. In: ME Schrader GL, editor. Modern approaches to wettability. New York: Plenum1992.
143. Fowkes FM. Determination of Interfacial Tensions, Contact Angles, and Dispersion Forces in Surfaces by Assuming Additivity of Intermolecular Interactions in Surfaces. J Phys Chem-Us. 1962;66(2):382-&.
144. Fowkes FM. Attractive Forces at Interfaces. Ind Eng Chem. 1964;56(12):40-&.
145. Owens DK, Wendt RC. Estimation of Surface Free Energy of Polymers. Journal of Applied Polymer Science. 1969;13(8):1741-&.
146. Bonzani IC, Adhikari R, Houshyar S, Mayadunne R, Gunatillake P, Stevens MM. Synthesis of two-component injectable polyurethanes for bone tissue engineering. Biomaterials. 2007;28(3):423-33.
147. Park J-M, Kim D-S, Kim S-R. Interfacial properties and microfailure degradation mechanisms of bioabsorbable fibers/poly-l-lactide composites using micromechanical test and nondestructive acoustic emission. Compos Sci Technol. 2003;63(3-4):403-19.
148. Webster TJ, Ergun C, Doremus RH, Siegel RW, Bizios R. Specific proteins mediate enhanced osteoblast adhesion on nanophase ceramics. Journal of biomedical materials research. 2000;51(3):475-83.
149. Abou Neel EA. Collagen-Phosphate Glass Fibres for Biomedical and Tissue Engineering Applications. London: University College London; 2006.
150. De Diego MA, Coleman NJ, Hench LL. Tensile properties of bioactive fibers for tissue engineering applications. Journal of biomedical materials research. 2000;53(3):199-203.
151. Choueka A, Charvet JL, Alexander H, Oh YH, Joseph G, Blumenthal NC, et al. Effect of Annealing Temperature on the Degradation of Reinforcing Fibers or Absorbable Implants. Journal of biomedical materials research. 1995;29(11):1309-15.
152. Clupper DC, Gough JE, Hall MM, Clare AG, LaCourse WC, Hench LL. In vitro bioactivity of S520 glass fibers and initial assessment of osteoblast attachment. J Biomed Mater Res A. 2003;67A(1):285-94.
153. Orefice RL, Hench LL, Clark AE, Brennan AB. Novel sol-gel bioactive fibers. Journal of biomedical materials research. 2001;55(4):460-7.
154. SJ Lee JL, HB Lee. Korea Polym J. 1999;7(2):102.
155. Abou Neel EA, Young AM, Nazhat SN, Knowles JC. A facile synthesis route to prepare microtubes from phosphate glass fibres. Adv Mater. 2007;19(19):2856-62.
156. Chen GP, Ushida T, Tateishi T. Scaffold design for tissue engineering. Macromol Biosci. 2002;2(2):67-77.
157. Hutmacher DW. Scaffold design and fabrication technologies for engineering tissues - state of the art and future perspectives. J Biomat Sci-Polym E. 2001;12(1):107-24.
158. Griffith LG. Polymeric biomaterials. Acta Mater. 2000;48(1):263-77.
159. Shoichet MS. Polymer Scaffolds for Biomaterials Applications. Macromolecules. 2010;43(2):581-91.

160. Sokolsky-Papkov M, Agashi K, Olaye A, Shakesheff K, Domb AJ. Polymer carriers for drug delivery in tissue engineering. Adv Drug Deliv Rev. 2007;59(4-5):187-206.
161. Dang JM, Leong KW. Natural polymers for gene delivery and tissue engineering. Adv Drug Deliver Rev. 2006;58(4):487-99.
162. Ko HF, Sfeir C, Kumta PN. Novel synthesis strategies for natural polymer and composite biomaterials as potential scaffolds for tissue engineering. Philos Transact A Math Phys Eng Sci. 2010;368(1917):1981-97.
163. Tibbitt MW, Anseth KS. Hydrogels as Extracellular Matrix Mimics for 3D Cell Culture. Biotechnol Bioeng. 2009;103(4):655-63.
164. Lavik E, Langer R. Tissue engineering: current state and perspectives. Appl Microbiol Biot. 2004;65(1):1-8.
165. Lee CH, Singla A, Lee Y. Biomedical applications of collagen. International journal of pharmaceutics. 2001;221(1):1.
166. Schmidt CE, Baier JM. Acellular vascular tissues: natural biomaterials for tissue repair and tissue engineering. Biomaterials. 2000;21(22):2215-31.
167. SilVIO LD. Bone tissue engineering and biomineralization. In: Gough ABaJ, editor. Tissue engineering using ceramics and polymers. Cambridge: Woodhead publishing Ltd; 2007.
168. Holy CE, Fialkov JA, Davies JE, Shoichet MS. Use of a biomimetic strategy to engineer bone. J Biomed Mater Res A. 2003;65A(4):447-53.
169. P.A. Gunatillake RA. Biodegradable synthetic polymers for tissue engineering. Eur Cells Mater. 2003;5:1-16.
170. Pitt CG. Poly-ε-caprolactone and its copolymers. In: Chasin RLaM, editor. Biodegradable Polymers as Drug Delivery Systems. New York: Marcel Dekker; 1990. p. 71-120.
171. C.G. Pitt ALA, Y.T. Bao, and N.K.P. Samuel. Estimation of rate of drug diffusion in polymers. In: Good PILaWR, editor. Controlled-Release Technology, Pharmaceutical Applications, ACS Symposium Series; Washington DC, USA: American Chemical Society
1987. p. 49-70.
172. J.E. Potts RACaSC. Biodegradable plastic containers for seeding transplants. Soc Plast Eng Tech Pap. 1975;21:567-9.
173. Pitt CG, Chasalow FI, Hibionada YM, Klimas DM, Schindler A. Aliphatic Polyesters .1. The Degradation of Poly(Epsilon-Caprolactone) Invivo. Journal of Applied Polymer Science. 1981;26(11):3779-87.
174. Woodward SC, Brewer PS, Moatamed F, Schindler A, Pitt CG. The Intracellular Degradation of Poly(Epsilon-Caprolactone). Journal of biomedical materials research. 1985;19(4):437-44.
175. J.V. Koleske. Blends containing poly(ε-caprolactone) and related polymers In: Newman DRPaS, editor. Polymer Blends; New York, NY, USA: Academic Press; 1978. p. 369-89.
176. Hartmann MH. Biopolymers from Renewable Resources. Berlin: Springer-Verlag; 1998. p. 367-411.
177. Garlotta D. A literature review of poly(lactic acid). J Polym Environ. 2001;9(2):63-84.

178. Spinu M, Jackson C, Keating MY, Gardner KH. Material design in poly(lactic acid) systems: Block copolymers, star homo- and copolymers, and stereocomplexes. J Macromol Sci Pure. 1996;A33(10):1497-530.
179. Hyon SH, Jamshidi K, Ikada Y. Effects of residual monomer on the degradation of DL-lactide polymer. Polym Int. 1998;46(3):196-202.
180. SK Misra AB. Biodegradable and bioactive polymer/ceramic composite scaffolds. In: AR Boccaccini JG, editor. Tissue engineering using ceramics and polymers. Cambridge: Woodhead publishing; 2007.
181. Maquet V, Boccaccini AR, Pravata L, Notingher I, Jerome R. Preparation, characterization, and in vitro degradation of bioresorbable and bioactive composites based on Bioglass (R)-filled polylactide foams. J Biomed Mater Res A. 2003;66A(2):335-46.
182. Lu HH, El-Amin SF, Scott KD, Laurencin CT. Three-dimensional, bioactive, biodegradable, polymer-bioactive glass composite scaffolds with improved mechanical properties support collagen synthesis and mineralization of human osteoblast-like cells in vitro. J Biomed Mater Res A. 2003;64A(3):465-74.
183. Blaker JJ, Maquet V, Jerome R, Boccaccini AR, Nazhat SN. Mechanical properties of highly porous PDLLA/Bioglass (R) composite foams as scaffolds for bone tissue engineering. Acta Biomaterialia. 2005;1(6):643-52.
184. Kim HW, Lee EJ, Jun IK, Kim HE, Knowles JC. Degradation and drug release of phosphate glass/polycaprolactone biological composites for hard-tissue regeneration. J Biomed Mater Res B. 2005;75B(1):34-41.
185. Blaker JJ, Gough JE, Maquet V, Notingher I, Boccaccini AR. In vitro evaluation of novel bioactive composites based on Bioglass (R)-filled polylactide foams for bone tissue engineering scaffolds. J Biomed Mater Res A. 2003;67A(4):1401-11.
186. Jiang G, Evans ME, Jones IA, Rudd CD, Scotchford CA, Walker GS. Preparation of poly(epsilon-caprolactone)/continuous bioglass fibre composite using monomer transfer moulding for bone implant. Biomaterials. 2005;26(15):2281-8.
187. Thomson RC, Yaszemski MJ, Powers JM, Mikos AG. Hydroxyapatite fiber reinforced poly(alpha-hydroxy ester) foams for bone regeneration. Biomaterials. 1998;19(21):1935-43.
188. Blaker JJ, Bismarck A, Boccaccini AR, Young AM, Nazhat SN. Premature degradation of poly(alpha-hydroxyesters) during thermal processing of Bioglass (R)-containing composites. Acta Biomaterialia. 2010;6(3):756-62.
189. Navarro M, Ginebra MP, Planell JA, Zeppetelli S, Ambrosio L. Development and cell response of a new biodegradable composite scaffold for guided bone regeneration. J Mater Sci-Mater M. 2004;15(4):419-22.
190. Georgiou G, Mathieu L, Pioletti DP, Bourban PE, Manson JAE, Knowles JC, et al. Polylactic acid-phosphate glass composite foams as scaffolds for bone tissue engineering. J Biomed Mater Res B. 2007;80B(2):322-31.
191. Ahmed I, Cronin PS, Abou Neel EA, Parsons AJ, Knowles JC, Rudd CD. Retention of Mechanical Properties and Cytocompatibility of a Phosphate-Based Glass Fiber/Polylactic Acid Composite. J Biomed Mater Res B. 2009;89B(1):18-27.
192. Ahmed I, Jones IA, Parsons AJ, Bernard J, Farmer J, Scotchford CA, et al. Composites for bone repair: phosphate glass fibre reinforced PLA with varying fibre architecture. J Mater Sci-Mater M. 2011;22(8):1825-34.

193. Khan RA, Parsons AJ, Jones IA, Walker GS, Rudd CD. Preparation and Characterization of Phosphate Glass Fibers and Fabrication of Poly(caprolactone) Matrix Resorbable Composites. J Reinf Plast Comp. 2010;29(12):1838-50.
194. Blaker JJ, Knowles JC, Day RM. Novel fabrication techniques to produce microspheres by thermally induced phase separation for tissue engineering and drug delivery. Acta Biomaterialia. 2008;4(2):264-72.
195. Lin ST, Krebs SL, Kadiyala S, Leong KW, Lacourse WC, Kumar B. Development of Bioabsorbable Glass-Fibers. Biomaterials. 1994;15(13):1057-61.
196. Andriano KP DA, Smutz WP, Wyatt WB. Preliminary biocompatibility screening of several biodegradable phosphate fibre reinforced polymers. J Appl Biomater 1993;4:1-12.
197. Lowry KJ, Hamson KR, Bear L, Peng YB, Calaluce R, Evans ML, et al. Polycaprolactone/glass bioabsorbable implant in a rabbit humerus fracture model. Journal of biomedical materials research. 1997;36(4):536-41.
198. Nazhat SN, Abou Neel EA, Kidane A, Ahmed I, Hope C, Kershaw M, et al. Controlled microchannelling in dense collagen scaffolds by soluble phosphate glass fibers. Biomacromolecules. 2007;8(2):543-51.
199. Ikada Y. Tissue engineering: fundamentals and applications. Oxford: Elsevier; 2006.
200. Ma PX. Scaffolds for tissue fabrication. Materials Today. 2004;7(5):30-40.
201. Reynaud B, Quinn TM. Anisotropic hydraulic permeability in compressed articular cartilage. J Biomech. 2006;39(1):131-7.
202. Ramanujan S, Pluen A, McKee TD, Brown EB, Boucher Y, Jain RK. Diffusion and convection in collagen gels: Implications for transport in the tumor interstitium. Biophys J. 2002;83(3):1650-60.
203. Tabata Y. Tissue regeneration based on tissue engineering technology. Congenit Anom (Kyoto). 2004;44(3):111-24.
204. Chung HJ, Park TG. Surface engineered and drug releasing pre-fabricated scaffolds for tissue engineering. Adv Drug Deliver Rev. 2007;59(4-5):249-62.
205. Park JB, Lakes RS. Biomaterials: An Introduction. New York, N.Y: Springer; 2007.
206. Hollister SJ. Porous scaffold design for tissue engineering. Nat Mater. 2005;4(7):518-24.
207. Liu C, Xia Z, Czernuszka JT. Design and development of three-dimensional scaffolds for tissue engineering. Chem Eng Res Des. 2007;85(A7):1051-64.
208. Howard D, Buttery LD, Shakesheff KM, Roberts SJ. Tissue engineering: strategies, stem cells and scaffolds. J Anat. 2008;213(1):66-72.
209. Eisenbarth E. Biomaterials for tissue engineering. Adv Eng Mater. 2007;9(12):1051-60.
210. Mikos AG, Thorsen AJ, Czerwonka LA, Bao Y, Langer R, Winslow DN, et al. Preparation and Characterization of Poly(L-Lactic Acid) Foams. Polymer. 1994;35(5):1068-77.
211. Yang SF, Leong KF, Du ZH, Chua CK. The design of scaffolds for use in tissue engineering. Part 1. Traditional factors. Tissue Eng. 2001;7(6):679-89.
212. ME Gomes AS. Polymer Based Systems on Tissue Engineering, Replacement and Regeneration. 1st ed. The Netherlands: Kluwer, Dordrecht; 2002.

213. Q Chen JR, AR Boccaccini. Tissue engineering scaffolds from bioactive glass and composite materials. In: N Ashammakhi RR, F Chiellini, editor. Topics in Tissue Engineering2008.
214. Boccaccini AR, Blaker JJ. Bioactive composite materials for tissue engineering scaffolds. Expert Rev Med Devic. 2005;2(3):303-17.
215. Keshaw H, Georgiou G, Blaker JJ, Forbes A, Knowles JC, Day RM. Assessment of Polymer/Bioactive Glass-Composite Microporous Spheres for Tissue Regeneration Applications. Tissue Eng Pt A. 2009;15(7):1451-61.
216. Pang L, Hu YY, Yan YN, Liu L, Xiong Z, Wei YY, et al. Surface modification of PLGA/beta-TCP scaffold for bone tissue engineering: Hybridization with collagen and apatite. Surf Coat Tech. 2007;201(24):9549-57.
217. Shor L, Guceri S, Wen XJ, Gandhi M, Sun W. Fabrication of three-dimensional polycaprolactone/hydroxyapatite tissue scaffolds and osteoblast-scaffold interactions in vitro. Biomaterials. 2007;28(35):5291-7.
218. Hutmacher DW, Cool S. Concepts of scaffold-based tissue engineering-the rationale to use solid free-form fabrication techniques. J Cell Mol Med. 2007;11(4):654-69.
219. Xiong Z YY, Wang SG, Zhang RJ. Fabrication of porous scaffolds for bone tissue engineering via low temperature deposition Sci Mater. 2002;46:771-6.
220. Leong KF, Cheah CM, Chua CK. Solid freeform fabrication of three-dimensional scaffolds for engineering replacement tissues and organs. Biomaterials. 2003;24(13):2363-78.
221. Barry JJA, Silva MMCG, Popov VK, Shakesheff KM, Howdle SM. Supercritical carbon dioxide: putting the fizz into biomaterials. Philos T Roy Soc A. 2006;364(1838):249-61.
222. Woods HM, Silva MMCG, Nouvel C, Shakesheff KM, Howdle SM. Materials processing in supercritical carbon dioxide: surfactants, polymers and biomaterials. J Mater Chem. 2004;14(11):1663-78.
223. Cooper AI. Polymer synthesis and processing using supercritical carbon dioxide. J Mater Chem. 2000;10(2):207-34.
224. Goel SK, Beckman EJ. Generation of Microcellular Polymeric Foams Using Supercritical Carbon-Dioxide .1. Effect of Pressure and Temperature on Nucleation. Polym Eng Sci. 1994;34(14):1137-47.
225. Arora KA, Lesser AJ, McCarthy TJ. Preparation and characterization of microcellular polystyrene foams processed in supercritical carbon dioxide. Macromolecules. 1998;31(14):4614-20.
226. McHugh MA KV. Supercritical fluid extraction: principles and practice. 2nd ed. Boston: Butterworth-Heinemann; 1994.
227. Quirk RA, France RM, Shakesheff KM, Howdle SM. Supercritical fluid technologies and tissue engineering scaffolds. Curr Opin Solid St M. 2004;8(3-4):313-21.
228. Alavi SH, Gogoi BK, Khan M, Bowman BJ, Rizvi SSH. Structural properties of protein-stabilized starch-based supercritical fluid extrudates. Food Res Int. 1999;32(2):107-18.
229. Goel SK, Beckman EJ. Generation of Microcellular Polymeric Foams Using Supercritical Carbon-Dioxide .2. Cell-Growth and Skin Formation. Polym Eng Sci. 1994;34(14):1148-56.

230. Park CB, Baldwin DF, Suh NP. Effect of the Pressure Drip Rate on Cell Nucleation in Continuous Processing of Microcellular Polymers. Polym Eng Sci. 1995;35(5):432-40.
231. Sheridan MH, Shea LD, Peters MC, Mooney DJ. Bioadsorbable polymer scaffolds for tissue engineering capable of sustained growth factor delivery. J Control Release. 2000;64(1-3):91-102.
232. Howdle SM, Watson MS, Whitaker MJ, Popov VK, Davies MC, Mandel FS, et al. Supercritical fluid mixing: preparation of thermally sensitive polymer composites containing bioactive materials. Chem Commun. 2001(01):109-10.
233. Kazarian SG, Vincent MF, Bright FV, Liotta CL, Eckert CA. Specific intermolecular interaction of carbon dioxide with polymers. J Am Chem Soc. 1996;118(7):1729-36.
234. Tai HY, Mather ML, Howard D, Wang WX, White LJ, Crowe JA, et al. Control of pore size and structure of tissue engineering scaffolds produced by supercritical fluid processing. Eur Cells Mater. 2007;14:64-76.
235. Mathieu LM, Montjovent MO, Bourban PE, Pioletti DP, Manson JAE. Bioresorbable composites prepared by supercritical fluid foaming. J Biomed Mater Res A. 2005;75A(1):89-97.
236. Mathieu LM, Mueller TL, Bourban PE, Pioletti DP, Muller R, Manson JAE. Architecture and properties of anisotropic polymer composite scaffolds for bone tissue engineering. Biomaterials. 2006;27(6):905-16.
237. Jacobs LJM, Kemmere MF, Keurentjes JTF. Sustainable polymer foaming using high pressure carbon dioxide: a review on fundamentals, processes and applications. Green Chem. 2008;10(7):731-8.
238. Mooney DJ, Baldwin DF, Suh NP, Vacanti LP, Langer R. Novel approach to fabricate porous sponges of poly(D,L-lactic-co-glycolic acid) without the use of organic solvents. Biomaterials. 1996;17(14):1417-22.
239. Singh L, Kumar V, Ratner BD. Generation of porous microcellular 85/15 poly ((DL)-lactide-co-glycolide) foams for biomedical applications. Biomaterials. 2004;25(13):2611-7.
240. Hu X NA, Naguib HE, Day M, Ueda K, Lia X. Ploylactic acid (PLA)-CO2 foams at sub-critical conditions. ANTEC. 2005:2670-3.
241. Pietak AM, Reid JW, Stott MJ, Sayer M. Silicon substitution in the calcium phosphate bioceramics. Biomaterials. 2007;28(28):4023-32.
242. Carlisle EM. Silicon . A Possible Factor in Bone Calcification. Science. 1970;167(3916):279-&.
243. Jugdaohsingh R, Tucker KL, Qiao N, Cupples LA, Kiel DP, Powell JJ. Dietary silicon intake is positively associated with bone mineral density in men and premenopausal women of the Framingham Offspring cohort. J Bone Miner Res. 2004;19(2):297-307.
244. Ma PX, Zhang RY, Xiao GZ, Franceschi R. Engineering new bone tissue in vitro on highly porous poly(alpha-hydroxyl acids)/hydroxyapatite composite scaffolds. Journal of biomedical materials research. 2001;54(2):284-93.
245. Navarro M, Ginebra MP, Planell JA, Barrias CC, Barbosa MA. In vitro degradation behavior of a novel bioresorbable composite material based on PLA and a soluble CaP glass. Acta Biomaterialia. 2005;1(4):411-9.

246. Charles-Harris M, del Valle S, Hentges E, Bleuet P, Lacroix D, Planell JA. Mechanical and structural characterisation of completely degradable polylactic acid/calcium phosphate glass scaffolds. Biomaterials. 2007;28(30):4429-38.
247. Nazhat SN, Kellomaki M, Tormala P, Tanner KE, Bonfield W. Dynamic mechanical characterization of biodegradable composites of hydroxyapatite and polylactides. Journal of biomedical materials research. 2001;58(4):335-43.
248. Bleach NC, Nazhat SN, Tanner KE, Kellomaki M, Tormala P. Effect of filler content on mechanical and dynamic mechanical properties of particulate biphasic calcium phosphate-polylactide composites. Biomaterials. 2002;23(7):1579-85.
249. Dupraz AMP, deWijn JR, vanderMeer SAT, deGroot K. Characterization of silane-treated hydroxyapatite powders for use as filler in biodegradable composites. Journal of biomedical materials research. 1996;30(2):231-8.
250. I. Engleberg JK. Physico-mechanical properties of degradable polymers used in medical applications: a comprehensive study. Biomaterials. 1991;12:292-304.
251. Kokubo T, Takadama H. How useful is SBF in predicting in vivo bone bioactivity? Biomaterials. 2006;27(15):2907-15.
252. V Vitins MD, J Middleton, G Limbert, I Knets. Flexural and creep properties of human jaw compact bone for FEA studies
Comput Methods Biomech Biomed Engin 2003;6(5-6):299-303
253. Niemela T, Niiranen H, Kellomaki M, Tormala P. Self-reinforced composites of bioabsorbable polymer and bioactive glass with different bloactive glass contents. Part 1: Initial mechanical properties and bioactivity. Acta Biomaterialia. 2005;1(2):235-42.
254. Niiranen H, Pyhalto T, Rokkanen O, Kellomaki M, Tormala P. In vitro and in vivo behavior of self-reinforced bioabsorbable polymer and self-reinforced bioabsorbable polymer/bioactive glass composites. J Biomed Mater Res A. 2004;69A(4):699-708.
255. RAD. Williams JE. Basic and applied dental biochemistry. Edinburgh: Churchill Livingstone; 1989.
256. Johnsson MSA, Nancollas GH. The Role of Brushite and Octacalcium Phosphate in Apatite Formation. Crit Rev Oral Biol M. 1992;3(1-2):61-82.
257. Bohner M. Silicon-substituted calcium phosphates - A critical view. Biomaterials. 2009;30(32):6403-6.
258. Boccaccini AR, Blaker JJ, Maquet V, Day RM, Jerome R. Preparation and characterisation of poly(lactide-co-glycolide) (PLGA) and PLGA/Bioglass((R)) composite tubular foam scaffolds for tissue engineering applications. Mat Sci Eng C-Bio S. 2005;25(1):23-31.
259. ASTM Standard D2584-94. Test method for ignition loss of cured reinforced resins
ASTM International.
260. Marasinghe GK, Karabulut M, Ray CS, Day DE, Shumsky MG, Yelon WB, et al. Structural features of iron phosphate glasses. J Non-Cryst Solids. 1997;222:144-52.
261. Cox HL. The Elasticity and Strength of Paper and Other Fibrous Materials. Brit J Appl Phys. 1952;3(Mar):72-9.
262. Kelly A, Tyson WR. Tensile Properties of Fibre-Reinforced Metals - Copper/Tungsten and Copper/Molybdenum. J Mech Phys Solids. 1965;13(6):329-&.
263. Blasi P, D'Souza SS, Selmin F, DeLuca PP. Plasticizing effect of water on poly(lactide-co-glycolide). J Control Release. 2005;108(1):1-9.

264. Grimau M, Laredo E, Perez MCY, Bello A. Study of dielectric relaxation modes in poly(epsilon-caprolactone): Molecular weight, water sorption, and merging effects. J Chem Phys. 2001;114(14):6417-25.
265. Sun HF, Mei L, Song CX, Cui XM, Wang PY. The in vivo degradation, absorption and excretion of PCL-based implant. Biomaterials. 2006;27(9):1735-40.
266. Onal L, Cozien-Cazuc S, Jones IA, Rudd CD. Water absorption properties of phosphate glass fiber-reinforced poly-epsilon-caprolactone composites for craniofacial bone repair. Journal of Applied Polymer Science. 2008;107(6):3750-5.
267. Verrier S, Blaker JJ, Maquet V, Hench LL, Boccaccini AR. PDLLA/Bioglass (R) composites for soft-tissue and hard-tissue engineering: an in vitro cell biology assessment. Biomaterials. 2004;25(15):3013-21.
268. Lin ASP, Barrows TH, Cartmell SH, Guldberg RE. Microarchitectural and mechanical characterization of oriented porous polymer scaffolds. Biomaterials. 2003;24(3):481-9.
269. Bitar M, Knowles JC, Lewis MP, Salih V. Soluble phosphate glass fibres for repair of bone-ligament interface. J Mater Sci-Mater M. 2005;16(12):1131-6.
270. Shah R, Sinanan ACM, Knowles JC, Hunt NP, Lewis MP. Craniofacial muscle engineering using a 3-dimensional phosphate glass fibre construct. Biomaterials. 2005;26(13):1497-505.
271. Ma S, Yang Y, Carnes DL, Kim K, Park S, Oh SH, et al. Effects of dissolved calcium and phosphorous on osteoblast responses. The Journal of oral implantology. [; Research Support, Non-U.S. Gov't; Research Support, U.S. Gov't, P.H.S.]. 2005;31(2):61-7.
272. II. Doron AL. Bone graft substitutes. Opt Tech Plas Recon Surg. 2002;9:151-60.
273. Paolinelis G, Banerjee A, Watson TF. An in vitro investigation of the effect and retention of bioactive glass air-abrasive on sound and carious dentine. Journal of Dentistry. 2008;36(3):214-8.
274. Xynos ID, Edgar AJ, Buttery LDK, Hench LL, Polak JM. Ionic products of bioactive glass dissolution increase proliferation of human osteoblasts and induce insulin-like growth factor II mRNA expression and protein synthesis. Biochem Bioph Res Co. 2000;276(2):461-5.
275. Keeting PE, Oursler MJ, Wiegand KE, Bonde SK, Spelsberg TC, Riggs BL. Zeolite-a Increases Proliferation, Differentiation, and Transforming Growth-Factor-Beta Production in Normal Adult Human Osteoblast-Like Cells-Invitro. J Bone Miner Res. 1992;7(11):1281-9.
276. Gibson IR, Best SM, Bonfield W. Chemical characterization of silicon-substituted hydroxyapatite. Journal of biomedical materials research. 1999;44(4):422-8.
277. Ruys A. Silicon-doped hydroxyapatite. J Aust Ceram Soc. 1993;29:71-80.
278. G. Gupta SK, A. El-Ghannam. Effect of exogenous phosphorous and silicon on osteoblast differentiation at the interface with bioactive ceramics. Journal of Biomedical Materials Research A. 2010;95:882-90.
279. Reffitt DM, Ogston N, Jugdaohsingh R, Cheung HFJ, Evans BAJ, Thompson RPH, et al. Orthosilicic acid stimulates collagen type 1 synthesis and osteoblastic differentiation in human osteoblast-like cells in vitro. Bone. 2003;32(2):127-35.

280. Beck GR, Moran E, Knecht N. Inorganic phosphate regulates multiple genes during osteoblast differentiation, including Nrf2. Experimental Cell Research. 2003;288(2):288-300.
281. Meleti Z, Shapiro IM, Adams CS. Inorganic phosphate induces apoptosis of osteoblast-like cells in culture. Bone. 2000;27(3):359-66.
282. Navarro M, Ginebra MP, Planell JA. Cellular response to calcium phosphate glasses with controlled solubility. J Biomed Mater Res A. 2003;67A(3):1009-15.
283. Kirkpatrick RJ, Brow RK. Nuclear-Magnetic-Resonance Investigation of the Structures of Phosphate and Phosphate-Containing Glasses - a Review. Solid State Nuclear Magnetic Resonance. 1995;5(1):9-21.
284. Brow RK, Tallant DR, Hudgens JJ, Martin SW, Irwin AD. The Short-Range Structure of Sodium Ultraphosphate Glasses. J Non-Cryst Solids. 1994;177:221-8.
285. M. Shah Mohammadi IA, N. Muja, S. Almeida, CD. Rudd, MN. Bureau, SN. Nazhat. Effect of Si and Fe doping on calcium phosphate glass fibre reinforced polycaprolactone bone analogous composites. Acta Biomaterialia. 2012:in press.
286. Brow RK, Tallant DR, Warren WL, McIntyre A, Day DE. Spectroscopic studies of the structure of titanophosphate and calcium titanophosphate glasses. Phys Chem Glasses. 1997;38(6):300-6.
287. Strauss UP, Smith EH, Wineman PL. Polyphosphates as Polyelectrolytes .1. Light Scattering and Viscosity of Sodium Polyphosphates in Electrolyte Solutions. J Am Chem Soc. 1953;75(16):3935-40.
288. Owen TA, Aronow M, Shalhoub V, Barone LM, Wilming L, Tassinari MS, et al. Progressive Development of the Rat Osteoblast Phenotype Invitro - Reciprocal Relationships in Expression of Genes Associated with Osteoblast Proliferation and Differentiation during Formation of the Bone Extracellular-Matrix. J Cell Physiol. 1990;143(3):420-30.
289. Usui Y, Uematsu T, Uchihashi T, Takahashi M, Takahashi M, Ishizuka M, et al. Inorganic Polyphosphate Induces Osteoblastic Differentiation. J Dent Res. 2010;89(5):504-9.
290. Ryan LM, Wortmann RL, Karas B, Lynch MP, Mccarty DJ. Pyrophosphohydrolase Activity and Inorganic Pyrophosphate Content of Cultured Human-Skin Fibroblasts - Elevated Levels in Some Patients with Calcium Pyrophosphate Dihydrate Deposition Disease. J Clin Invest. 1986;77(5):1689-93.
291. Terkeltaub RA. Inorganic pyrophosphate generation and disposition in pathophysiology. Am J Physiol-Cell Ph. 2001;281(1):C1-C11.
292. Bellows CG, Heersche JNM, Aubin JE. Inorganic-Phosphate Added Exogenously or Released from Beta-Glycerophosphate Initiates Mineralization of Osteoid Nodules Invitro. Bone Miner. 1992;17(1):15-29.
293. Huang MS, Sage AP, Lu JX, Demer LL, Tintut Y. Phosphate and pyrophosphate mediate PKA-induced vascular cell calcification. Biochem Bioph Res Co. 2008;374(3):553-8.
294. Nakano Y, Addison WN, Kaartinen MT. ATP-mediated mineralization of MOT3-E1 osteoblast cultures. Bone. 2007;41(4):549-61.
295. Hutmacher DW, Garcia AJ. Scaffold-based bone engineering by using genetically modified cells. Gene. 2005;347(1):1-10.
296. Langer R, Vacanti JP. Tissue engineering. Science. 1993;260(5110):920-6.

297. CT. Laurencin HL. Polymer-ceramic composites for bone tissue engineering. In: Davies J, editor. Bone engineering2000. p. 462-72.
298. Wang M. Developing bioactive composite materials for tissue replacement. Biomaterials. 2003;24(13):2133-51.
299. Moroni L, De Wijn JR, Van Blitterswijk CA. Integrating novel technologies to fabricate smart scaffolds. J Biomat Sci-Polym E. 2008;19(5):543-72.
300. Fu Q, Rahaman MN, Dogan F, Bal BS. Freeze-cast hydroxyapatite scaffolds for bone tissue engineering applications. Biomed Mater. 2008;3(2).
301. Nakamatsu J, Torres FG, Troncoso OP, Yuan ML, Boccaccini AR. Processing and characterization of porous structures from chitosan and starch for tissue engineering scaffolds. Biomacromolecules. 2006;7(12):3345-55.
302. Sultana N, Wang M. Fabrication of HA/PHBV composite scaffolds through the emulsion freezing/freeze-drying process and characterisation of the scaffolds. J Mater Sci-Mater M. 2008;19(7):2555-61.
303. Gomes ME, Azevedo HS, Moreira AR, Ella V, Kellomaki M, Reis RL. Starch-poly(epsilon-caprolactone) and starch-poly(lactic acid) fibre-mesh scaffolds for bone tissue engineering applications: structure, mechanical properties and degradation behaviour. J Tissue Eng Regen M. 2008;2(5):243-52.
304. Ghosh S, Viana JC, Reis RL, Mano JF. The double porogen approach as a new technique for the fabrication of interconnected poly(L-lactic acid) and starch based biodegradable scaffolds. J Mater Sci-Mater M. 2007;18(2):185-93.
305. Ghosh S, Vianac JC, Reis RL, Mano JF. Development of porous lamellar poly(L-lactic acid) scaffolds by conventional injection molding process. Acta Biomaterialia. 2008;4(4):887-96.
306. Tuzlakoglu K, Alves CM, Mano JF, Reis RL. Production and characterization of chitosan fibers and 3-D fiber mesh scaffolds for tissue engineering applications. Macromol Biosci. 2004;4(8):811-9.
307. Liang D, Hsiao BS, Chu B. Functional electrospun nanofibrous scaffolds for biomedical applications. Adv Drug Deliver Rev. 2007;59(14):1392-412.
308. Duarte ARC, Mano JF, Reis RL. Perspectives on: Supercritical Fluid Technology for 3D Tissue Engineering Scaffold Applications. J Bioact Compat Pol. 2009;24(4):385-400.
309. Cooper AI. Porous materials and supercritical fluids. Adv Mater. 2003;15(13):1049-59.
310. Marelli B, Ghezzi CE, Barralet JE, Boccaccini AR, Nazhat SN. Three-Dimensional Mineralization of Dense Nanofibrillar Collagen-Bioglass Hybrid Scaffolds. Biomacromolecules. 2010;11(6):1470-9.
311. Reignier J, Gendron R, Champagne MF. Extrusion foaming of poly(lactic acid) blown with Co-2: Toward 100% green material. Cellular Polymers. 2007;26(2):83-115.
312. Karageorgiou V, Kaplan D. Porosity of 3D biornaterial scaffolds and osteogenesis. Biomaterials. 2005;26(27):5474-91.
313. R. Gendron MB. Challenging the paradigm of microcellular foams: Mechanical properties of low-density cyclo-olefin copolymer foams. Antec2009.
314. A. Qaiss HS, O. Fassi-Fehri, M. Bousmina. Porosity formation by biaxial stretching in polyolefin films filled with calcium carbonate particles. Journal of Applied Polymer Science. 2012;123:3425-36.

315. Bureau M. The relationship between morphology and mechanical properties in thermoplastic foams. In: Gendron R, editor. Thermoplastic foam processing: Principles and development: CRC press; 2005. p. 235-81.
316. dos Santos E, Farina M, Soares G, Anselme K. Surface energy of hydroxyapatite and β-tricalcium phosphate ceramics driving serum protein adsorption and osteoblast adhesion. Journal of Materials Science: Materials in Medicine. 2008;19(6):2307-16.